A THEORETICAL AND EXPERIMENTAL INVESTIGATION OF PRESTRESSED CYLINDRICAL SHELL ROOFS

A thesis presented for the
degree of Doctor of Philosphy in Civil Engineering
in the University of Canterbury,
Christchurch, New Zealand

by

A. H. Bryant, B.E. (hons.).

1966

N O T E

A factor of 2 has been omitted in the equation relating shear stresses and strains (section 7.6). Hence, the experimental shear stresses should be one half the values given in figures 9.1 - 9.8 and on pages 188 - 195 with the agreement between theoretical and experimental shear stresses being similar to that for transverse stresses. Some of the discussions and conclusions on shear and principal stresses can now be disregarded.

A B S T R A C T

This thesis deals with the experimental and theoretical analysis of cylindrical shells that are prestressed within the curved surface.

An existing solution to the D.K.J. equation is presented and extended so that cylindrical shells can be analysed with line-loads applied along pairs of generators. A method of replacing the loads on a cylindrical shell from prestressing cables within the curved surface by actions along a finite number of generators is given. Computer programs have been written to carry out this process and analyse prestressed cylindrical shells.

The construction and testing of an aluminium alloy model of a cylindrical shell from which strain and deflection readings were obtained from eight different symmetrical prestressing cable lay-outs is described. Particular emphasis was placed on the obtaining of accurate experimental readings.

Comparisons between theory and experiment showed that the behaviour of the model shell was close to that described by the D.K.J. equation and that a Levy type solution gave satisfactory stresses and deflections over most of the shell surface.

Of particular interest is the variation of transverse moments with different prestressing cable lay-outs and different shell spans.

A C K N O W L E D G E M E N T S

The author is grateful to Professor H. J. Hopkins, Head of the Department of Civil Engineering, University of Canterbury, under whose overall guidance this research was carried out.

For detailed supervision, the author is indebted to Dr. J. C. Scrivener.

Thanks are also due to:

Dr. G. H. Powell for his assistance on shell theory.

Dr. D. G. Elms for helpful comments on experimental technique.

The Technical Staff of the Civil Engineering Department for their help with testing.

The staff of the Mobil Computer Laboratory, University of Canterbury, for the punching of cards and the processing of programs.

The University Grants Committee for financial assistance under a Research Fellowship, and for equipment under the Research Grant 63/116.

C O N T E N T S

LIST OF FIGURES

LIST OF TABLES

INDEX OF NOTATION

Each notation is defined where it first appears in the manuscript and the more important are listed below:

$\underline{A}, A, A_1, A_2$	:	coefficient matrices of complementary function
$\mathbf{a}$	:	column vector of arbitrary constants, (a_1, a_2, a_3, a_4), from left hand edge
a	:	constant defining parabola
a_n	:	nth Fourier coefficient in the x direction
a_{ni}	:	nth Fourier coefficient from the ith strip
a_m	:	mth Fourier coefficient in the y direction
$\underline{B}, B, B_1, B_2$	:	coefficient matrices of the complementary function
$\mathbf{b}$	:	column vector of arbitrary constants, (b_1, b_2, b_3, b_4), from right hand edge
b	:	constant defining parabola
b	:	shell arc length from one edge to the other
$\underline{\mathbf{b}}$	:	unit binormal
C	:	resistance correction coefficient
c	:	complex number describing solution to auxiliary equation
c	:	parameter describing parabolic cable
D	:	flexural rigidity
d	:	anchorage eccentricity as an arc distance from the crown
E	:	Young's modulus
e	:	$\frac{1}{4}$ period of general function

$\mathbf{F}^y, \mathbf{F}^z$	:	matrices of damping factors
F_x, F_y, F_z, F	:	constants of particular integral solution
f	:	general action or displacement
f	:	drape of prestressing cable as an arc length
f(x)	:	general function of x
G	:	constant in complementary function solution
GF_b	:	gauge factor set on strain indicator
GF_g	:	gauge factor of strain gauge
g	:	arc distance of prestressing cable from generator
$g_i(x)$	:	equation of i th strip
h	:	height of gauge point above centroid of cross section
h	:	arc distance of prestressing cable from generator
H_x, H_y, H_z, H	:	constants of particular integral solution
i	:	name for general term, junction, shell
$\mathbf{J}$	:	unit diagonal matrix (1, -1, 1, -1)
j	:	name for general term etc.
j, j_1	:	roots of auxiliary equation
$\mathbf{K}$	:	stiffness matrix
K	:	transverse gauge cross sensitivity
k, k_1	:	roots of auxiliary equation
L	:	shell span
L_c, L_f, L	:	line loads along cable per unit cable length
L'_c, L'_f, L'	:	line loads along cable per unit longitudinal length

$\underline{\mathbf{M}}$	:	diagonal coefficient matrix of complementary function solution
M_2	:	moment per unit length exerted by junction on shell or edge stiffening member
m_1, m_2, m_{12}	:	shell moments per unit length
m	:	positive integer (generally describing Fourier harmonic in y direction)
$\underline{\mathbf{N}}$	:	diagonal coefficient matrix of complementary function solution
N_{12}, N_2	:	actions per unit length exerted by junction on shell or edge stiffening member
n	:	positive integer (generally describing Fourier harmonic in x direction)
$\mathbf{n}$	:	column vector of edge actions (n_{12}, n_2, r_2, m_2)
n_1, n_2, n_{12}	:	shell membrane actions per unit length
P	:	prestressing force
P_a	:	prestressing force at anchorages
P_f	:	Friction loss in prestressing force - from diaphragms to mid-span
P_1, P_2	:	constants of particular integral solution
p_1, p_2	:	principal stresses
Q'	:	reading of strain gauge at gauge
Q_b	:	reading of strain gauge at strain indicator
$\mathbf{q}$	:	column vector of junction actions (N_{12}, N_2, R_2, M_2)
q_1, q_2	:	shell transverse shears per unit length
R	:	radius of shell middle surface
R_2	:	action per unit length exerted by junction on shell or edge stiffening member

r	:	number of strips considered in ½ shell length or ¼ period
r_1, r_2	:	shell reactions per unit length
r	:	vector function of path of prestressing cable
s	:	distance along prestressing cable
T	:	carry over matrix
t	:	shell thickness
t	:	parameter describing parabola
t	:	unit tangent
U	:	displacement in X direction
u	:	displacement in x direction
u	:	column vector of displacements $(Eu, Ev, Ew, E\theta_2)$
V	:	displacement in Y direction
v	:	displacement in y direction
v	:	displacement column vector $(EU, EV, EW, E\theta_2)$
W	:	force per unit length of cable to move prestressing cable
X	:	junction axes
X	:	surface load per unit area in x direction
x	:	shell axis
Y	:	junction axis
Y	:	surface load per unit area in y direction
y	:	shell axis
y	:	arc distance from left hand shell edge
y_m	:	arc distance from crown to shell edge
Z	:	junction axis

Z	:	surface load per unit area in z direction
Z_p, Z_m	:	plate and membrane surface loads
z	:	shell axis
z	:	arc distance from right hand shell edge
$\alpha, \beta, \gamma, \eta, \lambda, \nu$	:	constants describing complementary function solution
ε	:	strain
κ	:	curvature
φ_k	:	half shell opening angle
φ_s	:	half angle between 2 loaded generators
σ	:	stress
$\Theta_1, \Theta_2, \Theta_2$	:	rotations
μ	:	Poisson's ratio
μ	:	coefficient of friction

SUBSCRIPTS AND SUPERSCRIPTS

i or j	:	i th or j th general term
s	:	in shell axes
o	:	at y = 0 or z = 0
b	:	at y = b or x = b
f	:	at a fixed edge
1,2,3 or x,y,z		in x, y, z directions
y,z	:	at y = y, z = z

CHAPTER ONE

INTRODUCTION TO PRESTRESSED CYLINDRICAL SHELLS

1.1 PRESTRESSED SHELL ROOFS

The prestressing of shell roofs offers many advantages to shell designers and builders. Greater architectural freedom is allowed in the design with the possibility of larger spans, thinner shells, and the rejection of edge-beams. Cracking of the concrete can be reduced or eliminated and the waterproofing of the shell is no longer such a problem.

Prestressing supplies a method of joining precast shell sections together. Shell sections could be easily and accurately cast in a precision mould in a precasting factory or on the site of a shell roof under construction and then lifted into position and prestressed together. Building shells would be much easier because there would no longer be the necessity of building complex boxing and the problem of pouring and curing the concrete in situ.

Prestressing within the curved surface of shells allows a greater choice of prestressing cable positions and profiles than does prestressing within edge-beams.

1.2 DEVELOPMENT OF SHELL THEORY

The general process of solution in which the state of equilibrium and continuity of a shell element is expressed as

a single characteristic equation which is then solved with the aid of Fourier analysis, has become a widely used approach to cylindrical shell theory.

About this approach, Bouma[1] states:

"It was not until after 1940 that Donnell's equations for cylindrical shells gained the recognition that they so well deserved. In establishing these equations, non-essential or only slightly important terms have been rigorously discarded. In many publications giving ever-different characteristic equations, there is something refreshing about the equations developed by Donnell. Von Karman and Tsien, Jenkins and Wlassov adopted the same approach and many others followed them. The accuracy of these equations was investigated, and, although they were not in all cases exact, they were, in general, found reliable."

The D.K.J. (Donnel, von Karman, and Jenkins) equation, as given by Jenkins[2], has been adopted, in this thesis, as the characteristic equation describing the behaviour of a cylindrical shell.

As well as the so called "exact" solutions, there is a whole body of approximate solutions such as the membrane theory or the extended beam theory of Lundgren[3] which have been developed to simplify design computations. These elementary methods may produce acceptable results under particular favourable circumstances but, with the advent of electronic digital computers, they are becoming less important as the vast amount of arithmetic manipulation, necessary for

the solution of the differential equations describing shell behaviour accurately, can be carried out without much effort and time once computer programs are written.

1.3 KNOWLEDGE OF PRESTRESSED CYLINDRICAL SHELLS AT THE START OF THIS INVESTIGATION

The solution of cylindrical shells with prestressed edge-beams[4] is basically no different from that for reinforced concrete shells. More Fourier loading terms than are commonly used for dealing with self-weight are necessary to describe the effects of prestressing on edge-beams. Care must be taken because mid-span and the shell ends are not always the most highly stressed areas of the shell.

The problem of solving cylindrical shells with prestressing cables within the curved surface is more difficult. Rather than the cables lying in a rectangular beam whose deflections and stresses can be easily calculated, the cables now lie within parts of cylindrical shells whose behaviour is more complex. Before the age of electronic digital computers, the use of severe approximations, such as the beam theory or replacing the loads on a shell from cable curvature by statically equivalent actions along the shell edges (method described by Dehouse[5]), were required so that solutions could be obtained from a reasonable amount of arithmetic manipulation.

de Sitter[6], in 1963, gave a method that is described in section 11.1 of this thesis, for the solution of prestressed

cylindrical shells with straight prestressing cables by treating the anchorage loads as boundary direct stresses at the curved ends of the shell. Recent multi-shell computer programs, such as that of Scordelis and Lo[7], (published since the start of this investigation in 1964), have been used for the solution of cylindrical shells with straight prestressing cables by treating the cable positions as junctions between shells of a multi-shell and applying the anchorage loads as point shear loads at the ends of these junctions.

Little systematic experimental work has been done to verify the large number of theoretical solutions to many shell problems. The field of prestressed cylindrical shells is no exception, the set of tests of de Sitter[6], in which a plastic model was tested with a number of straight cable positions, appearing to be the only set of such tests. All other tests appear to be isolated tests; usually as aids to the design of particular prestressed cylindrical shells.

There appeared to be no existing accurate theoretical solutions to cylindrical shells with draped prestressing cables within the curved surface and no existing satisfactory model tests, in which prestressing cable positions and profiles were varied in a systematic manner.

1.4 SCOPE OF THIS RESEARCH

The main objects of this research project were:

(a) To build an elastic model of a cylindrical shell without edge-beams and to carry out a systematic set of tests on this model, in which the stresses and deflections, resulting from different symmetrical prestressing cable positions and profiles, were to be accurately measured.

(b) To develop a solution to the D.K.J. equation for the stresses in a cylindrical shell with prestressing cables in the curved surface.

(c) To compare theoretical and experimental model stresses.

1.5 COMPUTER FACILITIES

The only available electronic digital computer at the University of Canterbury was an I.B.M. 1620, model 1. The total storage capacity of this machine was only 40,000 decimal digits. Using Fortran II, 11,000 of these positions were required for basic instructions, leaving 29,000 decimal digits of storage for programs and data. One 8 figure floating point number takes 10 decimal digits of storage. Computing speed was also very slow.

With these limitations in view, computer programs must be very carefully written. Program lengths and storage requirements must be carefully watched and programs must be written so that everything is calculated as efficiently as possible.

The solving of shell problems on a 1620 is rather futile because of the complexity of shell theory. Even with all possible short cuts and limitations on the generality, the computer program developed for the solution of cylindrical shells with prestressing cables in the curved surface consisted of 5 separate chapters. The computer storage had to be cleared between chapters and the card output from one chapter fed directly into the next.

All computer programs were written in I.B.M. Fortran II for the 1620[8].

CHAPTER TWO

BENDING SOLUTION FOR A CYLINDRICAL SHELL

2.1 INTRODUCTION TO SHELL THEORY

A brief description of the formation of the D.K.J. equation and its solution is given in this chapter. Nearly all that has been included is necessary for a clear definition of the meaning of all the terms in the complementary function and the particular integral solutions. This solution to the D.K.J. equation has been taken as the basis for the multi-shell and the generator line-load theory given in chapter 3 and used for the solution of prestressed cylindrical shells.

The solution closely follows the method of Jenkins[2] and is a simplification of that used by Powell[9] for shells with curvature in both the longitudinal and the transverse directions. A slightly different notation and sign convention from that of Jenkins has been used and Poisson's ratio has been included.

2.2 NOTATION AND SIGN CONVENTION

Figure 2.1 shows the positive directions of the axes (x, y, z), shell actions per unit length (extensional actions n_1, n_2, n_{12} ; moments m_1, m_2, m_{12} ; transverse shears q_1, q_2 ; and reactions r_1, r_2), displacements (u, v, w), and rotations (θ_1, θ_2).

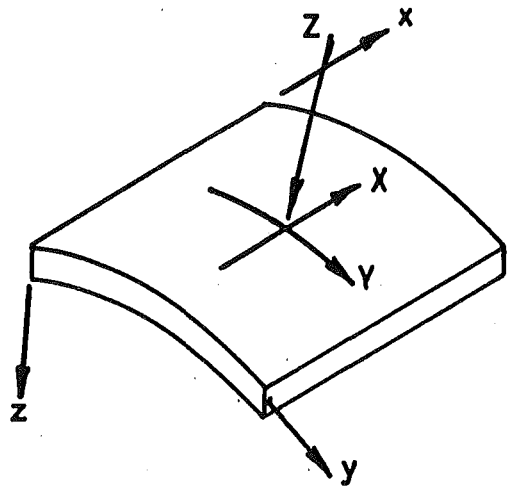

(a) Surface loads and shell axes

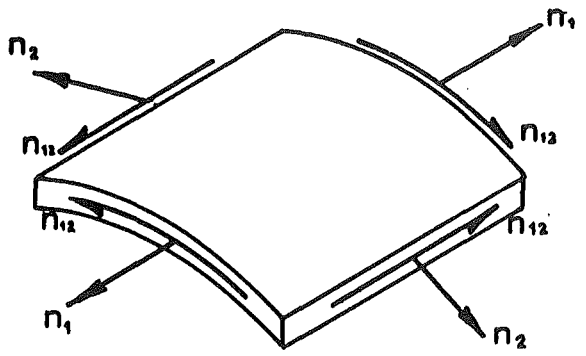

(b) Extensional actions

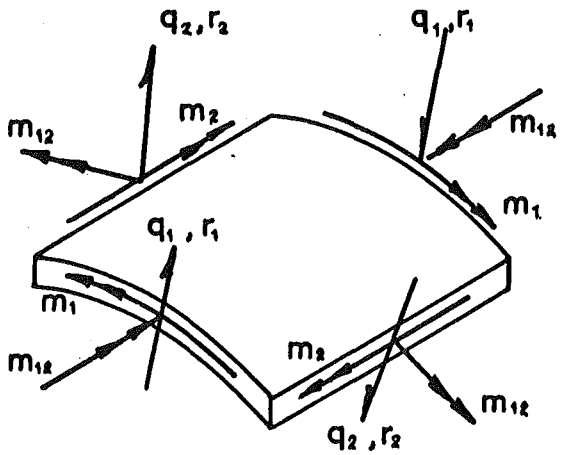

(c) Flexural actions

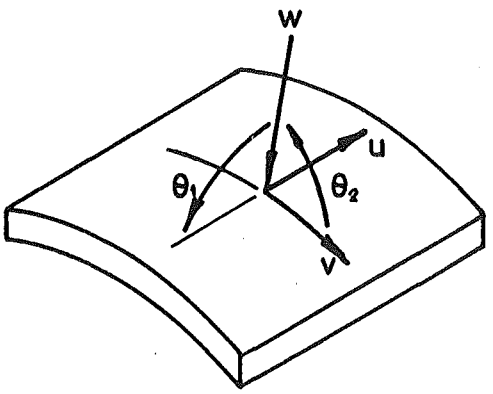

(d) Displacements

Fig. 2.1 Conventially positive shell axes, actions, surface loads, and displacements

The rotations are defined by

$$\theta_1 = -\frac{\partial w}{\partial x} \quad , \qquad \theta_2 = -\frac{\partial w}{\partial y} \, .$$

At the shell edges the actions can be represented by four actions as in figure 2.2 where

$$r_1 = q_1 + \frac{\partial m_{12}}{\partial y} \quad , \quad r_2 = q_2 + \frac{\partial m_{12}}{\partial x} \, .$$

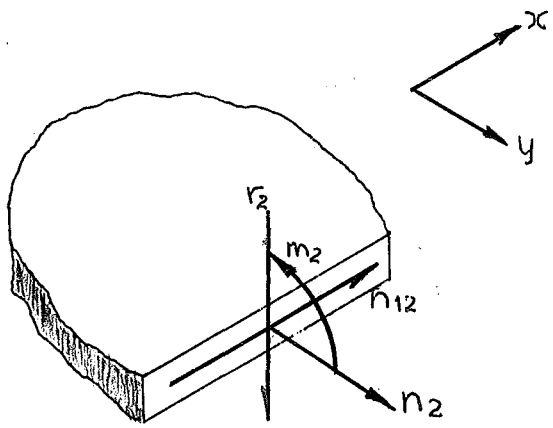

Fig. 2.2 Boundary actions at y = constant

2.3 EQUILIBRIUM EQUATIONS

$$\left.\begin{aligned} \frac{\partial n_1}{\partial x} + \frac{\partial n_{12}}{\partial y} + X &= 0 \\ \frac{\partial n_{12}}{\partial x} + \frac{\partial n_2}{\partial y} + Y &= 0 \\ \frac{n_2}{R} + Z_m &= 0 \end{aligned}\right\} \text{ membrane . . (1)}$$

$$\left.\begin{aligned} \frac{\partial m_1}{\partial x} + \frac{\partial m_{12}}{\partial y} - q_1 &= 0 \\ \frac{\partial m_{12}}{\partial x} + \frac{\partial m_2}{\partial y} - q_2 &= 0 \\ \frac{\partial q_1}{\partial x} + \frac{\partial q_2}{\partial y} + Z_p &= 0 \end{aligned}\right\} \text{flexural . . (2)}$$

where $Z_m + Z_p = Z$,

R = shell radius.

2.4 CONTINUITY EQUATIONS

$$\left.\begin{aligned} n_1 &= \frac{Et}{(1-\mu^2)}\left[\frac{\partial u}{\partial x} + \mu\left(\frac{\partial v}{\partial y} - \frac{w}{R}\right)\right] \\ n_2 &= \frac{Et}{(1-\mu^2)}\left[\frac{\partial v}{\partial y} - \frac{w}{R} + \mu\frac{\partial u}{\partial x}\right] \\ n_{12} &= \frac{Et}{2(1+\mu)}\left[\frac{\partial u}{\partial y} + \frac{\partial v}{\partial x}\right] \end{aligned}\right\} \text{membrane . . (3)}$$

$$\left.\begin{aligned} m_1 &= -\frac{Et^3}{12(1-\mu^2)}\left[\frac{\partial^2 w}{\partial x^2} + \mu\frac{\partial^2 w}{\partial y^2}\right] \\ m_2 &= -\frac{Et^3}{12(1-\mu^2)}\left[\mu\frac{\partial^2 w}{\partial x^2} + \frac{\partial^2 w}{\partial y^2}\right] \\ m_{12} &= -\frac{Et^3}{12(1+\mu)}\left[\frac{\partial^2 w}{\partial x \partial y}\right] \\ q_1 &= -\frac{Et^3}{12(1-\mu^2)}\left[\frac{\partial}{\partial x}\nabla^2 w\right] \end{aligned}\right\} \text{flexural . . (4)}$$

$$
\left.
\begin{aligned}
q_2 &= \frac{-Et^3}{12(1-\mu^2)} \left[\frac{\partial}{\partial y}\nabla^2 w\right] \\
r_1 &= \frac{-Et^3}{12(1-\mu^2)} \frac{\partial}{\partial x}\left[\frac{\partial^2 w}{\partial x^2} + (2-\mu)\frac{\partial^2 w}{\partial y^2}\right] \\
r_2 &= \frac{-Et^3}{12(1-\mu^2)} \frac{\partial}{\partial y}\left[\frac{\partial^2 w}{\partial y^2} + (2-\mu)\frac{\partial^2 w}{\partial x^2}\right]
\end{aligned}
\right|
$$

t = shell thickness, E = Young's modulus,

μ = Poisson's ratio, $\nabla^2 = \frac{\partial^2}{\partial x^2} + \frac{\partial^2}{\partial y^2}$.

2.5 THE CYLINDRICAL SHELL (D.K.J.) EQUATION

Equations (1) and (3) yield the cylindrical shell membrane equation

$$
\frac{Et}{R^2}\frac{\partial^4 w}{\partial x^4} = \nabla^4 Z_m + \frac{1}{R}\left[\frac{\partial^2}{\partial y^2} - \mu\frac{\partial^2}{\partial x^2}\right]\frac{\partial X}{\partial x}
$$

$$
- \frac{1}{R}\left[\frac{\partial^2}{\partial y^2} + (2+\mu)\frac{\partial^2}{\partial x^2}\right]\frac{\partial Y}{\partial y} \quad \ldots \quad (5)
$$

Similarly equations (2) and (4) give Lagrange's equation for the plate,

$$
\frac{Et^3}{12(1-\mu^2)}\nabla^4 w = Z_p
$$

or

$$
\frac{Et^3}{12(1-\mu^2)}\nabla^8 w = \nabla^4 Z_p . \quad \ldots \quad (6)
$$

Adding equations (5) and (6) gives the D.K.J. equation,

$$\frac{Et^3}{12(1-\mu^2)}\nabla^8 w + \frac{Et}{R^2}\frac{\partial^4 w}{\partial x^4} = \nabla^4 Z + \frac{1}{R}\left[\frac{\partial^2}{\partial y^2} - \mu\frac{\partial^2}{\partial x^2}\right]\frac{\partial X}{\partial x} - \frac{1}{R}\left[\frac{\partial^2}{\partial y^2} + (2+\mu)\frac{\partial^2}{\partial x^2}\right]\frac{\partial Y}{\partial y}, \quad \ldots (7)$$

where $\nabla^{2n} \equiv (\nabla^2)^n \equiv \left(\frac{\partial^2}{\partial x^2} + \frac{\partial^2}{\partial y^2}\right)^n$.

2.6 METHOD OF SOLUTION

A Levy type method of solution can be applied to reduce (7) to an ordinary differential equation. If loading functions are of the form

$$\left.\begin{aligned} X &= X(x, y) = X(y) \sin \alpha x, \\ Y &= Y(x, y) = Y(y) \cos \alpha x, \\ Z &= Z(x, y) = Z(y) \cos \alpha x, \end{aligned}\right\} \quad \ldots\ldots\ldots (8)$$

where α is some constant it may easily be shown that (7) is satisfied by

$$w = w(x, y) = w(y) \cos \alpha x$$

and reduces to

$$\frac{Et^3}{12(1-\mu^2)}\left[\frac{d^2}{dy^2} - \alpha^2\right]^4 w(y) + \frac{Et}{R^2}\alpha^4 w(y) = \left[\frac{d^2}{dy^2} - \alpha^2\right]^2 Z(y) + \frac{\alpha}{R}\left[\frac{d^2}{dy^2} + \mu\alpha^2\right] X(y) - \frac{1}{R}\left[\frac{d^2}{dy^2} - \alpha^2(2+\mu)\right]\frac{dY(y)}{dy}. \quad \ldots (9)$$

It can also be shown that any other action or displacement, f , will be one of the two similar forms:

$$f = f(x, y) = f(y) \sin \alpha x$$

or $$f = f(x, y) = f(y) \cos \alpha x$$

$\cos \alpha x$ applies to n_1, n_2, m_1, m_2, q_2, r_2, v, θ_2

$\sin \alpha x$ applies to n_{12}, m_{12}, q_1, r_1, u, θ_1.

In the following solutions the maximum values of actions, displacements, and loads are used with the multipliers $\cos \alpha x$ and $\sin \alpha x$ being implied.

If the constant α is defined by $\alpha = n\pi/L$ where n equals a positive integer and L = shell length, the boundary conditions at the curved ends ($x = \pm L/2$) are

$n_1 = n_2 = m_1 = m_2 = q_2 = r_2 = v = w = \theta_2 = 0.$

These conditions are satisfied by a "simple support" - a diaphragm normal to the shell surface having:

(a) infinite stiffness in its own plane,

(b) zero stiffness normal to its own plane.

The Levy solution allows 4 boundary conditions along each of the two straight edges to be satisfied.

e.g. Boundary conditions at a free edge:

$$m_2 = r_2 = n_2 = n_{12} = 0.$$

The column vectors **n**,**u**, given below, are directly obtained during the solution of (9).

$$\mathbf{n} = \begin{bmatrix} n_{12} \\ n_2 \\ r_2 \\ m_2 \end{bmatrix}, \qquad \mathbf{u} = \begin{bmatrix} Eu \\ Ev \\ Ew \\ E\theta_2 \end{bmatrix}.$$

All other actions and displacements can be found from the elements of $\mathbf{n}$ and $\mathbf{u}$.

$$\left.\begin{aligned}
n_1 &= \alpha t E u + \mu n_2 \\
m_1 &= \mu m_2 + \frac{\alpha^2 t^3}{12} E w \\
m_{12} &= \frac{-\alpha t^3}{12(1+\mu)} E\theta_2 \\
q_2 &= r_2 - \alpha m_{12} \\
q_1 &= \frac{-\alpha}{1+\mu}(m_1 + m_2) \\
r_1 &= q_1 + \frac{\alpha}{1-\mu^2}(m_2 - \mu m_1)
\end{aligned}\right\} \quad \ldots\ldots (10)$$

2.7 COMPLEMENTARY FUNCTION SOLUTION

2.7.1 Solution of the auxiliary equation

The homogeneous form of (9) is

$$\frac{Et^3}{12(1-\mu^2)}\left[\frac{d^2}{dy^2}-\alpha^2\right]^4 w(y) + \frac{Et}{R^2}\alpha^4 w(y) = 0 \quad \ldots (11)$$

which has a solution in the form

$w(y) = G\, e^{cy}$ with 8 complex values of c, G = a constant.

The auxiliary equation is

$$\left(\frac{c^2}{\lambda^2} - \nu\right)^4 + 4 = 0, \quad \text{where}$$

$$\beta = \sqrt[4]{\frac{3(1-\mu^2)}{R^2t^2}}\,,$$

$$\lambda = \sqrt{\alpha\beta}\,, \quad \nu = \frac{\alpha}{\beta}\,,$$

and has 8 complex roots

$$\frac{c}{\lambda} = \pm(j \pm ik) \;\&\; \pm(j_1 \pm ik_1)\,,$$

where

$$j = \sqrt{\frac{\sqrt{1+(1+\nu)^2}+1+\nu}{2}}\,, \qquad j_1 = \sqrt{\frac{\sqrt{1+(1-\nu)^2}-(1-\nu)}{2}}\,,$$

$$k = \frac{1}{2j}\,, \qquad k_1 = \frac{1}{2j_1}\,,$$

also

$$j^2 - k^2 = 1+\nu\,, \qquad j_1^2 - k_1^2 = -(1-\nu)\,.$$

The solution can be expressed in two sets of damped, oscillating functions originating at the left hand edge ($y = 0$, $z = b$) and at the right hand edge ($y = b$, $z = 0$). y and z are arc lengths from the left and right hand shell edges to a point on the shell middle surface.

$$w = e^{-j\lambda y}(a_1 \cos k\lambda y + a_2 \sin k\lambda y) + e^{-j_1\lambda y}(a_3 \cos k_1\lambda y + a_4 \sin k_1\lambda y)$$
$$+ e^{-j\lambda z}(b_1 \cos k\lambda z + b_2 \sin k\lambda z) + e^{-j_1\lambda z}(b_3 \cos k_1\lambda z + b_4 \sin k_1\lambda z),$$

where a_1, a_2, a_3, a_4 are arbitrary constants determined from the left hand edge,

b_1, b_2, b_3, b_4 are arbitrary constants determined from the right hand edge.

2.7.2 Complete complementary function solution

The complementary function solution can be expressed in the form

$$\mathbf{n} = \left[\mathbf{A}\mathbf{F}^{y}\mathbf{a} - \mathbf{J}\mathbf{A}\mathbf{F}^{z}\mathbf{b}\right], \quad \ldots \quad (13)$$

$$\mathbf{u} = \left[\mathbf{B}\mathbf{F}^{y}\mathbf{a} + \mathbf{J}\mathbf{B}\mathbf{F}^{z}\mathbf{b}\right], \quad \ldots \quad (14)$$

where $\mathbf{A} = \underline{\mathbf{M}}\,\underline{\mathbf{A}}$, $\mathbf{B} = \underline{\mathbf{N}}\,\underline{\mathbf{B}}$,

and $\mathbf{n} = \begin{bmatrix} n_{12} \\ n_2 \\ r_2 \\ m_2 \end{bmatrix}$, $\mathbf{u} = \begin{bmatrix} Eu \\ Ev \\ Ew \\ E\Theta_2 \end{bmatrix}$, $\mathbf{a} = \begin{bmatrix} a_1 \\ a_2 \\ a_3 \\ a_4 \end{bmatrix}$, $\mathbf{b} = \begin{bmatrix} b_1 \\ b_2 \\ b_3 \\ b_4 \end{bmatrix}$,

$\mathbf{J} = \mathrm{Diag}\begin{bmatrix} 1 \\ -1 \\ 1 \\ -1 \end{bmatrix}$, $\underline{\mathbf{N}} = \mathrm{Diag}\begin{bmatrix} \frac{\alpha^2}{2R\lambda^2} \\ \frac{1}{2R\lambda} \\ 1 \\ \lambda \end{bmatrix}$, $\underline{\mathbf{M}} = \mathrm{Diag}\begin{bmatrix} \frac{t\alpha^3}{2R\lambda^3} \\ \frac{t\alpha^4}{2R\lambda^4} \\ \frac{t\alpha^4}{4R^2\lambda^5} \\ \frac{t\alpha^4}{4R^2\lambda^6} \end{bmatrix}$,

$$F^y = \begin{bmatrix} e^{-j\lambda y}\cos k\lambda y & e^{-j\lambda y}\sin k\lambda y & \cdot & \cdot \\ -e^{-j\lambda y}\sin k\lambda y & e^{-j\lambda y}\cos k\lambda y & \cdot & \cdot \\ \cdot & \cdot & e^{-j_1\lambda y}\cos k_1\lambda y & e^{-j_1\lambda y}\sin k_1\lambda y \\ \cdot & \cdot & -e^{-j_1\lambda y}\sin k_1\lambda y & e^{-j_1\lambda y}\cos k_1\lambda y \end{bmatrix},$$

$$\underline{A} = \begin{bmatrix} -k & -j & k_1 & j_1 \\ \cdot & -1 & \cdot & 1 \\ j[1-\nu(1-\mu)]-k & -k[j-\nu(1-\mu)]-j & -j_1[1+\nu(1-\mu)]-k_1 & k_1[1+\nu(1-\mu)]-j_1 \\ -1-\nu(1-\mu) & 1 & 1-\nu(1-\mu) & 1 \end{bmatrix},$$

$$\underline{B} = \begin{bmatrix} 1 & 1+\nu(1+\mu) & -1 & 1-\nu(1+\mu) \\ -k[1-\nu(1+\mu)]-j & -j[1-\nu(1+\mu)]+k & -k_1[1+\nu(1+\mu)]+j_1 & -j_1[1+\nu(1+\mu)]-k_1 \\ 1 & \cdot & 1 & \cdot \\ j & -k & j_1 & -k_1 \end{bmatrix}.$$

2.7.3 Determination of arbitrary constants

For a symmetrically loaded symmetrical cylindrical shell

$$a = b = a_s$$

and the complementary function solution becomes

$$n_s = \left[AF^y - JAF^z\right]a_s, \quad \ldots \quad (15)$$

$$u_s = \left[BF^y + JBF^z\right]a_s. \quad \ldots \quad (16)$$

For an antisymmetrically loaded cylindrical shell

$$a = -b = a_a$$

and the complementary function solution becomes

$$n_a = \left[AF^y + JAF^z\right]a_a, \quad \ldots \quad (17)$$

$$u_a = \left[BF^y - JBF^z\right]a_a, \quad \ldots \quad (18)$$

where subscript s : symmetrical,

subscript a : antisymmetrical.

Equations (13), (14) can be split into two parts

$$n = \left[AF^y - JAF^z\right]\frac{a+b}{2} + \left[AF^y + JAF^z\right]\frac{a-b}{2}, \quad \cdots (19)$$

$$u = \left[BF^y + JBF^z\right]\frac{a+b}{2} + \left[BF^y - JBF^z\right]\frac{a-b}{2} \quad \cdots (20)$$

which are the sums of symmetrical and antisymmetrical solutions in which

$$a_s = \frac{a+b}{2}, \qquad a_a = \frac{a-b}{2}.$$

Let

$$\left.\begin{aligned} A_1 &= A - JAF^b, & A_2 &= A + JAF^b \\ B_1 &= B + JBF^b, & B_2 &= B - JBF^b \end{aligned}\right\} \cdots (21)$$

where $y = 0$, $z = b$ and $y = b$, $z = 0$ are the left and right hand edges of the shell.

Then

$$\left.\begin{aligned} n_o &= A_1 a_s + A_2 a_a \\ u_o &= B_1 a_s + B_2 a_a \\ n_b &= -JA_1 a_s + JA_2 a_a \\ u_b &= JB_1 a_s - JB_2 a_a \end{aligned}\right\} \cdots\cdots (22)$$

subscript o stands for the left hand edge,

subscript b stands for the right hand edge.

It follows directly that:

for a given edge displacement

$$\left.\begin{aligned} \mathbf{a}_s &= \tfrac{1}{2}\mathbf{B}_1^{-1}\left[\mathbf{u}_o + \mathbf{J}\mathbf{u}_b\right], \\ \mathbf{a}_a &= \tfrac{1}{2}\mathbf{B}_2^{-1}\left[\mathbf{u}_o - \mathbf{J}\mathbf{u}_b\right], \end{aligned}\right\} \quad \ldots\ldots (23)$$

and for given edge actions

$$\left.\begin{aligned} \mathbf{a}_s &= \tfrac{1}{2}\mathbf{A}_1^{-1}\left[\mathbf{n}_o - \mathbf{J}\mathbf{n}_b\right], \\ \mathbf{a}_a &= \tfrac{1}{2}\mathbf{A}_2^{-1}\left[\mathbf{n}_o + \mathbf{J}\mathbf{n}_b\right]. \end{aligned}\right\} \quad \ldots\ldots (24)$$

$\mathbf{a}, \mathbf{b}$ can be obtained directly, if necessary:

$$\left.\begin{aligned} \mathbf{a} &= \mathbf{a}_s + \mathbf{a}_a, \\ \mathbf{b} &= \mathbf{a}_s - \mathbf{a}_a. \end{aligned}\right\} \quad \ldots\ldots (25)$$

2.8 PARTICULAR INTEGRAL SOLUTIONS

2.8.1 Form of the solution

An exact particular integral solution has been used rather than a solution based on the membrane theory. Higher Fourier terms than those usually considered for self weight are necessary to obtain a reasonably accurate representation of the effects of a point load or a prestressing cable.

From these higher terms, bending rather than membrane stresses predominate and a particular integral solution that excludes bending stresses would be unsatisfactory.

Equation (9) is of the form.

$$\frac{R^2 t^2}{12(1-\mu^2)} \left[\left(\frac{d^2}{dy^2} - \alpha^2\right)^4 + \alpha^4\right] w(y) = P_1 \alpha^4 Q(y) \quad \ldots \quad (26)$$

If Q(y) is of the form cos γy or sin γy
then the particular integral is of the same form.
i.e. $w(y) = P_2 \cos \gamma y$ or $P_2 \sin \gamma y$,
where P_1, P_2, γ are constants.

$$P_2 \left[\frac{R^2 t^2}{12(1-\mu^2)} (\alpha^2 + \gamma^2)^4 + \alpha^4\right] = P_1 \alpha^4.$$

$$\text{ie} \quad w(y) = \frac{P_1 Q(y)}{1 + \frac{r^4}{4}(1+\eta^2)^4}, \quad \ldots \quad (27)$$

$$\eta = \frac{\alpha}{\gamma}.$$

2.8.2 Particular integral tables

Loads

Symmetrical axial $X = X \sin \alpha x \cos \gamma y$

Symmetrical tangential $Y = Y \cos \alpha x \cos \gamma y$ (28)

Symmetrical radial $Z = Z \cos \alpha x \sin \gamma y$

n, u can be expressed in terms of F, H, such that

$$H_x = \frac{R}{\alpha t} \frac{\mu - \eta^2}{1 + \frac{\nu^4}{4}(1+\eta^2)^4} X$$

$$H_y = \frac{R}{\alpha t} \frac{\eta^3 + \eta(2+\mu)}{1 + \frac{\nu^4}{4}(1+\eta^2)^4} Y$$

$$H_z = \frac{R^2}{t} \frac{(1+\eta^2)^2}{1 + \frac{\nu^4}{4}(1+\eta^2)^4} Z$$

$$F_x = \frac{1}{\alpha^3} \frac{\frac{\nu^4}{4}(1+\eta^2)^2(\eta^2-\mu)}{1 + \frac{\nu^4}{4}(1+\eta^2)^4} X$$

$$F_y = \frac{1}{\alpha^2\gamma} \frac{\left[\frac{\nu^4}{4}(1+\eta^2)^2(1-\mu\eta^2)+1\right]}{1 + \frac{\nu^4}{4}(1+\eta^2)^4} Y$$

$$F_z = \frac{R}{\alpha^2} \frac{1}{1 + \frac{\nu^4}{4}(1+\eta^2)^4} Z$$

$$H = H_x + H_y + H_z$$

$$F = F_x + F_y + F_z$$

$$D = \frac{t^3}{12(1-\mu^2)}$$

$$n_{12} = -\alpha\gamma F \sin\alpha x \sin\gamma y$$

$$n_2 = \left[-\alpha^2 F + \frac{Y}{\gamma}\right] \cos\alpha x \cos\gamma y$$

$$r_{12} = -D\alpha^3 \left[\zeta^3 + (2-\mu)\zeta\right] H \cos\alpha x \sin\gamma y$$

$$m_2 = D\alpha^2 \left[\mu + \zeta^2\right] H \cos\alpha x \cos\gamma y$$

$$E_U = \left[\frac{\alpha(\mu-\zeta^2)}{t} F + \frac{X}{t\alpha^2} - \frac{\mu Y}{t\alpha\gamma}\right] \sin\alpha x \cos\gamma y$$

$$E_V = \left[\frac{\alpha^2(\mu\zeta^2-1)}{t\gamma} F - \frac{\mu X}{t\alpha\gamma} + \frac{Y}{t\gamma^2} + \frac{H_y}{\gamma R} + \frac{H_z}{\gamma R}\right] \cos\alpha x \sin\gamma y$$

$$E_W = H \cos\alpha x \cos\gamma y$$

$$E\Theta_2 = \gamma H \cos\alpha x \sin\gamma y$$

CHAPTER THREE

MULTI-SHELL THEORY

3.1 INTRODUCTION

Most of the material in section 3.2 is a summary of portions of a paper by Powell[10]. Its main use, in this thesis, is as a definition of terms used in multi-shell theory and as an illustration of how multi-shells are usually solved.

In section 3.3 a solution for cylindrical shells with line loads along any number of generators is given. The solution has been arranged for symmetrical loads or antisymmetrical loads on any number of pairs of symmetrically placed generators. Any load on a symmetrical structure can be expressed as the sum of symmetrical plus antisymmetrical loads with the solution normally requiring less arithmetic manipulation when the loads are split in this manner.

The problem is reduced to the solution of sets of 4th order simultaneous equations rather than the solution of much higher order (at least four times the number of pairs of loaded generators) simultaneous equations that is required for the usual multi-shell theory. Such a solution is suitable for programming for limited computer facilities.

Various subscripts and superscripts are used in this chapter for a variety of purposes.

Subscripts i or j indicate general shell junctions i or j and a superscript s implies that a stiffness or carry-over matrix has been defined in shell axes while no superscript usually implies junction axes.

In chain-type multi-shell structures, as in figure 3.3, where there is only one structural member between two adjacent junctions, subscripts and superscripts are used in the following manner with:

subscripts ij : shell from junction i to j ,
ii : edge-beam at junction i ,
i : of junction i ,
superscript f : fixing action .

In tube structures, as in figure 3.4, where there is more than one shell between the junctions i and j , a different system is used in which subscripts o and b stand for left and right hand edges of a shell and a general superscript i means through shell i .

e.g. $\mathbf{K}_b^1$ means the stiffness of the right hand edge of shell 1 .

3.2 ORDINARY MULTI-SHELL THEORY

3.2.1 Sign convention for edge actions and displacements in junction axes.

Before the actions and displacements of members meeting at a junction can be easily compared, they must be defined in a common set of junction axes. Actions and displacements can be changed from expressions in one set of axes to expressions in another set of axes by simple orthogonal and translatory transformations.[2,9,10].

When considering the signs of edge actions it is convenient to think of the junction exerting actions on the members meeting there. The sign convention for edge actions and displacements is given in figures 3.1 and 3.2. Upper case letters signify actions and displacements in junction axes corresponding to the lower case letters for actions and displacements in shell axes. The column vectors $\mathbf{q}$ and $\mathbf{v}$, corresponding to $\mathbf{n}$ and $\mathbf{u}$, are defined by

$$\mathbf{q} = \begin{bmatrix} N_{12} \\ N_2 \\ R_2 \\ M_2 \end{bmatrix}, \qquad \mathbf{v} = \begin{bmatrix} E\,U \\ E\,V \\ E\,W \\ E\,\Theta_2 \end{bmatrix}.$$

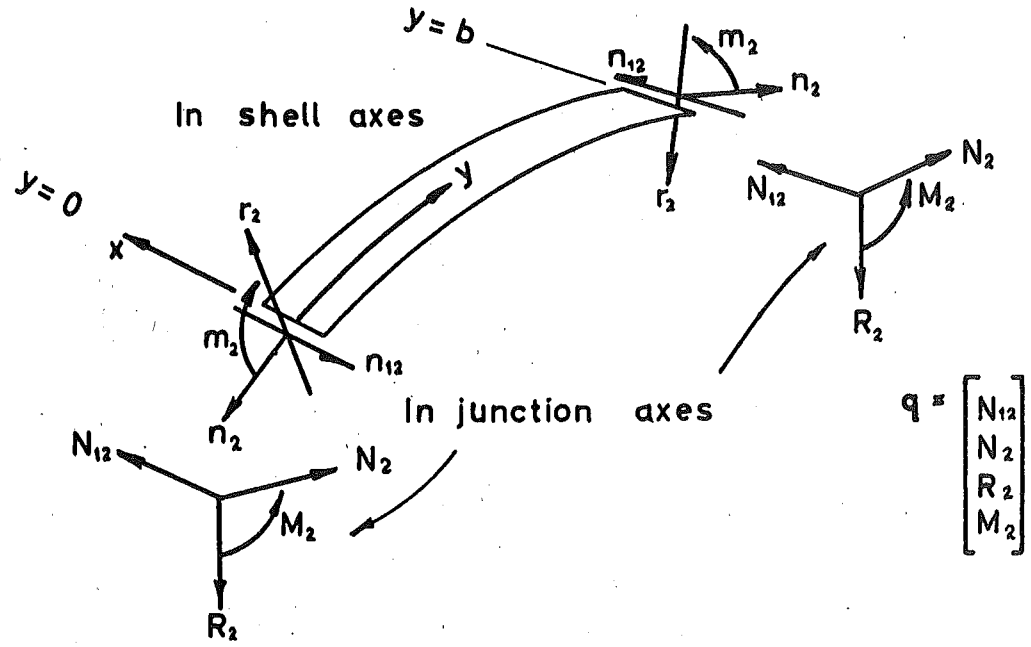

Fig. 3.1 Conventionally positive actions in shell and junction axes

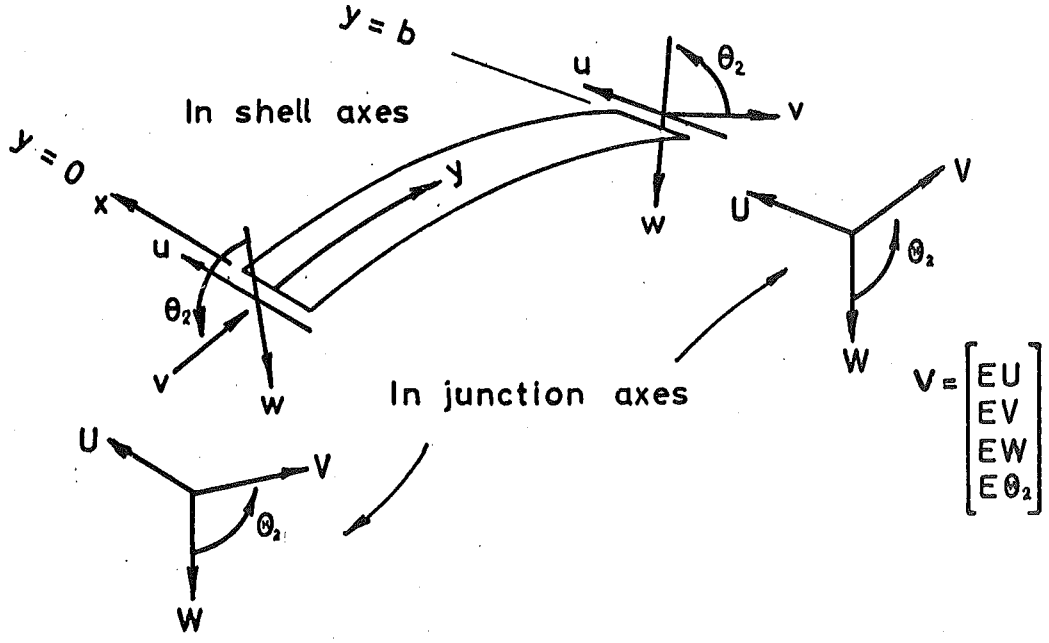

Fig. 3.2 Conventionally positive displacements in shell and junction axes

3.2.2 Stiffness and carry over

Most workers in multi-shell theory have defined the stiffness and carry over as follows. Consider a shell, carrying no external load, extending from junction i to j. If junction j is held clamped, any action q_{ij}, applied to the shell through junction i, will produce a displacement v_{ij} at junction i and a carried over action q_{ji} at junction j. The relationships between these effects can be expressed by 4 x 4 stiffness and carry over matrices $\mathbf{K}$ and $\mathbf{T}$ such that

$$\mathbf{q}_{ij} = \mathbf{K}_{ij}\,\mathbf{v}_{ij}\,, \qquad \ldots\ldots\ldots (31)$$

$$\mathbf{q}_{ji} = \mathbf{T}_{ij}\,\mathbf{v}_{ij}\,. \qquad \ldots\ldots\ldots (32)$$

It is not necessary to restrict the definition of stiffness and carry over to the case of a clamped far joint.

Consider a symmetrical shell with both edges symmetrically loaded. If the stiffness is defined by

$$\mathbf{q}_{ij} = \mathbf{K}_{ij}\,\mathbf{v}_{ij} \quad \text{when} \quad \mathbf{v}_{ij} = \mathbf{J}\,\mathbf{v}_{ji}$$

$$\text{and} \quad \mathbf{q}_{ij} = \mathbf{J}\,\mathbf{q}_{ji}$$

then $\mathbf{T}_{ij} = 0$ and, in many cases, only one junction of the shell needs to be considered, as no actions are carried over from one junction to the other. This process is carried out in section 3.3.

The concepts of stiffness and carry over in shell analysis are analogous to those in frame analysis with 4 x 4 matrices to deal with the 4 actions and 4 interrelated displacements rather than numbers dealing with moments and rotations as in most frame analyses.

3.2.3 Slope deflection equations

Figure 3.3 shows actions that can exist on the boundaries of a shell. As the loading is a general loading, stiffness and carry over matrices as defined by equations (31) and (32) have been used. For convenience in drawing, the actions are shown as moments and the displacements as rotations. Slope deflection equations can be set up for each member at any junction.

e.g. the edge i of the shell in figure 3.3.

$$\begin{aligned} \mathbf{q}_{ij} &= \mathbf{q}'_{ij} + \mathbf{q}''_{ij} + \mathbf{q}'''_{ij} \\ &= \mathbf{q}^{\phi}_{ij} + \mathbf{K}_{ij}\mathbf{v}_{ij} + \mathbf{T}_{ji}\mathbf{v}_{ji} . \end{aligned}$$

Consider the structure shown in figure 3.4. Because the displacements of all members meeting at a joint must be identical

$$\mathbf{q}_{11} = \mathbf{q}^{\phi}_{11} + \mathbf{K}_{11}\mathbf{v}_1 ,$$

$$\mathbf{q}_{12} = \mathbf{q}^{\phi}_{12} + \mathbf{K}_{12}\mathbf{v}_1 + \mathbf{T}_{21}\mathbf{v}_2 ,$$

$$\mathbf{q}_{21} = \mathbf{q}^{\phi}_{21} + \mathbf{T}_{12}\mathbf{v}_1 + \mathbf{K}_{21}\mathbf{v}_2 ,$$

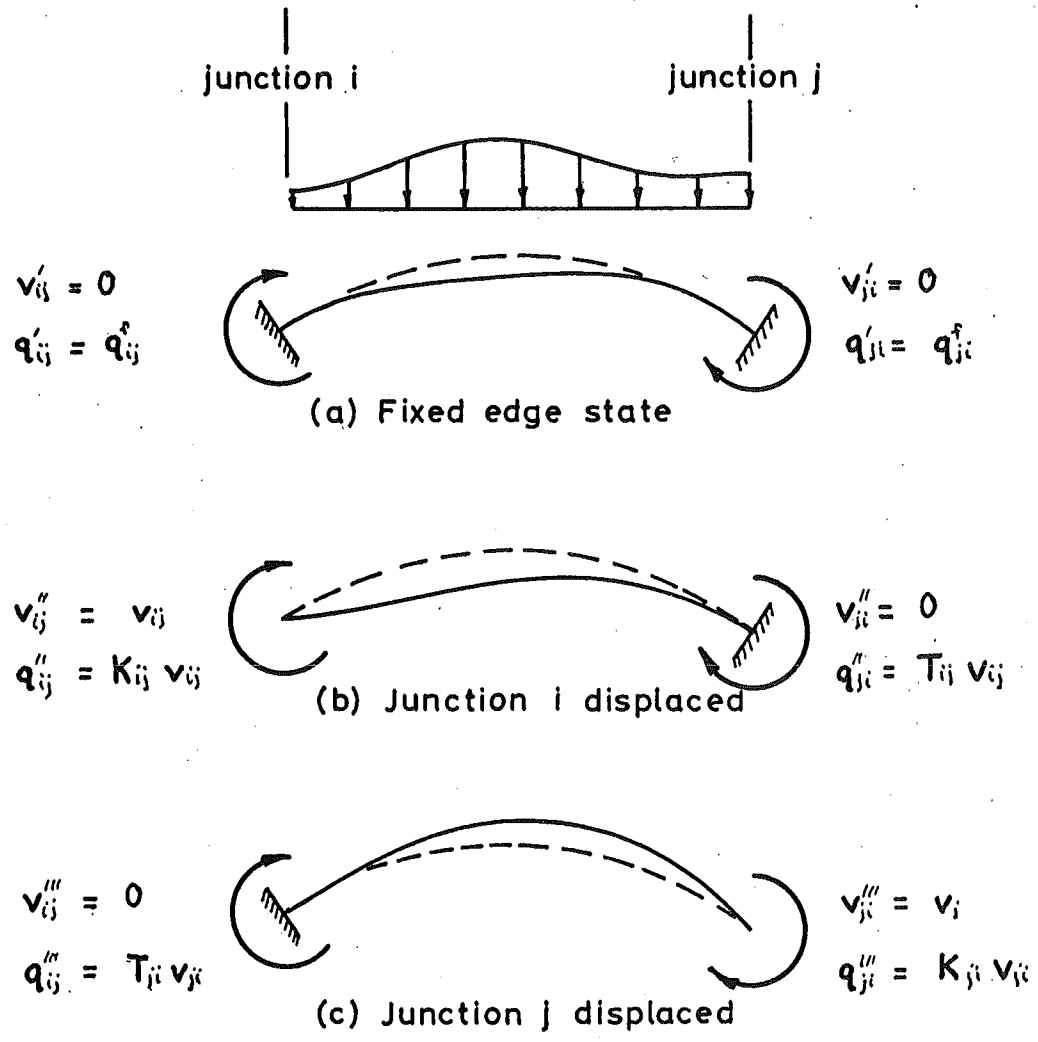

Fig. 3.3 Actions on the edges of a shell

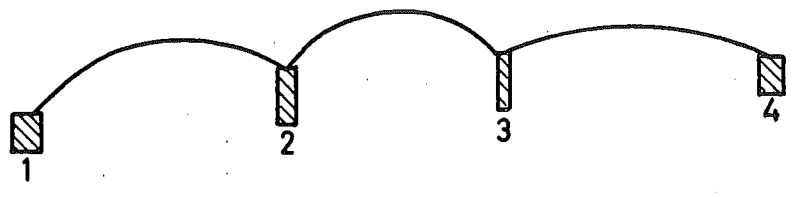

Fig. 3.4 Typical chain type multi-shell structure

$$q_{22} = q^f_{22} + K_{22} v_2 ,$$

$$q_{23} = q^f_{23} + K_{23} v_2 + T_{32} v_3 ,$$

etc. where shells referred to by subscripts 12, 23 etc.,

edge beams referred to by subscripts 11, 33,

q^f_{12} = fixed edge action for shell 12 ,

q^f_{11} = fixing action for edge beam 11 ,

v_1 = displacement of joint 1.

For equilibrium

$$\begin{bmatrix} K_1 & T_{21} & \cdot & \cdot \\ T_{12} & K_2 & T_{32} & \cdot \\ \cdot & T_{23} & K_3 & T_{43} \\ \cdot & \cdot & T_{34} & K_4 \end{bmatrix} \begin{bmatrix} v_1 \\ v_2 \\ v_3 \\ v_4 \end{bmatrix} = - \begin{bmatrix} q^f_1 \\ q^f_2 \\ q^f_3 \\ q^f_4 \end{bmatrix} ,$$

where $K_2 = K_{21} + K_{22} + K_{23}$,

q^f_1 = applied external action at joint 1.

3.3 LINE-LOADS ALONG GENERATORS OF A CYLINDRICAL SHELL

3.3.1 Symmetrical loads applied along symmetrical pairs of generators of a cylindrical shell

The solution is carried out in the two stages diagramatically shown in figure 3.5 and described below:

(1) For each pair of loaded generators the shell is treated as a complete tube with the loaded generators forming the junctions between a pair of shells. If the stiffness is

defined by $q_i = K_i v_i$ when $v_i = J v_j$ there is no carry over from one junction to the other and only one junction of the tube need be considered because $q_j = J q_i$. This step can be repeated for each pair of loaded generators.

(2) The cylindrical tube can now be cut at the shell edges and the ordinary complementary function solution can be used to remove the unwanted edge actions or deflections and to restore the shell edges to equilibrium. Edge-beams could be included in this step or fixing actions could be calculated so that the shell with loaded generators could be included in a multi-shell structure without the necessity of treating each loaded generator as a general shell junction.

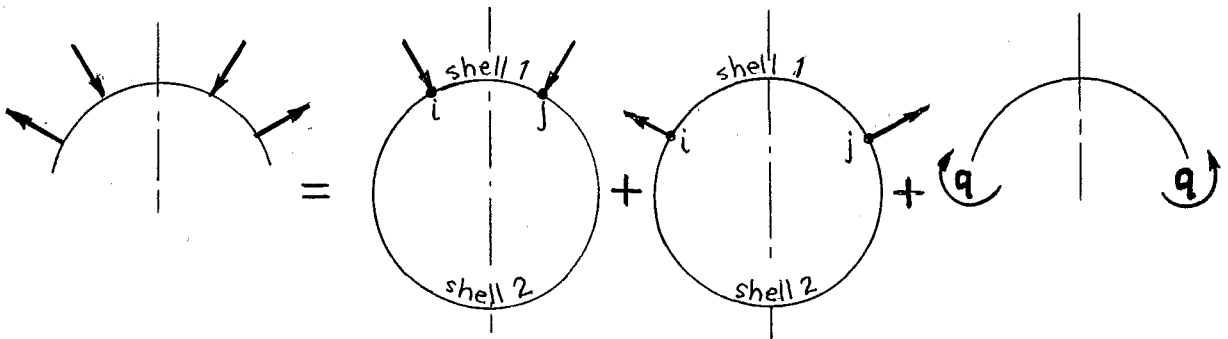

1. pairs of multi-shells with loaded junctions.

2. ordinary C.F. solution to remove unwanted edge actions.

Fig. 3.5 Symmetrically loaded generators - method of solution

Stiffness and carry over for symmetrically loaded shells

For the left hand edge:

$$n_o = K_o^s u_o \qquad \text{with} \qquad u_b = J u_o .$$

From section 2.7.3

$$n_o = A_1 a ,$$

$$u_o = B_1 a .$$

Hence

$$a = B_1^{-1} u_o .$$

$$\therefore \quad K_o^s = A_1 B_1^{-1} .$$

By definition

$$T_{ob}^s = 0 .$$

superscript s : in shell axes,

subscript o : left hand edge,

subscript b : right hand edge,

For the right hand edge

$$n_b = K_b^s u_o \qquad \text{with} \qquad u_o = J u_b .$$

From section 2.7.3

$$n_b = -J A_1 a ,$$

$$u_b = J B_1 a . \quad \text{ie} \quad J u_b = B_1 a .$$

$$\therefore \quad a = B_1^{-1} J u_b .$$

$$\therefore \quad K_b^s = -J A_1 B_1^{-1} J = -J K_o^s J .$$

By definition

$$T_{bo}^s = 0 .$$

As the shell is continuous through the junctions no rotation or translation transformations are necessary to change from shell to junction axes. Only a sign change for actions at the left hand edge is necessary.

$$\therefore \quad K_o = -K_o^s ,$$

$$K_b = K_b^s .$$

$$T_{ob} = T_{bo} = T_{ob}^s \quad T_{bo}^s = 0.$$

Slope deflection equation

Consider junction j of the shell in figure 3.6.

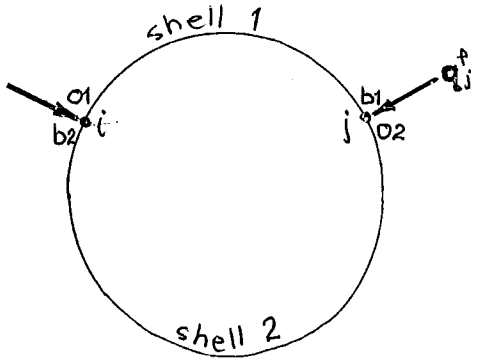

Fig. 3.6 Complete tube

$$q_j^1 = K_{bj}^1 v_j ,$$

$$q_j^2 = K_{oj}^2 v_j .$$

$$\therefore \quad \left[K_{bj}^1 + K_{oj}^2\right] v_j = -q_j^f ,$$

where superscript 1, 2 : of shells 1, 2.

3.3.2 Antisymmetrical loads applied along symmetric pairs of generators

The process of solution is identical with that for symmetrical loads except that different stiffnesses are used.

Stiffness and carry over

For the left hand edge

$$n_o = K_o^s u_o \quad \text{with} \quad u_b = -J u_o .$$

From section 2.7.3 and equations (21), (22) in a manner similar to that for symmetric loads

$$K_o^s = A_2 B_2^{-1} .$$

Similarly for the right hand edge

$$K_b^s = -J A_2 B_2^{-1} J = -J K_o^s J .$$

In junction axes

$$K_o = -K_o^s ,$$

$$K_b = K_b^s ,$$

$$T_{ob} = T_{bo} = T_{ob}^s = T_{bo}^s = 0.$$

CHAPTER FOUR

PRESTRESSING CABLES WITHIN THE CURVED SURFACE

4.1 GENERAL DISCUSSION

Figure 4.1 gives dimensional details of a prestressed cylindrical shell. The notation of these dimensions corresponds with dimensions already given in chapter 2.

The anchorage eccentricity d, the drape f, and y_m, are distances measured around the shell middle surface in the direction of the y axes. φ_k is half the shell opening angle in radians.

Of the loads on the shell from the anchorages, only the longitudinal component need be considered in the theoretical analysis as all other components are directly absorbed by the diaphragms.

From the curvature of a prestressing cable there is, in the direction of the principal normal of the cable, a line-load L_c per unit cable length given by

$$L_c = P\kappa,$$ where P = cable tension at a point,

κ = cable curvature at that point.

In the direction of a cable, from frictional effects, there is a line-load L_f per unit cable length given by

$$L_f = \mu L_c + W,$$

where μ = coefficient of friction,

W = force per unit length to bodily move the cable.

For the purpose of this thesis, W has been assumed insignificant compared with frictional forces dependent on normal pressure, and the following equation has been assumed to apply for friction effects:

$$L_f = \mu L_c .$$

The coefficient of friction can be obtained from the friction loss in prestress force along a cable from

$$\text{Friction loss from A to B} = \int_A^B \mu L_c \, ds,$$

where s = distance along the cable.

Cables with a parabolic profile in the developed shell surface are the only profiles for which general expressions for the curvature, unit tangent, and principal normal have been given in this thesis, although other profiles could be easily considered. The rest of the analysis applies for general cable profiles.

Two different methods are given for expressing these loads on a shell in a suitable form for the solution of the D.K.J. equation. Initially, computer programs were written for the first of these, method A, in which the loads are

treated as surface loads and expanded as double Fourier series. Some of the shell actions did not appear to converge satisfactorily and the use of this method was discontinued.

A computer program written for method B, in which the loads are replaced by actions along a number of generators, quickly gave satisfactory results and therefore was used for all theoretical investigations.

The difference between these methods is in the manner in which the transverse variation of load is considered. The load on a shell from a prestressing cable can be considered as a series of point loads making up a line-load. In method A these point loads are replaced by a loading made up from terms of Fourier series while in method B the point loads are replaced by actions along generators. Experimental results show that the transverse stresses are very dependent on the prestressing cable position. In method B the loads are more precisely defined with respect to the prestressing cable positions than in method A, where the loads are spread out over considerable portions of the shell width by virtue of the poor approximation of point loads by a reasonable number of terms of Fourier series. The computing time for method B was about one half that used for the nonconverged solutions from method A.

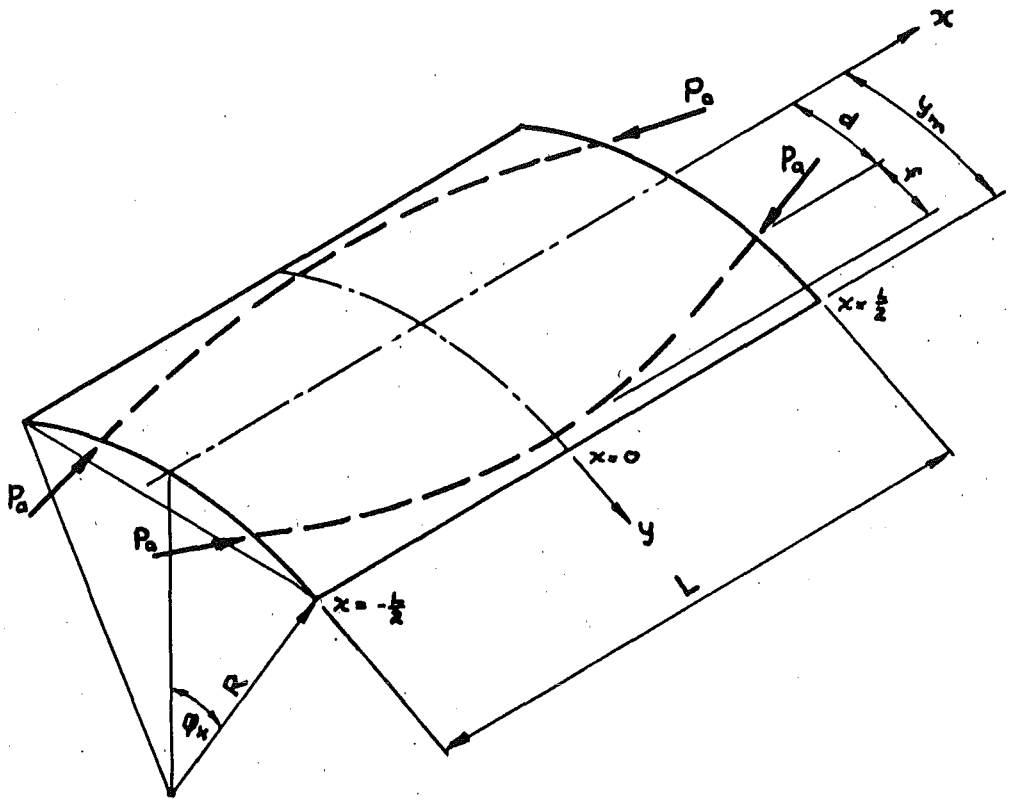

Fig. 4.1 Notation of shell and prestressing details

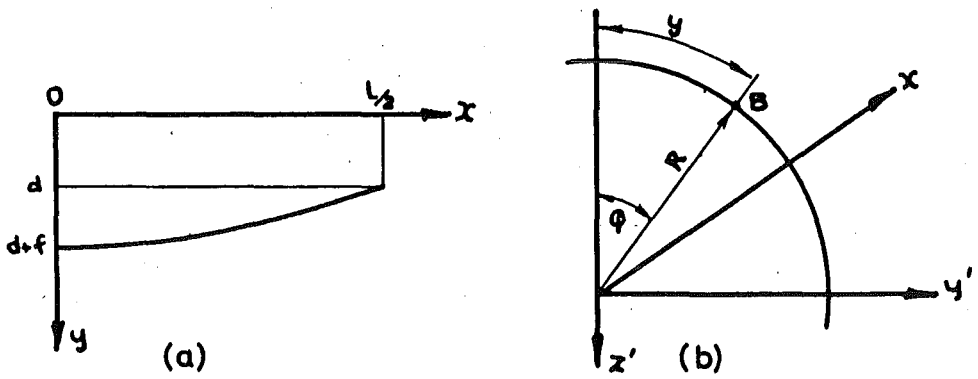

Fig. 4.2 Mathematical expression of a parabola in the developed shell surface

4.2 PROPERTIES OF A PARABOLA IN THE DEVELOPED SHELL SURFACE

Consider the symmetrical parabolic cable as shown in figure 4.2. The parametric equation of the parabola in the xy plane of figure 4.2(a) is

$$x = \frac{t}{2a}, \quad y = b - \frac{t^2}{4a} = \frac{4ab - t^2}{4a}.$$

i.e. $y = b - ax^2$

where $b = d + f$,

$$a = \frac{4f}{L^2}.$$

In figure 4.2(b) the y axes has become the arc of a circle in the $y'z'$ plane of radius R. If B is a point on the cable,

$$\varphi = \frac{y}{R} = \frac{4ab - t^2}{4aR}.$$

y' and z' are rectangular axes through the centre of curvature of the shell.

Hence $z' = -R\cos\varphi$,

$y' = R\sin\varphi$,

and $x = \frac{t}{2a}$.

This is a parametric form of the cable profile and, as such, is in a suitable form for obtaining the curvature, principal normal and the unit tangent[11]. Let the path of the prestressing cable be defined by the position vector $\mathbf{r}$. With respect to the axes x, y', and z',

$$\mathbf{r} = \left(\frac{t}{2a} \;,\; R\sin\varphi \;,\; -R\cos\varphi\right),$$

$$\frac{d\mathbf{r}}{dt} = \frac{1}{2a}\left(1 \;,\; -t\cos\varphi \;,\; -t\sin\varphi\right),$$

$$\frac{d^2\mathbf{r}}{dt^2} = \frac{1}{2a}\left(0 \;,\; -\cos\varphi + c\sin\varphi \;,\; -\sin\varphi - c\cos\varphi\right),$$

where $c = -\frac{t^2}{2aR}$.

And in the axes x, y, and z

$$\frac{d\mathbf{r}}{dt} = \frac{1}{2a}\left(1 \;,\; -t \;,\; 0\right),$$

$$\frac{d^2\mathbf{r}}{dt^2} = \frac{1}{2a}\left(0 \;,\; -1 \;,\; -c\right),$$

$$\frac{ds}{dt} = \frac{1}{2a}\sqrt{1 + t^2},$$

where s = distance along the cable.

Now $\frac{d\mathbf{r}}{dt} = \frac{ds}{dt}\cdot\mathbf{t}$

and $\frac{d\mathbf{r}}{dt} \times \frac{d^2\mathbf{r}}{dt^2} = \kappa\left(\frac{ds}{dt}\right)^3 \mathbf{b}$,

where $\mathbf{t}$ = unit tangent,

$\mathbf{b}$ = unit binormal.

i.e. $\mathbf{b}\times\mathbf{t}$ = unit principal normal.

Therefore

$$\kappa = \frac{2a\left[t^2c^2 + c^2 + 1\right]^{\frac{1}{2}}}{\left[1 + t^2\right]^{\frac{3}{2}}},$$

the principal normal has the direction cosines of

$$\frac{1}{\left[1+t^2\right]^{\frac{1}{2}}\left[t^2c^2 + c^2 + 1\right]^{\frac{1}{2}}}\left(-t \;,\; -1 \;,\; -c\left(t^2 + 1\right)\right),$$

and the unit tangent the direction cosines of

$$\frac{1}{\left[1 + t^2\right]^{\frac{1}{2}}} \left(1, - t , 0 \right).$$

The line-loads are given by

$$L'_c = L_c \frac{ds}{dx} = P \mathcal{K} \sqrt{1 + t^2}$$

and

$$L'_f = L_f \frac{ds}{dx} = (\mu P \mathcal{K} + W) \sqrt{1 + t^2}$$

where L'_f and L'_c are loads per unit length in the x direction.

4.3 FOURIER ANALYSIS

Consider a function $f(x)$ symmetrical about $x = 0$ and antisymmetrical about $x = \pm e$ with period of $4e$ as is shown in figure 4.3.

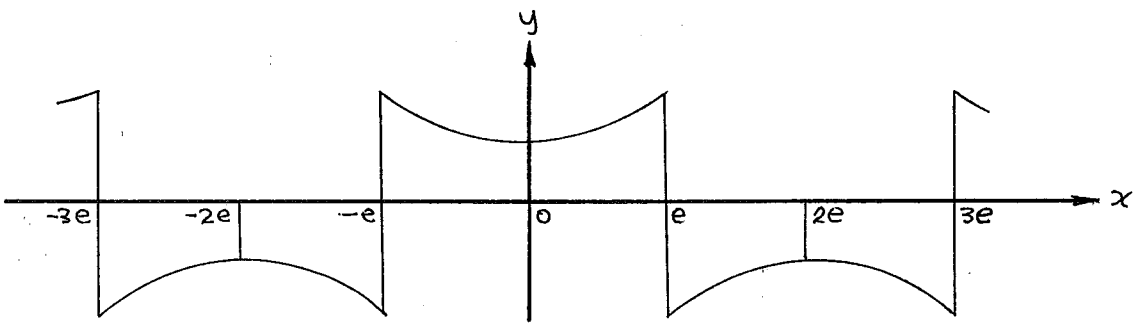

Fig. 4.3 General symmetric load function.

Divide the function into a sufficiently large number of strips of width $\frac{e}{r}$ such that the pulse function, formed by making each strip a rectangle, is a reasonable approximation of $f(x)$.

Consider the i th strip as shown in figure 4.4.

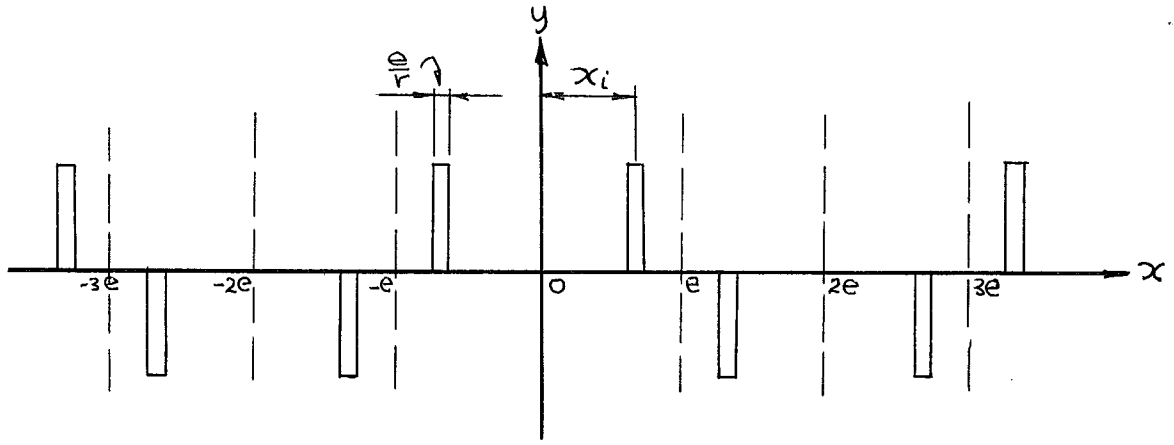

Fig. 4.4 General symmetric pulse function

Let $g_i(x)$ = equation of the i th rectangular strip. By Fourier analysis

$$g_i(x) = f(x_i) \frac{8}{\pi} \sum_n a_{ni} \cos\left[\frac{n\pi}{2e} x\right],$$

where $a_{ni} = \frac{1}{n} \sin\left[\frac{n\pi}{4r}\right] \cos\left[\frac{n\pi}{2e} x_i\right]$,

and $n = 1, 3, 5, \ldots$

From the sum of all the strips

$$f(x) = \sum_{i=1}^{r} g_i(x)$$

$$= \frac{8}{\pi} \sum_n a_n \cos\left[\frac{n\pi}{2e} x\right],$$

where $a_n = \sum_{i=1}^{r} a_{ni} f(x_i)$,

$n = 1, 3, 5, \ldots$

In a similar manner, functions, antisymmetric about $x = 0$ and $x = \pm e$ with a period of $4e$, can be expanded as a sine series.

$$f(x) = \frac{8}{\pi} \sum_{n} a_n \sin\left[\frac{n\pi}{2e} x\right],$$

$$\text{where} \quad a_n = \sum_{i=1}^{r} f(x_i)\, a_{ni},$$

$$n = 1, 3, 5, \ldots.$$

4.4 PRESTRESSING LOADS TREATED AS SURFACE LOADS, METHOD A

The loads from the prestressing cables can be expanded in the form

$$\sum_{n} a_n \begin{Bmatrix} \sin \alpha x \\ \cos \alpha x \end{Bmatrix} \sum_{m} a_m \begin{Bmatrix} \sin \gamma y \\ \cos \gamma y \end{Bmatrix},$$

where n and m are integers,

γ = constant times m,

$\alpha = \frac{n\pi}{L}$,

and treated as surface loads on the shell. Consider the i th section of the cable. Each component of load from this section can be considered as a block load as shown in figure 4.5. Over the i th block

$$\left[X_i, Y_i, Z_i\right] = \frac{r}{y_m} \left[L'_{ci} + L'_{fi} \right],$$

where $\frac{y_m}{r}$ = transverse width of the block.

The double Fourier expansion for such a load, obtained by multiplying the Fourier series for the variation of load in the x direction with that in the y direction is

$$F_i(x,y) = \begin{matrix}\text{Intensity}\\ \text{of block}\\ \text{load}\end{matrix} \cdot \frac{64}{\pi^2} \sum_n a_{ni} \begin{Bmatrix}\sin & \alpha x\\ \cos & \alpha x\end{Bmatrix} \sum_m a_{mi} \begin{Bmatrix}\sin & \gamma y\\ \cos & \gamma y\end{Bmatrix},$$

$$\text{where} \quad a_{ni} = \frac{1}{n} \sin \frac{n\pi}{4r} \begin{Bmatrix}\sin & \alpha x_i\\ \cos & \alpha x_i\end{Bmatrix},$$

$$a_{mi} = \frac{1}{m} \sin \frac{m\pi}{4r} \begin{Bmatrix}\sin & \gamma y_i\\ \cos & \gamma y_i\end{Bmatrix},$$

$$n, m = 1, 3, 5, \ldots.$$

At the r th block there is an additional X surface load from the anchorages of intensity $P/(\frac{L}{2r} \cdot \frac{y_m}{r})$.

The sum of the loads from all the blocks gives

$$F(x,y) = \sum_{i=1}^{r} F_i(x,y).$$

For symmetrical prestressing cables the loads will be of the form

$$X = X_o \sin \alpha x \cos \gamma y,$$

$$Y = Y_o \cos \alpha x \sin \gamma y,$$

$$Z = Z_o \cos \alpha x \cos \gamma y,$$

where X_o, Y_o, Z_o are constants depending on n, m, and the prestressing. The particular integral solution, given in section 2.8, can be used as the first part of the solution of the D.K.J. equation.

When a term of the form $\begin{Bmatrix}\cos\\ \sin\end{Bmatrix}$ appears in any of the above expressions it is implied that sin applies for odd functions and cos for even functions.

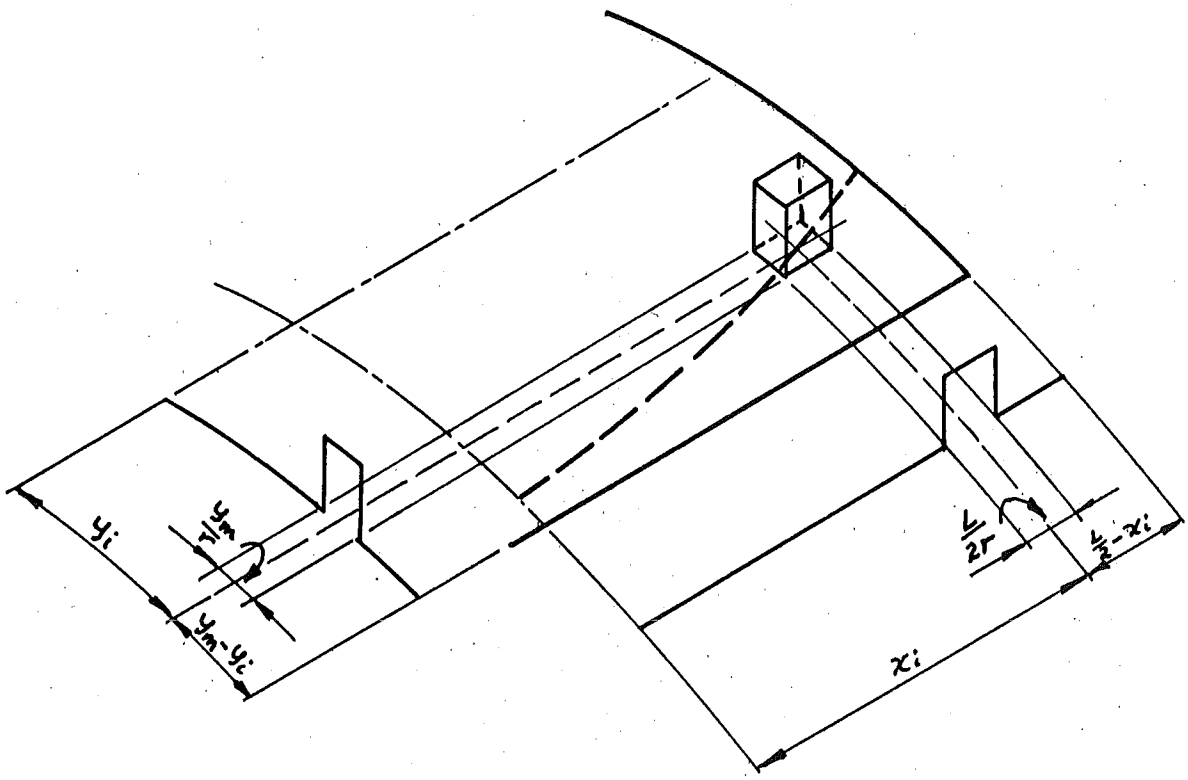

Fig. 4.5 Block surface load from a prestressing cable

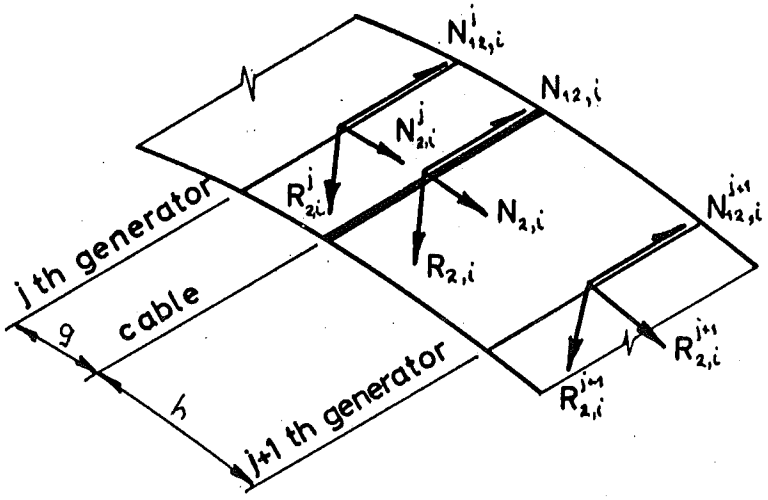

Fig. 4.6 Curvature loads split between generators

4.5 PRESTRESSING LOADS TREATED AS LOADS ALONG GENERATORS - METHOD B.

4.5.1 Mathematical representation

The loads from a prestressing cable can be represented by sets of actions along a finite number of closely spaced generators. The sets of actions can be then treated as loads on the junctions of multi-shells or as line-loads along generators as described in section 3.3.

The shell is divided into transverse strips of width $\frac{L}{2r}$. Throughout each strip the cable position and the line-load intensity can be considered to be constant. Consider the i th strip where the cable lies between the j th and the $j+1$ th generator at distances of g and h from the j th and the $j+1$ th generators as shown in figure 4.6. The line-load from the i th strip can be divided between the two generators such that

$$\left[N^{j}_{12,i},\ N^{j}_{2,i},\ R^{j}_{2,i}\right] = \frac{h}{g+h}\left[L'_{c\,i} + L'_{f\,i}\right],$$

$$\left[N^{j+1}_{12,i},\ N^{j+1}_{2,i},\ R^{j+1}_{2,i}\right] = \frac{g}{g+h}\left[L'_{c\,i} + L'_{f\,i}\right].$$

In figure 4.7,

$$\left[N_{12,i},\ N_{2,i},\ R_{2,i}\right] \equiv \left[L'_{c\,i} + L'_{f\,i}\right],$$

where subscript i : i th strip,

superscript j : j th generator.

The anchorage load is considered to be a shear load spread a short distance into the shell from the anchorages along one or two generators passing through the anchorages and is expanded as a Fourier series along with the loads from cable curvature, using the method outlined in section 4.3.

4.5.2 Physical interpretation

One must remember that the anchorage forces are, in reality, applied to the shell as boundary forces and not as actions spread along generators. These shear actions do not exist and, if they are of appreciable size relative to the actual shear stresses in a shell near the anchorages, the theoretical shear stresses, and possibly other stresses, in the vicinity of the anchorages must be in error. By Saint-Venant's principle[12] the stresses and displacements away from the anchorages will not be affected if the applied shear actions are statically equivalent to the anchorage loads. The stresses in the vicinity of the ~~actions~~ anchorages will be dependent on the anchorage loads and not shell action. They can be calculated from local considerations.

Similar problems do not arise from replacing the line-loads along the cables by actions along generators, because these actions are of a lower order of magnitude than the actions existing from shell action. Consider, as an example, the section of a shell between two loaded generators

(say 1.7" wide, 40" long, and 20" radius - similar dimensions to those used in calculations for the model tests). Provided that the transferred actions at the edges of the section are equivalent to and of the same form as the loads on the section from the prestressing cable, the overall behaviour of the shell will hardly be altered as the stresses, resulting from transferring the loads, will be a small part of the overall stresses that result from supporting the long straight edges of the section of the shell as part of the shell. Small local errors will arise from transferring the loads.

e.g. error in m_2 at cable $\triangleq g R^j_{2,i}$.

Errors in longitudinal actions will be negligible.

Curvature of the shell was neglected when the loads were being divided between the generators. Errors from this source are of the same order as the differences between φ_s and $\sin \varphi_s$ compared with φ_s where $2\varphi_s$ is the angle subtended at the centre of curvature of the shell by two adjacent loaded generators. For the generators at 1.7" spacing and 20" radius these errors are less than 0.2 percent.

The validity of applying the loads from prestressing as line-loads along generators, can best be checked by comparisons of theoretical solutions with other theoretical solutions using the same method and different parameters such as generator spacing, comparisons with results from other methods of solution (section 11.1), and comparisons with experimental results.

C H A P T E R F I V E

SOLUTIONS USING THE GENERATOR LINE-LOAD THEORY

5.1 GENERATOR LINE-LOAD COMPUTER PROGRAM

The computer program, written to solve prestressed cylindrical shells with draped cables within the curved surface, consisted of five separate chapters, with the card output from one chapter being fed directly into the next. The program was named "P.C.S. gen. line-loads" and the five chapters are as follows:

Chapter 1 calculated the curvature, principal normal and unit tangent at a number of points (usually 20 on half the shell length) along each cable. A coefficient of friction was assumed (initially calculated for a circular cable profile) and a numerical integration process was used to determine friction losses along the cables from mid-span to the diaphragms. If the friction losses so obtained did not agree with the given friction loss, a new estimate of the coefficient of friction was made and the numerical integration process was repeated. Thus, the distribution of prestressing forces and hence the line-loads along the cables could be calculated. The line-loads were then transferred to the generators and Fourier coefficients of their distributions were calculated and then punched.

Chapter 2 used the complementary function solution given in section 2.7 and the generator line-load theory given in section 3.3 to obtain the arbitrary constants necessary to describe the actions and displacements originating from all the loaded generators and the shell edges.

Chapter 3 calculated the column vectors $\mathbf{n}$ and $\mathbf{u}$ at a number of points on the shell cross section (usually 7 on half the cross section). This chapter took about two-thirds of the total computing time.

Chapter 4 calculated the required actions and displacements at a grid of points spread over one quarter of the shell surface. From $\mathbf{n}$ and $\mathbf{u}$ all the shell actions and displacements can be obtained as is shown in section 2.6, equations (10).

Chapter 5 added multiples of the solutions given by chapter 4, for the same shell with different prestressing cable lay-outs, to obtain the effects of superposition of different prestressing systems or to obtain curvature and anchorage effects separately.

Block diagrams for chapters 1 - 4 are given in figures 5.1 to 5.4 and in appendix IV listings of all the chapters are given.

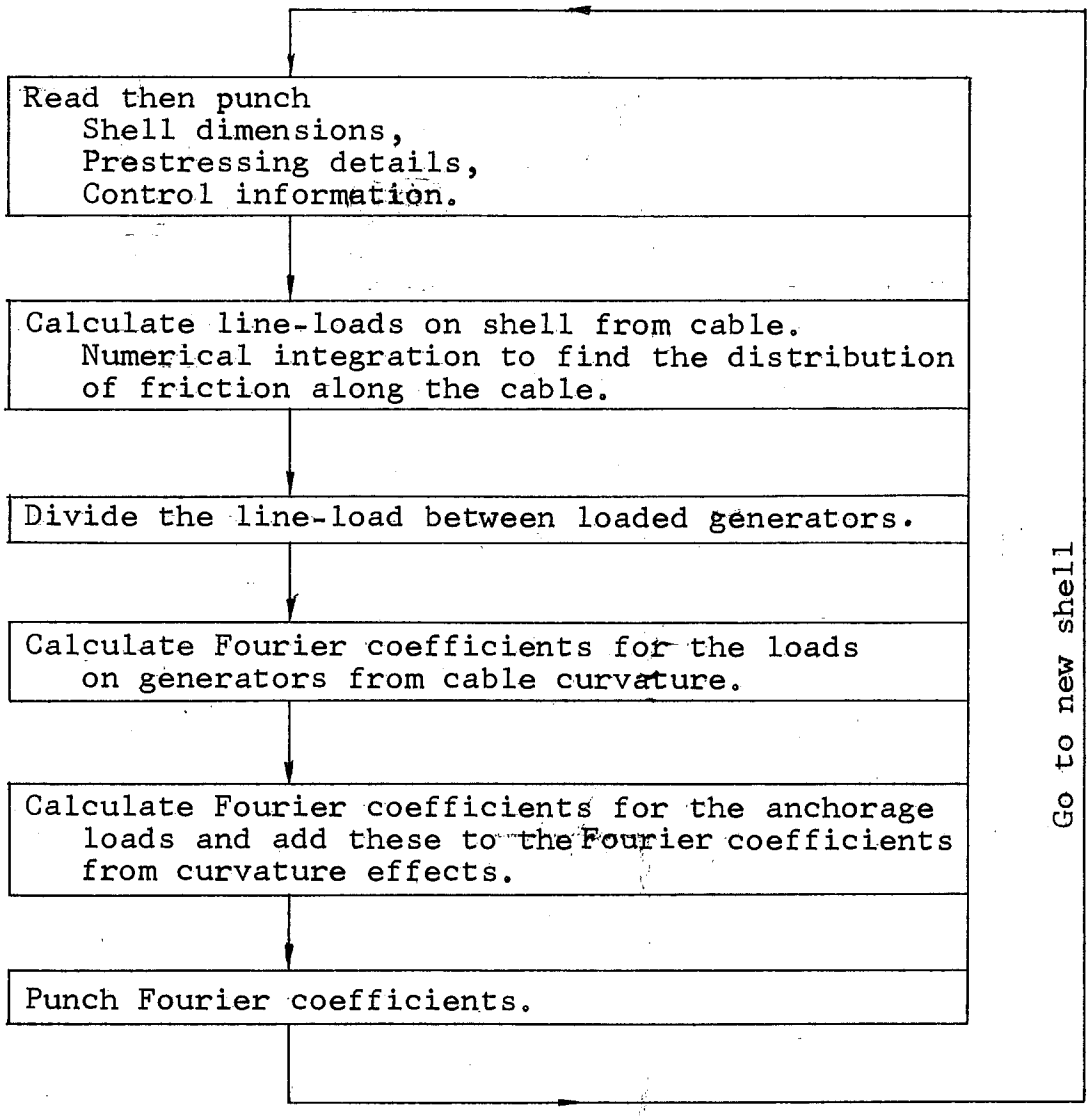

Fig. 5.1 Block diagram for Chapter 1 of the computer program

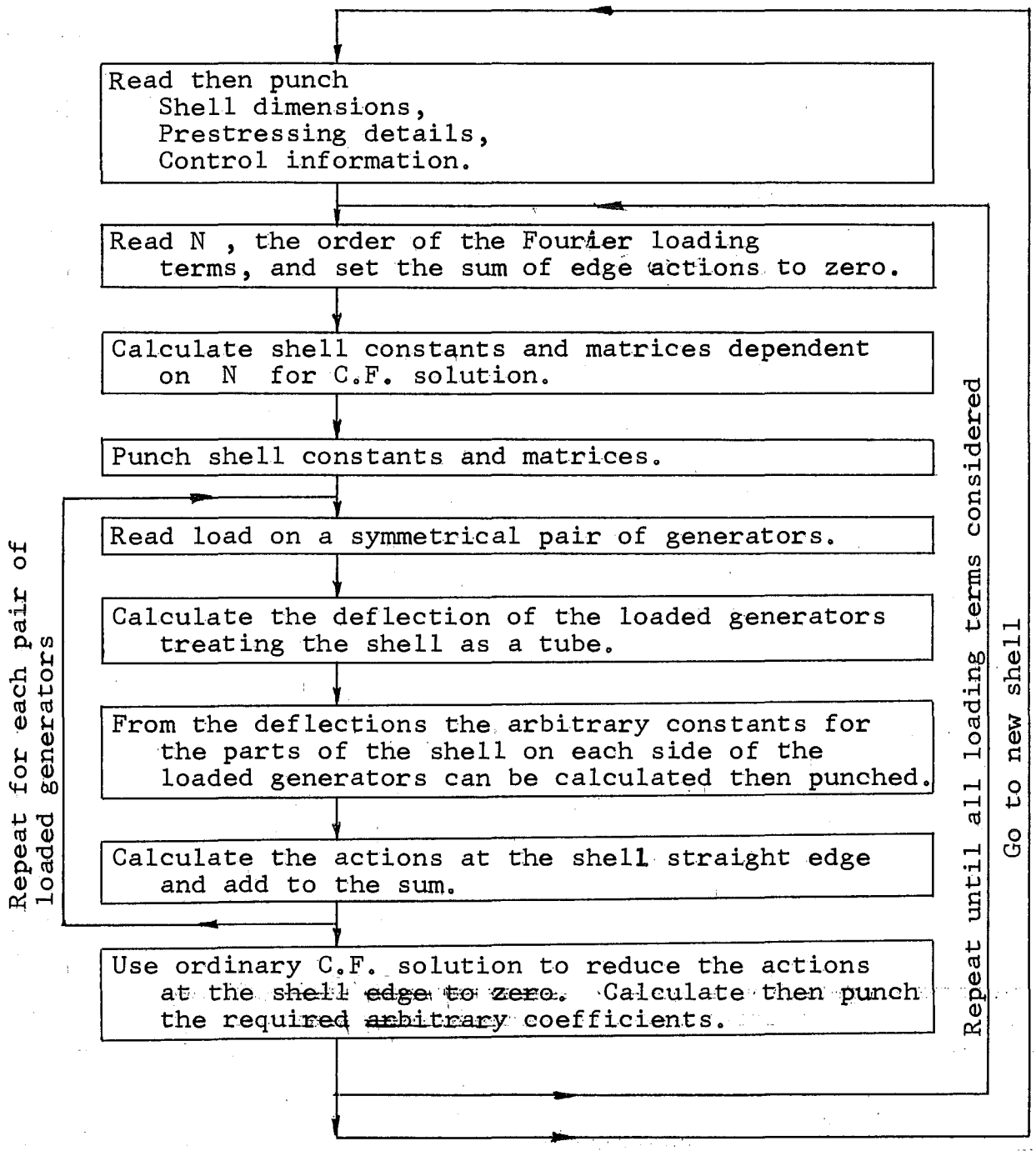

Fig. 5.2 Block diagram for Chapter 2

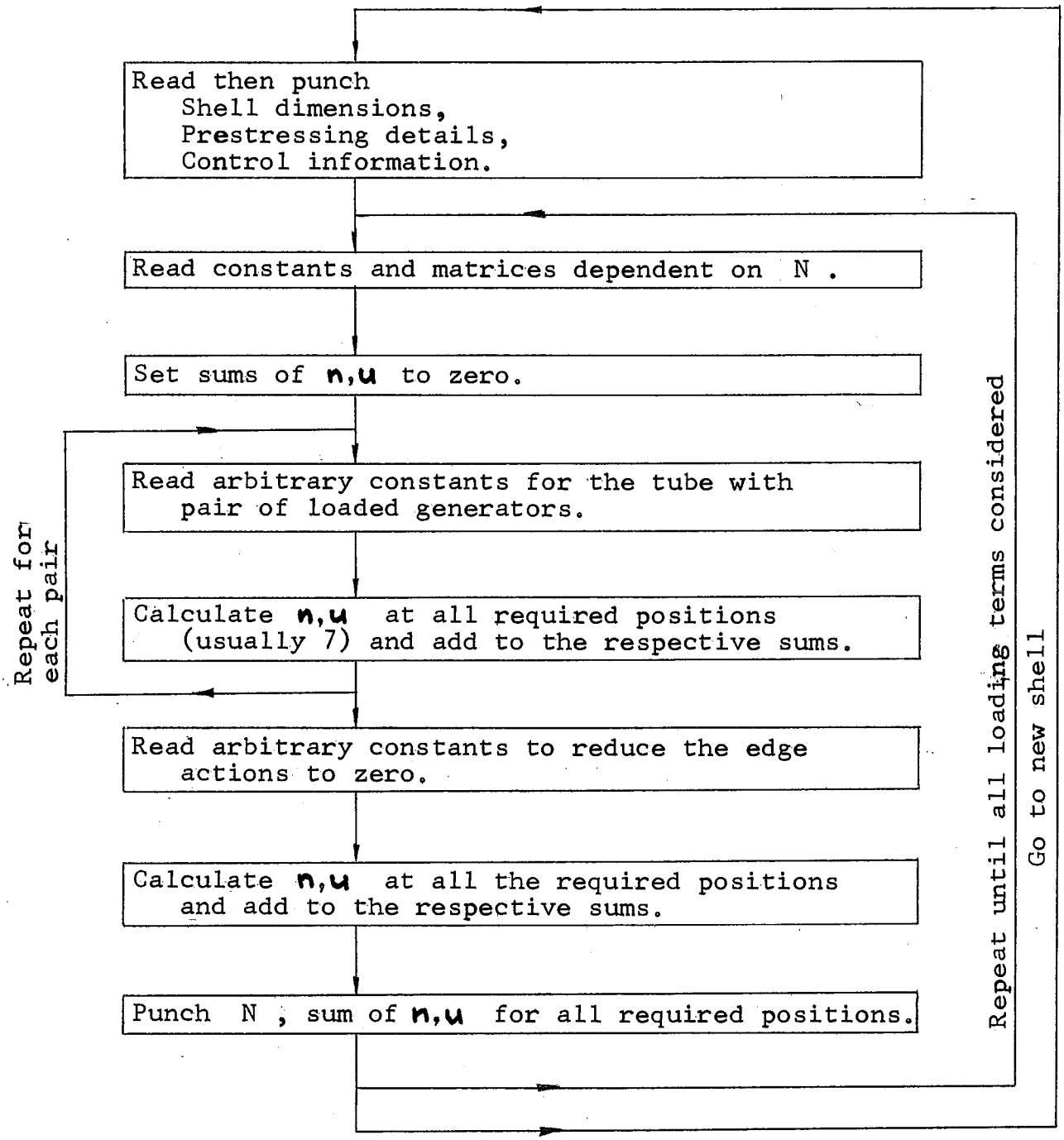

Fig. 5.3 Block diagram for Chapter 3

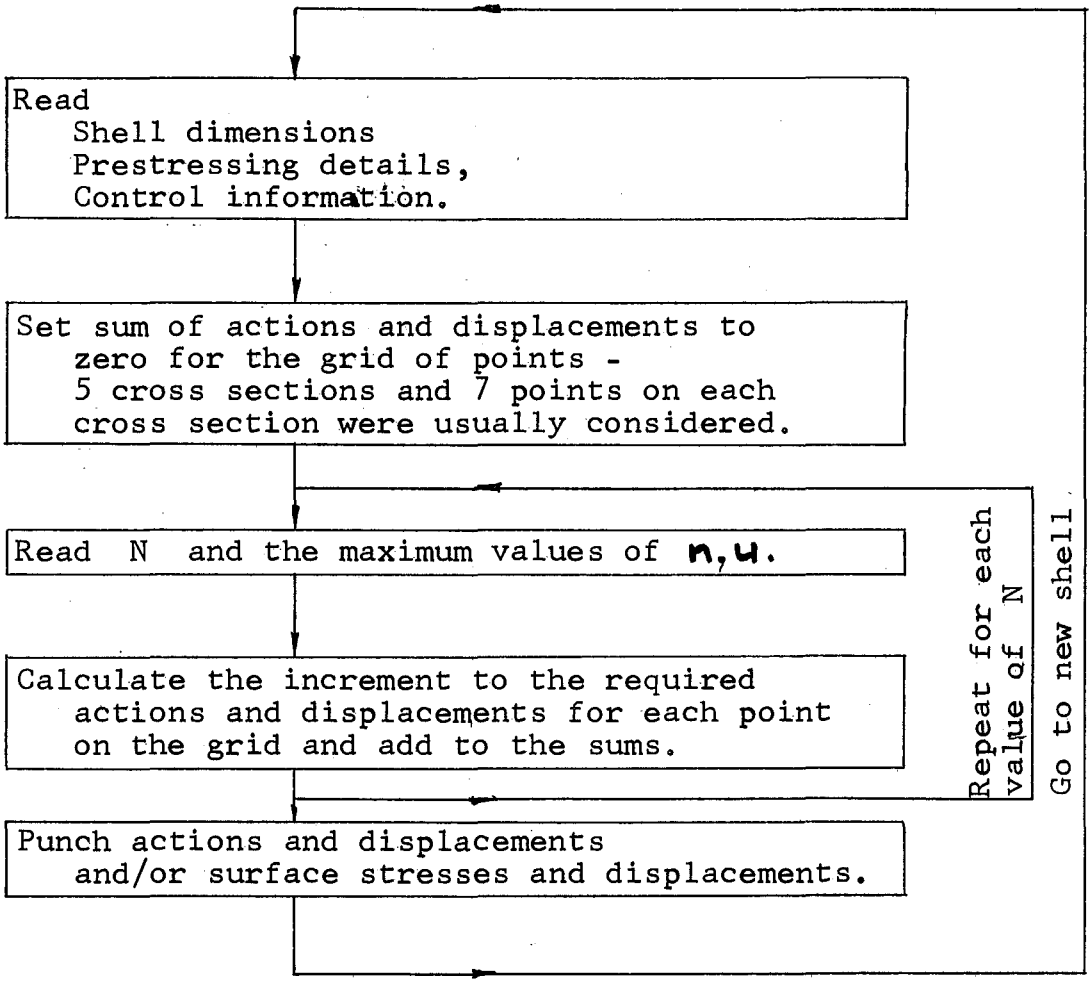

Fig. 5.4 Block diagram for Chapter 4

5.2 NUMERICAL DETAILS OF SOLUTIONS

5.2.1 General discussion

While the generator line-load computer program was being written provision was made so that the various parameters, describing the replacement of loads from prestressing cables by loads made up from a finite number of terms of Fourier series expansions of actions along a finite number of generators, could be varied. These parameters were then chosen so that a sufficiently accurate solution could be obtained from as little arithmetic as possible.

In the following discussion, the anchorage and the curvature loads are treated separately because they are of completely different natures. They are therefore, handled most satisfactorily by different combinations of the various parameters. Some of the points that are raised in this discussion are fairly trivial while others can bring considerable improvements to accuracy with a reduction in the amount of arithmetic manipulation.

5.2.2 Anchorage loads

A study of the convergence of Fourier series expansions of rectangular pulse functions soon shows by the expansion of the anchorage loads, as block shear loads spread a distance 0.05 L down the shell, rather than their expansion as point shear loads, leads to a quicker solution. The Fourier expansion for a

rectangular pulse converges more slowly as the period over which the pulse is spread decreases.

However, the shear loads are supposed to be applied at the anchorages and they should not be spread too far down the shell.

In figure 5.6 the sums of the first 10 terms (n = 1,19) of Fourier expansions of the same anchorage load as block shear loads spread down the shell distances of 0.05 L and 0.0125 L are shown, with the series for 0.05 L clearly converging most rapidly. In figure 5.8 the longitudinal stresses obtained from using the first 10 terms of these series are compared with experimental results from one of the model tests. The solution for the shear load spread over 0.05 L , shows no sign of the disturbances along the line of the prestressing cables that are evident in the solutions for the shear load spread over 0.0125 L .

Chapter 2 of the computer program listed the vector **n** for the actions at the shell edges before the complementary function solution was applied to reduce the edge actions to zero. This gave an indication of the contribution to the total solution of each term of the Fourier series loading. Table 5.1 gives a typical listing of these actions. At the tenth term (n = 19) the contribution to the total solution from each term has become insignificant compared with the sum of the first 3 or 4 terms.

		n			
Term	n	n_{12} lb./in.	n_2 lb./in.	r_2 lb./in.	m_2 lb.
1	1	-40.38	-4.20	.53	-1.98
2	3	21.62	.15	- .575	.33
3	5	-11.53	2.19	.43	.05
4	7	5.31	-3.34	.27	- .04
5	9	- 1.72	3.70	.16	.06
6	11	- .06	-3.42	- .07	- .05
7	13	.73	2.74	.03	.04
8	15	- .75	-1.84	- .00	- .02
9	17	.48	.98	0.00	0.00
10	19	- .15	- .27	0.00	0.00

Table 5.1 Contributions to the total solution from each Fourier term - P_a = 1200 lb., $d = 0.833y_m$, f = 0, shear load over 0.05 L

In fact, the sum of the first 5 terms (n = 1,9) gave a reasonably satisfactory solution over much of the shell surface. But, along the line of the anchorages, there were appreciable local variations in longitudinal stresses caused by the small oscillating loads that are the sum of the first 5 terms. The solution from the sum of the first 10 terms did not show these local

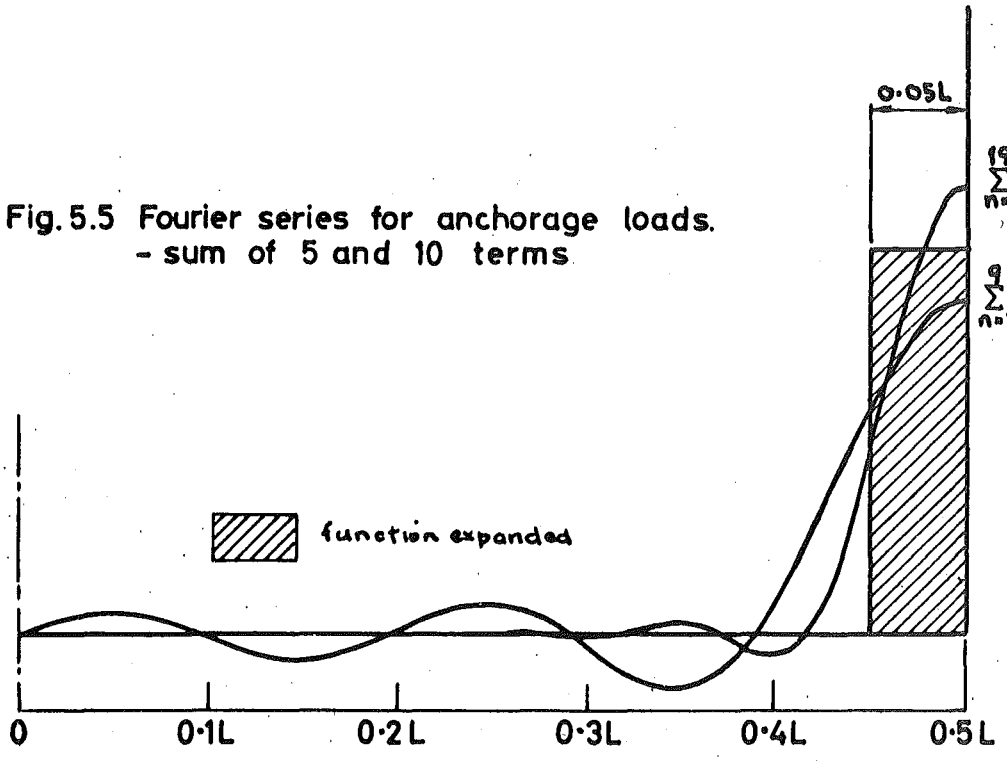

Fig. 5.5 Fourier series for anchorage loads. - sum of 5 and 10 terms

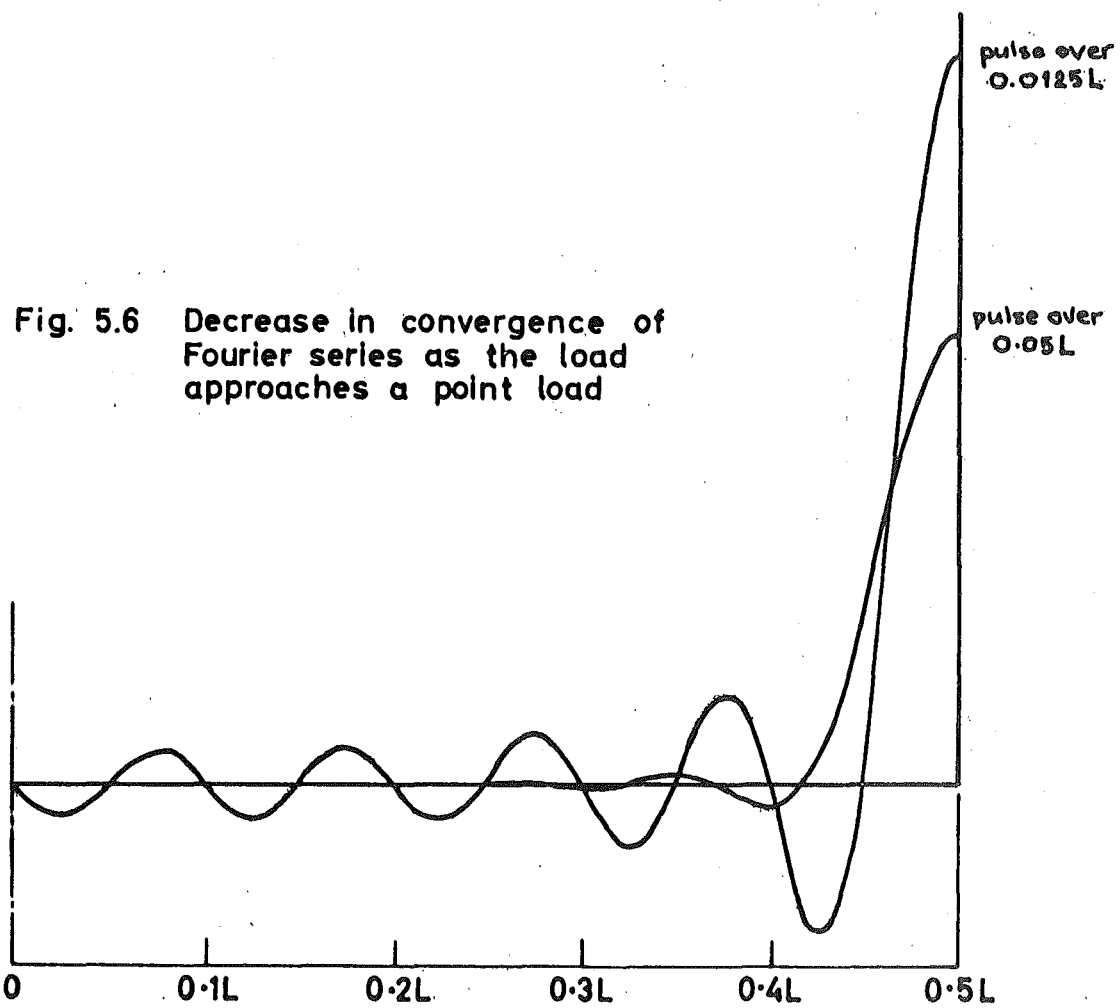

Fig. 5.6 Decrease in convergence of Fourier series as the load approaches a point load

disturbances, as can be easily understood from figure 5.5 where the sums of the first 5 and 10 terms of the Fourier expansion of a block shear load spreading 0.05 L down the shell are shown.

When the anchorage loads were spread down two closely spaced generators there appeared to be an improvement in theoretical stresses as can be seen from figures 5.7 and 5.8. This is probably due to a lowering of the intensity of the shear loading by spreading it between two generators.

Thus, the sums of the first 10 terms (n = 1,19) of Fourier expansions of block shear loads spread a distance 0.05 L down two closely spaced generators were found to give satisfactory solutions for the anchorage loads with a minimum of arithmetic manipulation and, therefore, were used for all the results given in this thesis.

5.2.3 Loads on the shell from cable curvature

For the loading on the shell from curvature effects (normal pressure and friction) the first 6 terms of the Fourier series expansions of the actions along the generators produced a solution of similar accuracy to that of 10 terms for anchorage loads. When the curvature loads are replaced by actions along generators, the actions are of a lower order of magnitude than those from anchorage loads. As the curvature effects are spread along considerable lengths of the shell the Fourier expansions

of these loads converge more rapidly than those for the anchorage loads.

In section 4.5 the shell was divided into r transverse strips between mid-span and the diaphragms. Through each of these strips the line-load on the shell from cable curvature was considered to be constant. From each of these strips the line-load was transferred to adjacent generators. This r was also the r used in finding the Fourier expansion of the actions along the generators (analysis as in section 4.3). For all the curvature effects a value of r equals 20 (the maximum value allowed by storage requirements of chapter 1 of the computer program) was used although identical solutions were obtained for r equals 15. This process becomes more accurate in both the transferring of the actions and in the Fourier analysis as the value of r increases.

The generator spacing is another parameter that could be varied. Figure 5.9 shows the mid-span transverse moments, the action most affected by transferring the line-loads along the cables to the generators, for various generator spacings for the theoretical analysis of model set-up 8 (see section 8.1). Although there is little difference between the actions with the generator spacing at 1.65" and 2.475" a spacing of about 1.7" or its equivalent for shells of other dimensions was used.

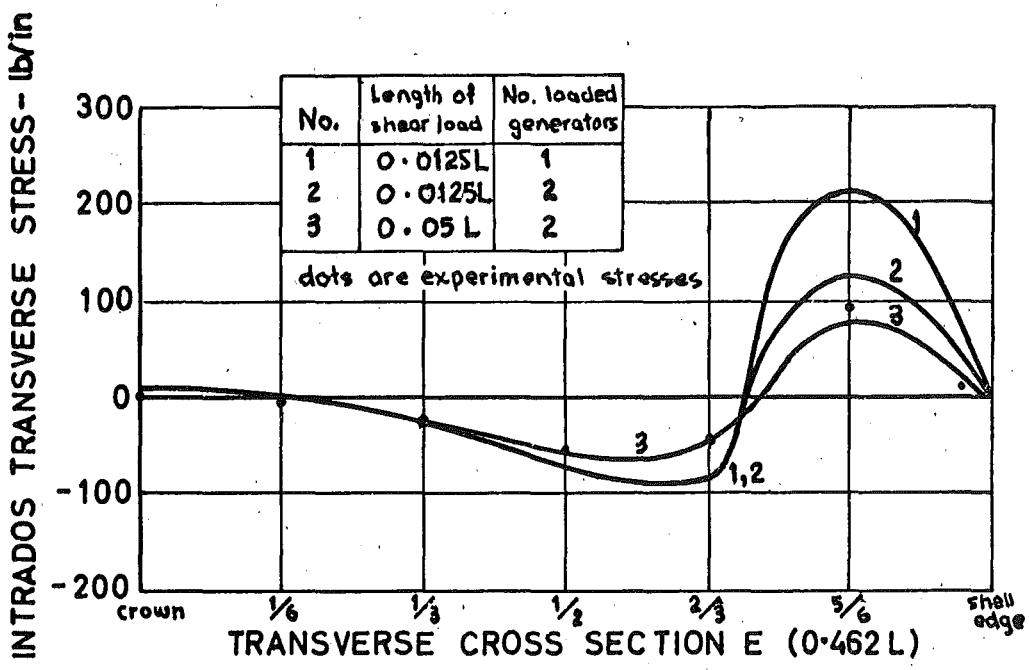

Fig. 5.7 Intrados transvese stress at $x = 0.462\ L$ for 10 terms of different Fourier series expansions of the loads - $R = 19{\cdot}94''$, $L = 39{\cdot}12''$, $t = 0{\cdot}1309''$, $\varphi_k = 0{\cdot}526$ rad, $P_a = 1200$ lb, $d = 0{\cdot}833\ y_m$, $f = 0$

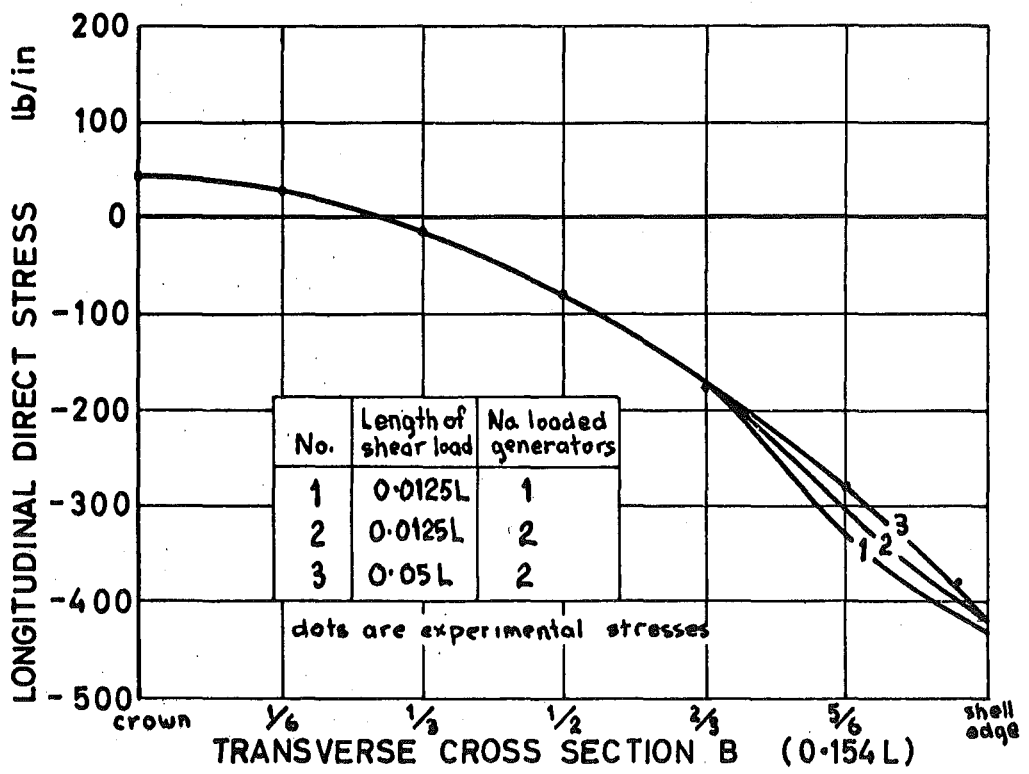

Fig. 5.8 Disturbance to longitudinal stresses from non-converged Fourier series loading - example as in fig. 5.7

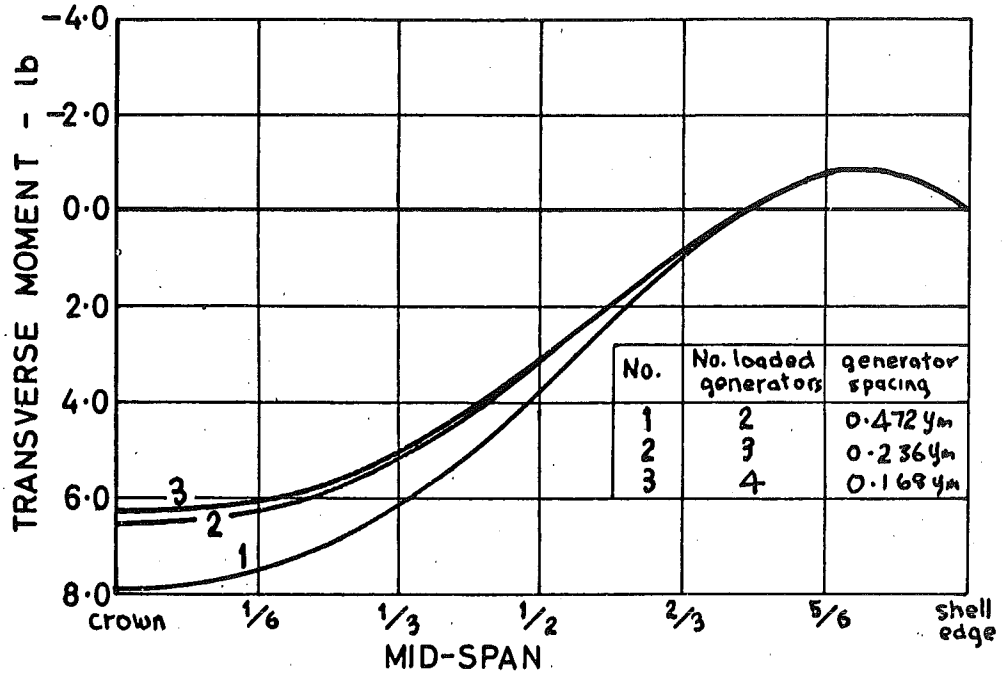

Fig. 5.9 Mid-span transverse moments from cable curvature showing the effect of generator spacing - $R = 19{\cdot}94''$, $L = 39{\cdot}12''$, $t = 0{\cdot}1309''$, $P_n = 1200$ lb, $d = 0{\cdot}500 y_m$, $f = 0{\cdot}472 y_m$, $\varphi_k = 0{\cdot}526$ rad

CHAPTER SIX

MODEL SHELL

6.1 MODEL MATERIALS

6.1.1 General discussion

Before the choice of a model material can be made, the aim of an experimental investigation must be fully understood. If, as in this case, the model test is to check the validities of mathematical theories that assume elastic, isotropic, and homogeneous materials, then the model should, in the first instance, be made from a material closely meeting these requirements. If the behaviour of a prototype structure before and after cracking or the mode of failure is required, the model must be made from a material such as micro-concrete that exhibits the same properties as reinforced or prestressed concrete (Rowe[13], Haas and Bouma[14]).

Investigators have found that the problems in making and testing micro-concrete shell models are considerable. Satisfactory strain readings have seldom been obtained (Scrivener[15]) because of the uncertainty of Young's modulus and Poisson's ratio[16] and cracking within or just outside gauge lengths.

Accurate stresses can be readily obtained from the strains recorded from an elastic model. Provided that the

stresses in a model are kept within the elastic limit of the model material, tests can be repeated as many times as is necessary and different loading systems can be used on any one model.

As prestressing tends to eliminate high tensile stresses it should be noted that prestressed concrete, under normal working loads, behaves closer to an elastic material than does reinforced concrete.

Plastics, such as "Perspex" have been commonly used in shell models (Powell[9], de Sitter[6], Arcan and Nicolau[17], Hergenröder and Rüsch[18]) as so called "elastic" materials because of their low Young's moduli and ease of moulding into shapes of double curvature. But they suffer from the drawbacks: of creeping under load; of elastic constants varying with temperature; and the difficulty of accurate strain measurement, because of the stiffening effect of electric resistance strain gauges on thin models and the warm up drifts that occur as a result of the low heat sink properties and high coefficients of expansion.

If a model can be constructed from a metal and high enough loads applied to produce reasonable strains and deflections (Young's modulus of aluminium is about 20 times that of most plastics), a metal model will usually give more accurate results because of the stable elastic properties with

no appreciable creep or temperature effects. Accurate strain measurements can easily be made because of the availability of temperature compensated strain gauges and the high heat sink properties of metals. Thickness tolerances on metal sheets are much better than those on plastics.

High strength aluminium alloy was chosen as the most suitable of available metals because of its low Young's modulus (about one-third that of steel).

6.1.2 Properties of H30-WP aluminium alloy as used on the model shell

	Typical specifications (reference 19)	From tests as in appendix II
Type-British Standard designation	H30-WP	
Thickness	10 S.W.G.	0.1309 in.
0.1% proof stress	18.5 tons/in.^{2}	
Ultimate tensile strength	22 tons/in.^{2}	
Bearing yield stress	22 tons/in.^{2}	
Young's modulus	10 x 10^6 lb./in.^{2}	10.23 x 10^6 lb./in.^{2}
Poisson's ratio	0.3	0.307
B.H.N.	95	

Table 6.1 Properties of the aluminium alloy used in the shell model

The model shell was constructed from aluminium alloy of the specifications and properties as given in table 6.1. In appendix II, the tests, from which the elastic constants were accurately obtained, are described.

6.2 MODEL DIMENSIONS

A shell of intermediate length, L/R = 2, for which approximate methods of solution such as the beam theory of Lundgren[3] would give doubtful solutions because transverse stresses would be a significant part of the shell behaviour, was chosen as being of suitable proportions for the model shell. Table 6.2 and figure 6.1 give the model dimensions.

When scaled up to a thickness of 3" these dimensions give a shell of some 80 foot span.

Radius - R	of shell middle surface	19.94"
Width	of shell middle surface	19.97"
Span - L	centre line diaphragm to centre line diaphragm	39.12"
Thickness - t		0.1309"
½ opening angle - φ_k		0.526 rad.

Table 6.2 Model shell dimensions

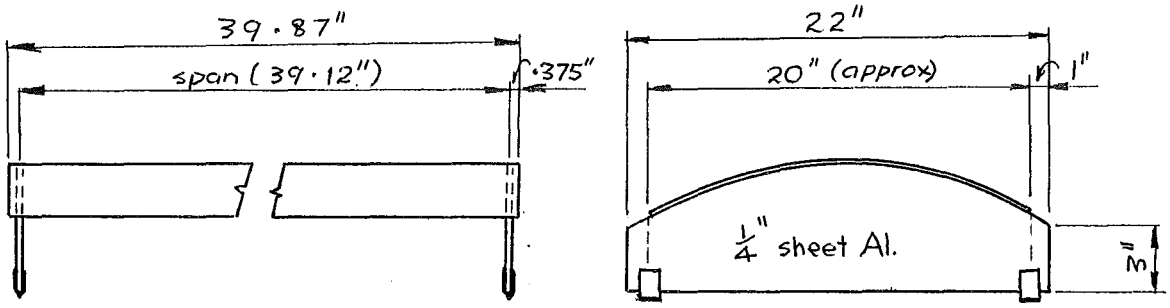

Fig. 6.1 Model shell dimensions

6.3 MANUFACTURE OF THE MODEL

6.3.1 Shaping of the shell surface

The curved surface of the shell was formed by rolling a 40" x 27" sheet of aluminium alloy in sheet metal rollers until all the generators were straight and, to within 2½" of the straight edges, the radius was constant. 3" wide strips were then cut off each side of the shell with a band saw. As the strips were being cut off, the straight edges of the shell bowed up about ⅛". Two 7 lb. weights, hung near mid-span along each straight edge, were found to remove this unwanted bowing and to restore the shell to a constant radius with straight generators all over the surface.

Although the difference in strains and deflections between the preliminary tests in which weights were left hanging

on the shell edges and those with no weights hanging on the shell edges were small, the weights were left hanging on the shell edges during all other tests.

6.3.2 Gluing of structural joints

All structural joints on the model shell were made with Araldite 106, a gap filling, room temperature curing, epoxy resin. As suggested by the manufacturer[20], the adhesive was mixed in the proportions of 100 parts by weight of adhesive to 80 parts by weight of hardener 953U.

To improve the bond strength and decrease the setting time the resin was cured in an oven at 40^{o} C or under infra red lamps. All surfaces were roughened with fine emery paper and carefully degreased with strain gauge cleaning fluid before gluing.

6.3.3 Shell supports

1" long hardened steel knife edges were glued to thickened sections of the diaphragms directly under each corner of the shell. At one end of the model the two knife edges rested on rollers (figure 6.2) and at the other end they rested on steel blocks (figure 6.3).

Symmetric longitudinal movement, the only theoretical displacement of the diaphragms for symmetrical prestressing, could occur without any restraint. A system of supports, allowing universal movement, such as Kelly[21], Scrivener[15], or

Powell[9] used was thought to be unnecessary. As the only load on the knife edges was the self weight of the shell, the normal pressure of the knife edges was very low and the shell could easily be bodily moved across the supports. This would have allowed any type of movement to take place with little restraint.

6.3.4 Testing table

As no suitable test bed was available a table with a top of stiffened ¼" mild steel plate was constructed. To enable the bolting down of supports and attachments a grid of ¼" B.S.W. tapped holes at 1" centres was supplied. The table top rested on adjustable "Dexion" legs.

The roller blocks and steel pads of the shell supports were glued to the tops of 6" high columns that were carefully shimmed and bolted to the testing table with their tops true and level. The columns were made from 1½" diameter steam pipe with ¼" steel flanges welded to each end. With the shell sitting on the columns, the shell curved surface was far enough from the testing table to allow easy access to the intrados of the shell during testing.

6.4 PRESTRESSING SYSTEM

6.4.1 Introduction

The aim of this model study was to investigate the effects of prestressing on a cylindrical shell. Considerable

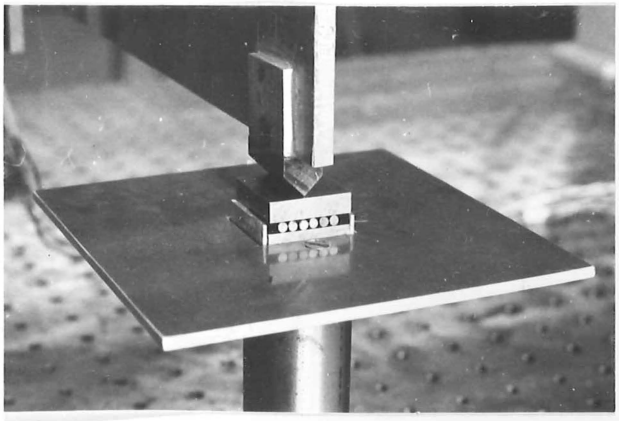

Fig. 6.2 Roller support of the model shell

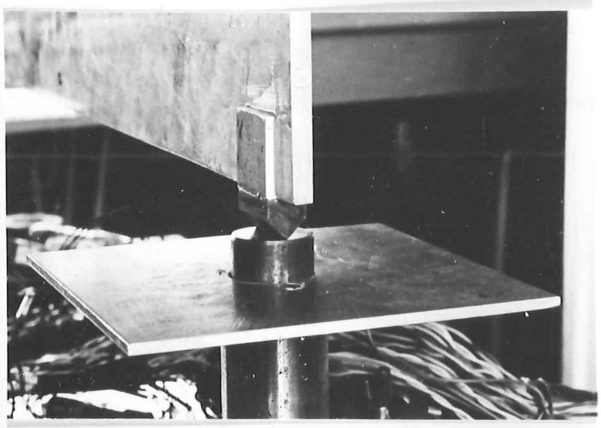

Fig. 6.3 Hinge support of the model shell

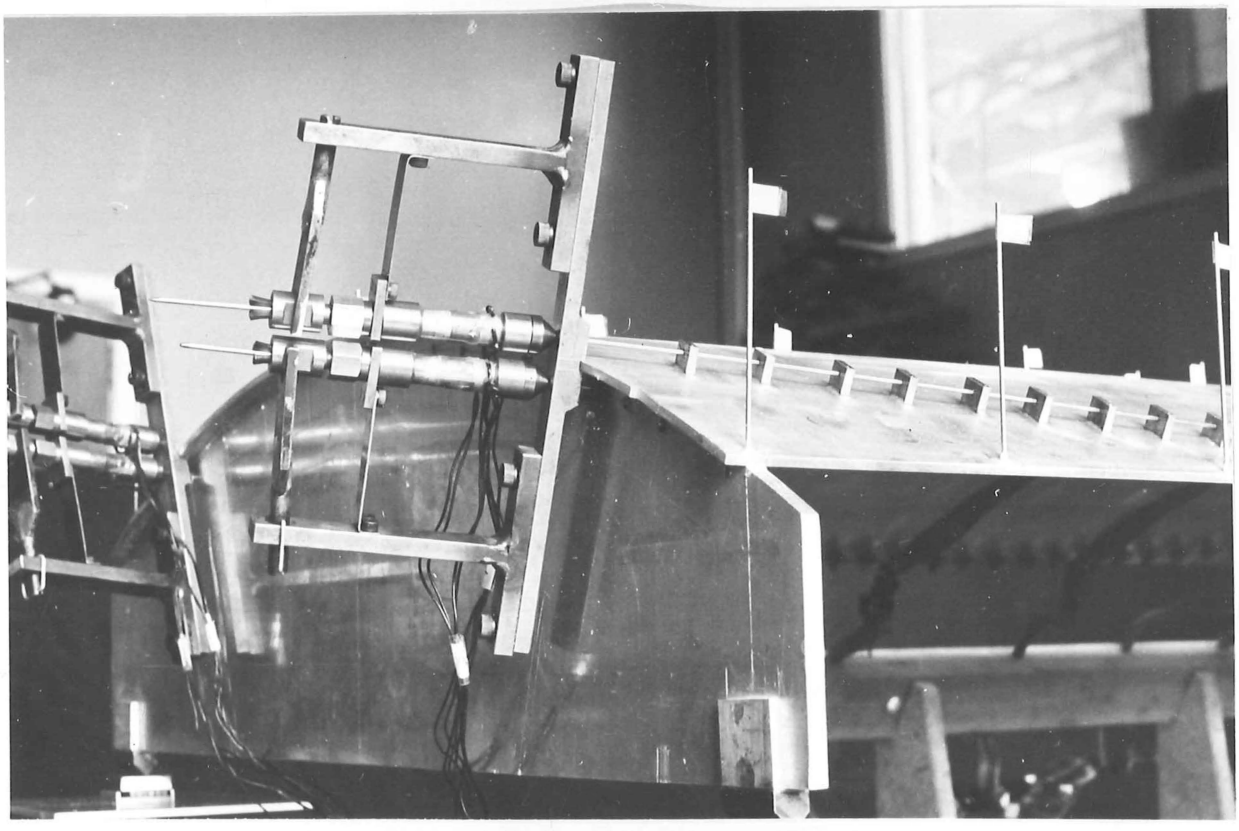

Fig. 6.4 The prestressing system

time, therefore, was spent on the development of a suitable system for the accurate application and measurement of varying prestressing forces of up to 1600 lb. per cable position (800 lb. per wire for a two wire system having a wire at the intrados and one at the extrados of the shell). The prestressing system also had to be suitable for use throughout a series of repeated tests on the same model shell with different prestressing cable positions and profiles.

In the Proceedings of the Symposium on Shell Research, Delft, 1961, there are described several different systems (Hergenröder and Rüsch[18], Arcan and Nicolau[17], Franz and Teepe[22], and Röntsch[23]) which have been used for prestressing plastic and gypsum models. The forces that these prestressing systems apply are not high enough for metal models. The interesting demountable force measuring device, as used by Bouma and van Koten[24,25] on a prestressed micro-concrete model tested in a series of model shells, was considered to be unsuitable for use on an elastic model with wires on the intrados and on the extrados of the shell.

The system developed, consisting of 0.064" diameter piano wires passing through steel guides glued to the shell surface, screw jacks to tension the wires, and load cells to measure the forces, is shown in figure 6.4.

6.4.2 Prestressing wires

0.064" diameter silver plated piano wire was chosen for prestressing wires, because its high ultimate strength of 1100 lb. would give a safe working load of 800 lb., and its smooth surface finish would give minimum friction losses.

As purchased, the wire was tightly coiled into a 5" diameter spool. It was straightened by pulling it slowly through a wire straightener made from a bent piece of ½" water pipe spinning in a lathe at 750 R.P.M. (see figure 6.5).

Twisted wire cables were also considered but rejected because: they stretched when loaded; it was difficult to grip the ends symmetrically and securely; and it was felt that they would give high friction losses as a result of the cables deforming when they passed through guides.

6.4.3 Prestressing jacks

The simple screw thread and nut arrangement shown in figures 6.6 and 6.8 was used to tension the wires. The thread of 40 threads per inch was chosen because it gave a low mechanical advantage. After the first few tests, Glacier DU (polytetrafluoroethylene impregnated bronze with a steel backing) thrust washers were added between the prestressing nuts and the load cells. The setting of prestressing forces was now much easier because "sticking" was eliminated and torsional effects were no longer picked up in the load cells.

The prestressing wires were anchored in the prestressing jacks by wedges made from grinding down 0.125" P.C.S. sleeves as is illustrated in figure 6.7. Many different solders were also tried during the search for a suitable method of anchoring the wires but, either the solder failed or the wires broke prematurely from the effects of overheating during soldering.

The device used to push the pairs of wedges into the prestressing jacks, thus anchoring the wires, is shown in operation in figure 6.11.

6.4.4 Load cells for measuring the forces in the prestressing wires

The prestressing force measuring load cells, dimensioned in figure 6.8, were made from heat treatable steel. They were not heat treated, as was originally intended, because of fear of distortion. The heavy end billets were added to an initial design, using a straight tube with protecting pieces at each end, after inconsistent readings had been obtained in preliminary calibration tests.

After hardening, the bull noses were ground into their respective load cells.

Four Budd, C6 - 121A steel temperature compensated strain gauges, wired with two pairs of two gauges in series in parallel to give 120 ohms resistance, were used as active strain gauges on each load cell. The load cells were all connected to switch-box A (described in section 7.4.1) and

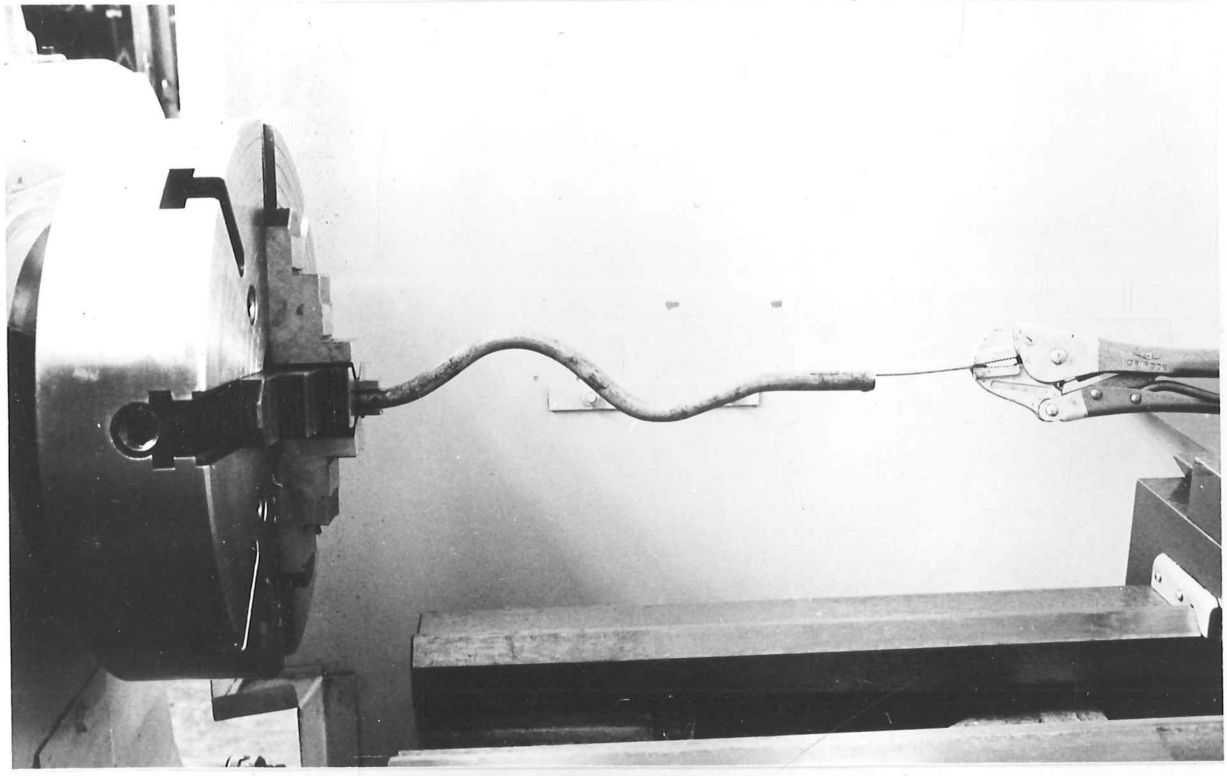

Fig. 6.5 Wire straightener in the lathe

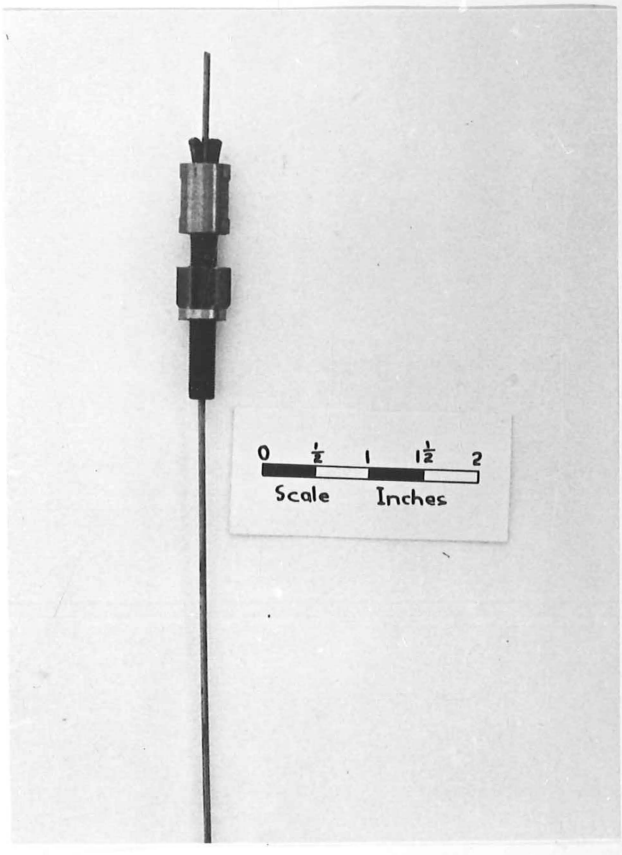

Fig. 6.6 Prestressing jack

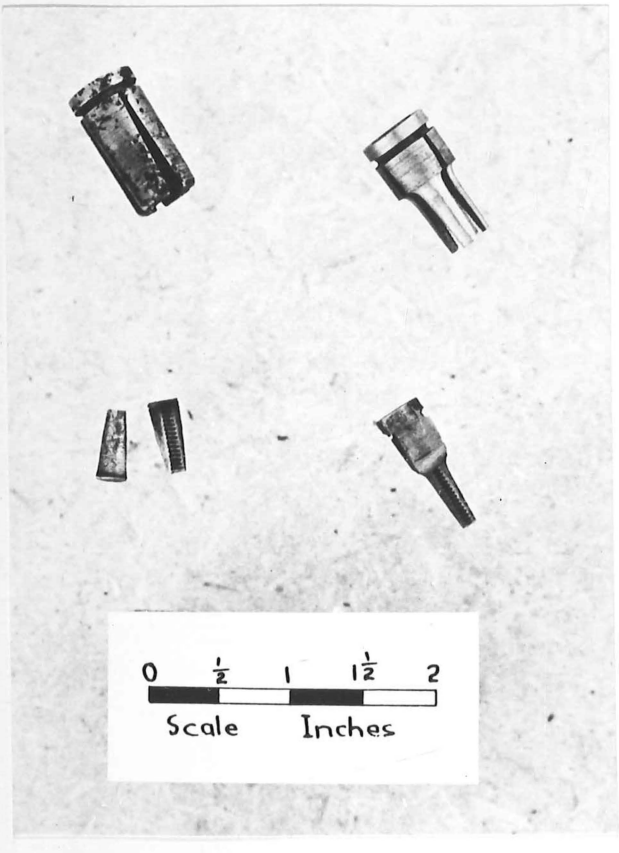

Fig. 6.7 Making of wedges

read along with the strain gauges on the model shell. One of the gauges on an aluminium alloy test piece was used as a dummy.

6.4.5 Complete anchorage assembly

The prestressing wires, jacks, and load cells were kept in place by anchorage-holding pieces (as in figure 6.4) which also served the various functions of: preventing the load cells and the prestressing jacks from rotating when the prestressing nuts were turned; holding the load cells so that only axial forces could act on them; and transmitting the anchorage forces from the prestressing wires to the shell.

6.4.6 Surface guides

The loads on the shell from cable curvature were applied to the shell through mild steel guides glued with Araldite to the shell surface at 1" centres for draped cables, and at 3" centres for straight cables. The guides are dimensioned in figure 6.9.

Although the forces from the cable curvature were applied as a series of point loads, it was considered that this system was preferable to one with continuous guides such as Arcan and Nicolau[17] describe using plastic tube cemented to a plastic shell. Since the guides were not continuous they had little effect on the shell stiffness (see appendix II).

The guides were drilled in a bench drill press with a simple jig holding the guides so that the holes were accurately

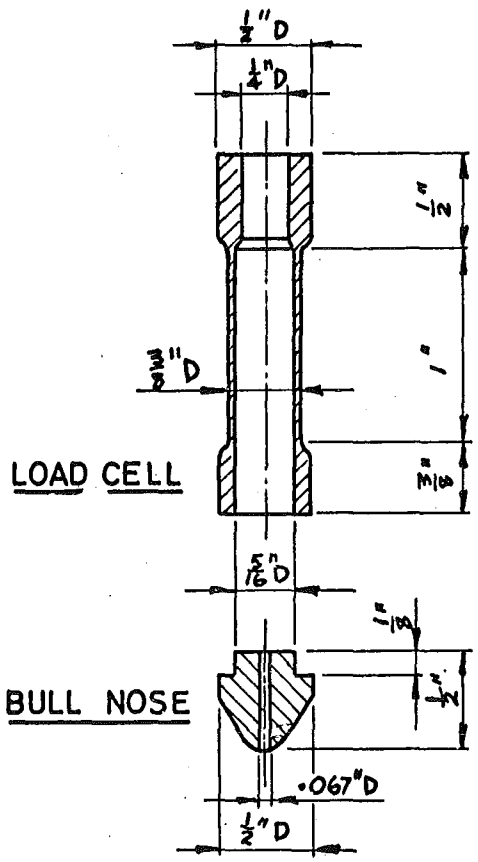

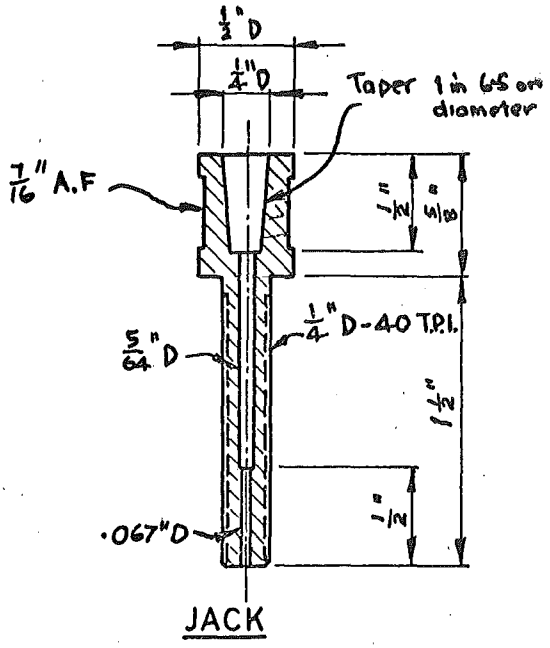

Fig. 6.8 Dimensions of prestressing load cells and jacks

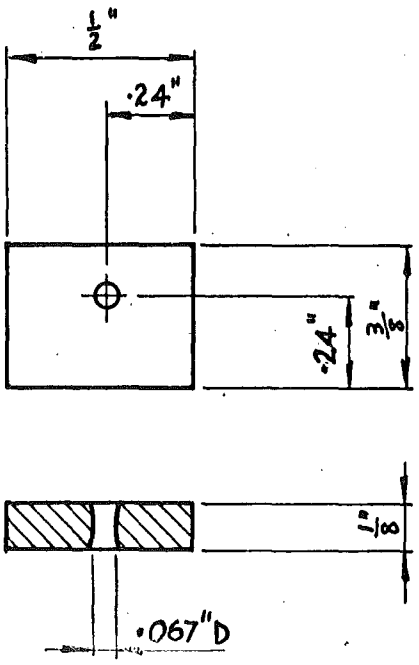

Fig. 6.9 Surface guides

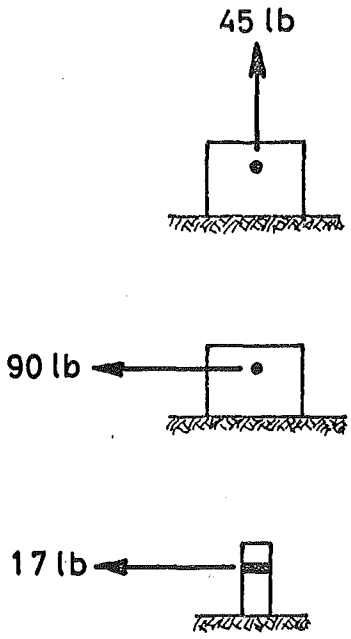

Fig. 6.10 Failure loads of glued joints between surface guides and the shell

positioned with respect to the base and one edge. The top corner of the guides, above the edge from which the holes were positioned, was marked. The guides could be accurately positioned on the shell surface by butting this edge against a straight edge or a bent steel rod clamped to the shell surface (figure 8.1).

The glued joint between the shell and the guides was of ample strength as can be seen from the test results, shown in figure 6.10, on guides glued to a strip of aluminium. The guides could be removed from the shell by a sharp tap from a small hammer. Soaking the guides in Episolve 299 removed all the adhering Araldite.

Molybdenum disulphide grease was used to reduce friction between the wires and the guides.

6.4.7 Calibration of the prestressing load cells

During all calibration tests the load cells were held in an anchorage-holding piece in the same way that they were held during the actual testing of the shell model and loaded through a piece of prestressing wire as indicated in figure 6.12.

Calibration tests were made with an Avery 25,000 lb. universal test machine, working in its lowest range of 0 - 1250 lb., supplying the load. There was doubt as to the repeatability of the load cells until it was realized that shifts of up to 10 lb. in the zero of the test machine load

indicating mechanism were occurring during some runs, and that frictional effects in hydraulic test machines can make them unreliable if the direction of loading is changed (B.S. 1610 recognizes this and only requires hydraulic test machines to be calibrated for load increasing).

A 400 lb. spring balance with a simple bolt arrangement to wind the tension up was used to show that the load cells gave repeatable results with random load changes.

A straight line through the readings of 3 runs, with strain readings at 100 lb. intervals going up to 800 lb., was taken as the calibration curve for each cell. Before the start of the initial calibration the load cells were loaded up and down five or six times to remove hysteresis effects. Between each run the bull noses and the load cells were rotated separately in the holding pieces.

The sensitivity of the load cells was such that 100 μstrain was equivalent to 100 lb. Thus the prestress forces could be set to within 2 lb. of the desired loads.

Calibration tests at the end of straight cable testing and at the finish of testing were within 0.5 per cent of the initial calibration.

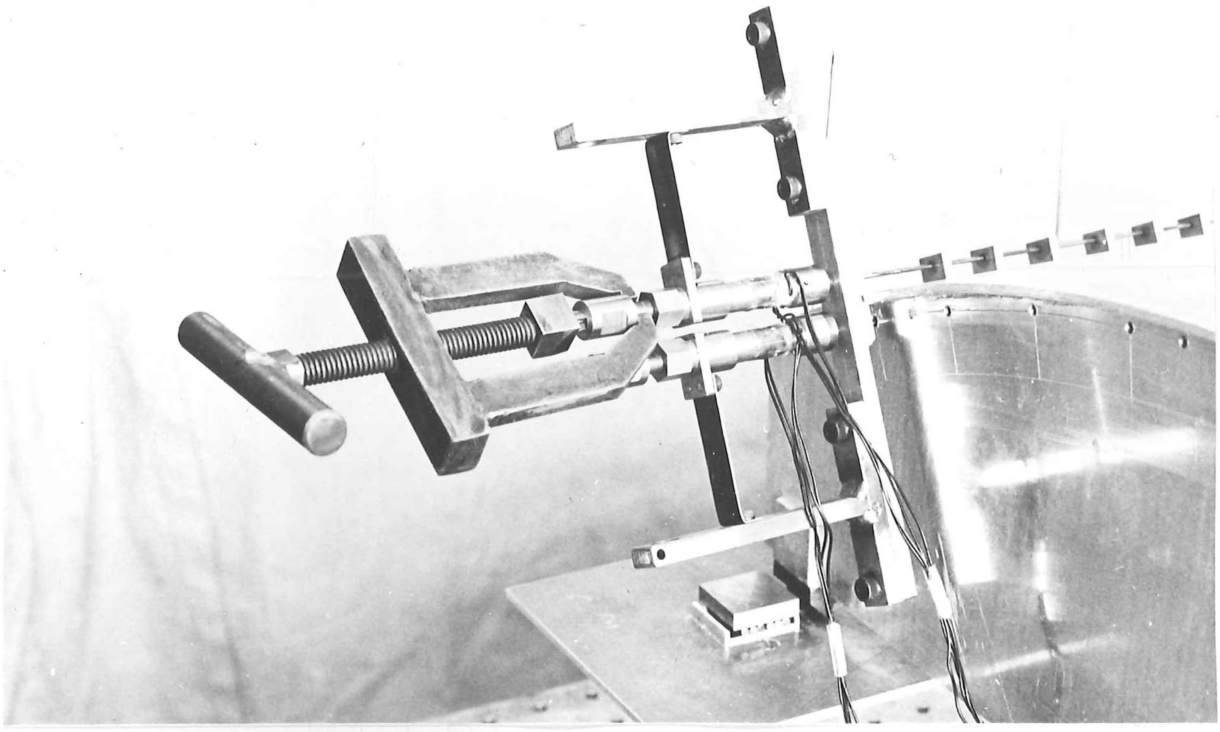

Fig. 6.11 Pushing in wedges

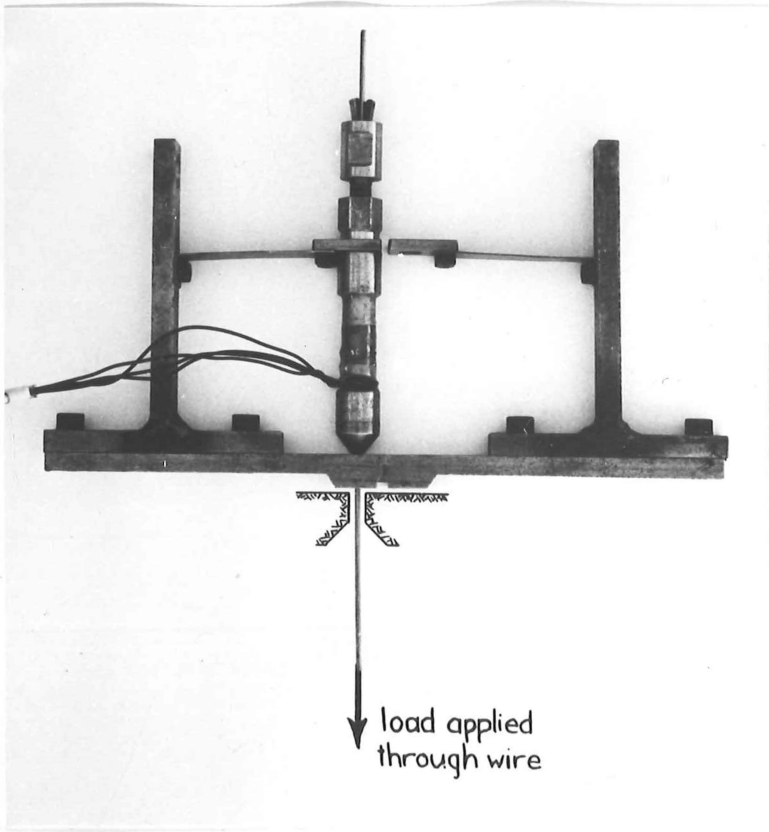

Fig. 6.12 Calibration of prestressing load cells

CHAPTER SEVEN

STRAIN AND DEFLECTION MEASUREMENT

7.1 DISTRIBUTION OF STRAIN GAUGES ON THE MODEL SHELL

Electric resistance rosette strain gauges were positioned on the intrados and extrados of one quarter of the shell in the rectangular grid pattern shown in figure 7.1.

120^{o} delta rosette strain gauges were used to measure the shear as well as the direct strains at transverse cross sections D and E near the diaphragms and to check symmetrical behaviour about mid-span and the shell crown.

At cross section A, B, and C, where shear strains were considered to be relatively unimportant, 90^{o} rosettes were placed so that the two gauges measured direct longitudinal and transverse strains.

The number of strain gauges which would have been required to strain gauge more of the shell was prohibitive. Unless strain gauges are close together the drawing of stress profiles becomes almost impossible. Investigators have almost invariably stated that there were insufficient strain gauges on their models at the places that mattered. It was hoped that the strain gauges would be sufficiently closely spaced on a number of transverse cross sections to obtain a good indication of the changes in stress over the whole shell surface.

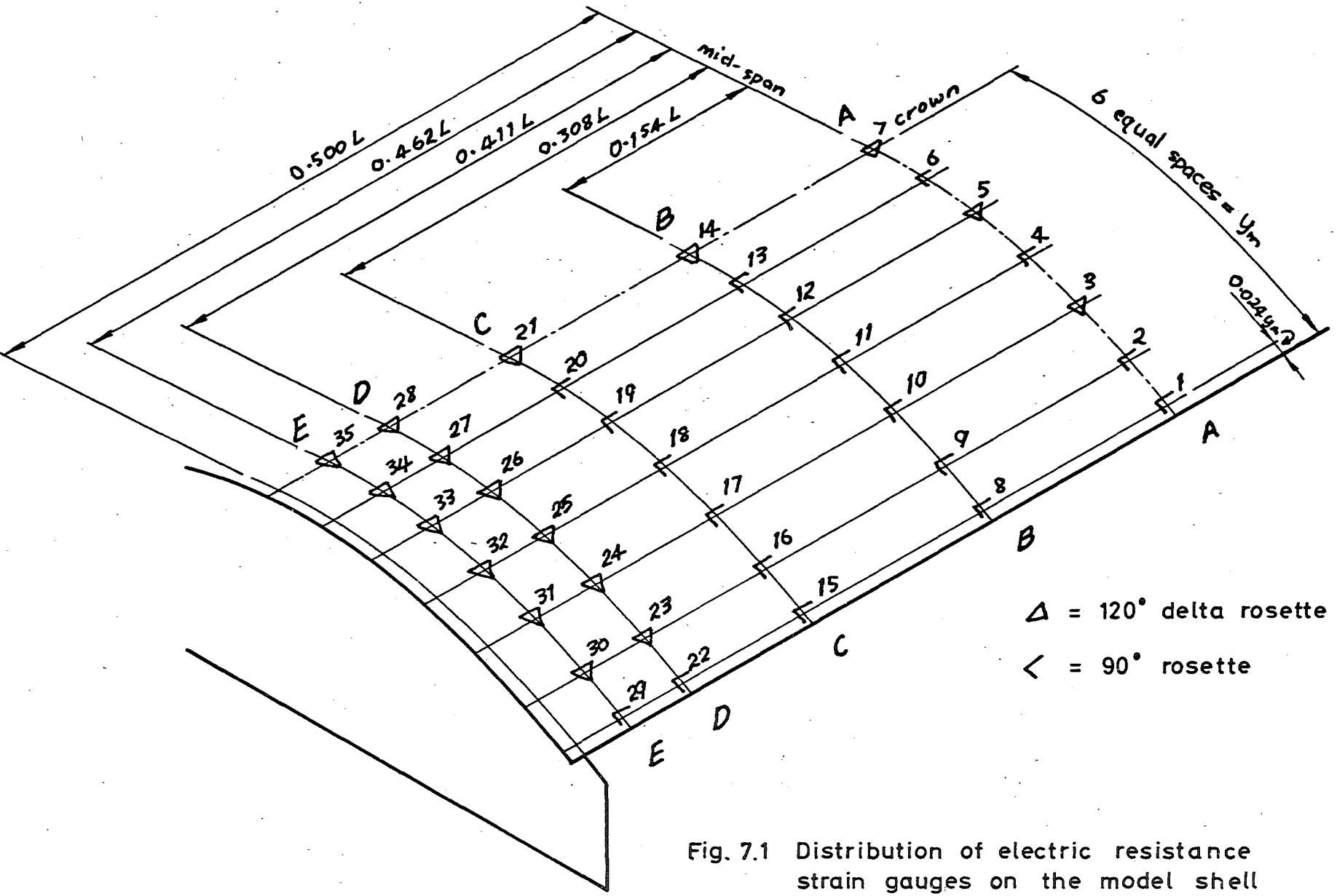

Fig. 7.1 Distribution of electric resistance strain gauges on the model shell

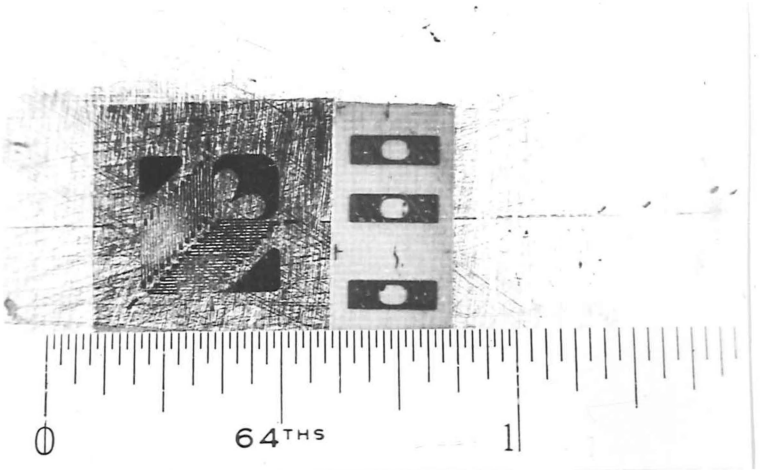

(a) 90° rosette (C12 - 121 - R2VC) plus terminal strip

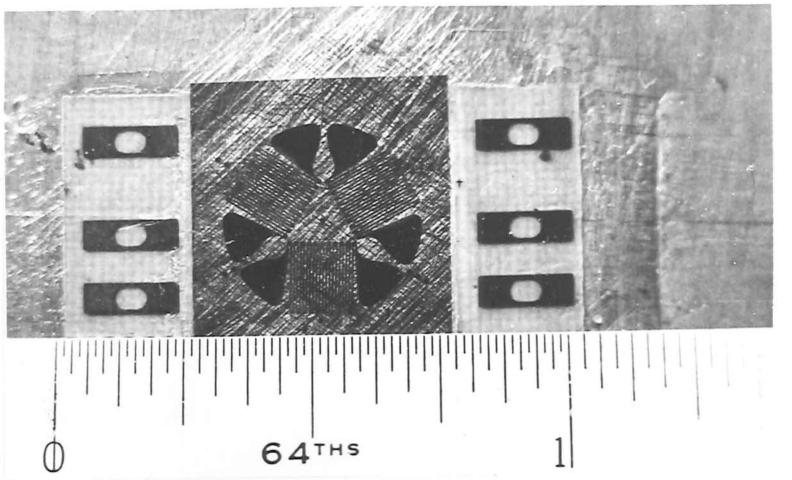

(b) 120° delta rosette (C12 - 121 -R3Y) plus terminal strips

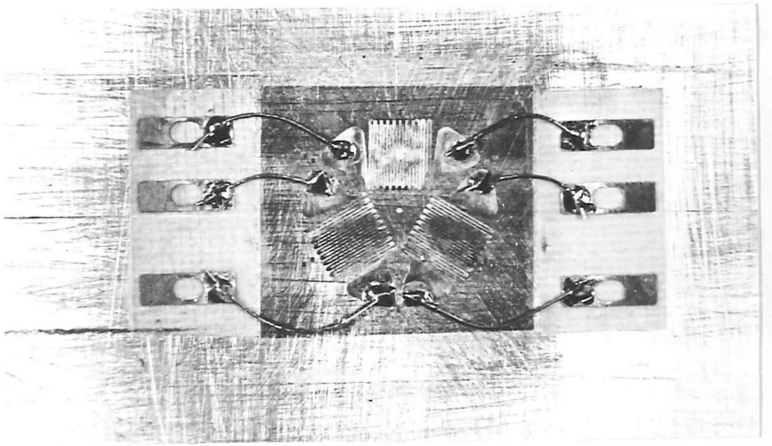

(c) Wires soldered from gauge to terminal strips

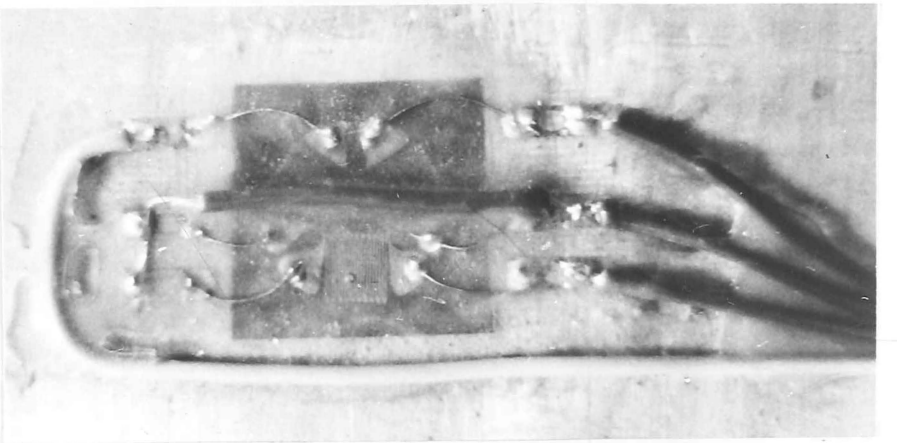

(d) Completed waterproofed gauge installation

Fig. 7.2 Budd metalfilm strain gauges

7.2 ELECTRIC RESISTANCE STRAIN GAUGES AND THEIR ACCESSORIES

Budd metalfilm electric resistance strain gauges and accessories were used throughout this series of tests to measure all strains. Points in favour for the use of these gauges were:

(a) The availability of straight and rosette gauges of suitable small size ($\frac{1}{8}$" gauge length was chosen as being suitable).

(b) Metalfilm gauges are temperature compensated for a wide range of materials.

(c) The close control of electrical and physical characteristics of the metalfilm gauges during manufacture.

(d) The metalfilm gauges are very thin with high flexibility.

In tables 7.1 and 7.2 the strain gauges and their accessories are listed.

7.3 INSTALLATION OF THE STRAIN GAUGES

The gauges and the terminal strips were affixed to the shell surface with Eastman 910 contact cement according to the recommended procedures of the Budd Company[27]. Strain gauge installation was very fast because of the immediate bond formation when the gauges were pressed into the cement. No clamps were necessary.

Budd catalogue[26] designation	Description	Use
C12 - 121	straight aluminium temperature compensated - $\frac{1}{8}$" gauge length	test gauges on aluminium alloy test pieces
C12 - 121 - R2VC	2 gauge 90° rosette, aluminium temperature compensated - $\frac{1}{8}$" gauge length	measuring longitudinal and transverse strains on the model shell
C12 - 121 - R3Y	3 gauge 120° delta rosette, aluminium temperature compensated - $\frac{1}{8}$" gauge length	measuring longitudinal, transverse, and shear strains on the model shell
C6 - 121A	straight steel temperature compensated - $\frac{1}{8}$" gauge length	gauges on prestressing load measuring load cells

Table 7.1 Strain gauges used during the model tests

Budd catalogue[26] designation	Accessory	Description
GA1	contact cement kit	Eastman 910 plus accelerator
GS - 3	terminal strips	
GS - 350	solder	0.015" dia. low melting point
	cleaning solvent	2 parts by vol. of methyl ethyl ketone to 1 part of zylol
	"waterproofing"	flexible epoxy - Araldite 106 plus 20% by weight of Thikol as plasticizer

Table 7.2 Strain gauge accessories

The use of terminal strips can be seen from figure 7.2. The terminal strips protect the strain gauges. If the lead wires are pulled the terminal strips break in two and the actual strain gauge is unharmed. After the soldering of the connecting wires from a rosette to its terminal strips, the rosette and half the terminal strips can be waterproofed before the lead wires are attached. Moisture cannot penetrate between the lead wires and the waterproofing.

A flexible epoxy resin coating of Araldite 106 plus 20 per cent by weight of Thikol as a plasticizer, was painted over the strain gauges. The main purpose of this so called waterproofing was protecting the gauges and wiring from mechanical damage. No stiffening effect from the waterproofed strain gauges was noticeable on aluminium alloy test strips (see appendix II).

Each lead wire was made in three sections, as in table 7.3, with the lengths of each section being measured to ensure that the lead wire resistances were all equal and that there would be no apparent drifts in strain gauge zeros as the temperature of all the lead wires changed.

To reduce the number of lead wires a common lead wire system was used for the gauges of each cross section. To prevent interference between the prestressing guides and the lead wires, the lead wires were kept in $\frac{3}{4}$" wide bands across the shell (see figure 7.4).

	Type of wire	Length
gauge to terminal strip	1 strand from 7/.0076" insulated copper cable	¼"
terminal strip to shell edge	7/.0040" plastic insulated copper cable	1' - 11"
shell edge to switch-box	7/.0076" plastic insulated copper cable	10' - 0"

Table 7.3 Strain gauge lead wires

7.4 STRAIN GAUGE INSTRUMENTATION

7.4.1 Switch-boxes

Two switch-boxes were made so that all the strain gauges (some 182 separate gauges when the prestressing load cells were included) could be read from one strain indicator. Originally, only the making of one switch-box (98 way) was intended. For the rest of the readings the use of existing equipment or the data logger (an automatic strain gauge reader and recorder under construction at the time) was envisaged. After switch-box A was made and successfully tested, it was obvious that the easiest solution to the switching problems was to make another switch-box, B , to handle the rest of the gauges.

Each switch-box was connected to an active set of gauges and to a dummy gauge which was a gauge on one of the

aluminium alloy test strips. The two switch-boxes were then connected together so that one strain indicator could be used without any additional switching in the active arms of the Wheatstone bridge circuits.

The switches used in the switch-boxes were type S.P.I. Croydon rotary stud switches. The switches performed satisfactorily without any noticeable switching resistance differences. Switch-box A had zero setting, consisting of a 10,000 ohm wire wound resistance and a 10,000 ohm variable resistance in parallel with each strain gauge, giving a balance of $\pm$ 0.35 ohms for 120 ohm strain gauges. Switch-box B had no zero setting.

7.4.2 Strain indicators

A Budd P-350 portable strain indicator (serial number 1810) was used for reading strains during most of the testing. Before the arrival of the Budd instrument, a BLH Model 120 strain indicator was used during some of the preliminary testing.

The Budd instrument was easier and faster to use and did not have the annoying 2 - 3 μstrain "backlash" of the BLH instrument (the BLH instrument was damaged during delivery and the suspension of the micro-ammeter could have been damaged).

The instruments are shown in figure 7.3.

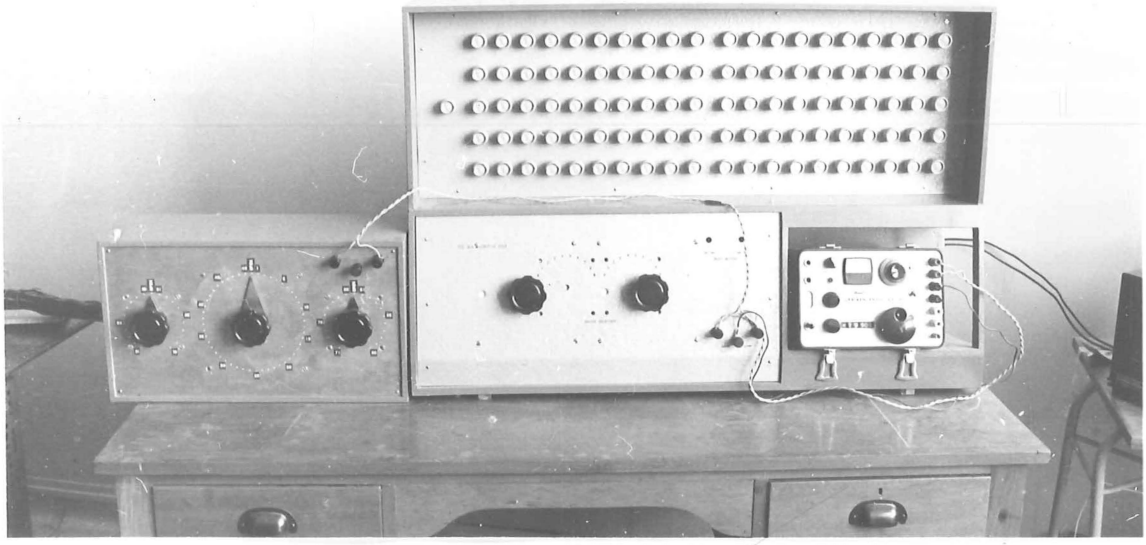

Fig. 7.3 Switch-boxes and Budd P-350 strain indicator

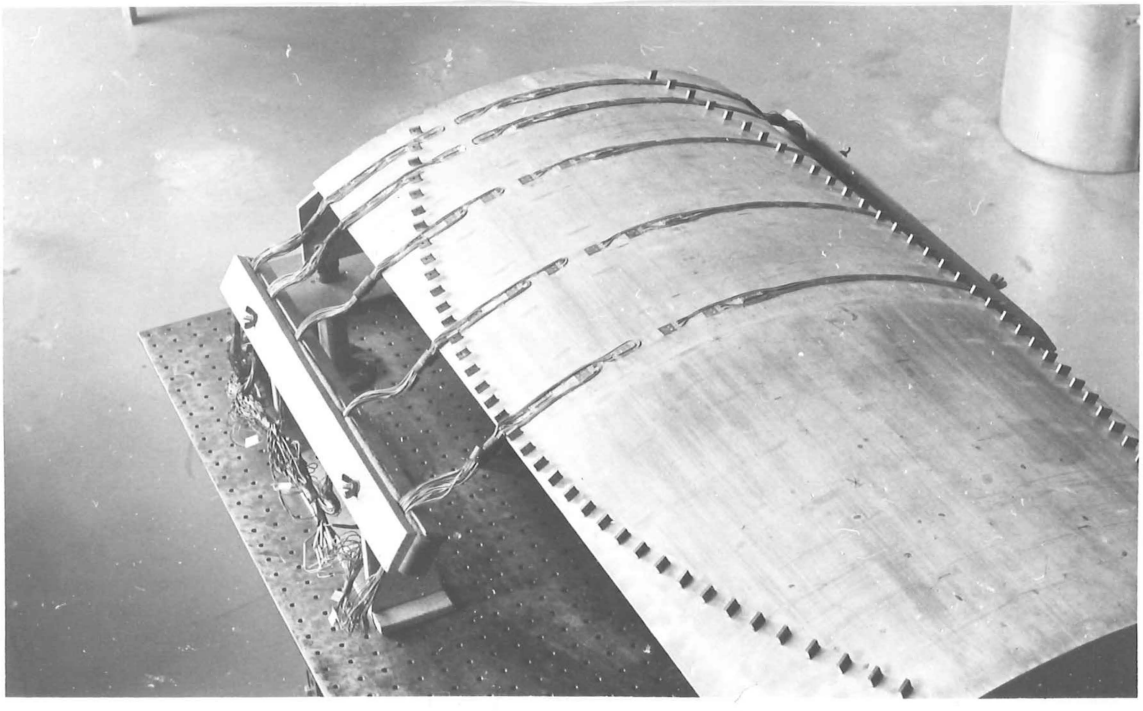

Fig. 7.4 Strain gauge wiring across the shell surface

7.5. CORRECTIONS TO STRAIN READINGS

Certain corrections must be made to the readings of strain gauges at a strain indicator if accurate surface strains are required.

In appendix I the equation

$$Q' = C \frac{GF_b}{GF_g} Q_b ,$$

where Q' = reading of gauge at gauge,

Q_b = reading of gauge at strain indicator,

C = resistance correction coefficient,

GF_b = gauge factor set on the strain indicator,

GF_g = gauge factor of the strain gauge,

is obtained for the corrections to strain readings from lead-wire and switch-box resistance and the gauge factor set on the bridge.

$C = 1.017$ for strain gauges wired through switch-box A and $C = 1.008$ for strain gauges wired through switch-box B.

The following equations apply as corrections for strain gauge cross sensitivity[28].

For 120^o delta rosettes

$$\epsilon_1' = Q_1' - K(Q_2' + Q_3'),$$

$$\epsilon_2' = Q_2' - K(Q_3' + Q_1'),$$

$$\varepsilon_3' = Q_3' - K(Q_1' + Q_2'),$$

and for 90° rosettes

$$\varepsilon_1' = Q_1' - K\,Q_2',$$

$$\varepsilon_2' = Q_2' - K\,Q_1',$$

where K = transverse sensitivity,

Q_j' = reading of strain in j direction,

ε_j' = strain of gauge in j direction.

For the Budd metalfilm strain gauges K was taken as zero and, in reality, no transverse sensitivity corrections were made to the model shell strain readings

The surface strain under a strain gauge is not, in general, the same as the strain of the metalfilm of a strain gauge because the metalfilm is a small distance t_1, from the surface. From figure 7.5 in which surface and metalfilm strains are superimposed

$$\varepsilon_b = \frac{t + t_1}{t + 2t_1}\,\varepsilon_b' + \frac{t_1}{t + 2t_1}\,\varepsilon_t',$$

$$\varepsilon_t = \frac{t + t_1}{t + 2t_1}\,\varepsilon_t' + \frac{t_1}{t + 2t_1}\,\varepsilon_b',$$

where t = model thickness,

t_1 = effective strain gauge thickness,

ε_t' and ε_b' = metalfilm strains,

ε_t and ε_b = surface strains.

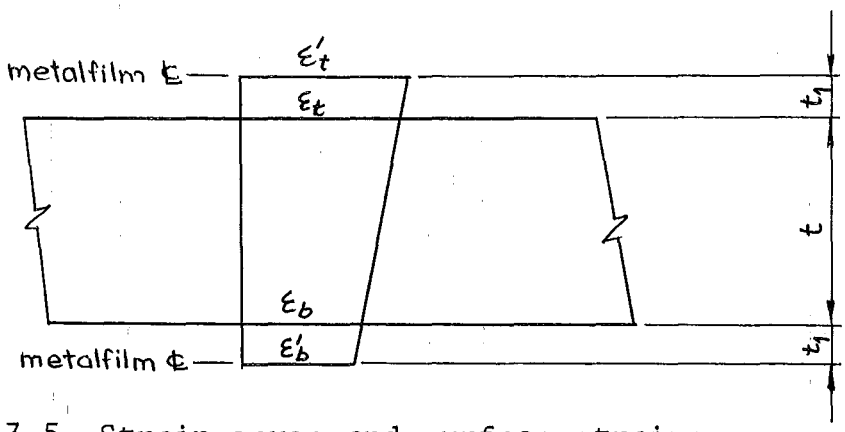

Fig. 7.5 Strain gauge and surface strains

7.6 SURFACE STRESSES FROM SURFACE STRAINS

If the directions of the gauges of rosettes compared with the shell axes x and y are as shown in figure 7.6 the following equations apply[29].

For the 120^o delta rosettes

$$\varepsilon_x = \varepsilon_1 ,$$

$$\varepsilon_{xy} = \frac{2}{\sqrt{3}} (\varepsilon_3 - \varepsilon_2) ,$$

$$\varepsilon_y = \frac{1}{3} \left[2(\varepsilon_2 + \varepsilon_3) - \varepsilon_1 \right] ,$$

and for the 90^o rosettes

$$\varepsilon_x = \varepsilon_1 ,$$

$$\varepsilon_y = \varepsilon_2 .$$

Stresses can be obtained from strains from the well known relationships

$$\sigma_x = \frac{E}{1 - \mu^2} (\varepsilon_x + \mu \varepsilon_y) ,$$

$$\sigma_{xy} = \frac{E}{2(1+\mu)} \epsilon_{xy} ,$$

$$\sigma_y = \frac{E}{1-\mu^2} (\epsilon_y + \mu\epsilon_x) ,$$

where ϵ_x, ϵ_y = strains in the x,y directions,
ϵ_{xy} = shear strain,
σ_x, σ_y = direct stress in the x,y directions,
σ_{xy} = shear stress.

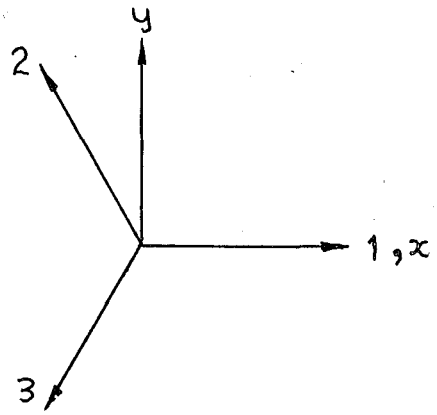

(a) 120° delta rosette

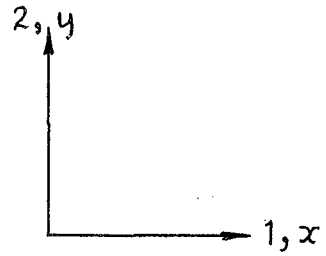

(b) 90° rosette

Fig. 7.6 Orientation of strain gauges compared with shell axes

7.7 DEFLECTION MEASUREMENTS ON SHELL MODELS

The measurement of deflections on a shell model is quite a difficult problem because of the three dimensional nature of the surface and the deflections. Shells are very sensitive to point loads and the deflection measuring system must not load the shell with varying point loads.

Dial gauges have been used to measure the deflections on many shell models. Unfortunately, there are certain drawbacks to their use which become more noticeable as the scale of a model is reduced. A "forest" of dial gauges is needed if the deflections of a large number of points is required. Dial gauges are usually set up radially to the shell surface. If, as is often the case, the shell does not move radially, the dial gauge stems will slip over the shell surface giving friction in the dial gauges from sideways loadings on their stems. The deflection readings so obtained will not be the deflection readings of the points on the shell over which the dial gauges were set up. If the deflections of the shell are small, the point loads on the shell from the dial gauges remain effectively constant, and the shell is little affected by the dial gauges. But, when the deflections are large compared with the total movement of the dial gauges, or when the dial gauges are moved during tests, the point loads on the shell from the dial gauges could become important.

7.8 TRAVELLING LEVEL DEFLECTION MEASUREMENT

Wherever vertical deflections were required targets were attached to the shell. The height of each target above datum could be obtained by raising or lowering a surveying level by means of the micrometer drive mechanism of a travelling microscope until the line of sight coincided with the target, and reading the vertical height from the micrometer drive. By taking readings before and after loading, the vertical deflections of as many targets as was required could be obtained. This deflection measuring system has the advantages of:

(a) Measuring the true vertical deflections of the points on the shell to which the targets are attached.

(b) The shell surface is relatively uncluttered and the only loads on the shell are the self-weights of the targets.

(c) Only one instrument is required to measure the deflections of as many points as is required.

The reading speed was rather slow. 20 minutes were required for the reading of 35 deflection points. During this time 200 strain gauges could be read.

7.9 THE TRAVELLING LEVEL

The travelling level, shown in figure 7.8, was made up from:

(a) A travelling microscope, serial number 2843, made by J. Swift and Son.

(b) An automatic precise level, serial number S07247, made by Cooke, Troughton and Simms.

A steel base plate was bolted to the travelling microscope mechanism instead of the microscope. The level sat on this base plate supported by a 7½ lb. counterweight which removed all backlash and made the travelling movement easy to operate.

Different surveying levels were tried in the search for the most satisfactory level. The first to be tried was the automatic precise level which was initially rejected because of continual vibrations, set up by workshop and laboratory machinery, in the automatic level of the instrument, giving a slightly blurred image and cross hairs. During the first preliminary test an ordinary tilting level was used. Reading speed was rather slow because continual adjustments to the level of the instrument were necessary. Then the precise level was retried and, because a more consistent set of readings was obtained in about one-half the time, it was used during all further tests.

7.10 EXPERIMENTAL DEFLECTION READINGS

Deflection readings were taken at the pattern of points spread over the whole of the shell surface as shown in figure 7.7. To avoid coincidence between the strain gauges and the

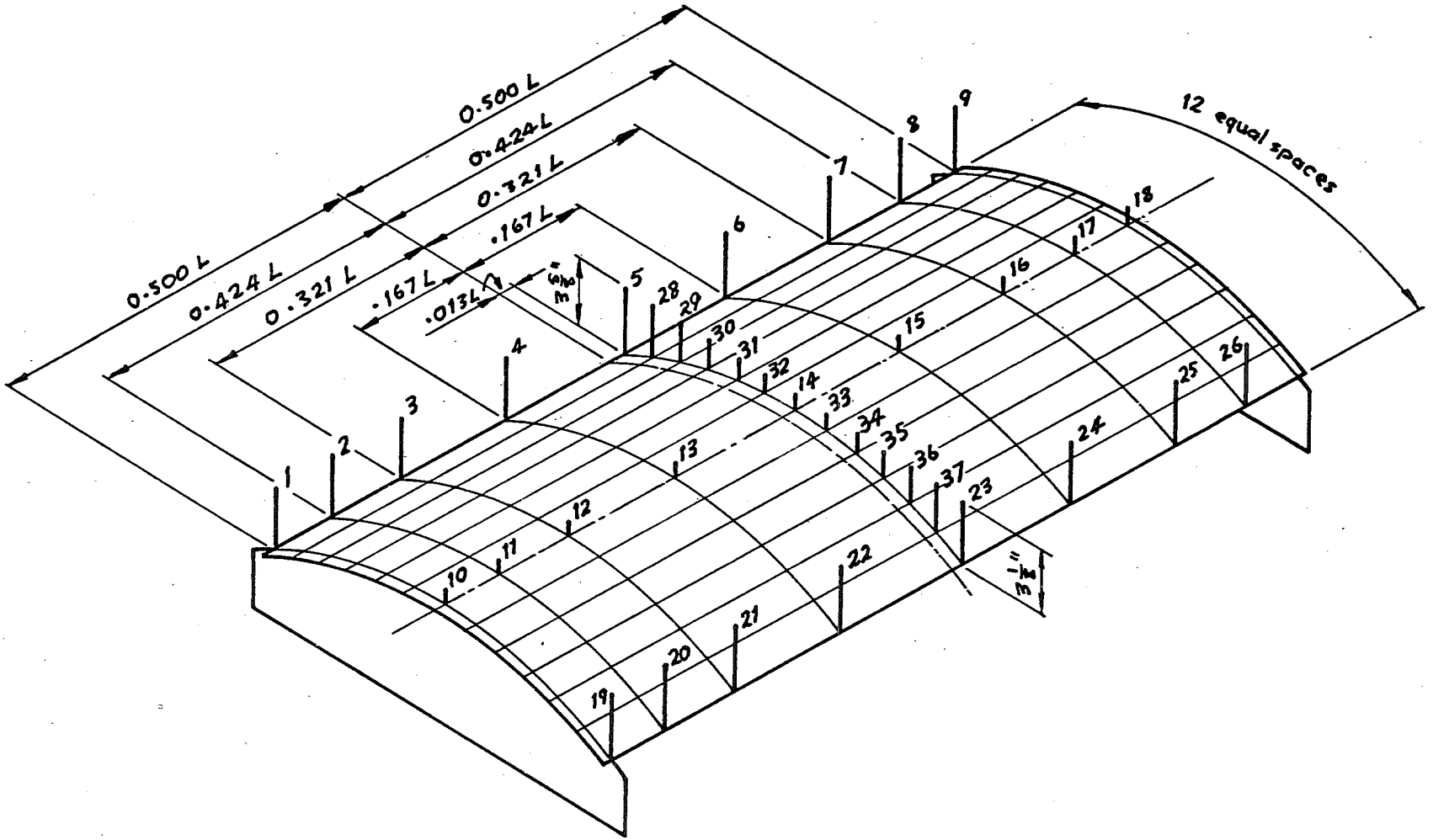

Fig. 7.7 Location of deflection targets on the model shell

deflection targets, the targets were displaced ½" further from mid-span than the adjacent strain gauges. For practical purposes the row of deflection targets across the shell, ½" from mid-span can be considered to be at mid-span.

The targets were vertical 1/16" diameter brass rods with their tops carefully filed square and polished with fine emery paper. The targets were glued to the shell surface with Philip's PR 9244/05 strain gauge waterproofing compound (used because of a setting time of 10 minutes). The targets on the near side of the shell to the travelling level were ½" shorter than those on the far side.

A 5 foot 80 watt fluorescent light tube with a tracing paper light diffuser in front, was placed behind the targets (see figure 7.9). The targets stood out as black outlines against this bright background.

A correction, consisting of the average deflection of the 6 diaphragm targets, was made to each set of readings to allow for relative movements between the shell supports and the travelling level tripod. This correction was frequently as high as 0.005" for a test spread over 6 hours.

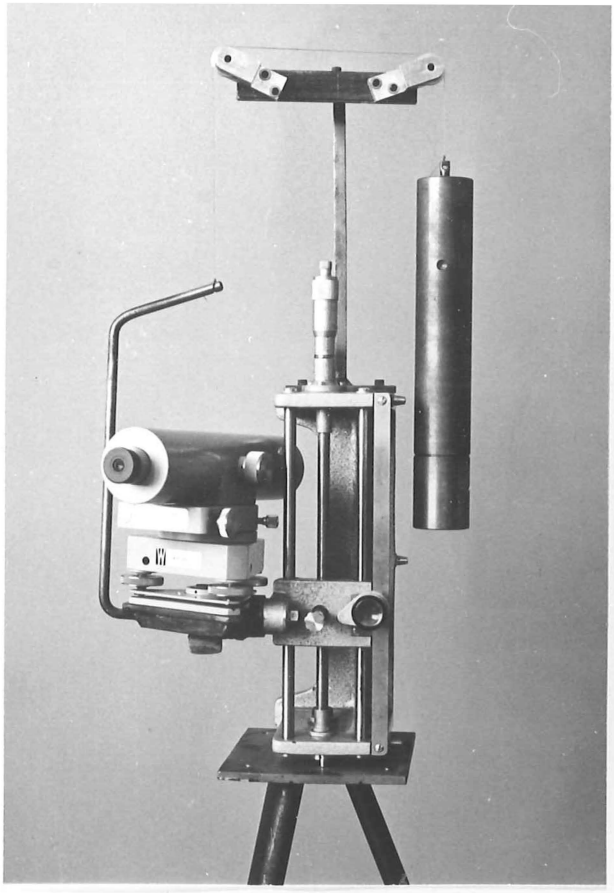

Fig. 7.8 Travelling level

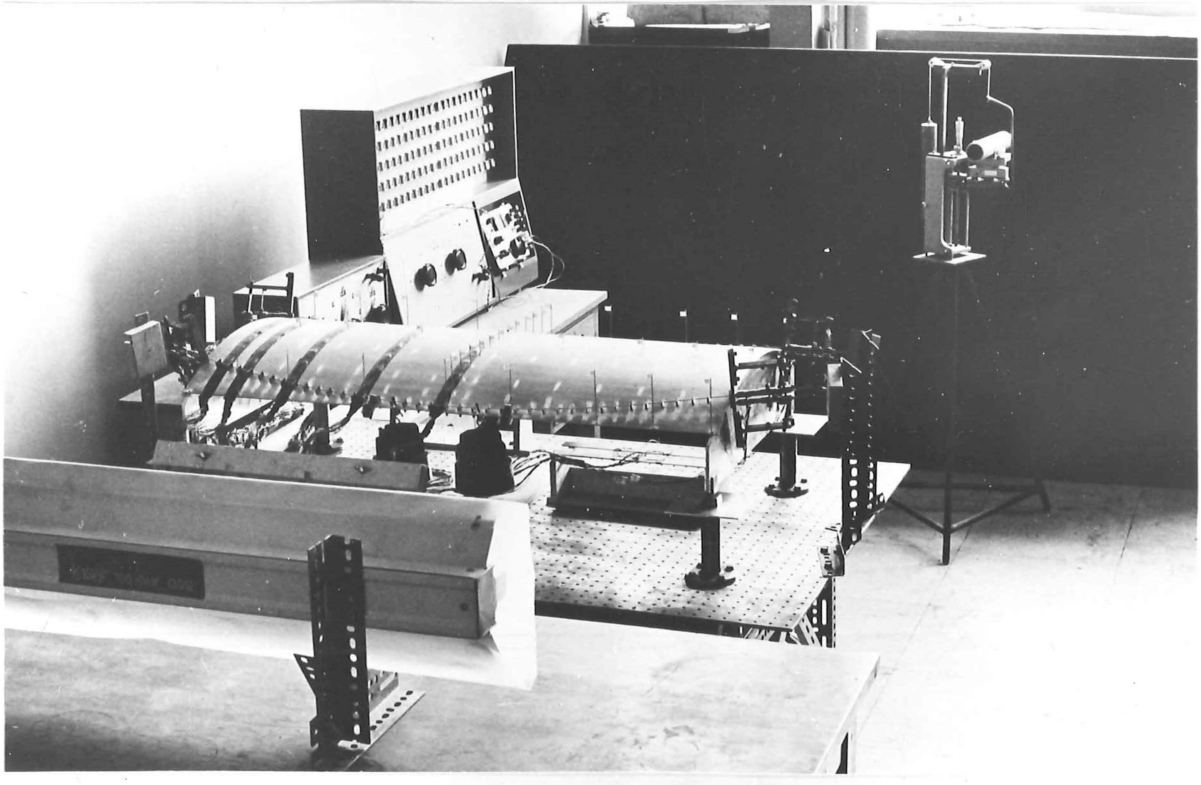

Fig. 7.9 Model shell ready for testing - fluorescent light is in the foreground and the level in the background

CHAPTER EIGHT

DESCRIPTION OF THE MODEL TESTS

8.1 INTRODUCTION TO THE MODEL TESTS

Strain and deflection readings were obtained from tests with eight different symmetrical prestressing cable lay-outs on the model whose construction, prestressing system, and instrumentation are described in the previous two chapters. In the first five cable lay-outs the effect of varying the position of straight cables was studied, and in the last three lay-outs the drape of parabolic in the developed shell surface cables with a constant mid-span cable position was varied. The actual lay-out details of the prestressing cables are given in table 8.1.

In general, for each model set-up, readings were taken during at least two runs in which the prestressing forces were varied in two different patterns. For loading pattern A, readings were taken at a series of different prestressing forces - say 0, 200, 400, 600, 600, 400, 0 lb. per wire. Pattern A was used to show that the model was behaving in a linear manner and to determine the effect of friction. This was obtained from the differences between readings taken at a given load after increases and after decreases in prestressing forces. Loading pattern B, for which repeated readings were

taken with repeated applications of full prestressed - say 0, 600, 0, 600, 0, 600, 0 lb. per wire - was used to improve the experimental accuracy.

About 15 minutes were required for the setting of the prestress forces on any given load, and about 25 minutes were required for the reading and recording of a complete set of strain and deflection readings, using three persons as follows:

(1) A person to read and record deflections.

(2) A person to read strains.

(3) A person to record strains.

Test	Anchorage eccentricity d	Drape f	d + f	
1	0.048	-	0.048	straight prestressing tendons, varying anchorage eccentricity
4	0.333	-	0.333	
3	0.667	-	0.667	
5	0.833	-	0.833	
2	0.972	-	0.972	curved prestressing tendons, constant mid-span position, varying drape and anchorage eccentricity
6	0.833	0.138	0.971	
7	0.667	0.305	0.972	
8	0.500	0.472	0.972	

Table 8.1 Prestressing cable lay-out details - quantities given in terms of y_m, d + f = mid-span cable position.

8.2 DETAILS OF INDIVIDUAL TESTS

In table 8.2 a complete list of all the tests on the different model set ups is given, with notes describing various special features of individual tests. These, however, were later found to be relatively unimportant.

Model tests 1 and 2 were treated as preliminary tests. Important features of these preliminary tests were:

(a) Temperature control of the testing room. Drifts of strain gauge zeros of up to 5 μstrain throughout each day were causing concern. Electric heaters, controlled by a Satchwell TM20 thermostat and a relay, were installed and the temperature was held at $20^{o} \pm 1^{o}C$. No improvement in zero stability was noticed and, when it became apparent that electrical interference from the heater wiring was occasionally affecting strain readings, the use of the heaters was discontinued and the electrical wiring was removed.

(b) Weights on the shell edges. As constructed, the edges of the shell were bowed up about $\frac{1}{8}$" (see section 6.2). Model 2 was tested with bowed edges, and with weights hanging from the edges to make them straight. Although the differences in readings were slight (less than 3 per cent for the more sensitive readings) the weights were included in all the following tests.

Model Test	Prestressing d	Prestressing f	Test	Load Pattern	Notes
1	0.048	-	A	A	test model and instruments, exercise strain gauges to remove zero drift - only some gauges read
			B	A	read all gauges and deflection points
			C	B	change from BLH to Budd strain indicator and ordinary tilting to the precise level
2	0.972	-	A	A	no weights on the shell edges
			B	A	weights on the shell edges
			C	B	weights on the shell edges
			D	B	no weights on the shell edges
3	0.667	-	A	A	
			B	B	
4	0.333	-	A	A	Glacier DU thrust washers added to reduce friction between jacks and the load cells - torsion effects no longer troublesome
			B	B	
5	0.833		A	A	nut on a prestressing jack failed in shear (nuts $\frac{1}{4}$" thick)- model dismantled and new nuts, $\frac{3}{8}$" thick, were made
6	0.833	0.138	A	A	
			B	B	
7	0.667	0.305	A	A	cable friction effects just noticeable
			B	B	
8	0.500	0.472	A	A	readings after increases in prestress
			B	B	readings after increases in prestress
			C	B	readings after decreases in prestress

Table 8.2 Notes on model tests - f, d in terms of y_m

(c) Different recording instruments were tried until the most satisfactory instruments were discovered.

The results from tests 1 and 2 were then completely analysed with the aid of computer programs RR1, RR2, and RR3 (programs described in section 8.6). As the results appeared to be satisfactory, with symmetrical behaviour and an overall equilibrium between internal stresses and external prestressing loads, the decision to carry on with the rest of the tests was made.

8.3 SETTING UP THE PRESTRESSING WIRES

Points on the line of the prestressing wires were laid out on the extrados of the model by measurements from the crown of the shell. Ample setting out accuracy could be obtained with dividers and a steel rule as, at any transverse cross section, the prestressing cable position relative to the whole cross section and not the thickness of the shell is of importance. The prestressing wires on the intrados of the shell were radially placed with respect to those on the extrados.

By butting the prestressing guides against a spring steel rod or a straight edge clamped to the shell surface as in figure 8.1, the guides could be held in position, with the holes in the guides forming a smooth cable profile, while the Araldite cured. The shell was held upside down as in

figure 8.2. so that the guides could be glued to the intrados of the shell.

For straight prestressing cables, one could see from one end of the shell to the other by looking down the holes through the guides. For curved prestressing cables with the guides placed at 1" centres, the prestressing wires could be fed through the guides by pushing from the ends with a force of some 5 lb. The free end of the wire did not require directing from one guide to the next. These points give an indication that the local variations of the positions of the holes through the guides were small.

Notches were filed in the ends of the shell so that the load cells and prestressing jacks lined up with the prestressing wires.

8.4 SETTING THE PRESTRESS FORCES

The prestress was always set in the two stages listed below and diagrammatically shown in figure 8.4.

Stage 1: The tension in each wire, at one end, was jacked up (load increasing) or down (load decreasing) until the correct tension, at the jacking end, was reached. The prestress forces at the far ends of each wire were then read to give twice the final friction loss.

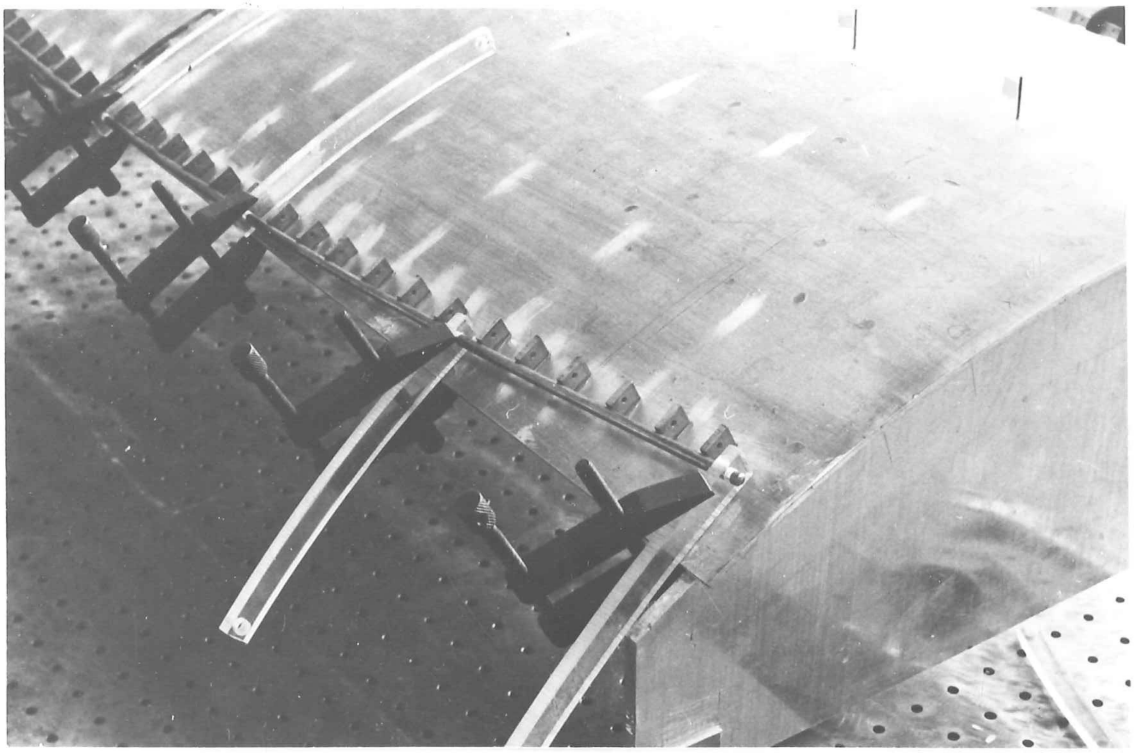

Fig. 8.1 Gluing guides to the extrados

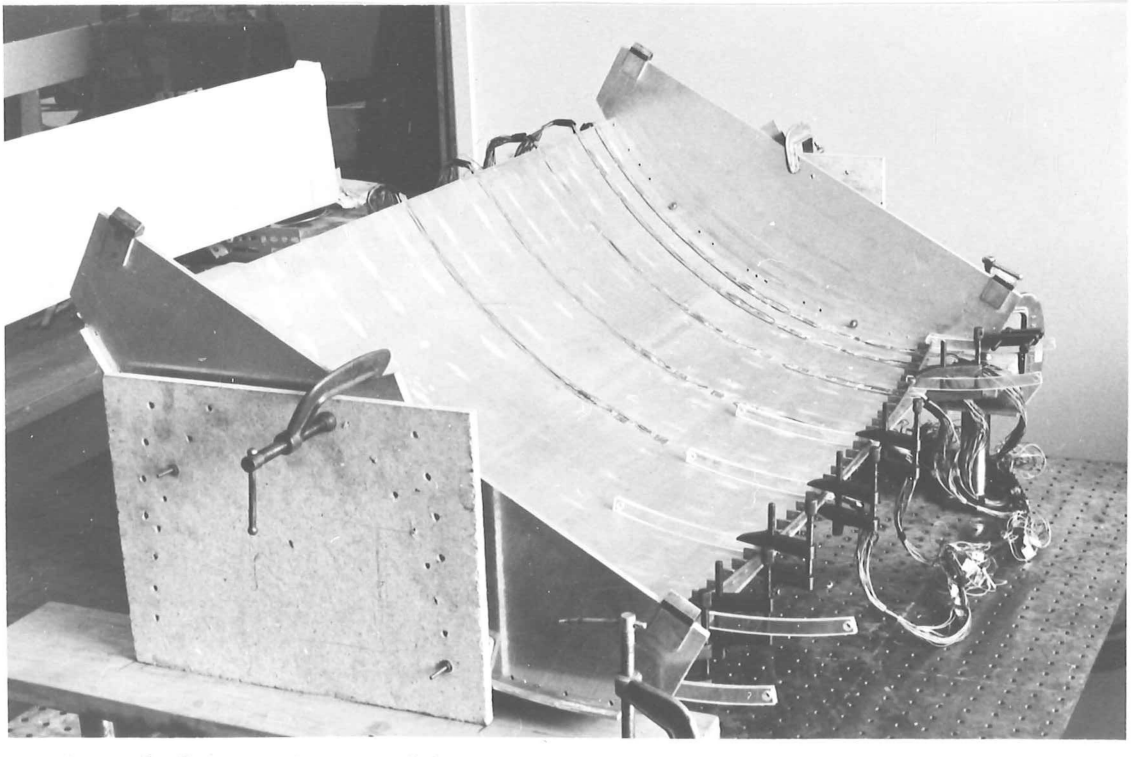

Fig. 8.2 Gluing guides to the intrados of the shell

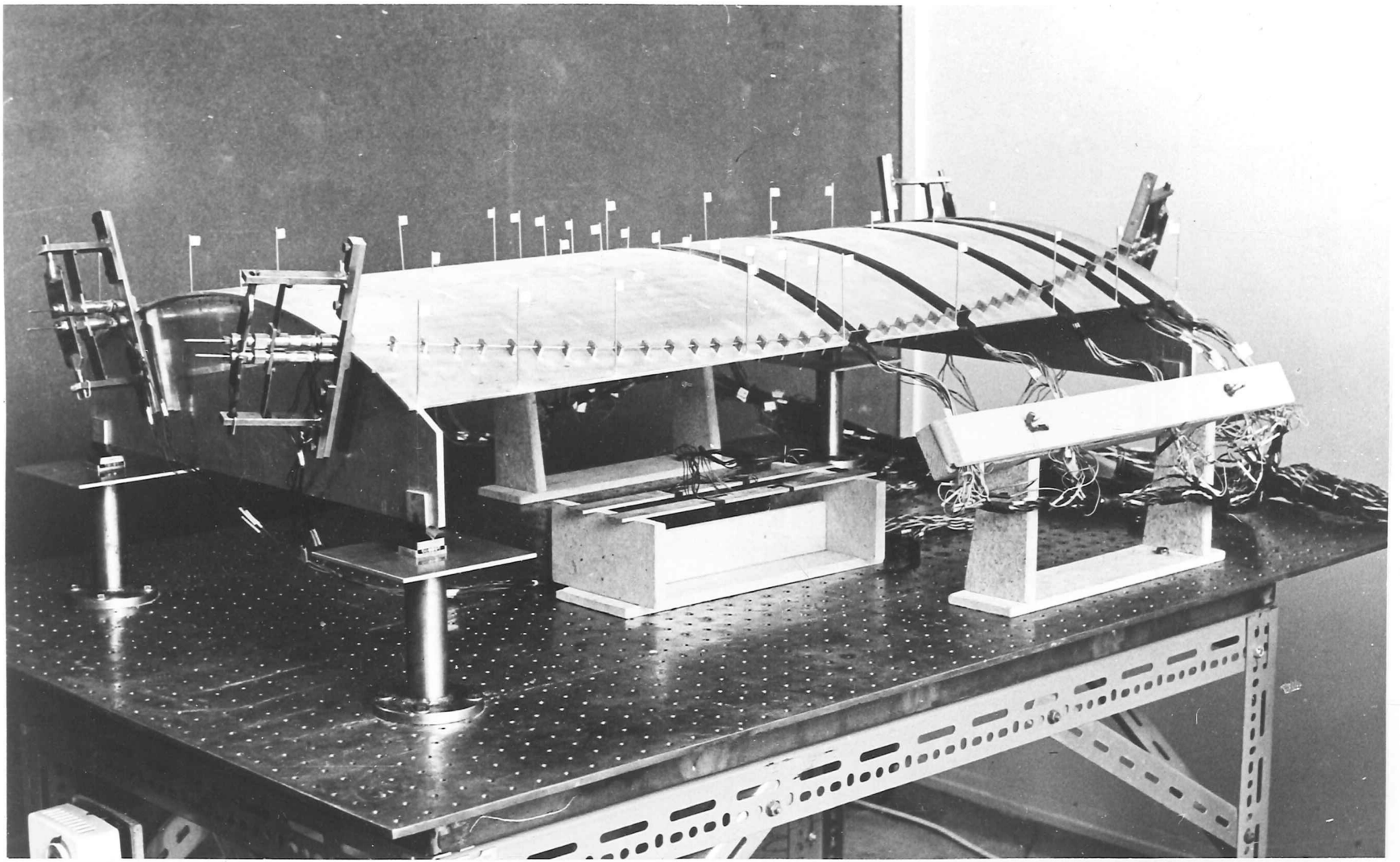

Fig. 8.3 Model shell ready for testing

Stage 2: The other end of each wire was jacked up (load increasing) or down (load decreasing) until the correct tension was indicated at that end. All the load cells were then read and any slight adjustments, if any, were made.

By this means the prestressing forces were set so that they were symmetrical about mid-span with an accurate measurement of the friction losses.

The repeatability, linearity, and the overall equilibrium of the experimental results show that the desired prestress was satisfactorily obtained at all times.

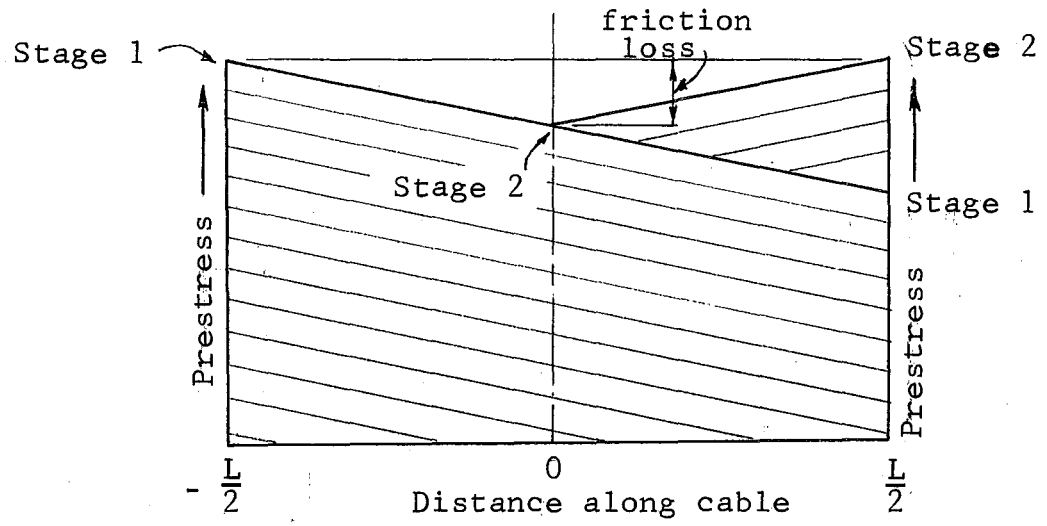

Fig. 8.4 Friction losses in prestressing cables

8.5 FRICTION LOSSES IN THE PRESTRESSING

For straight prestressing wires no noticeable friction losses were measured. As the drape of the prestressing wires was increased, the normal pressures between the guides and the wires increased, giving the expected increase in friction losses. In table 8.3 these friction losses are given. The coefficient of friction, calculated by numerical integration as described in section 5.1, remained reasonably constant at about 0.16.

Although included in the theoretical calculations, the effect of friction losses on the experimental stresses and deflections was slight. In model test 6 ($f = .138\, y_m$) the effects of cable friction were not noticeable on experimental stresses and deflections; in model test 7 ($f = 0.305\, y_m$) they were just noticeable on some readings; and in model test 8 ($f = 0.472\, y_m$) the friction effects accounted for a reduction in mid-span actions and deflections of about 3 or 4 percent corresponding to friction losses of 7 percent.

Model test	$\frac{f}{y_m}$	Prestress lb./wire	Loss lb./wire	Percentage Loss	Coefficient of friction
1 - 5	0	600	0	0	-
6	0.138	500	13	2.6	0.174
7	0.305	450	22.5	5.0	0.160
8	0.472	400	29	7.3	0.155

Table 8.3 Friction losses in prestressing wires

8.6 PROCESSING OF EXPERIMENTAL RESULTS

All experimental results were recorded directly on I.B.M. card punching detail sheets. These results were then punched onto cards. A series of three computer programs processed these results and ended up with experimental stresses and deflections.

Program RR1:

(a) Added a constant amount to all the strain or deflection readings at each prestressing load to allow for zero drift. These corrections were usually made only for deflection readings.

(b) Reduced all readings to an initial zero.

(c) Checked the deviations of readings from straight lines joining no load to the first full load readings. If these deviations exceeded the biggest of 5 μstrain or 5 per cent of the readings for strains, or 0.002" or 5 per cent of the readings for deflections, error messages were typed by the computer. This step was included so that reading or recording errors, such as a reversal of figures or 1999 instead of 1899, were eliminated although it did also check the linearity of experimental readings. Errors, if any, were manually corrected.

(d) Calculated a weighted mean of all the readings. Weights were proportional to the loads.

Program RR2:

(a) Compared the average readings from each test on the same model set-up. If the differences between readings exceeded the biggest of 5 μstrain or 5 per cent for strains, or 0.002" or 5 per cent for deflections, the readings were typed out by the computer. Recorded readings were checked, but no corrections were usually necessary.

(b) Calculated a weighted average of corresponding readings. Weights were obtained from a perusal of each day's test on each model set-up.

Program RR3:

(a) Solved for surface stresses and deflections and/or actions and deflections.

(b) Summed longitudinal thrusts and moments by integration of the 12th order polynomials through the actions at each transverse cross section.

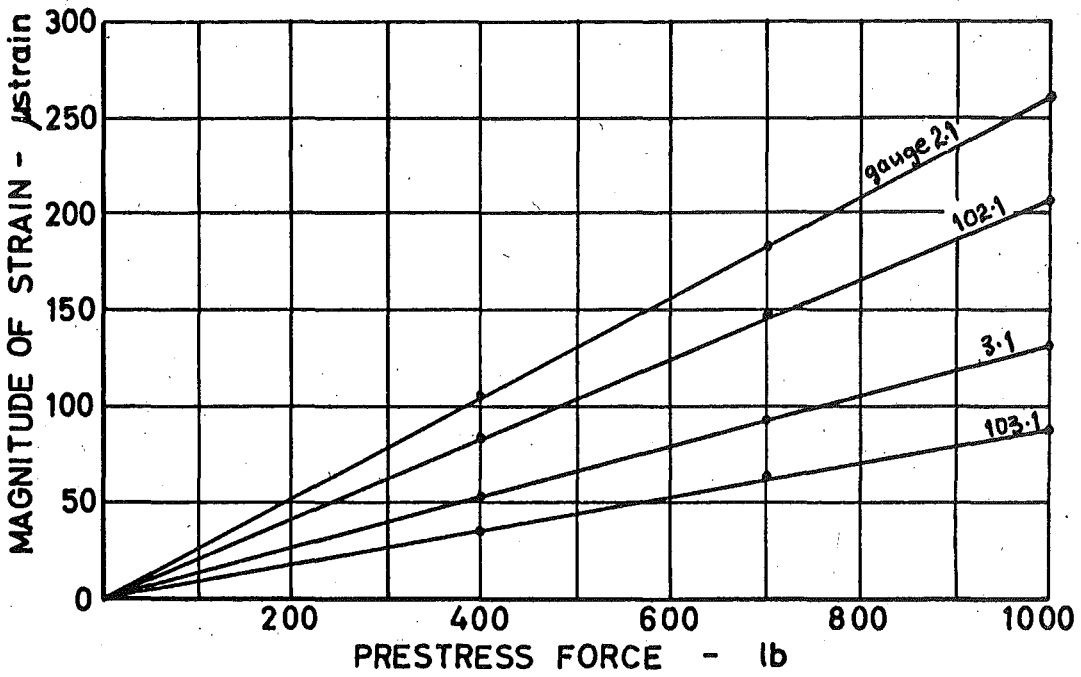

Fig. 8.5 Typical linearity of model behaviour - strains from model test 6A - dots are experimental readings

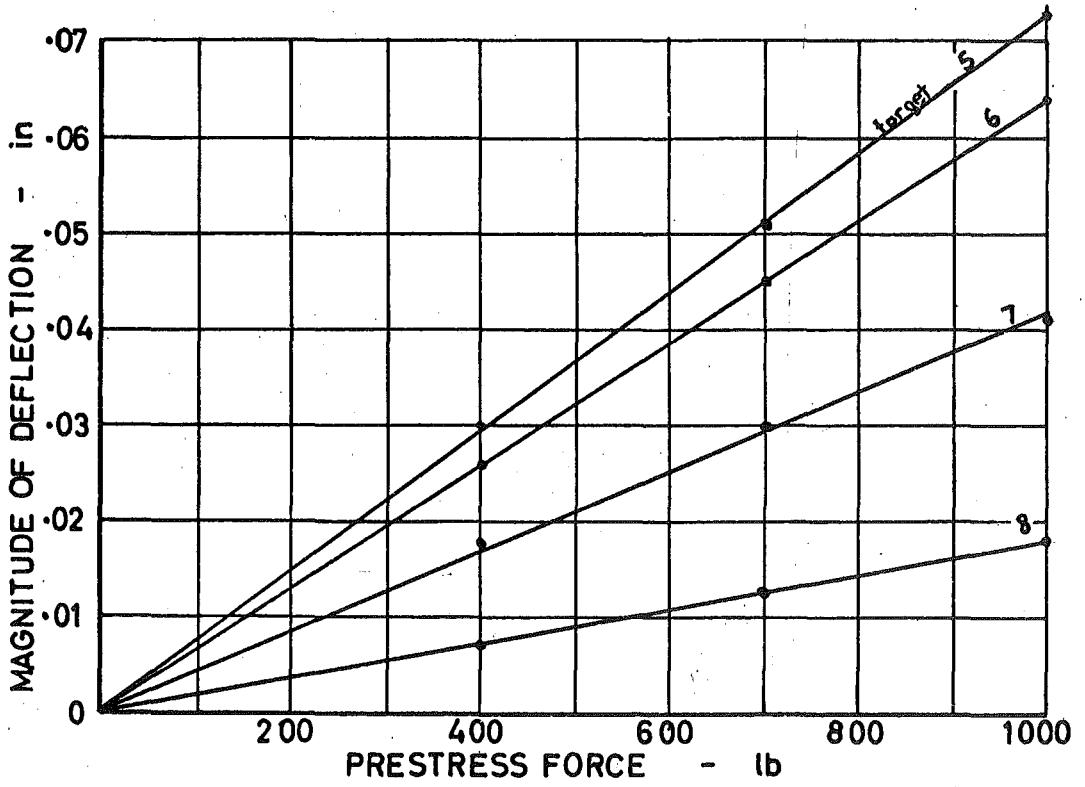

Fig. 8.6 Typical linearity of model behaviour - deflections from model test 6A - dots are experimental readings

8.7 LINEARITY OF MODEL BEHAVIOUR

In all the model tests no evidence of non-linear behaviour could be found. Tables 8.4 and 8.7 give a good indication of typical strain and deflection readings from a test with an A type loading pattern from which the linearity of results can be studied. The linearity of these results can be seen from figures 8.5 and 8.6 where a few of the readings are plotted against the prestressing loads. Any deviations off the straight lines can be attributed to inaccuracies of individual readings.

It should be commented that the loads and hence the deflections of the model were purposely kept low so that there would be little danger of non-linear behaviour from the changes in shell geometry as the loads were increased. One of the purposes of prestressing in a concrete structure is to reduce deflections. Therefore, a prestressed concrete shell, under normal working loads, is more likely to behave in a linear manner than a reinforced concrete shell.

8.8 ACCURACY OF EXPERIMENTAL READINGS

Tables 8.5 and 8.8 give an indication of the excellent repeatability of experimental readings under repeated applications of the prestressing loads. The accuracy of strain and deflection readings can best be judged from tables 8.6 and 8.9 where typical average readings from two different

P_a LB	1200	0	400	700	1000	1000	700	0
GAUGE	AVERAGE STRAIN	REDUCED STRAIN - MICROSTRAIN						
1 1	-522	0	-179	-305	-435	-434	-315	-5
1 2	146	0	50	80	117	116	82	-8
101 1	-451	0	-156	-266	-374	-374	-270	-3
101 2	139	0	47	76	114	114	80	-4
2 1	-313	0	-106	-183	-259	-258	-187	0
2 2	-27	0	-8	-18	-22	-22	-15	0
2 3	-19	0	-6	-12	-16	-16	-12	-1
102 1	-250	0	-85	-148	-207	-206	-151	-1
102 2	21	0	6	8	18	18	12	-1
102 3	-13	0	-5	-11	-9	-9	-8	0
3 1	-156	0	-54	-94	-130	-129	-95	-2
3 2	41	0	15	21	31	31	21	-5
103 1	-105	0	-36	-64	-87	-87	-64	-2
103 2	28	0	7	11	22	22	13	-5
4 1	-37	0	-11	-23	-29	-30	-23	1
4 2	26	0	9	12	22	22	14	-1
4 3	24	0	8	11	20	18	11	-3
104 1	-2	0	-1	-4	0	-1	1	1
104 2	-30	0	-10	-20	-23	-23	-16	2
104 3	-28	0	-9	-19	-21	-21	-14	2
5 1	29	0	11	15	24	25	18	0
5 2	72	0	24	39	59	59	41	-2
105 1	51	0	18	28	43	43	31	1
105 2	-98	0	-32	-58	-80	-80	-60	0
6 1	65	0	21	35	54	54	39	-1
6 2	93	0	32	52	77	78	55	-1
106 1	78	0	27	43	66	66	48	1
106 2	-132	0	-43	-78	-109	-108	-79	0
7 1	76	0	27	43	66	67	50	5
7 2	97	0	34	56	83	84	62	5
7 3	96	0	35	55	81	82	59	3
107 1	87	0	30	50	74	75	53	3
107 2	-88	0	-28	-53	-71	-70	-52	2
107 3	-88	0	-28	-53	-72	-70	-52	2

Table 8.4 Typical strain readings for load pattern A - from test 6A - output from program RR1

P_a LB	1200	0 1000	0 1000	0 1000	0
GAUGE	AVERAGE STRAIN	REDUCED STRAIN - MICROSTRAIN			
1 1	-524	0 -439	-3 -436	-3 -442	-3
1 2	147	0 121	-2 120	-4 118	-6
101 1	-452	0 -376	-4 -378	-3 -386	-4
101 2	143	0 119	0 118	0 119	-1
2 1	-314	0 -262	-2 -260	0 -264	0
2 2	-25	0 -23	-3 -21	-1 -23	1
2 3	-18	0 -16	-1 -15	-1 -17	-1
102 1	-248	0 -208	-2 -206	-1 -210	0
102 2	24	0 18	-2 20	-1 19	0
102 3	-11	0 -9	0 -7	2 -7	3
3 1	-154	0 -129	-1 -128	-1 -132	-2
3 2	40	0 32	-2 31	-3 29	-4
103 1	-104	0 -86	0 -86	0 -87	1
103 2	28	0 23	-1 24	-1 21	-2
4 1	-37	0 -31	0 -29	1 -30	3
4 2	26	0 22	0 23	1 23	2
4 3	25	0 20	-1 20	-1 20	0
104 1	-2	0 0	1 1	3 1	4
104 2	-29	0 -25	0 -22	2 -23	3
104 3	-26	0 -16	6 -14	8 -17	8
5 1	28	0 23	-1 23	0 23	1
5 2	74	0 60	-1 60	-2 61	-2
105 1	49	0 41	1 42	1 43	2
105 2	-97	0 -79	0 -80	1 -82	0
6 1	66	0 56	1 56	1 56	3
6 2	95	0 79	0 78	0 83	7
106 1	79	0 67	1 68	2 66	2
106 2	-133	0 -111	-2 -111	-1 -114	0
7 1	78	0 65	0 65	2 69	4
7 2	100	0 84	2 86	5 90	7
7 3	96	0 81	2 83	4 86	6
107 1	87	0 74	4 76	3 77	6
107 2	-89	0 -73	2 -71	1 -75	3
107 3	-90	0 -74	1 -71	3 -74	4

Table 8.5 Typical strain readings for load pattern B - from test 6B - output from program RR1

GAUGE	WEIGHTED AVERAGE STRAIN	AVERAGE STRAIN 6A	6B
1 1	-523	-522	-524
1 2	147	146	147
101 1	-452	-451	-452
101 2	142	139	143
2 1	-314	-313	-314
2 2	-26	-27	-25
2 3	-18	-19	-18
102 1	-249	-250	-248
102 2	23	21	24
102 3	-12	-13	-11
3 1	-155	-156	-154
3 2	40	41	40
103 1	-104	-105	-104
103 2	28	28	28
4 1	-37	-37	-37
4 2	26	26	26
4 3	25	24	25
104 1	-2	-2	-2
104 2	-29	-30	-29
104 3	-27	-28	-26
5 1	28	29	28
5 2	73	72	74
105 1	50	51	49
105 2	-97	-98	-97
6 1	66	65	66
6 2	94	93	95
106 1	79	78	79
106 2	-133	-132	-133
7 1	77	76	78
7 2	99	97	100
7 3	96	96	96
107 1	87	87	87
107 2	-89	-88	-89
107 3	-89	-88	-90

Table 8.6 Typical comparison of strains from two tests with different load patterns on same model - model test 6 - output from program RR2

P_a LB	1200	0	400	700	1000	1000	700	0
POINT	AVERAGE DEFLN	REDUCED DEFLN - 0.001 IN						
1	1	0	1	1	0	1	0	0
2	22	0	8	14	18	19	14	1
3	50	0	16	29	41	42	29	-1
4	80	0	28	48	66	67	47	0
5	87	0	30	51	72	73	50	-1
6	77	0	26	45	64	65	45	0
7	50	0	18	30	41	41	30	0
8	22	0	7	13	18	18	13	0
9	-1	0	0	0	-1	0	0	0

Table 8.7 Typical deflection readings for load pattern A - from test 6A - output from program RR1

P_a LB	1200	0	1000	0	1000	0	1000	0
POINT	AVERAGE DEFLN	REDUCED DEFLN - 0.001 IN						
1	0	0	0	0	0	0	0	-1
2	22	0	18	0	19	1	19	0
3	50	0	41	0	42	0	42	0
4	82	0	67	1	68	0	69	-1
5	87	0	72	0	73	1	73	-1
6	79	0	66	0	66	1	67	0
7	50	0	41	-1	41	0	41	0
8	21	0	19	2	20	2	19	1
9	0	0	0	1	0	2	1	1

Table 8.8 Typical deflection readings from load pattern B - from test 6B - output from program RR1

POINT	WEIGHTED AVERAGE DEFLN	AVERAGE DEFLN 6A	6B
1	0	1	0
2	22	22	22
3	50	50	50
4	81	80	82
5	87	87	87
6	78	77	79
7	50	50	50
8	21	22	21
9	0	-1	0

Table 8.9 Typical comparison of deflections from two tests with different load patterns on same model - model 6 - output from program RR2

tests, with different prestressing load patterns, on the same model set up are compared. The weighted average strain readings are usually within 1 or 2 μstrain of the individual averages from the different tests and the deflections are to the nearest 0.001".

Table 8.10 gives an indication of the overall experimental accuracy, as determined from equilibrium between internal actions and external applied prestressing loads. A full listing of these results is given in appendix V. At cross sections A, B, and C the agreement is usually within 3 per cent. The figures for the internal thrust and moment at cross section E are rather pointless because the polynomial through all the actions is not a good approximation of the action profile when one action is so much bigger than all the others.

Cross section	Longitudinal thrust - lb.			Longitudinal moment - lb.in.		
	Applied loads	Internal Actions	% diff.	Applied Loads	Internal Action	% diff.
A	1169	1172	0.3	-1920	-1925	0.3
B	1177	1229	4.4	-1854	-1821	1.8
C	1183	1221	3.2	-1632	-1651	1.2
D	1186	1178	0.7	-1405	-1387	1.3
E	1187	1302	9.7	-1271	-1462	14.7

Table 8.10 Typical equilibrium between applied loads and internal actions - from test 6

8.9 SYMMETRY OF MODEL BEHAVIOUR

During all the tests the model shell behaved symmetrically as can be seen from:

(a) Readings of delta rosette strain gauges placed along the crown and at mid-span of the shell. Gauges 2 and 3 of these rosettes were symmetrically placed about the centre-lines and their readings should be similar as is shown in table 8.11 where the readings of gauges 2 and 3 of these rosettes are generally within 2 or 3 μstrain of each other. The differences can be accounted for by the experimental accuracy of the orientation of the rosettes on the shell surface.

(b) Vertical deflection readings recorded from all quarters of the shell. In table 8.12, where the deflection of points symmetrically placed about the crown and/or mid-span are listed together, it can be seen that the deflection of corresponding points are usually within 0.002" of each other.

Rosette	Gauge μstrain			Rosette	Gauge μstrain		
	1	2	3		1	2	3
2	-314	-26	-18	102	-249	23	-12
4	- 37	26	25	104	- 2	-29	-27
7	77	99	96	107	87	-89	-89
14	69	87	85	114	- 90	-77	-75
21	56	60	61	121	74	-53	-56
28	32	41	41	128	42	-29	-31
35	-13	13	13	135	42	- 4	- 5

Table 8.11 Typical strain readings showing symmetrical behaviour - readings 2 and 3 of each rosette should be the same - from test 6

Vertical deflection - 0.001"							
0 0 0 0	22 21 20 20	50 50 48 49	81 78 81 81	87 90			along straight edges, diaphragms to mid-span
0 -1	10 10	17 18	25 25	26			along crown, diaphragms to mid-span
87 90	75 78	62 62	49 49	37 36	29 29	26	across mid-span, straight edges to the crown

Table 8.12 Typical deflection readings from points symmetrically placed about the crown and/or midspan - readings from corresponding points are grouped together - from test 6

CHAPTER NINE

EXPERIMENTAL AND THEORETICAL RESULTS FOR THE MODEL SHELL

9.1 GENERAL DETAILS OF RESULTS

The theoretical results given here have been obtained from the generator line-load computer program, described in chapter 5 along with a discussion of the numerical details of the solutions which can be summarised as follows:

(a) Anchorage loads were taken as the sum of the first 10 terms (n = 1,19) of the Fourier series expansion of equivalent block shear loads spread a distance 0.05L into the shell along two generators at ½" spacing passing through the anchorages.

(b) Curvature loads were considered to be equal to the sum of the first 6 terms (n = 1,11) of Fourier series expansions of actions spread along generators at about 1.7" spacing.

In figures 9.1 to 9.8 experimental results for P_a = 1200 lb., are plotted against theoretical solutions. The longitudinal stresses are plotted to one half the scale of the transverse and shear stresses. Full listings of experimental readings, experimental actions and deflections, and theoretical actions and deflections are given in appendix V.

Frequent references are to be made to the strain gauged transverse cross sections A - E. For easy reference, they are given again in table 9.1. Deflection readings were taken at targets displaced ½" further from mid-span than the strain gauged cross sections.

Cross section	Distance from mid-span	
	x - ins.	x/L
A	0.00	0.000
B	6.06	0.154
C	12.06	0.308
D	16.06	0.411
E	18.06	0.462

Table 9.1 Positions of strain gauged cross sections on the model

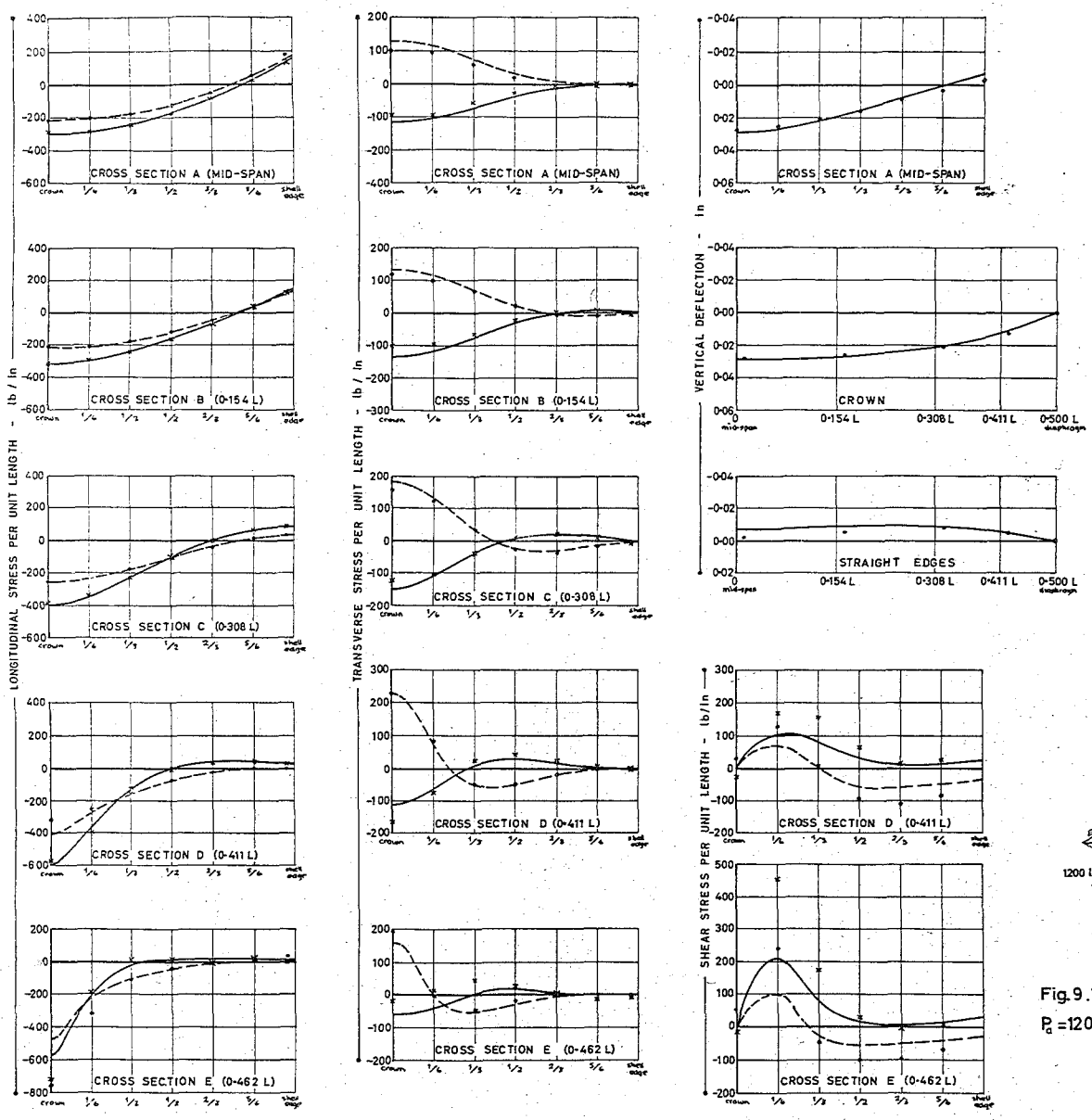

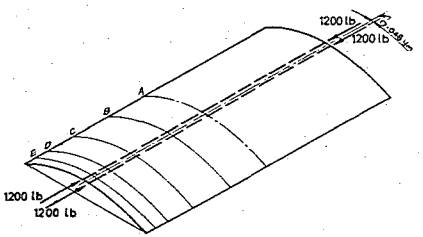

Fig. 9.1 Stresses and deflections for test 1.
P_a = 1200 lb, P_f = 0 lb, d = 0·048 y_m, f = 0 y_m

Intrados	theory	———
	exp.	• • •
Extrados	theory	———
	exp.	× × ×

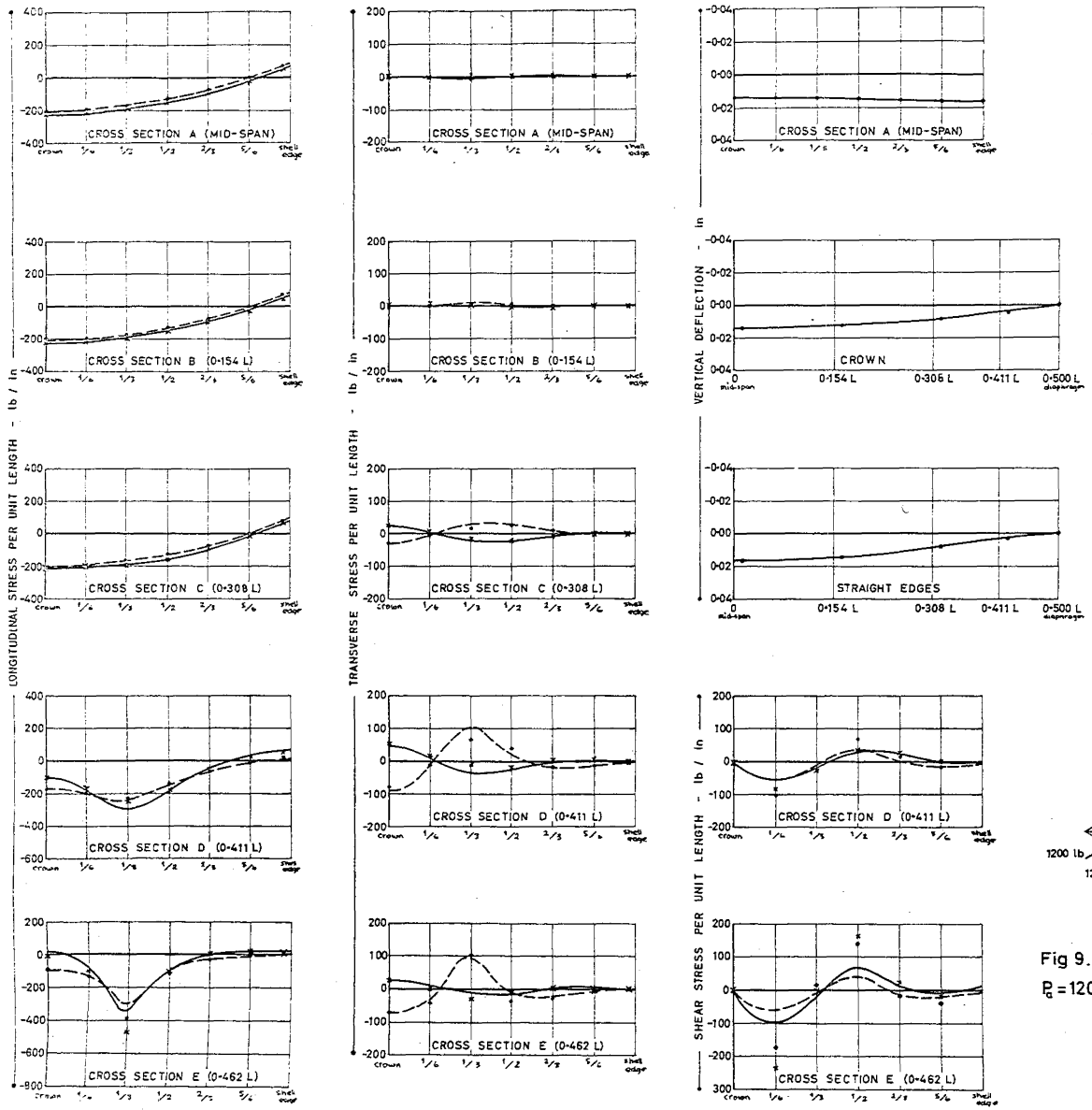

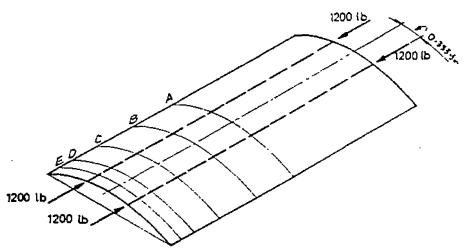

Fig 9.2 Stresses and deflections for test 4.
P_a = 1200 lb, P_f = 0 lb, d = 0·333 y_m, f = 0 y_m.

Intrados	theory
	exp.
Extrados	theory
	exp.

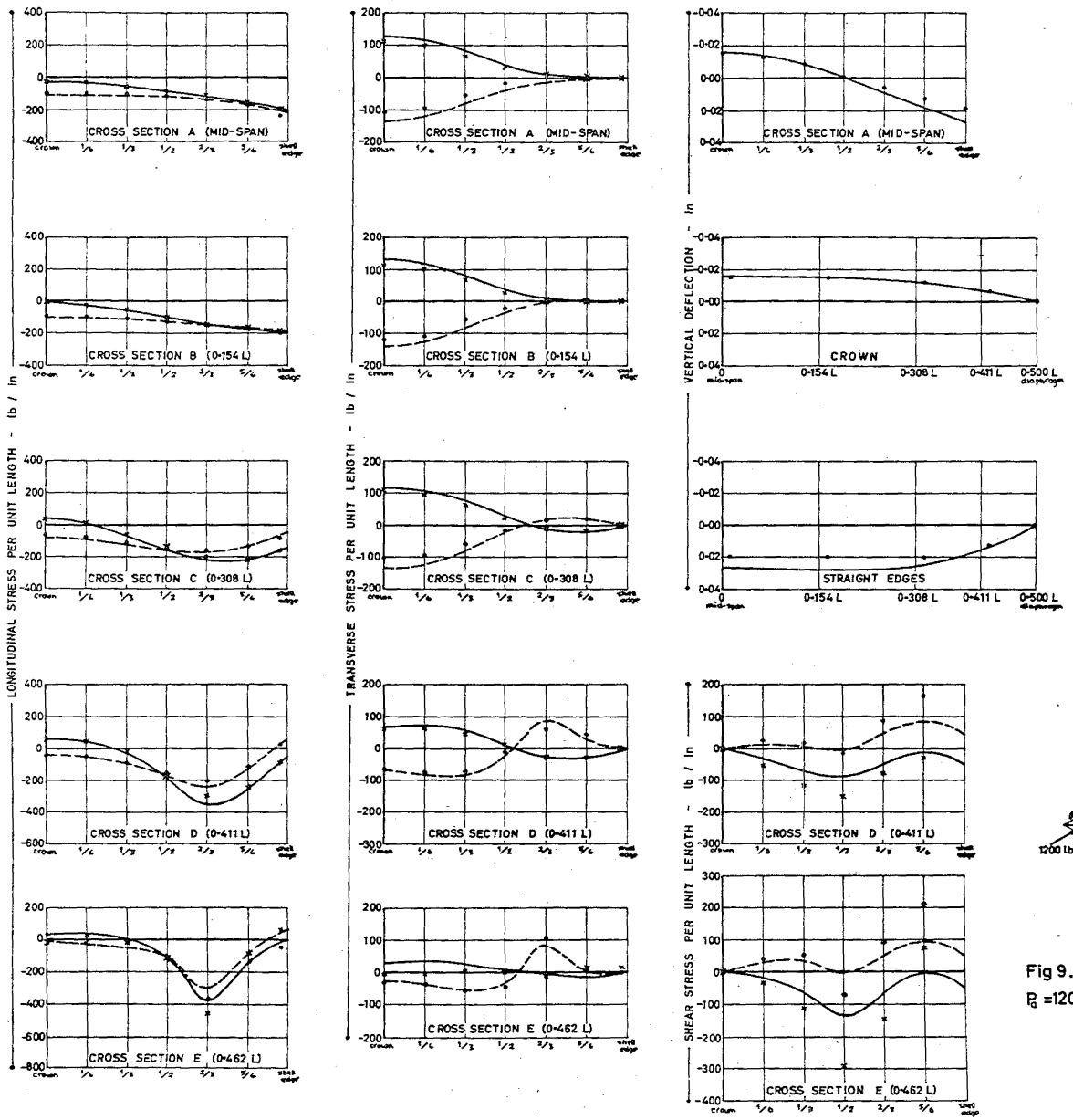

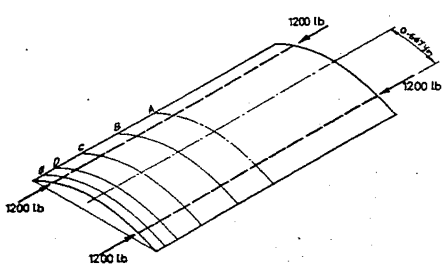

Fig 9.3 Stresses and deflections for test 3.
P_a =1200 lb, P_f=0 lb, d = 0·667 y_m , f = 0 y_m

Intrados	theory	-------
	exp.	• • •
Extrados	theory	———
	exp.	× × ×

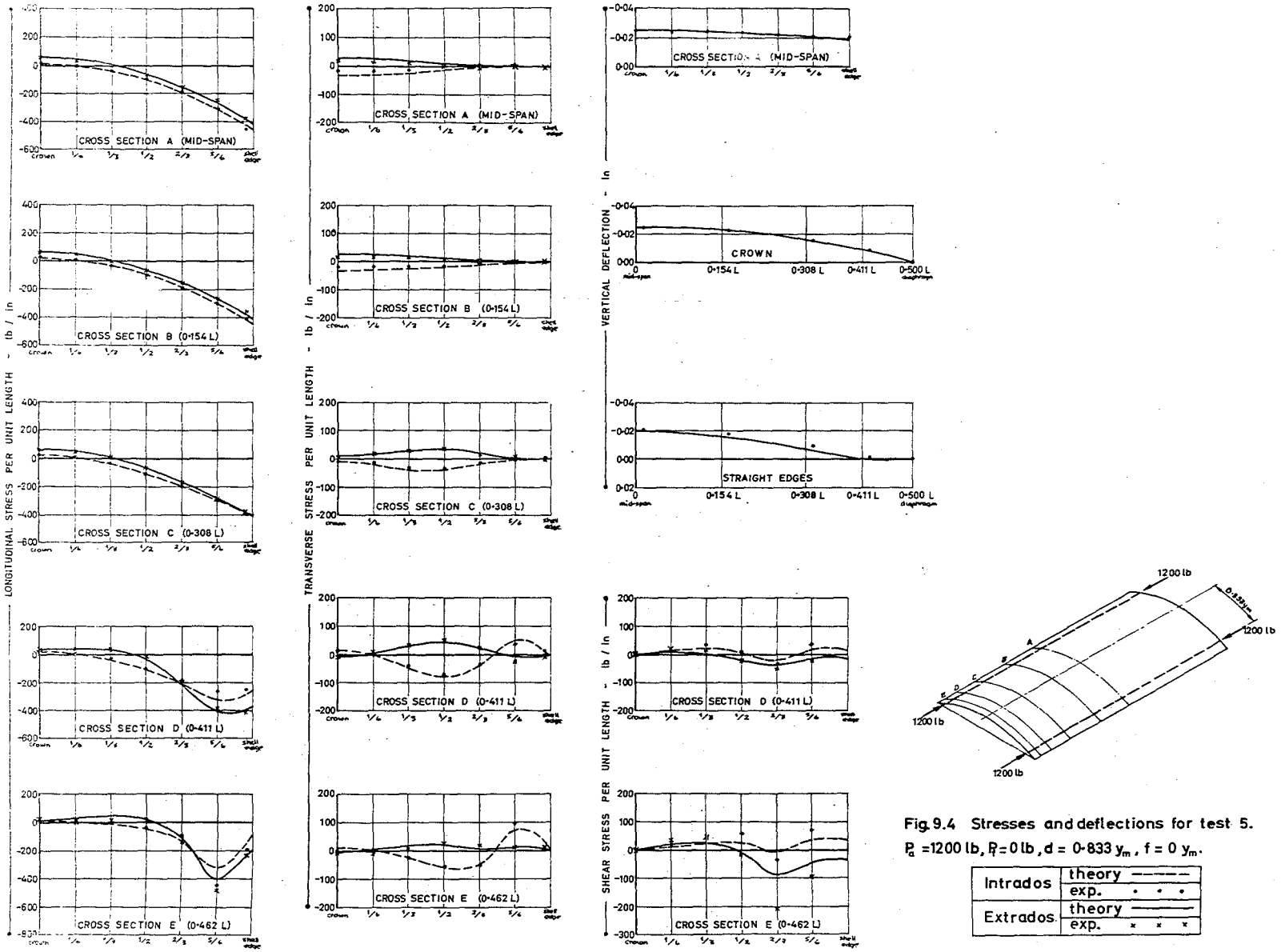

Fig. 9.4 Stresses and deflections for test 5.
P_a = 1200 lb, P_r = 0 lb, d = 0·833 y_m, f = 0 y_m.

Intrados	theory ———
	exp. · · ·
Extrados	theory ———
	exp. × × ×

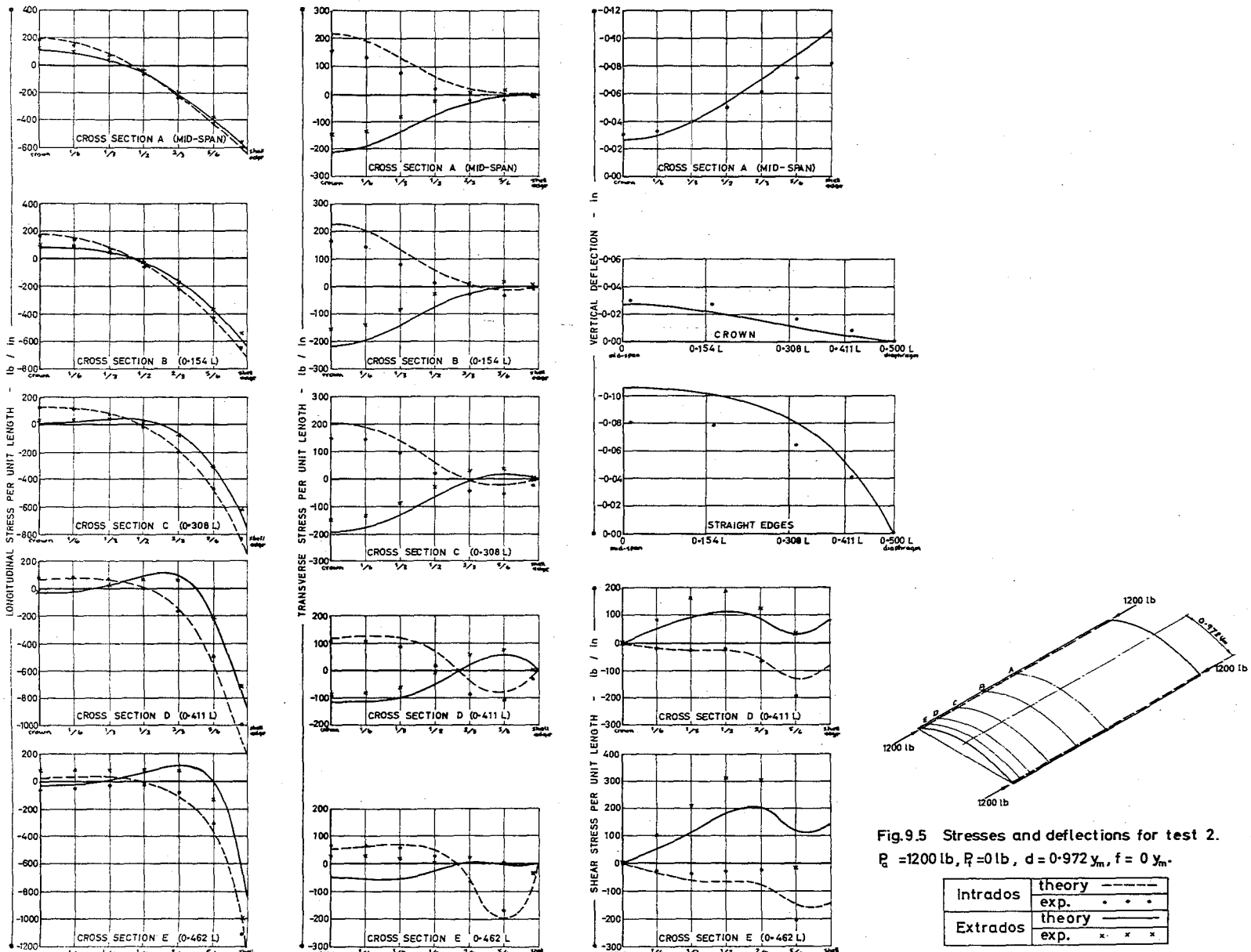

Fig. 9.5 Stresses and deflections for test 2.
P_a = 1200 lb, P_t = 0 lb, d = 0·972 y_m, f = 0 y_m.

Intrados	theory ———
	exp. · · ·
Extrados	theory ———
	exp. × × ×

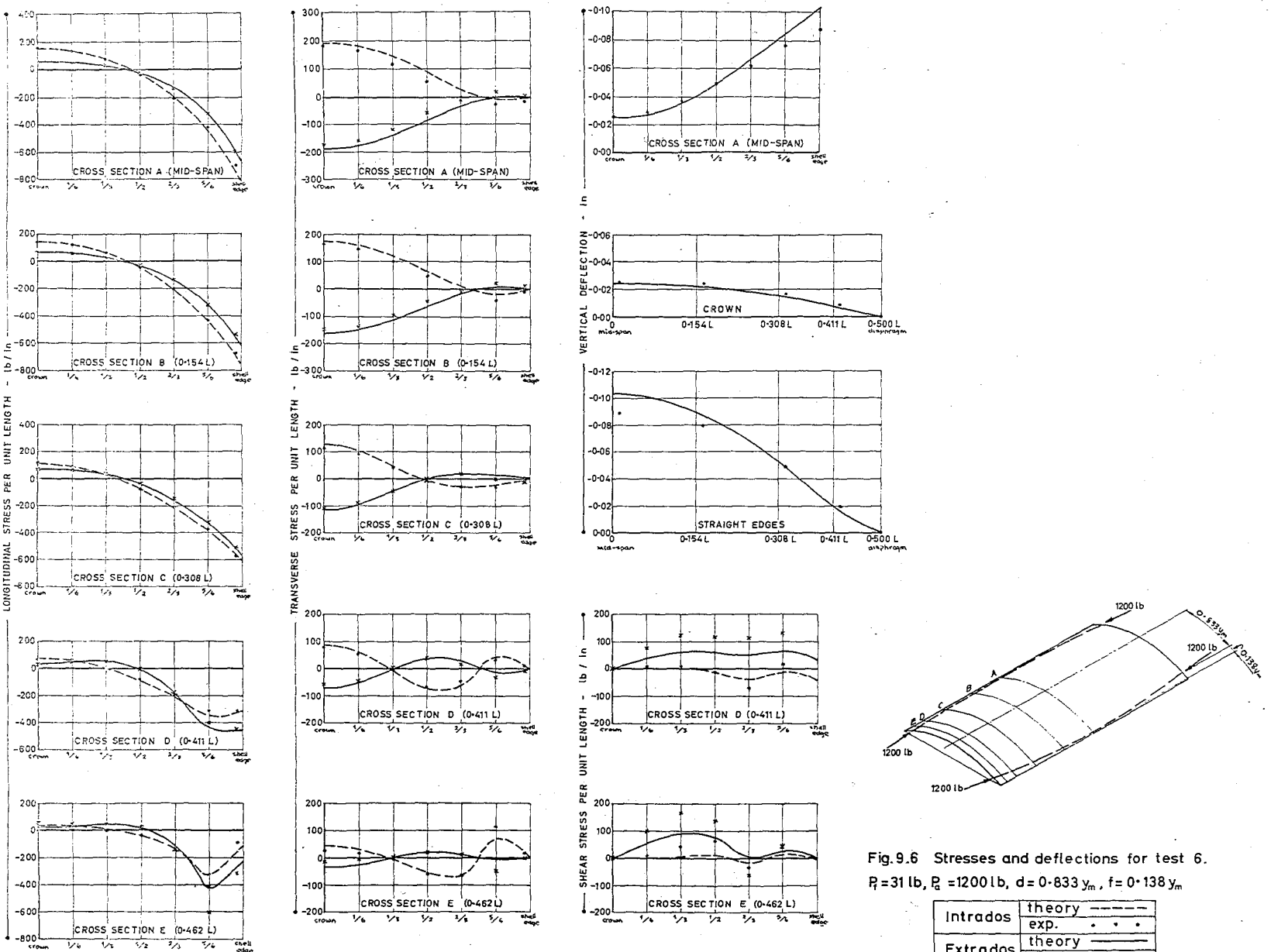

Fig. 9.6 Stresses and deflections for test 6.
P_t = 31 lb, P_a = 1200 lb, d = 0·833 y_m, f = 0·138 y_m

Intrados	theory ———
	exp. • • •
Extrados	theory ———
	exp. × × ×

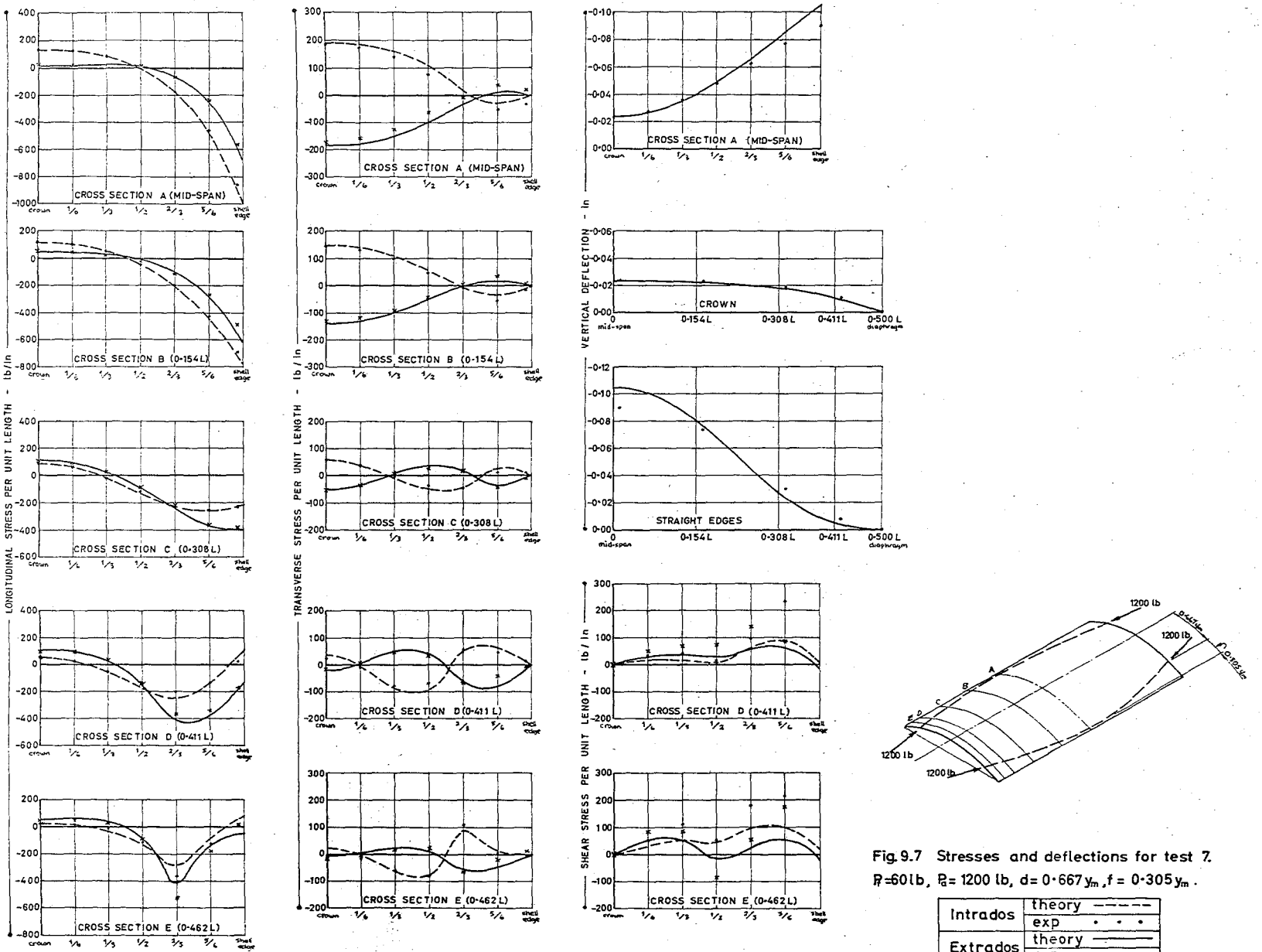

Fig. 9.7 Stresses and deflections for test 7.
R=60 lb, P_a= 1200 lb, $d = 0{\cdot}667\,y_m$, $f = 0{\cdot}305\,y_m$.

Intrados	theory ———
	exp • • •
Extrados	theory ———
	exp × × ×

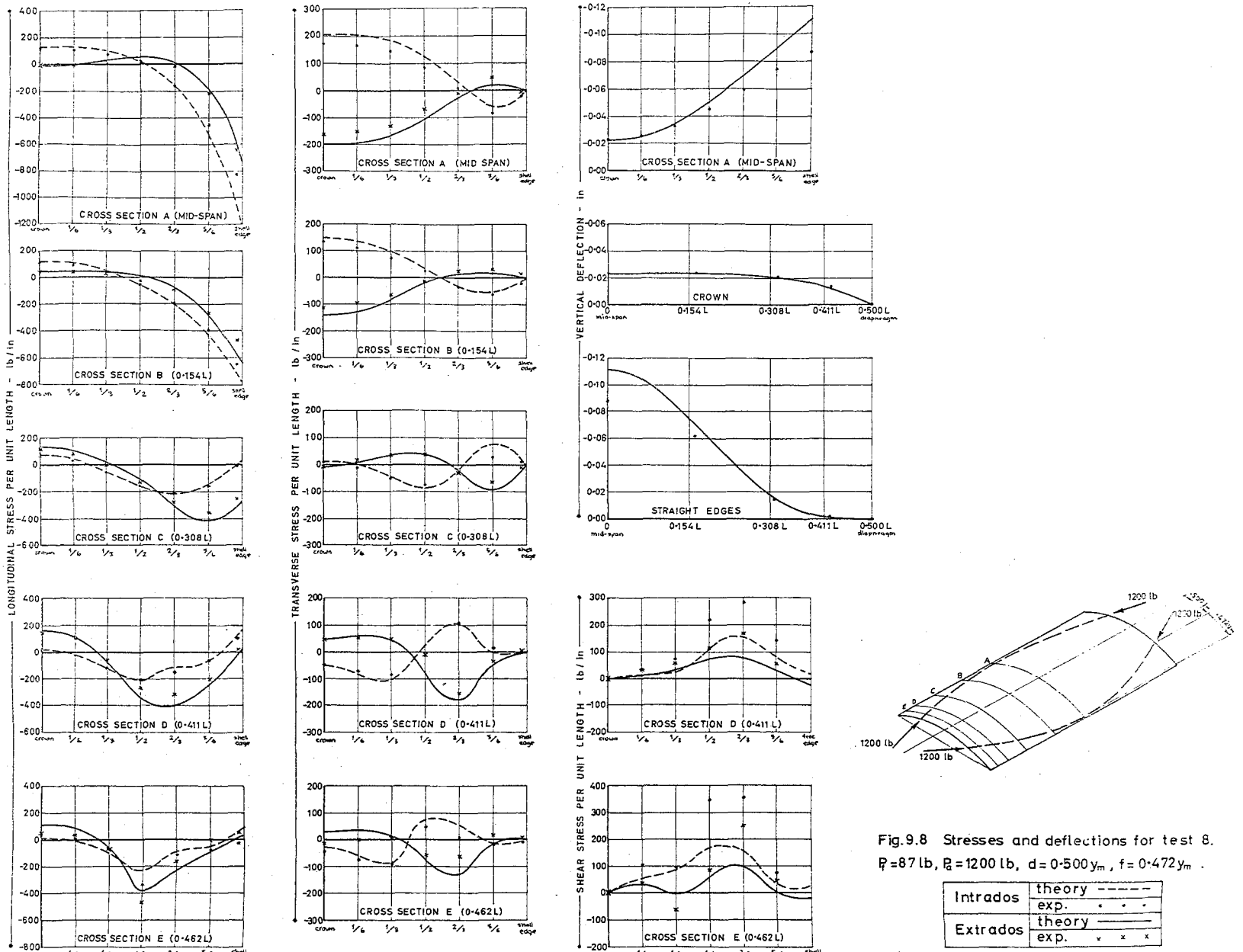

Fig.9.8 Stresses and deflections for test 8.
P_1=87 lb, P_2=1200 lb, d=0·500y_m, f=0·472y_m.

Intrados	theory -----
	exp. · · ·
Extrados	theory ——
	exp. × × ×

9.2 AGREEMENT BETWEEN THEORY AND EXPERIMENT

9.2.1 Longitudinal stresses

At cross sections A, B, and C there is perfect agreement between theory and almost all of the experimental longitudinal stresses. The direct as well as the longitudinal bending moment stresses are accurately forecast by the theory.

At cross sections D and E the agreement is not quite so good. Consider the sum of the terms of the Fourier series used to apply the anchorage loads as shear actions (see figure 5.5). At cross section E the Fourier series has not applied all the shear load and, as expected, the theoretical longitudinal stresses are rather low. At cross section D, where more than the correct shear stress has been applied by the Fourier series, the theoretical longitudinal stresses are rather high.

9.2.2 Transverse stresses

At all the strain gauged cross sections the theoretical solutions showed all the surprisingly frequent changes in sign of the experimental transverse moments and also obtained reasonable estimates of their magnitudes.

At cross sections A, B, and C, for tests where there were appreciable transverse moments at mid-span, the theoretical solutions tended to overestimate the transverse stresses by about 10 per cent.

At cross sections D and E the agreement between theory and experiment was better than expected, with the theoretical transverse stresses frequently being within a few per cent of the experimental stresses.

9.2.3 Vertical deflections

The theoretical and experimental deflections always showed similar trends. A comparison between figures 9.10 and 9.13 clearly shows the expected relationship between the mid-span deflections and the mid-span transverse moments.

For the tests where the mid-span prestressing cable positions were at the free edges (shell edges deflected by far the most for these cases) the theoretical deflections were some 10 to 25 per cent greater than the experimental deflections. Possibly, it could be argued, these low experimental deflections and corresponding mid-span transverse moments were a result of the change in cross sectional shape at mid-span as the free edges lifted more than the crown. This would give a smaller than theoretical eccentricity of the prestressing cables from the centroid of the transverse cross section with a lower than theoretically applied prestressing moment. In this case the shell would behave in a non-linear manner. No such non-linear effects were noticed. Model set-up 2 was tested with the shell edges bowed up about $\frac{1}{8}$" (as manufactured, see section 6.3.1) and with initially straight free edges. There was a difference

of less than 3 per cent between these two tests for most of the actions and deflections. Thus, the changes in cross sectional shape as the shell deflects, are very unlikely to account for even 3 per cent of the differences between theory and experiment because the experimental deflections were less than $\frac{1}{8}$".

For all other tests (mid-span prestressing cable positions not at the shell edge), where the deflections were generally much smaller, the theoretical deflections were usually within a few per cent of the experimental deflections.

9.2.4 Shear stresses

At cross sections D and E, shear stresses were obtained from the strain readings of the triple rosette strain gauges. These experimental shear stresses tended to be about twice the theoretical values.

In the vicinity of the anchorages the theoretical shear stresses are greatly affected by applying the anchorage loads as shear actions and not boundary forces. The number of terms considered and the particular Fourier series chosen greatly affects these disturbances to the shear stresses. The assumption of a diaphragm support at the ends of the shell will also make theoretical actions in the vicinity of the diaphragms open to question.

The experimental shear stresses are also the least accurate of the given experimental stresses (see appendix III) although this is unlikely to explain why all the experimental shear stresses are high.

9.2.5 Principal stresses

Instead of longitudinal, transverse, and shear stresses, principal stresses and their directions could have been considered. Using principal stresses is just another way of describing the same state of stress that is described by longitudinal, transverse, and shear stresses, and, as such, suffers from the same theoretical and experimental limitations. Longitudinal, transverse, and shear stresses have been used because the theory works directly in these stresses; longitudinal and transverse stresses were the only strains measured over much of the shell surface; and easier comparisons between the stresses at different points or cross sections can be made if stresses in fixed directions are considered.

However, a simple computer program was written to calculate principal stresses from longitudinal, transverse and shear stresses. In table 9.2 a sample set of theoretical and experimental principal stresses is given.

Of interest is the agreement in direction of the principal stresses between theory and experiment, and the large differences in direction between the principal stresses on the intrados

	Gauge		On the intrados			On the extrados		
			θ degrees	p_1 lb./in	p_2 lb./in	θ degrees	p_1 lb./in	p_2 lb./in
Cross section D	23	Exp	93	34	-318	108	12	-441
		Theor	89	48	-348	99	-4	-446
	24	Exp	68	-13	-218	114	67	-238
		Theor	76	-56	-205	103	41	-169
	25	Exp	51	-57	-84	129	141	-102
		Theor	64	-63	-81	129	89	-47
	26	Exp	147	13	-14	141	151	-99
		Theor	147	5	1	147	94	-51
	27	Exp	131	60	44	150	89	-87
		Theor	96	64	51	160	58	-67
	28	Exp	90	78	66	179	37	-59
		Theor	90	86	66	0	36	-69
Cross section E	30	Exp	95	119	-407	95	-44	-612
		Theor	93	75	-325	94	-1	-426
	31	Exp	67	-48	-141	70	35	-156
		Theor	76	-58	-130	92	12	-91
	32	Exp	140	24	-108	134	158	-125
		Theor	137	-34	-65	134	102	-60
	33	Exp	136	33	-49	138	194	-151
		Theor	136	3	-8	140	105	-72
	34	Exp	110	21	-10	142	131	-84
		Theor	81	31	23	147	56	-58
	35	Exp	90	26	-8	179	52	-10
		Theor	90	42	31	0	15	-32

Table 9.2 Comparison of theoretical and experimental principal stresses

model test 6, $d = 0.833\ y_m$, $f = 0.138\ y_m$,

θ = angle between x axis and p_1 direction, measured from x to y axes

p_1, p_2 = principal stresses per unit length

and the extrados of the shell due to large twisting moments.

A reasonable estimation of the sizes and the direction of the principal stresses near the diaphragms could be obtained from the theoretical solution if the known theoretical limitations of the solutions are kept in view.

9.3 MODEL SHELL BEHAVIOUR

Unless otherwise specified the discussion in this section refers to experimental results from the model tests. Theoretical results would bring out the same points with slightly different values to the stresses and deflections.

9.3.1 Longitudinal stresses

A study of the longitudinal stresses at the five strain gauged cross sections shows the expected progressive changes along the length of the shell. Near the diaphragms the effect of the anchorage loads is clearly visible and the longitudinal stresses are reminiscent of point loads on the ends of slabs. At mid-span, the longitudinal stresses have become similar to those of a prestressed beam with overall bending plus axial compression stresses predominating.

The stresses from longitudinal bending moments are generally small compared with the axial compressive stresses existing over most of the shell surface.

For straight cable prestressing the direct longitudinal stresses at cross section A (mid-span) and B (0.154 L) were close to those predicted by the beam theory as is shown in table 11.1. But, as the drape of the prestressing cables was increased, the longitudinal stresses became less like those predicted by beam theory. The beam theory implies that all the draped cable tests would have similar mid-span longitudinal stresses because all the mid-span cable positions were the same. This was not the case as can be seen from figure 9.9. For $d = 0.500y_m$, $f = 0.472y_m$ the free edge longitudinal stresses are 1½ times those for $d = 0.972y_m$, $f = 0$.

9.3.2 Transverse stresses

The variation of transverse moments with the positions of the prestressing cables is surprising. Figure 9.10 shows the mid-span transverse moment profiles for each of the straight cable tests and in figure 9.11 the mid-span crown transverse moments are plotted against the mid-span prestressing cable positions. Figure 9.12 shows the distribution of crown transverse moments for the straight cable tests and indicates that the mid-span transverse moments do not necessarily bear any relationship to the transverse moments near the diaphragms.

For the draped cable tests, the mid-span transverse moments have similar profiles (a coincidence as the theoretical analysis of shells of other lengths did not show this similarity,

section 10.2) with the sign change of moment near the straight edges becoming more pronounced as the drape increases. At other cross sections the moments change so much that simple trends are not obvious.

9.3.3 Vertical deflections

Figure 9.13 shows the mid-span deflection profiles for the straight cable tests and in figures 9.14 and 9.15, where the crown and straight edge deflections are plotted against the prestressing cable positions and the applied prestressing moments, the correspondence between mid-span deflections and applied prestressing moment is easily noticeable. In figures 9.16 and 9.17 the crown and free edge longitudinal deflection profiles for the straight cable tests are drawn. The free edge deflection for $d = 0.972y_m$ is of particular interest as it is 4 times that for $d = 0.833y_m$ for an applied moment of 1.7 times as much. For $d = 0.667y_m$ the deflection of the free edge at $\frac{1}{4}$ span is greater than that at mid-span.

The mid-span deflections are essentially the same for all the draped cable tests and the longitudinal deflection profiles of the crown are similar. As the drape increases the applied moment, at cross sections away from mid-span, decreases. The effect of this reduction in moment can be seen from the deflection profiles of the straight edges as shown in figure 9.18. The longitudinal deflection profiles of the

straight edges become less like those for a prestressed beam as the drape increases. This correlates with the changes in mid-span longitudinal stresses from those predicted by beam theory.

9.3.4 Shear stresses

From test to test, and from gauge to gauge during each test, the shear stresses varied considerably. Bearing in mind the limitations in the measurement of these shear stresses and in the method of theoretical analysis of the prestressed shells (discussed in section 9.2.4), it is rather difficult to make any worthwhile comments.

There seemed to be no connection between the magnitude and distribution of the shear stresses as the prestressing was varied. In the draped cable tests the prestressing applied membrane loads to the shell in the directions of the x and y axes. The effects of these loads were not noticeable in the shear stresses. The shear stresses for the tests with $f = 0.472y_m$ and $f = 0.0y_m$ were higher than those for $f = 0.305y_m$ and $f = 0.138y_m$.

9.4 CONCLUSIONS FROM THE MODEL TESTS

From the aluminium alloy model cylindrical shell with piano wire prestressing, accurate experimental strains and deflections, and hence stresses and deflections, could be and were obtained from a variety of prestressing cable lay-outs.

Replacing the loads on a shell from prestressing cables within the curved surface by actions spread along generators is a satisfactory method of considering the loads so that the D.K.J. equation can be solved and theoretical stresses and deflections obtained.

Deflections and direct stresses obtained from such solutions agreed well with the experimental values. Because diaphragms were assumed at the shell ends and the anchorage loads were applied as shear actions and not boundary stresses, the theoretical shear stresses, in the vicinity of the diaphragms, were not estimated particularly well by the theoretical solutions. One must remember that the stresses at the anchorages are predominantly compressive stresses resulting from the high anchorage point loads and not shell action. Also, the shear stresses are a small part of the total stresses as can be seen from a study of the principal stresses.

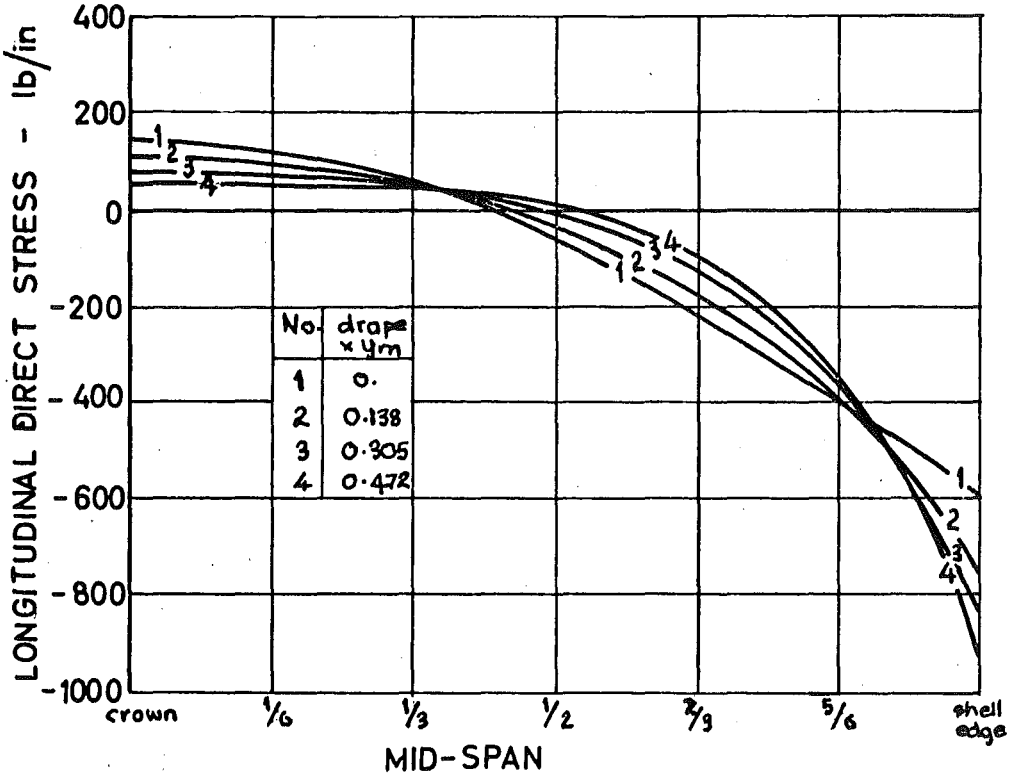

Fig. 9.9 Mid-span longitudinal stresses from the draped cable tests - P_a = 1200 lb.

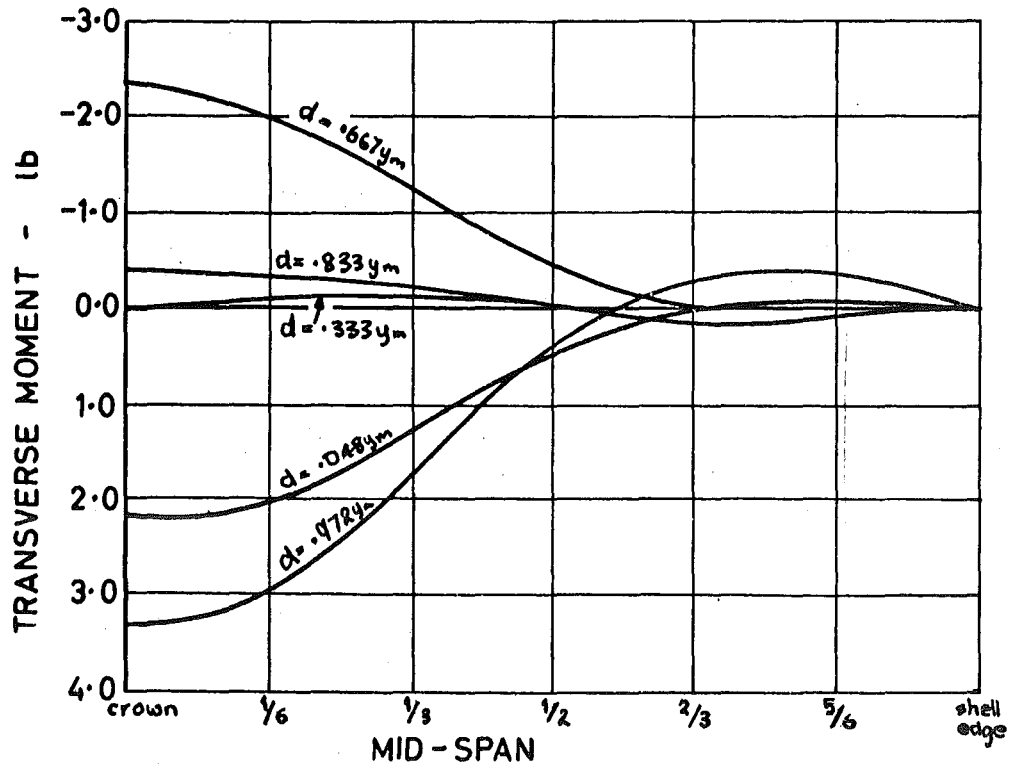

Fig. 9.10 Mid-span transverse moments for straight cable tests - P_a = 1200 lb.

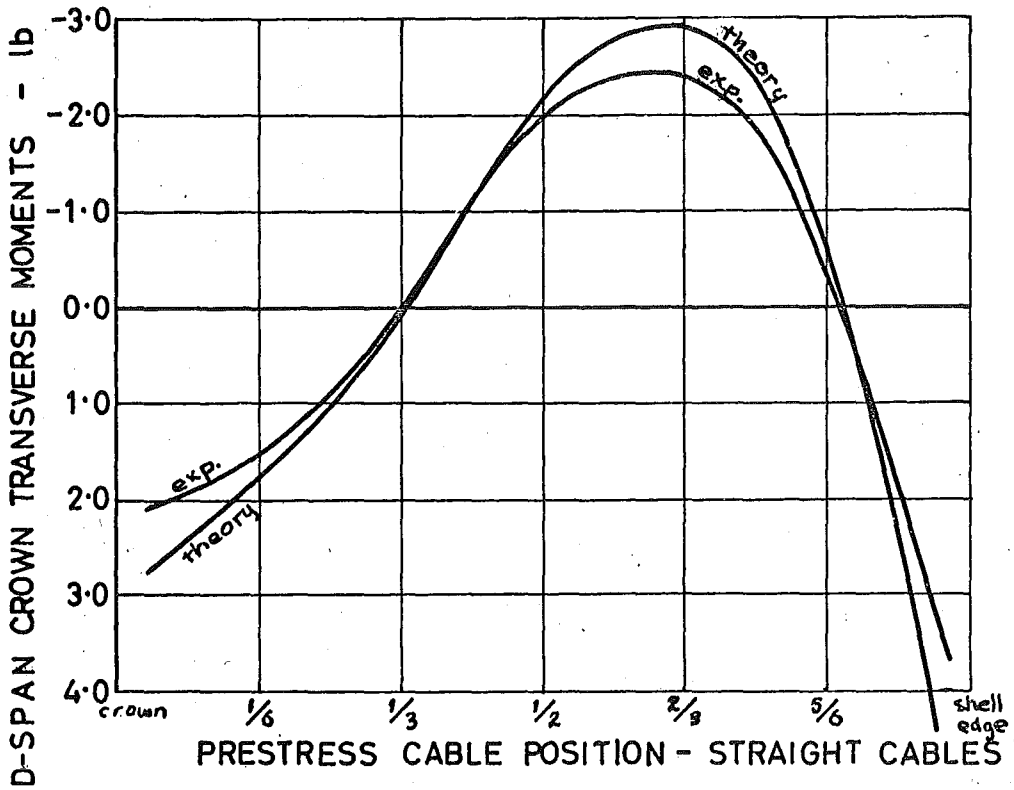

Fig.9.11 Variation of mid-span crown transverse moments with cable position - straight cables, P_a =1200 lb

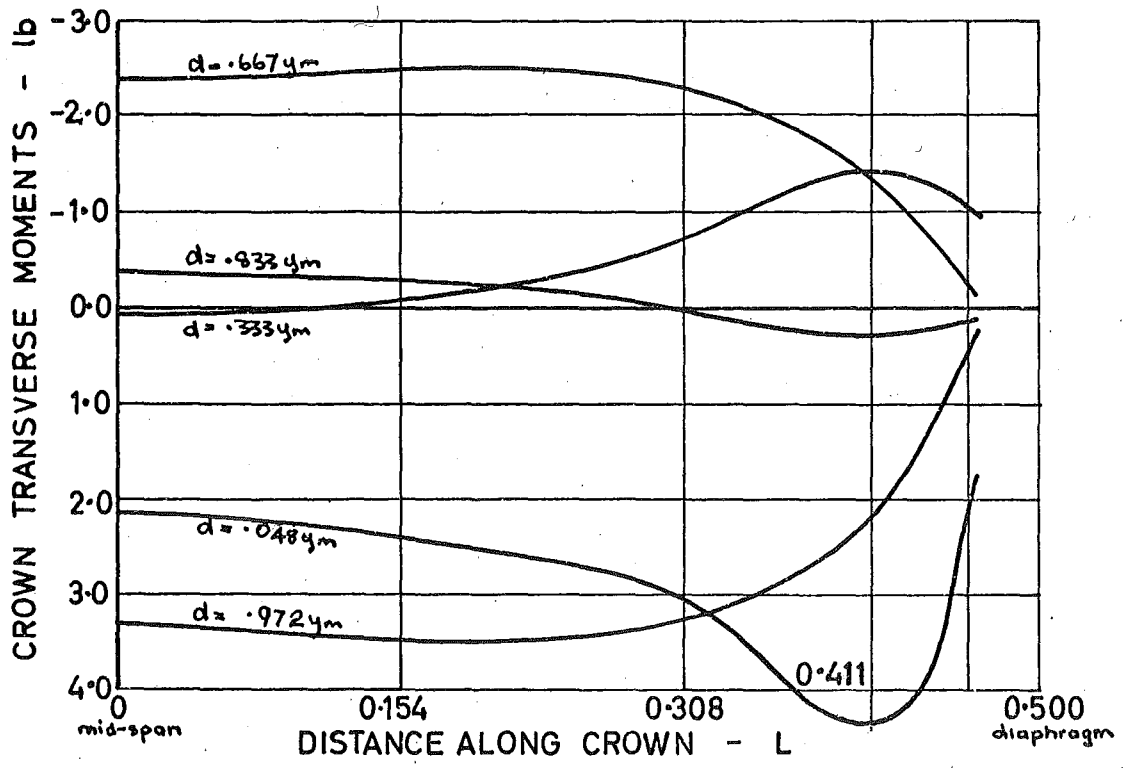

Fig. 9.12 Distribution of crown transverse moments for straight cables - P_a =1200 lb

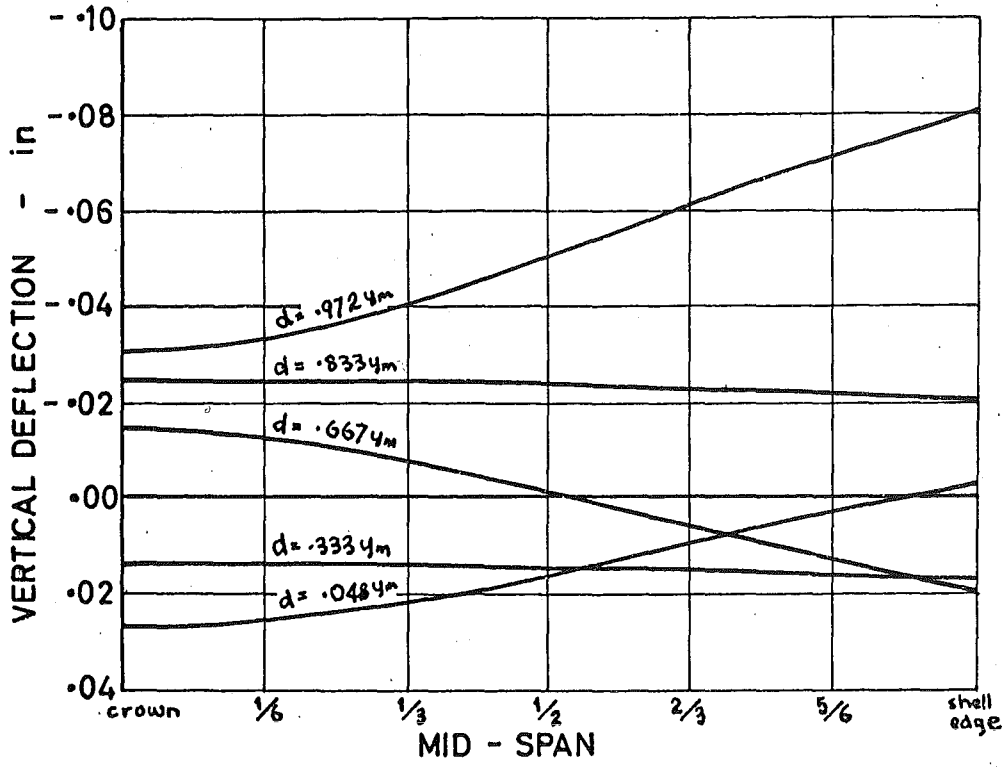

Fig. 9.13 Mid-span deflection profiles for straight cables - P_a = 1200 lb

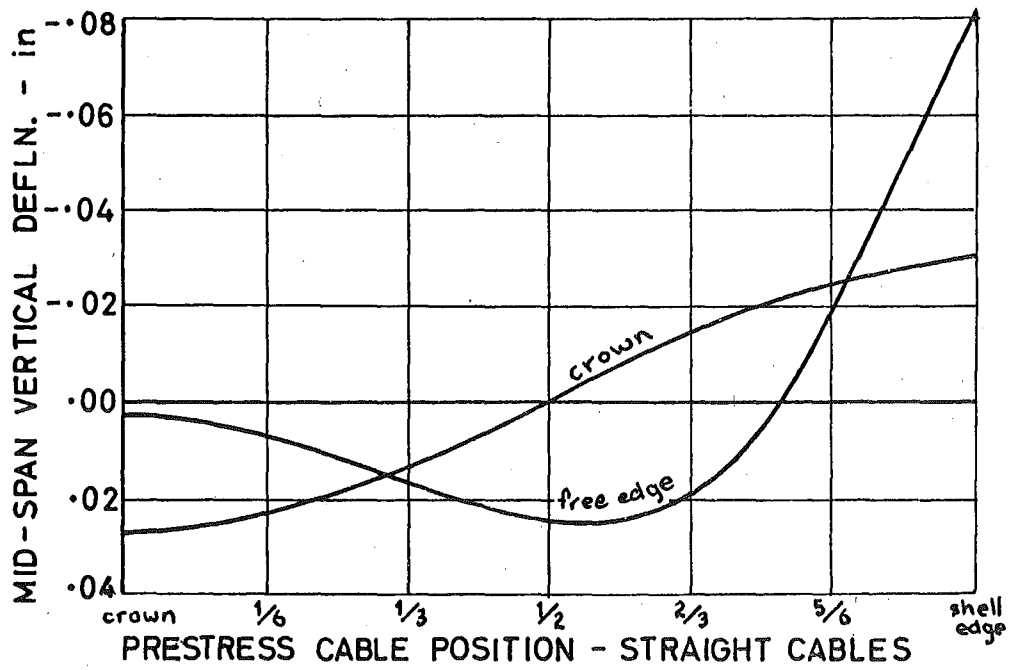

Fig. 9.14 Mid-span crown and free edge deflections against straight cable positions - P_a = 1200 lb

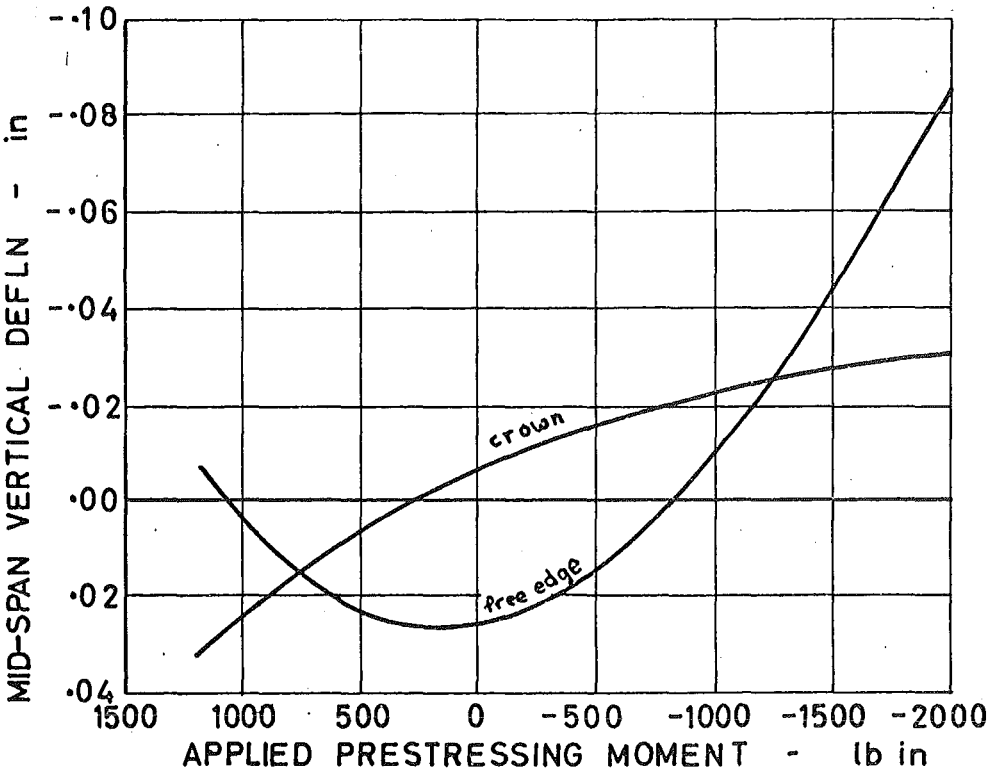

Fig. 9.15 Mid-span and free edge deflections versus applied prestressing moment - P_a = 1200 lb

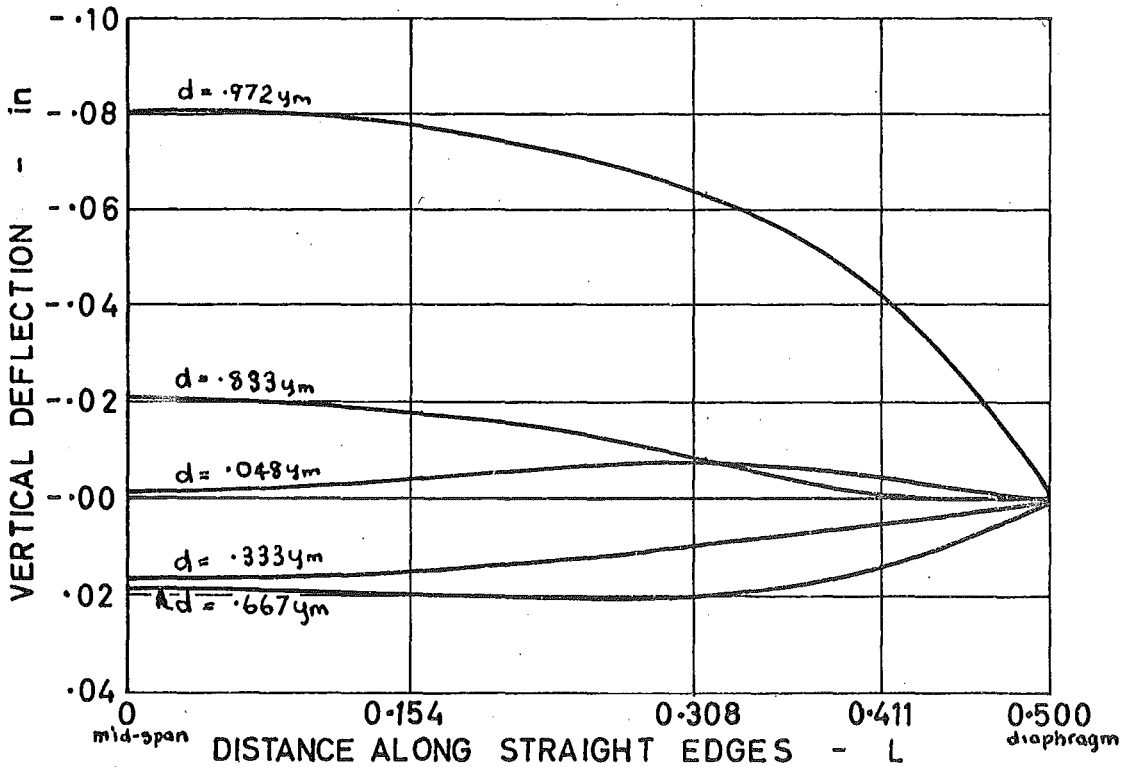

Fig. 9.16 Straight edge deflections for straight cables - P_a = 1200 lb

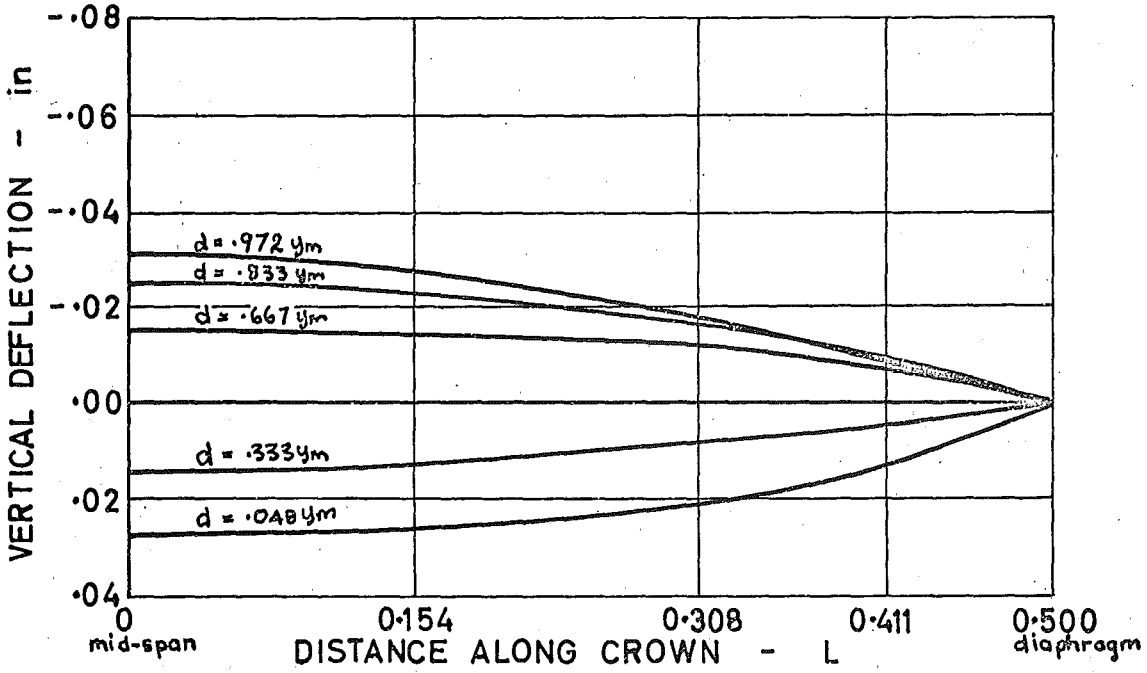

Fig. 9.17 Crown deflections for straight cables - P_a = 1200 lb

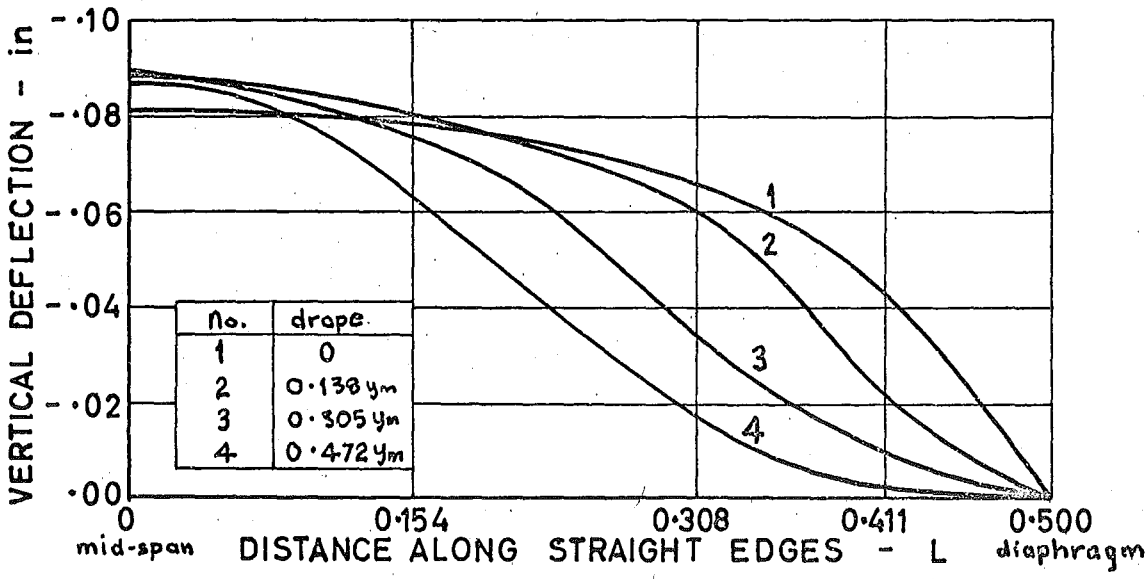

Fig. 9.18 Straight edge deflections for draped cables - P_a = 1200 lb

CHAPTER TEN

EFFECT OF SPAN ON THE STRESSES IN PRESTRESSED CYLINDRICAL SHELLS

10.1 DETAILS OF THE SHELLS AND THEIR SOLUTIONS

With the aid of the generator line-load computer program a series of shells with spans as given in table 10.1 was analysed. Apart from the spans, all dimensional and prestressing details were exactly the same as those used for the theoretical analysis of the model tests. Stresses and deflections were calculated at cross sections A - E at the fractional distances from mid-span as given in table 9.1. Numerical details of the solutions, as regards Fourier series and number of loaded generators, were the same as those summarised in section 9.1 for the theoretical solutions for the model tests.

If it is assumed that the beam theory applies, the longitudinal stresses should be the same and the transverse stresses should be inversely proportional to the span for shells with the same prestressing cable lay-outs and varying spans.

10.2 COMPARISON OF STRESSES

There were only small changes in the longitudinal stresses as the span was altered. For straight cable pre-stressing with the same prestressing cable positions the mid-

Shell	Span		L/R
	in.	x L_m	
A	28.34	0.724	1.42
B	39.12	1.0	1.97
C	58.685	1.5	2.95
D	78.24	2.0	3.93
E	117.36	3.0	5.89

Table 10.1 Spans of shells analysed
L_m = span of model shell

span longitudinal stresses hardly changed as L/R went from 1.97 to 5.89. As the span increased, the longitudinal stresses remained similar to the mid-span values for a greater proportion of the span. For curved cables, the mid-span longitudinal stresses became closer to those of the straight cable tests with the same mid-span cable positions as the span increased.

The transverse stresses did not necessarily reduce as the span was increased. Figure 10.1 shows the transverse moments at cross sections A, C, and D for the series of shells with $d = 0.972\ y_m$ and $f = 0$. At cross section A (mid-span) the transverse moments reduced considerably with the increase in span but at cross section D ($0.411\ L$) they increased with the span. This can be clearly seen from figure 10.2 where the

crown transverse moments at cross sections A and D are plotted against the L/R ratio.

For draped prestressing cables the transverse moments did not even reduce over much at mid-span as the span was increased. This is shown in figure 10.3 where the mid-span moments for $d = 0.500\, y_m$ and $f = 0.472\, y_m$ are plotted for L/R ratios of 1.97 and 3.93. These moments are also contrasted with those for $d = 0.972\, y_m$ and $f = 0$ (straight cables with the same mid-span position).

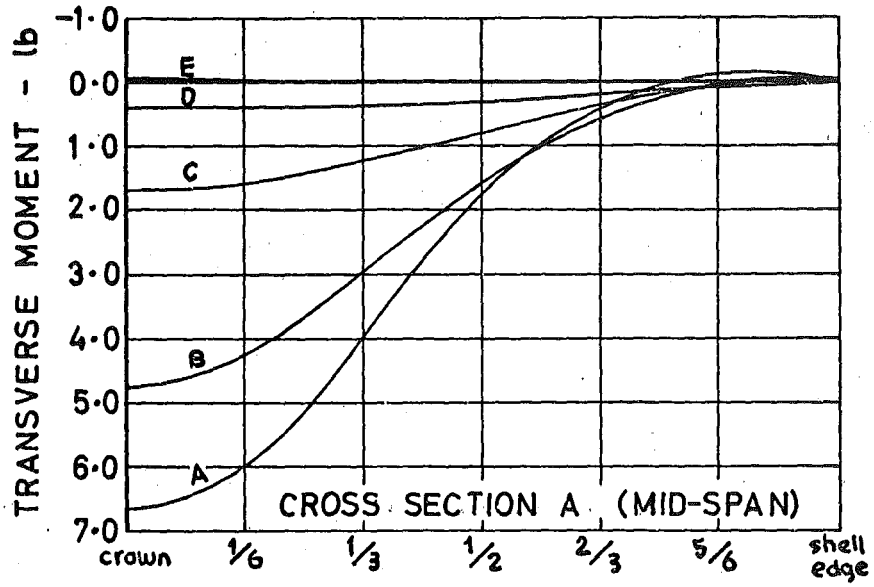

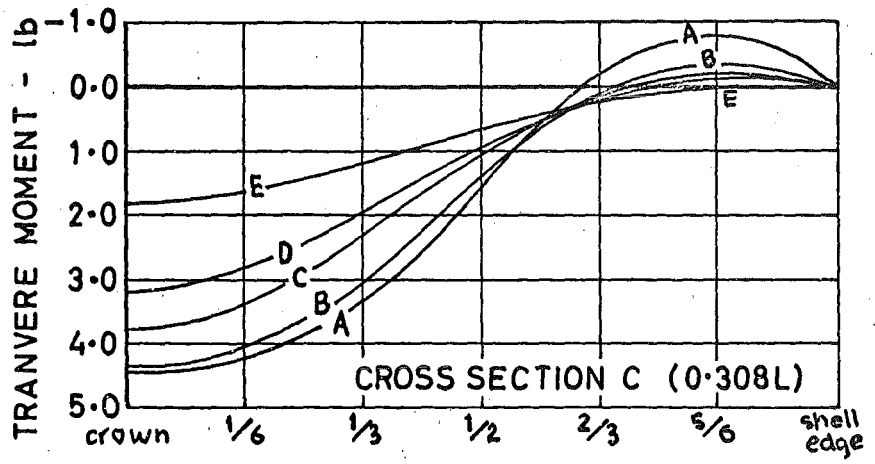

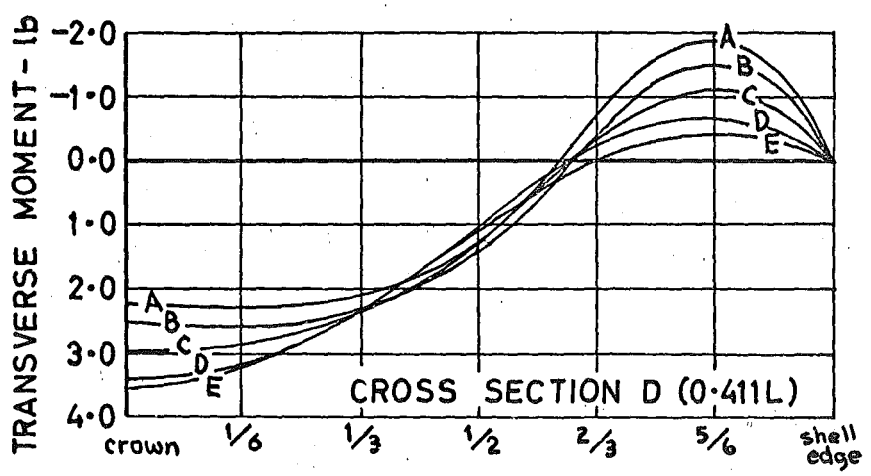

Curve	L/R
A	1·42
B	1·97
C	2·95
D	3·93
E	5·89

Fig. 10.1 Transverse moments for various spans - R = 19·94", t = 0·1309", φ_k=0·5263 rad., d = 0·972 y_m, f = 0, P_a = 1200 lb

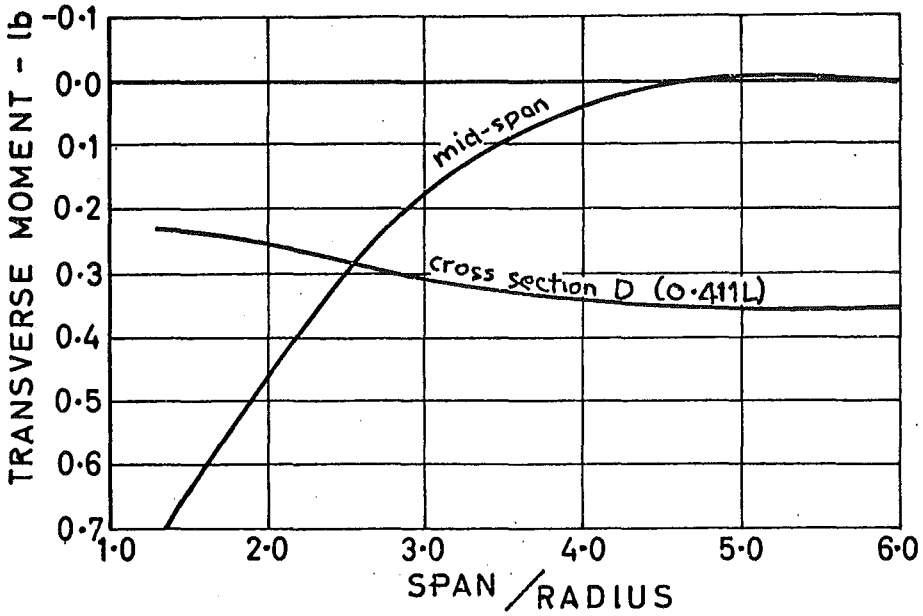

Fig. 10.2 Variation of crown transverse moments with span - same shells as those in fig.10.1

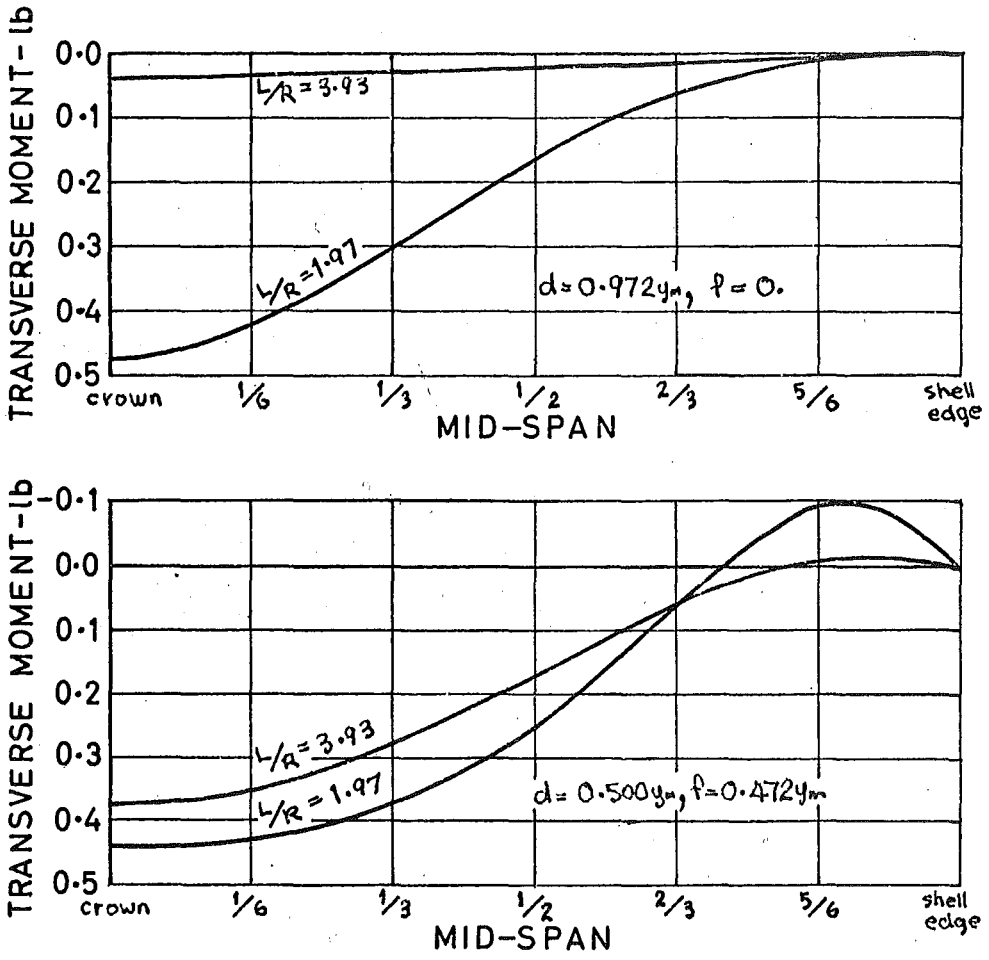

Fig. 10.3 Variation of mid-span transverse moment with span for draped cables - R = 19·94", t = 0·1309", φ_k = 0·5236 rad., P_a = 1200 lb

CHAPTER ELEVEN

OTHER METHODS OF SOLUTION

11.1 SOLUTIONS OF de SITTER

de Sitter's[6] series of tests consisted of straight cable tests on a plastic model of a cylindrical shell without edge beams. The model shell dimensions were $L = 51.4$ cm, $R = 33.0$ cm, $t = 0.2$ cm, and $\varphi_k = 0.597$ radians. The model was strain gauged with transverse and longitudinal strain gauges at transverse cross sections at $x = 0$, $\frac{1}{4}L$, and $5/12\,L$. The model was prestressed at $d = 0$, $\frac{1}{2}y_m$, $5/6\,y_m$, and y_m by loading the shell as a column with loads applied at the curved ends of the shell. The shell, under such a loading system, is unstable and much of the non-linearity in experimental results is probably from this cause and not from non-linear shell behaviour. This non-linearity was not discovered until the testing was almost complete.

The theoretical solutions were based on the D.K.J. equation. The shell was considered to be infinite in the y direction with the prestress applied through Fourier series as boundary stresses at $x = \pm \frac{L}{2}$, and a solution was obtained for each Fourier term with actions and displacements varying as sine or cosine functions in the y direction and damped

oscillating functions in the x direction. The actions, now existing along the straight edges as a result of considering the shell as infinite in the y direction, were expanded as a Fourier series and removed by ordinary complementary function solutions of the type described in section 2.7.

Although de Sitter's method is more complicated than the generator line-load method of solution it does have the advantage of allowing any boundary conditions at the curved ends and it should not upset the shear stresses near the diaphragms as does the generator line-load method when the anchorage loads are applied as shear loads. The transverse stresses are very dependent on the position of the prestressing cables and, because the Fourier series expansion of the anchorage loads as a boundary stress spreads the anchorage loads over a considerable portion of the shell ends, there is a possibility that the transverse stresses of de Sitter could be in error. There is no easy extension of the solution of de Sitter to handle the loads from cable curvature as accurately as those from the anchorages, although de Sitter does suggest and use in an example a method where the Y component of curvature loads is applied at the straight edges and the Z component is applied as a dome shaped surface loads by the first 2 terms of, presumably, Fourier series in the x and y directions.

The generator line-load method for straight prestressing cables is just a simple case of the draped cable solution.

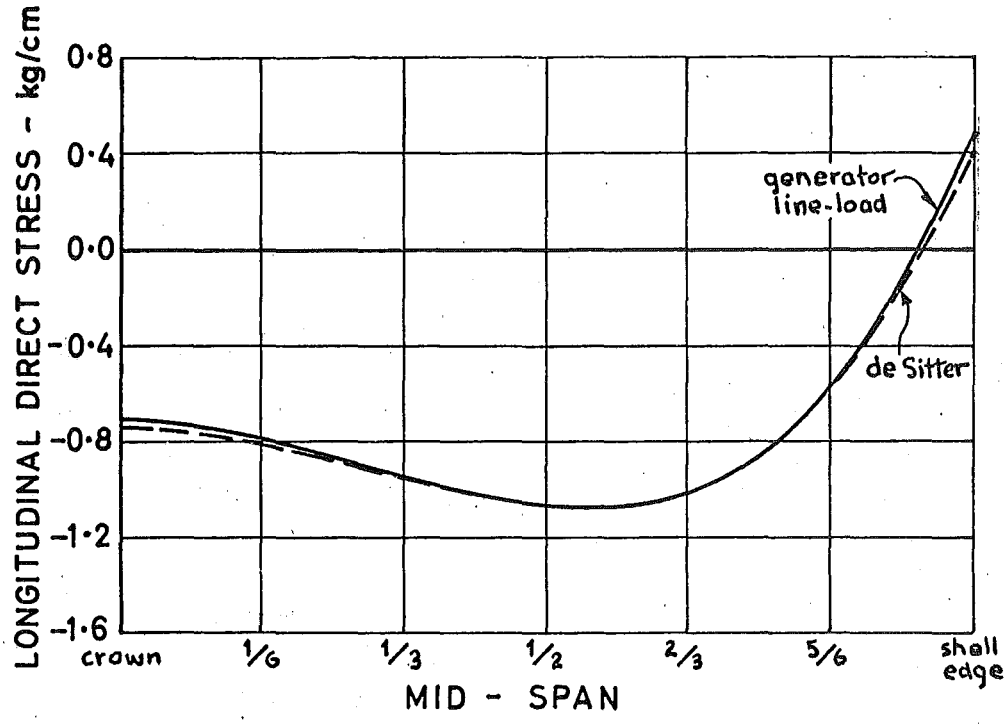

Fig. 11.1 Longitudinal stress - comparison between de Sitter's and generator line-load solutions - $L = 51{\cdot}4$ cm, $R = 33{\cdot}0$ cm, $t = 0{\cdot}2$ cm, $\varphi_k = 0{\cdot}597$ rad., $d = 0{\cdot}500\, y_m$, $f = 0$, $P_a = 15$ kg

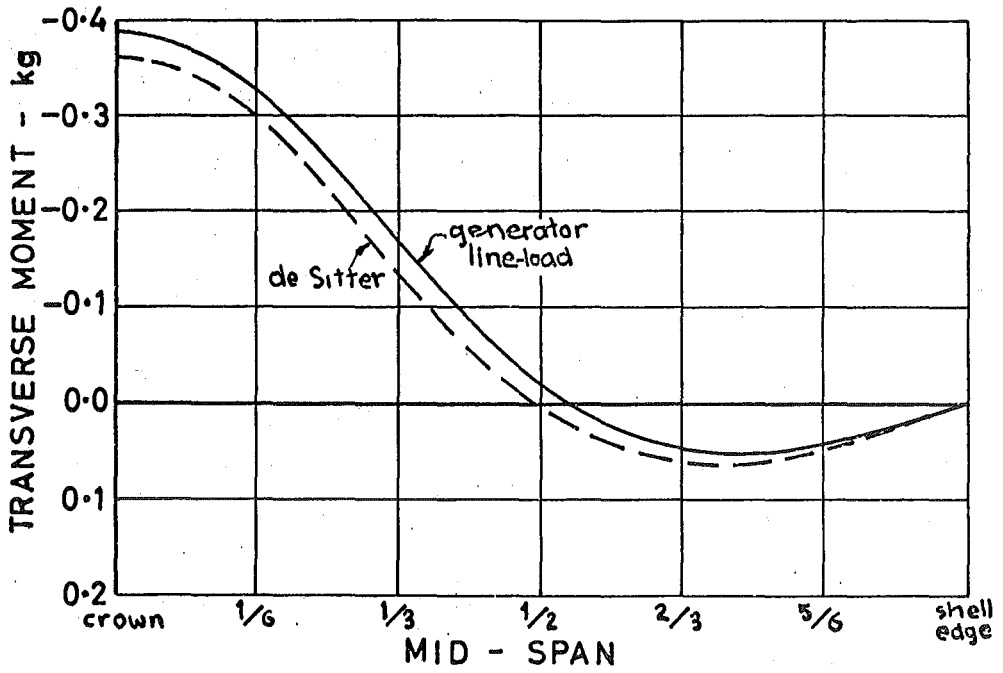

Fig 11.2 Transverse moments - comparison between de Sitter's and generator line-load solutions - same example as in fig. 11.1

The generator line-load solution is suitable for use in ordinary multi-shell computer programs such as that described by Scordelis and Lo[7] or computer programs can be easily written for limited computer facilities.

Figures 11.1 and 11.2 give an indication of the agreement between the theoretical solutions of de Sitter and those from the generator line-load computer program.

11.2 THE BEAM THEORY

The beam theory[30], first put forward by Lundgren[3], treats the shell as a beam spanning between diaphragms for the determination of longitudinal and shear stresses. To determine the transverse stresses the shell is divided into transverse strips which are loaded with surface loads, membrane forces (shear differences) along the curved edges, and actions at the straight edges if the shell is continuous. Nasser and Johnson[31] give a semi-graphical method for the analysis of long prestressed cylindrical shells.

The users of beam theory have always expressed their doubts on the applicability of the beam theory for short and intermediate single shells. The question is: how long must cylindrical shells be before the beam theory gives satisfactory solutions for longitudinal and transverse stresses over most of the shell surface?

Gauge	h		Direct longitudinal stress lb./in.				
		d	0.972	0.833	0.667	0.333	0.021
		M	-1973	-1175	-368	722	1082
1	1.667	beam	-598	-400	-203	62	150
		exp.	-581	-416	-223	78	165
2	0.980	beam	-396	-261	-167	-11	38
		exp.	-392	-279	-164	-2	36
3	0.307	beam	-203	-167	-130	-82	-65
		exp.	-215	-167	-124	-72	-71
4	-0.221	beam	-50	-76	-102	-137	-149
		exp.	-54	-72	-94	-132	-155
5	-0.602	beam	57	-8	-82	-179	-208
		exp.	55	-16	-75	-177	-212
6	-0.831	beam	125	29	-69	-202	-246
		exp.	123	24	-63	-193	-247
7	-0.908	beam	147	41	-65	-210	-257
		exp	149	42	-57	-204	-256

Table 11.1 Comparison of beam theory and experimental longitudinal direct stresses for straight prestressing cables

d = cable eccentricity in fractions of y_m,

M = total applied prestress moment,

h = height of strain gauges above centroid of cross section.

The model shell tested was well outside the limits for which the beam theory is considered to apply. However, the model test mid-span longitudinal direct stresses for straight cable prestressing agreed surprisingly well with those calculated from beam theory (table 11.1). The prestressing force and the cable eccentricity at any cross section determine the beam theory longitudinal stresses. Thus, all the draped cable model tests should have similar mid-span longitudinal stress distributions for the shell to be behaving according to the beam theory. This was not the case as is evident from figure 9.9. When L/R was increased to 3.93 the longitudinal stresses at midspan from the draped cable tests were close to the beam theory stresses.

For straight prestressing cables, however, the beam theory does not give any indication of the size or even the existence of transverse stresses because the beam shear is zero. Even when L/R was increased to 5.89 the transverse moments from straight cable prestressing, one of the controlling design values, were still significant (bigger than those for L/R = 1.97 near the diaphragms - see figures 10.1, 10.2).

Extending the beam theory for curved cables and using shear differences to calculate the transverse stresses would be rather pointless for these examples with L/R less than 6, because the transverse stresses from the anchorage loads, a significant portion of the transverse stresses, cannot be estimated by the beam theory.

CHAPTER TWELVE

SUMMARY OF CONCLUSIONS AND DISCUSSIONS

12.1 THE SHELL MODEL

The aluminium alloy proved to be an ideal model material. The shell was easily fabricated. The model tests showed that accurate and reliable strain readings could be obtained from electric resistance strain gauges with readings being repeatable to within $\pm$ 2 μstrain. The travelling level was very suitable for measuring vertical deflections to the nearest 0.001".

The desired prestress could be applied to the model shell with the prestressing system developed. Cable lay-outs could be easily altered and accurately set in position. The prestressing forces could be easily altered and set on any given loads with the screw jacks, and the load cells measured the prestressing forces to the nearest 2 - 3 lb.

The model shell behaved symmetrically and there was no evidence of non-linear behaviour.

An indication of the overall experimental accuracy is given by the agreement between internal actions and applied prestressing forces. Over the central half of the shell the differences between the sums of the internal actions and the applied prestressing forces were usually less than 3 per cent.

12.2 THEORETICAL SOLUTION BY GENERATOR LINE-LOADS

The method of replacing loads from the curvature and the anchorages of prestressing cables by actions along generators gave solutions that rapidly converged to unique values as the various parameters of replacing the loads were changed. The solutions obtained are true solutions to the D.K.J. equation, for the loads on a shell from prestressing cables within the curved surface, over a great part of the shell surface. Near the anchorages, the stresses (especially the shear stresses) were upset by applying the anchorage loads as shear loads and not boundary stresses. In this region the stresses can be considered as local effects arising from the high anchorage point loads.

Because of the limited available computer facilities, edge beams and surface loads were not included in the computer program written to solve prestressed cylindrical shells. Edge beams and surface loads could have been included with a consequent increase in the number of chapters of the computer program and an increase in the computing time required.

12.3 AGREEMENT BETWEEN THE MODEL TESTS AND THEORY

When the usual agreement between shell theory and experiment is considered it must be concluded that the model shell was definitely behaving according to the D.K.J. equation. Over a great part of the shell surface theoretical stresses and deflections were frequently within a few per cent of the

experimental stresses and deflections.

In the vicinity of the diaphragms, the theoretical solution did not give a very good estimate of some of the stresses. The differences between theory and experiment for longitudinal and transverse direct stresses can be explained from the limitations of theoretical method of solution. However, theoretical shear stresses near the diaphragms, tended to be about half the experimental shear stresses.

12.4 ANALYSIS OF SHELLS OF VARIOUS SPANS

The analysis of shells of varying L/R ratio soon showed that, although the longitudinal stresses behaved in a straight forward manner with the longitudinal stresses becoming closer to those of beam theory as L/R was increased to 6, the transverse stresses did not. At cross sections near the diaphragms the transverse stresses increased with the span. This is in direct contradiction to the beam theory and there is no way of calculating these transverse moments from the beam theory.

It must be remembered that this discussion is on single shells without edge-beams and the same points do not, necessarily, apply to shells of multi-shells or shells with edge-beams.

B I B L I O G R A P H Y

1. Bouma, A.L. "On approximate methods of shell analysis : a general survey". Proceedings of the World Conference on Shell Structures, San Francisco, October 1962. pp. 475 - 477.

2. Jenkins, R.S. "Theory and Design of Cylindrical Shell Structures". Ove Arup and Partners, London, 1947.

3. Lundgren, H. "Cylindrical Shells, Volume 1". The Danish Technical Press, Copenhagen, 1951.

4. Dabrowski, R. "Analysis of prestressed cylindrical shell roofs". Journal of the Structural Division, Proceedings of the American Society of Civil Engineers, Vol. 89, No. ST5, October 1963, pp. 91 - 116.

5. Dehouse, N.M. "Discussion on Prestressed and Precast Shells". Proceedings of the Second Symposium on Shell Roof Construction, Oslo, July 1957. pp. 368 - 369.

6. de Sitter, W.R. "Theoretisch en experimenteel onderzoek naar het gedrag van een voorgespannen tonschaal". Heron, Jaargang 11, No.1, 1963. pp. 28 - 47. Translation, University of Canterbury, 1964.

7. Scordelis, A.G. and Lo, K.S. "Computer analysis of cylindrical shells". Proceedings of the American Concrete Institute, Vol. 61, No.5, May 1964. pp. 539 - 560.

8. "IBM 1620 Fortran II Specifications". File No. 1620 - 25, IBM Product Publications, California, 1962.

9. Powell, G.H. "A study of reinforced concrete shell roofs employing observations on model structures". Ph.D. Thesis, University of Canterbury, 1964. pp. 19 - 38, 113 - 116.

10. Powell, G.H. "Elastic analysis of multi-shell and multi-plate structures". To be published in the Proceedings of the American Society of Civil Engineers.

11. Weatherburn, C.E. "Elementary vector analysis". 2nd edition, G. Bell and Sons, Ltd., London, 1955. pp. 97 - 103.

12. Southwell, R.V. "Theory of Elasticity", 2nd edition. Oxford University Press, London, 1941. pp. 98 - 100.

13. Rowe, R.E. "Experimental methods in the study of the behaviour of shell roofs". Proceedings of the World Conference on Shell Structures, San Francisco, October 1962. pp. 223 -228.

14. Bouma, A.L. and Haas, A.M. "General report". Proceedings of the Symposium on Shell Research, Delft, August 1961. pp. 8 - 9.

15. Scrivener, J.C. "An investigation of reinforced concrete hyperbolic parabaloid shells". Ph.D. Thesis, University of London, October 1962. pp. 136 - 138, 203 - 205.

16. Stöckl, S. "The effect of the behaviour of the outer fibres of concrete models on the deformation properties of the models". Proceedings of the Symposium on Shell Research, Delft, August 1961. pp. 340 - 341.

17. Arcan, M. and Nicolau, E. "Experimental stress analysis on shells by models of plastic". Proceedings of the Symposium on Shell Research, Delft, August 1961. pp. 277 - 281.

18. Hergenröder, A. and Rüsch, H. "Recent findings in the testing of models". Proceedings of the Symposium on Shell Research, Delft, August 1961, pp. 314 - 324.

19. "Structural Aluminium". The Northern Aluminium Co. Ltd., 1961.

20. "Instruction sheet for Araldite Adhesive 106". 9124 610.609/611.114, Plastics Department, CIBA Ltd., Switzerland.

21. Kelly, D.R. "The influence of edge beams and end diaphragm stiffness on the stress distribution in a cylindrical shell roof". Ph.D. Thesis, University of London, 1963. pp. 52 - 54.

22. Franz, G. and Teepe, W. "Untersuchungen an Schalenmodellen aus Kunstsoff". Proceedings of the Symposium on Shell Research, Delft, August 1961. Figs. 8, 15, between pp. 188 - 193.

23. Röntsch, G. "Über modellstatische Untersuchungen an trogförmig gekrümmten Mittelträgerschalen". Proceedings of the Symposium on Shell Research, Delft, August 1961. Fig. 4, pp. 351.

24. Bouma, A.L., van Riel, A.C., van Koten, H., and Beranek, W.J., "Investigations on models of eleven cylindrical shells made of reinforced and prestressed concrete". Proceedings of the Symposium on Shell Research, Delft, August 1961. pp. 79 - 101.

25. "Modelonderzoek van een voorgespannen tonschaal vervaardigd van microbeton". Report No. B-60-1464/8008, Instituut TNO voor Bouwmaterialen en Bouwconstructies, Delft, September 1960. Figs. 28 - 30.

26. "Budd strain gages and accessories, Catalog and Price list - BG 2400". Instruments Division, The Budd Co., Phoenixville, U.S.A.

27. "Instruction Manuals - BG 3100, BG 3110, and BG 3120". Instruments Division, The Budd Co., Phoenixville, U.S.A.

28. Dove, R.C. and Adams, P.H. "Experimental Stress Analysis and Motion Measurement". Charles E. Merril Books Ltd., Columbus, Ohio, 1964. pp. 243 - 251.

29. Dally, J.W. and Riley, W.F. "Experimental Stress Analysis". McGraw-Hill Book Co., New York, N.Y., 1965. pp. 429 - 432.

30. Chinn, J. "Cylindrical shell analysis simplified by beam method". Proceedings of the American Concrete Institute, Vol. 55, No. 11, May 1959. pp. 1183 - 1192.

31. Nasser, A.R. and Johnson, C.B. "Semigraphical analysis of long prestressed concrete vaulted shells". Proceedings of the American Concrete Institute, Vol. 59, No. 5, May 1962. pp. 659 - 672.

A P P E N D I X I

ANALYSIS OF STRAIN GAUGE CIRCUITS

The readings of a strain indicator depend not only on the strain gauges but also on the lead wire and switch-box resistances and the strain indicator and, if accurate strain readings are to be obtained, corrections must be made to the indicated strain readings.

A simplification of the strain gauge circuit, as seen by the strain indicator in the model tests, is shown in figure I.1.

$$Q' = C \frac{GF_b}{GF_g} Q_b$$

as $$Q_b = \frac{\delta R_t}{R_t \, GF_b}$$

and $$Q' = \frac{\delta R_g}{R_g \, GF_g} .$$

Now $$R_t = \frac{R_b(R_g + R_s)}{R_b + R_g + R_s} .$$

Hence $$C = \frac{R_b + R_g + R_s}{R_b} \cdot \frac{R_g + R_s}{R_g} .$$

GF_b = gauge factor set on bridge,

GF_g = gauge factor of strain gauge,

Q' = reading of gauge at gauge,

Q_b = reading of gauge at strain indicator,

C = resistance correction coefficient,

R_b = zero setting resistance,

R_g = strain gauge resistance,

R_s = series resistance of lead wires and switch-box,

R_t = total resistance as seen by strain indicator.

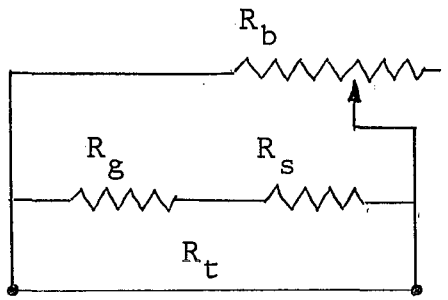

Fig. I.1 Simplified strain gauge circuit as seen by the strain indicator.

Switch-box	Resistance in ohms			C	
	R_g	R_s	R_b		
A	120	0.91	20,000 10,000	1.014 1.020	$C = 1.017 \pm 0.003$
B	120	0.91	-	1.008	$C = 1.008$

Table I.1 Lead wire and switch-box resistance correction coefficients

A P P E N D I X I I

TESTS ON H30-WP ALUMINIUM ALLOY

II.1 BENDING TESTS ON H30-WP ALLOY TEST PIECES

Two carefully machined and measured strips of the aluminium alloy used on the model shell were loaded in the test rig as shown in figure II.2 and measurements of central deflection and longitudinal and transverse strains were taken with:

(a) No strain gauges on the strips.

(b) A longitudinal and a transverse C12 - 121 strain gauge glued to the centre of each face of each strip and no waterproofing.

(c) The strain gauges from (b) waterproofed.

The strips were tested in 4 positions (end for end and upside-down end for end) with readings taken at loads of W = 0, 2, 4, 6, 8, 8, 6, 4, 2, 0 lb.

From theoretical considerations of an elastic beam loaded as in figure II.1 the following equations apply:

From the central deflection $E = \frac{Wd}{24\,Iy}(3L^2 - 4d^2)$

and from strain readings $E = \frac{Wd}{Z\,\varepsilon_l}$,

$\mu = \frac{\varepsilon_t}{\varepsilon_l}$,

where Z = section modulus,

I = section moment of inertia,

ϵ_ℓ = longitudinal strain,

ϵ_t = transverse strain.

The pertintent dimensions of both strips turned out to be the same:

width (average of 12 micrometer readings) = 0.9856",

thickness (average of 12 micromter readings)= 0.1309",

thickness of strain gauges = 0.0011",

span L = 11.00",

load distance d = 2.50".

Tests (a), (b), and (c) gave no discernable differences in readings and it was concluded that the strain gauges and waterproofing had negligible stiffening effect.

Average readings from all the tests were:

y = 0.0374"/2 lb. increment of each load,

ϵ_ℓ = 173.4 μstrain/2 lb. increment in each load,

ϵ_t = 52.9 μstrain/2 lb. increment in each load.

which give from deflection

$E = 10.26 \times 10^6$ lb./in.^{2},

and from strain readings

$E = 10.23 \times 10^6$ lb./in.^{2},

μ = 0.305.

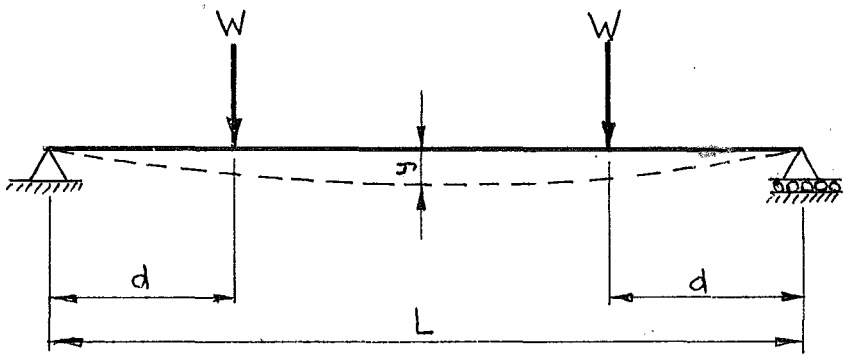

Fig. II.1 Bending of test strip

II.2 TENSION TESTS ON H30-WP ALUMINIUM ALLOY TEST STRIPS

The same two strips as were used in the bending tests were tested in tension in an Avery 25,000 lb. universal test machine.

During an initial test readings were taken with a Hounsfield extensometer as well as with the strain gauges. As the Hounsfield extensometer was of insufficient sensitivity compared with the strain gauges and it caused odd strain readings its use was discontinued and strains were only measured with electric resistance strain gauges.

A strip was placed in the test machine and loaded up and down three times before three sets of strain readings were taken at 100, 350, 600, 850, and 1100 lb. load. The strips were then removed, turned around, and retested. The results were:

area strip = 0.1307 $in.^2$,

$$\epsilon_\ell = 187.3\ \mu\text{strain/250 lb. tension},$$

$$\epsilon_t = 58.2\ \mu\text{strain/250 lb. tension},$$

which give $E = 10.21 \times 10^6$ lb./in.^{2},

$$\mu = 0.310.$$

II.3 THICKNESS OF MODEL SHELL AND STRAIN GAUGES

Micrometer measurements of the aluminium shell, test strips, and offcuts gave a thickness of 0.1309 ± 0.0005".

Strain gauge and glue layer thickness (distance from the surface of the shell to the metalfilm of the strain gauges) was 0.0011".

II.4 STIFFENING EFFECT OF THE PRESTRESSING GUIDES

The central deflection of a one inch wide strip of aluminium alloy, loaded as in figure II.3, was measured for tests with no guides and then with prestressing guides glued to both surfaces at 1" centres. The strip with guides is shown in figure II.3.

The prestressing guides increased the stiffness of the strip by 5 per cent. Since there were 2 rows of guides on the model shell in a width of 21", the average stiffening effect of the guides would not be noticeable. The strain gauges near the line of the prestressing wires might have been slightly affected by their proximity to the prestressing guides and their strain

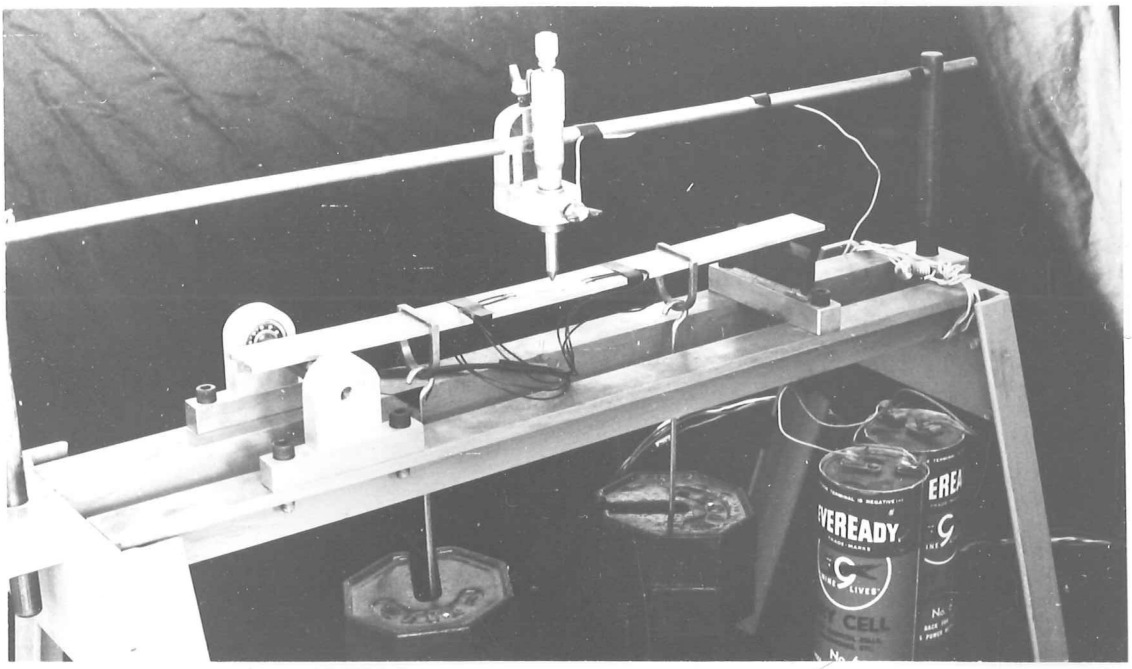

Fig. II.2 Bending test on aluminium alloy test strips

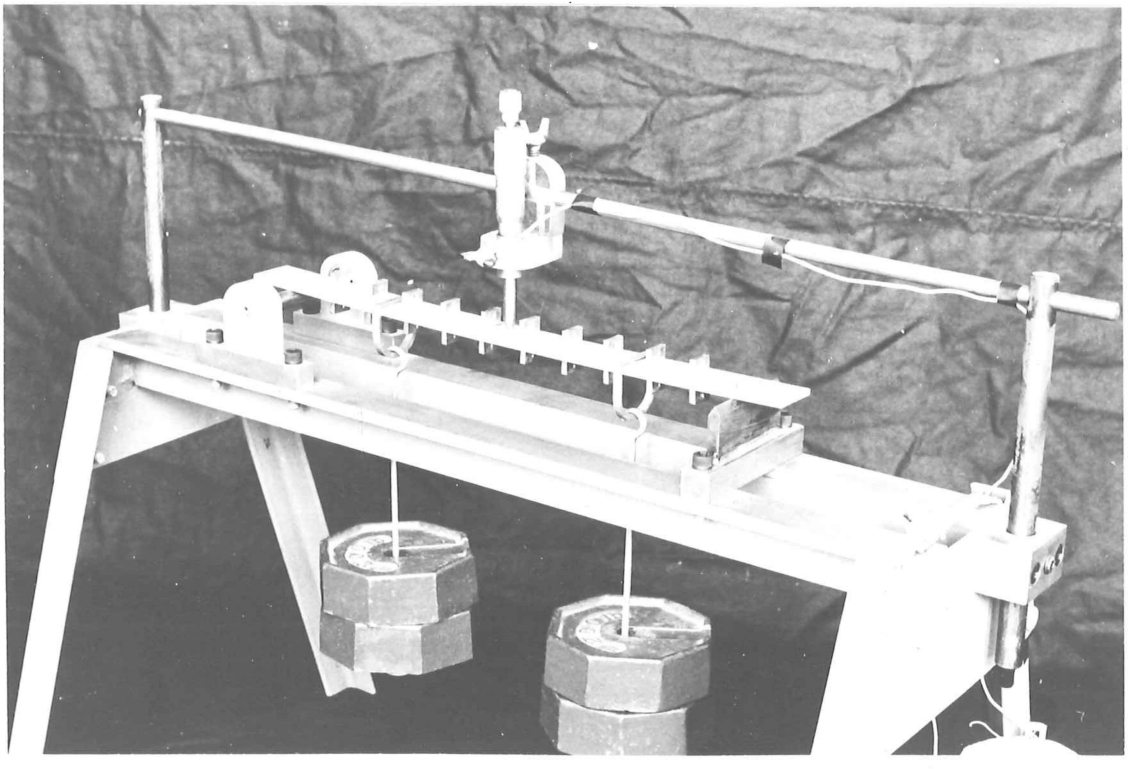

Fig. II.3 Stiffening effect of prestressing guides

readings could possibly have been a few per cent out. No such effects were noticeable in the experimental strain readings.

II.5 SUMMARY OF TESTS ON ALLOY STRIPS

(a) The strain gauges and waterproofing have negligible stiffening effect.

(b) Manufacturer's gauge factors were within their stated tolerances ($\pm$ 0.5%).

(c) Prestressing guides have little effect on the shell stiffness.

(d) The thickness of the shell was 0.1309" and the strain gauges had an effective thickness of 0.0011".

(e) Experimental values of elastic constants are given in table II.1.

	E lb./in.^{2}	μ
From strain gauges in tension test	10.21×10^6	0.310
From deflection readings in bending test	10.26×10^6	-
From strain readings in bending test	10.23×10^6	0.305
Values taken for determination of stresses and deflections in model tests	10.23×10^6	0.307

Table II.1 Elastic constants of H30-WP aluminium alloy

A P P E N D I X I I I

EFFECT OF STRAIN GAUGE ROSETTE SIZE

The 120^{o} delta rosettes strain gauges were glued to the shell with gauge 1 in the longitudinal direction and gauges 2 and 3 at 120^{o} on either side. Thus,

$$\epsilon_x = \epsilon_1,$$

$$\epsilon_{xy} = \frac{2}{\sqrt{3}} (\epsilon_3 - \epsilon_2),$$

$$\epsilon_y = \frac{1}{3} \left[2(\epsilon_2 + \epsilon_3) - \epsilon_1 \right],$$

as given in section 7.6.

The strains obtained from rosettes, such as were used in these model tests, are not average strains over the whole of the rosettes. They are the average strains of the individual gauges of the rosettes. The readings of gauges 2 and 3 of the rosettes commonly changed sign 2 or 3 times between the shell crown and the free edges while the longitudinal strains obtained from gauge 1 of each rosette gradually changed along the length of the shell. Therefore the readings of gauges 2 and 3 of the delta rosettes are likely to be considerably different from the strains in corresponding directions at the centres of the rosettes while the reading of gauge 1 will be close to the correct value.

The estimated shear stresses, obtained from the differences between gauges 2 and 3 of each rosette, could easily be very different from the actual shear stresses. The transverse stresses are generally more accurate because they depend to a large extent on the reading of gauge 1.

A P P E N D I X I V

THE GENERATOR LINE-LOAD COMPUTER PROGRAM

The five chapters of the computer program for solving cylindrical shells with symmetrical prestressing cables within the curved surface are listed in this appendix.

The program can be operated by reading the cards as described in table IV.1. The meanings of the input symbols are given in table IV.2.

Chapter	Cards	Format
1	R,XL,T,PHIK,E,XU P,FA,FB,FR NN,NB,NS,NC,IDENT	4E14.8 4E14.8 10I5
2	Output from chapter 1	
3	NY Output from chapter 2	I3
4	ND,NDO X(I),I=1,ND Output from chapter 3	10I5 4E14.8
5	II,M,IDE W(I),I=1,II Outputs from chapter 4	10I5 4E14.8

Table IV.1 Input to computer program

Chapter	Program	Theory	Meaning of symbol
1	R	R	shell radius
	XL	L	shell span
	T	t	shell thickness
	PHIK	φ_k	½ shell opening angle
	E	E	Young's modulus
	XU	μ	Poisson's ratio
	P	P_a	anchorage prestressing force
	FA	d	anchorage eccentricity
	FB	f	cable drape
	FR	P_f	friction loss
	NN	-	number of Fourier terms to be considered
	NB	r	number of points along cable for Fourier analysis
	NS	-	number of loaded generators
	NC	-	= 1 for straight cables with anchorage loads along 1 generator, = 2 for draped cables with anchorage effects, = 3 for draped cables without anchorage effects, = 4 for straight cables with anchorage loads along 2 generators
	IDENT	-	identification number
3	NY	-	number of points on transverse cross section for which actions required
4	ND	-	number of transverse cross sections
	NDO	-	= 1 for actions and deflections, = 2 for surface stresses and deflections = 3 for both 1 and 2
	X(5)	-	positions of transverse cross sections
5	II	-	number of solutions to be added
	M	-	= 1 for actions and deflections = 2 for surface stresses and deflections
	IDE	-	identification number
	W(5)	-	multiples of solutions to be added

Table IV.2 Meaning of input to computer program

```
C      P.C.S. GEN. LINE-LOAD. CHAPTER 1
C
C
C      READ DIMENSIONS AND CONTROL STATEMENTS
       DIMENSION Q(5,20,4),H(5,12,4),Y(5),X(20,5)
   19  READ100,R,XL,T,PHIK,E,XU
       READ100,P,FA,F,FR
       READ101,NN,NB,NS,NC,IDENT
  101  FORMAT(1015)
  100  FORMAT(4E14.8)
C
C  INITIALIZE
       XU1=1.-XU**2
       BETA=(3.*XU1/(R*T)**2)**.25
       PI=3.1415927
       YMAX=R*PHIK
       DO51=1,5
       DO5K=1,20
       DO5J=1,4
       H(I,K,J)=0.
    5  Q(I,K,J)=0.
       Y(1)=FA
       SNB=2*NB
       GO TO (1,2,11,2),NC
C
C      CURVATURE LOADS
    2  SNS=NS-1
       DY=F/SNS
       DO31=2,NS
    3  Y(I)=Y(I-1)+DY
       DX=XL/SNB
       X(1,1)=DX/2.
       DO41=2,NB
    4  X(I,1)=X(I-1,1)+DX
       CALL LINE(F,XL,X,PA,P,R,NB,FR)
       CALL EDGE(X,Q,DY,NB,NS,Y)
       CALL FOUR(PI,SNB,NB,NS,Q,H,X,XL,NN)
       GO TO (1,7,11,34),NC
C      ANCHORAGE LOADS
   11  Y(1)=FA-.25
       Y(2)=FA+.25
       NS=2.
       PA=P/2.
       GO TO 7
    1  PA=P
    7  PIT=PI/(2.*SNB)
       PA=8.*SNB/(PI*XL)*PA
       DO8N=1,NN
       XN=2*N-1
    8  H(1,N,1)=PA/XN*SINF(XN*PIT)*SINF(XN*PI/2.)+H(1,N,1)
C
C      OUTPUT
   34  PUNCH100,R,XL,T,PHIK,E,XU
       DO9K=1,4
       DO9I=1,NS
       DO9J=1,NN
    9  H(I,J,K)=-H(I,J,K)
       GO TO (12,12,13,12),NC
   13  DO14K=1,4
       DO14J=1,NN
   14  H(2,J,K)=H(1,J,K)
   12  PUNCH100,P,FA,F,FR
       PUNCH101,NN,NB,NS,NC,IDENT
       PUNCH100,XU1,BETA,YMAX,PI
       PUNCH100,(Y(I),I=1,NS)
       DO15J=1,NN
       PUNCH101,J
   15  PUNCH100,((H(I,J,K),K=1,4),I=1,NS)
       TYPE102
  102  FORMAT(//12HEND OF SHELL//)
       GO TO19
       END
```

```
C     SUBROUTINES FOR CHAPTER 1
C
C
C     TO CALCULATE LINE-LOADS ALONG CABLES
      SUBROUTINE LINE(F,XL,X,PA,P,R,NB,FR)
      DIMENSION X(20,5),E(20,8),PB(20),PC(20),PR(20)
      BN=2*NB
      A=4.*F/XL**2
      DX=XL/BN
      A2=2.*A
      DO11I=1,NB
      T=X(I,1)*A2
      T2=T**2
      X(I,2)=F-T2/(4.*A)
      D=-T2/(A2*R)
      D2=D**2
      AB=SQRTF(1.+D2+T2*D2)
      AC=SQRTF(1.+T2)
      E(I,1)=A2*AB/AC**3
      AD=-1./(AB*AC)
      E(I,2)=T*AD
      E(I,3)=AD
      E(I,4)=D*(T2+1.)*AD
      E(I,5)=DX*AC
      E(I,6)=1./AC
      E(I,7)=-T/AC
    1 E(I,8)=0.
      XU=FR*XL/(4.*P*F)
      PR(1)=P-FR*(BN-1.)/BN
      PB(1)=E(1,1)*PR(1)
    5 PC(1)=XU*PB(1)
      DO21=2,NB
      PR(I)=PR(I-1)+PC(I-1)*E(I-1,5)
      PB(I)=E(I,1)*PR(I)
    2 PC(I)=XU*PB(I)
      PRINT200,XU
  200 FORMAT(2HXU,F7.3)
      IF(XU)8,3,8
    8 PUN=(PR(NB)+PC(NB)*E(NB,5)*0.5-P)/FR
      IF(ABSF(PUN)-.02)3,3,4
    4 XU=(1.-PUN)*XU
      GO TO 5
    3 DO61=1,NB
      DO6J=1,3
    6 X(I,J+2)=-(E(I,J+1)*PB(I)+E(I,J+5)*PC(I))*AC
      AL=ATANF(4.*F/XL)
      PA=P*COSF(AL)
      RETURN
      END
```

```
C     TO DIVIDE LINE-LOADS BETWEEN GENERATORS
      SUBROUTINE EDGE (X,Q,DY,NB,NS,Y)
      DIMENSION X(20,5),Q(5,20,4),Y(5)
      DO1M=1,NB
      DO21=1,NS
      CA=X(M,2)+Y(1)-Y(I)
      IF(CA)3,3,2
    2 CONTINUE
    3 A=-CA/DY
      B=1.-A
      DO1J=1,3
      Q(I-1,M,J)=Q(I-1,M,J)+A*X(M,J+2)
    1 Q(I,M,J)=Q(I,M,J)+B*X(M,J+2)
      RETURN
      END
C
C     TO OBTAIN FOURIER COEFFICIENTS FOR DISTRIBUTED LOADS
      SUBROUTINE FOUR (PI,SNB,NB,NS,Q,H,X,XL,NN)
      DIMENSION X(20,5),H(5,12,4),Q(5,20,4)
      TQ=8./PI
      TS=PI/(2.*SNB)
      DO3N=1,NN
      XN=N*2-1
      SI=TQ/XN*SINF(XN*TS)
      AN=XN*PI/XL
      DO3M=1,NB
      C=X(M,1)*AN
      CU=COSF(C)
      SU=SINF(C)
      DO31=1,NS
      DO3L=1,3
      G=Q(I,M,L)
      IF(G)4,3,4
    4 GO TO (5,6,6),L
    5 CB=SU
      GO TO 7
    6 CB=CU
    7 H(I,N,L)=H(I,N,L)+CB*SI*G
    3 CONTINUE
      RETURN
      END
```

```
C     P.C.S. GEN. LINE-LOAD. CHAPTER 2
C
C
      DIMENSION A(4,4),B(4,4),QF(4),F(4,2),EN(4),C1(4,4),
     1C2(4,4),A1(4,4),B1(4,4),B2(4,4),A2(4,4),E1(4,4),
     2E2(4,4),AK1(4,4),AK2(4,4),V(4),AB1(4),AB2(4),ABT(4),
     3EB(4),G(4),VA(4),EU(4)
      COMMON AJ,AK,BJ,BK,BM
      TYPE102
  102 FORMAT(20HSWITCH 1 ON TYPE ANS)
    5 READ100,R,XL,T,PHIK,E,XU
      READ100,P,FA,FB,FR
      READ101,NN,NB,NS,NC,IDENT
  101 FORMAT(10I5)
  100 FORMAT(4E14.8)
      READ100,XU1,BETA,YMAX,PI
      READ100,(V(I),I=1,NS)
      PUNCH100,R,XL,T,PHIK,E,XU
      PUNCH100,P,FA,FB,FR
      PUNCH101,NN,NB,NS,NC,IDENT
      PUNCH100,(V(I),I=1,NS)
      TYPE100,R,XL,T,PHIK,E,XU
      TYPE100,P,FA,FB,FR
      TYPE101,NN,NB,NS,NC,IDENT
C
      D=T**3/(12.*XU1)
      Y2=2.*PI*R
      DO21I=1,4
    2 QF(I)=0.
C
C     COMPLIMENTARY FUNCTION SOLUTION
    1 READ101,N
      XN=2*N-1
      DO14I=1,4
   14 EN(I)=0.
      AN=XN*PI/XL
      AN3=AN**3
      BM=SQRTF(AN*BETA)
      CM=AN/BETA
      AJ=SQRTF((SQRTF(1.+(1.+CM)**2)+1.+CM)/2.)
      AK=.5/AJ
      BJ=SQRTF((SQRTF(1.+(1.-CM)**2)-1.+CM)/2.)
      BK=.5/BJ
      A(1,1)=-AK
      A(1,2)=-AJ
      A(1,3)=BK
      A(1,4)=+BJ
      A(2,1)=0.
      A(2,2)=-1.
      A(2,3)=0.
      A(2,4)=1.
      EP=1.-CM*(1.-XU)
      EQ=1.+CM*(1.-XU)
      A(3,1)=AJ*EP-AK
      A(3,2)=-AK*EP-AJ
      A(3,3)=-BJ*EQ-BK
      A(3,4)=BK*EQ-BJ
      A(4,1)=EP-2.
      A(4,2)=1.
      A(4,3)=EP
      A(4,4)=1.
      EB(1)=T/2.*AN3/(R*BM**3)
      EB(2)=EB(1)/BM*AN
      EB(3)=EB(2)/(2.*R*BM)
      EB(4)=EB(3)/BM
      EQ=1.+CM*(1.+XU)
      EP=1.-CM*(1.+XU)
      B(1,1)=1.
      B(1,2)=EQ
      B(1,3)=-1.
      B(1,4)=EP
      B(2,1)=-AK*EP-AJ
      B(2,2)=-AJ*EP+AK
      B(2,3)=-BK*EQ+BJ
      B(2,4)=-BJ*EQ-BK
      B(3,1)=1.
      B(3,2)=0.
      B(3,3)=1.
      B(3,4)=0.
      B(4,1)=AJ
      B(4,2)=-AK
      B(4,3)=BJ
      B(4,4)=-BK
      G(1)=AN/(2.*R*BM**2)
      G(2)=1./(2.*R*BM)
      G(3)=1.
      G(4)=BM
      DO13I=1,4
      DO13J=1,4
      A(I,J)=A(I,J)*EB(I)
   13 B(I,J)=B(I,J)*G(I)
      PUNCH104,N,AJ,AK,BJ,BK,BM,AN
  104 FORMAT(I3,2E14.8/4E14.8)
      PUNCH100,A,B
```

```
C     ARBITARY CONSTANTS FROM LOADED GENERATORS
      DO151=1,NS
      READ100,QF
      Y=Y2-2.*V(I)
      CALL COMFUN(Y,F)
      CALL FMULT(C1,F,B)
      CALL JADD(B1,B,C1)
      CALL FMULT(C2,F,A)
      CALL JSUB(A1,A,C2)
      CALL INVER(B1,E2,KO,4)
      GO TO (5,4),KO
    4 CALL MMULT(AK2,A1,E2)
      Y=2.*V(I)
      CALL COMFUN(Y,F)
      CALL FMULT(C1,F,B)
      CALL JADD(B1,C1,B)
      CALL FMULT(C2,F,A)
      CALL JSUB(A1,C2,A)
      CALL INVER(B1,E1,KO,4)
      GO TO (5,6),KO
    6 CALL MMULT(AK1,A1,E1)
      DO8L=1,4
      DO8J=1,4
    8 AK1(L,J)=AK1(L,J)-AK2(L,J)
      CALL INVER(AK1,AK2,KO,4)
      GO TO (5,7),KO
    7 CALL RMULT(VA,AK2,QF)
C
C     CAL COM FUN
      CALL RMULT(AB1,E1,VA)
      CALL RMULT(AB2,E2,VA)
      Y=YMAX-V(I)
      Z=Y2-2.*V(I)-Y
      CALL COMFUN(Y,F)
      CALL FMULT(C2,F,A)
      CALL COMFUN(Z,F)
      CALL FMULT(C1,F,A)
      CALL JSUB(A1,C2,C1)
      CALL RMULT (EU,A1,AB2)
      DO9L=1,4
    9 EN(L)=EN(L)-EU(L)
   15 PUNCH100,AB1,AB2
C
C     ARBITARY CONSTANTS FOR EDGE OF SHELL
      CALL COMFUN(2.*YMAX,F)
      CALL FMULT(C2,F,A)
      CALL JSUB(A1,C2,A)
      CALL INVER(A1,A2,KO,4)
      GO TO(5,54),KO
   54 CALL RMULT(ABT,A2,EN)
      PUNCH100,ABT
      IF(SENSE SWITCH 1)10,1
   10 TYPE106,N,EN
  106 FORMAT(/15,(4E14.8/))
      IF(NN-N)16,16,1
   16 TYPE107
  107 FORMAT(/12HEND OF SHELL////)
      GO TO 5
      END
```

```
C     P.C.S. GEN. LINE-LOAD. CHAPTER 3
C
C
      COMMON AJ,AK,BJ,BK,BM
      DIMENSION V(10),VA(5),EU(4),EN(4),FY(4,2),FZ(4,2),
     1A(4,4),B(4,4),AB1(4),AB2(4),ABT(4),A1(4,4),A2(4,4),
     2B1(4,4),B2(4,4),H(35,8)
      PI=3.1415927
C
C     READ AND PUNCH DIMENSIONS AND CONTROL
      TYPE103
  103 FORMAT(19H1ST CARD I3 LESS 10)
      READ104,NY
  104 FORMAT(I3)
      XNY=NY-1
      V(1)=0.
   14 READ100,R,XL,T,PHIK,E,XU
      READ100,P,FA,F,FR
      READ101,NN,NB,NS,NC,IDENT
  100 FORMAT(4E14.8)
  101 FORMAT(10I5)
      READ100,(VA(I),I=1,NS)
      NX=2*NN-1
      Y2=2.*PI*R
      YMAX=R*PHIK
      DY=YMAX/XNY
      DO11I=2,NY
    1 V(I)=V(I-1)+DY
      PUNCH100,R,XL,T,PHIK,E,XU
      PUNCH100,P,FA,F,FR
      PUNCH101,NN,NB,NS,NC,IDENT,NY
      PUNCH100,(V(I),I=1,NY)
      PUNCH100,(VA(I),I=1,NS)
C
C     OBTAIN VECTORS N AND U
   15 READ105,N,AJ,AK,BJ,BK,BM,AN
  105 FORMAT(I3,2E14.8/4E14.8)
      READ100,A,B
      DO21I=1,NY
      DO2J=1,8
    2 H(I,J)=0.
      KA=2
      DO6K=1,NS
      READ100,AB1,AB2
      Y1=VA(K)
      DO61I=1,NY
      IF(Y1-V(I))4,5,5
    5 KU=2
      Y=Y1+V(I)
      Z=Y1-V(I)
      GO TO 7
    4 KU=3
      Y=V(I)-Y1
      Z=Y2-2.*Y1-Y
      GO TO 7
    6 CONTINUE
      KU=1
      KA=1
      READ100,ABT
      DO131=1,NY
      Y=V(I)+YMAX
      Z=YMAX-V(I)
      GO TO 7
   13 CONTINUE
      PUNCH104,N
      PUNCH100,((H(I,J),J=1,8),I=1,NY)
      IF(NN-N)14,14,15
    7 CALL COMFUN (Y,FY)
      CALL COMFUN (Z,FZ)
      CALL FMULT (A1,FY,A)
      CALL FMULT (A2,FZ,A)
      CALL FMULT (B1,FY,B)
      CALL FMULT (B2,FZ,B)
      CALL JSUB (A1,A1,A2)
      CALL JADD (B1,B1,B2)
      GO TO (8,9,10),KU
    9 CALL RMULT (EN,A1,AB1)
      CALL RMULT (EU,B1,AB1)
      GO TO 11
   10 CALL RMULT (EN,A1,AB2)
      CALL RMULT (EU,B1,AB2)
      GO TO 11
    8 CALL RMULT (EN,A1,ABT)
      CALL RMULT (EU,B1,ABT)
   11 DO12J=1,4
      H(I,J)=EN(J)+H(I,J)
   12 H(I,J+4)=EU(J)+H(I,J+4)
      GO TO (13,6,6),KA
      END
```

```
C     SUBROUTINES FOR SHELL MATRICES
C
C
C     TO INVERT MATRICES
      SUBROUTINE INVER(A,B,KO,N)
      DIMENSIONA(4,4),B(4,4)
      DO31I=1,N
      DO3J=1,N
      IF(I-J)1,2,1
    1 B(I,J)=0.
      GO TO 3
    2 B(I,J)=1.
    3 CONTINUE
      DO121=1,N
      BIG=ABSF(A(I,I))
      JJ=I
      IF(I-N)14,15,15
   14 MM=N-1
      DO6J=I,MM
      IF(BIG-ABSF(A(J+1,I)))7,6,6
    7 BIG=ABSF(A(J+1,I))
      JJ=J+1
    6 CONTINUE
   15 IF(BIG-1.E-07)8,8,9
    8 PRINT36
   36 FORMAT(22HILL CONDITIONED MATRIX)
      KO=1
      RETURN
    9 IF(JJ-I)18,4,18
   18 DO10K=1,N
      C=A(I,K)
      D=B(I,K)
      A(I,K)=A(JJ,K)
      B(I,K)=B(JJ,K)
      A(JJ,K)=C
   10 B(JJ,K)=D
    4 P=1./A(I,I)
      DO11L=1,N
   11 B(I,L)=P*B(I,L)
      DO16L=1,N
   16 A(I,L)=P*A(I,L)
      DO12L=1,N
      IF(L-I)13,12,13
   13 P=A(L,I)
      DO17M=1,N
   17 A(L,M)=A(L,M)-P*A(I,M)
      DO24M=1,N
   24 B(L,M)=B(L,M)-P*B(I,M)
   12 CONTINUE
      KO=2
      RETURN
      END

C C=A+J*B
      SUBROUTINE JADD(C,A,B)
      DIMENSION C(4,4),B(4,4),A(4,4)
      DO11=1,3,2
      DO1J=1,4
      C(I,J)=A(I,J)+B(I,J)
    1 C(I+1,J)=A(I+1,J)-B(I+1,J)
      RETURN
      END

C     C=A-J*B
      SUBROUTINE JSUB(C,A,B)
      DIMENSION A(4,4),B(4,4),C(4,4)
      DO11=1,3,2
      DO1J=1,4
      C(I,J)=A(I,J)-B(I,J)
    1 C(I+1,J)=A(I+1,J)+B(I+1,J)
      RETURN
      END
C     B=A*F
      SUBROUTINE FMULT(B,F,A)
      DIMENSION B(4,4),F(4,2),A(4,4)
      DO11=1,4
      DO1J=1,2
      B(I,J)=A(I,1)*F(1,J)+A(I,2)*F(2,J)
    1 B(I,J+2)=A(I,3)*F(3,J)+A(I,4)*F(4,J)
      RETURN
      END

C     C=A*B
      SUBROUTINE MMULT(C,A,B)
      DIMENSION A(4,4),B(4,4),C(4,4)
      DO11=1,4
      DO1J=1,4
      S=0.
      DO2K=1,4
    2 S=S+A(I,K)*B(K,J)
    1 C(I,J)=S
      RETURN
      END

C     C=B*A
      SUBROUTINE RMULT(C,A,B)
      DIMENSION C(4),A(4,4),B(4)
      DO11=1,4
      S=0.
      DO2J=1,4
    2 S=S+A(I,J)*B(J)
    1 C(I)=S
      RETURN
      END

C     TO OBTAIN MATRIX F FOR Y=Y
      SUBROUTINE COMFUN(Y,F)
      DIMENSION F(4,2)
      COMMON AJ,AK,BJ,BK,BM
      P=BM*Y
      Q1=EXPF(-AJ*P)
      Q2=EXPF(-BJ*P)
      P1=COSF(AK*P)
      P2=SINF(AK*P)
      P3=COSF(BK*P)
      P4=SINF(BK*P)
      F(1,1)=Q1*P1
      F(1,2)=Q1*P2
      F(2,1)=-Q1*P2
      F(2,2)=Q1*P1
      F(3,1)=Q2*P3
      F(3,2)=Q2*P4
      F(4,1)=-Q2*P4
      F(4,2)=Q2*P3
      RETURN
      END
```

```
C     P.C.S. GEN. LINE-LOAD. CHAPTER 4
C
C
      DIMENSION X(5),CH(10),SH(10),EN(4),EU(4),Q(40,10),
     1V(10),C(10),S(10),HC(7),VA(5),HD(7),QA(40,10)
      PI=3.1415927
      READ101,ND,NDO
      READ100,(X(I),I=1,ND)
   27 READ100,R,XL,T,PHIK,E,XU
      READ100,P,FA,FB,FR
      READ101,NN,NB,NS,NC,IDENT,NY
      READ100,(V(I),I=1,NY)
      READ100,(VA(I),I=1,NS)
  100 FORMAT(4E14.8)
  101 FORMAT(1015)
      KU=ND*NY
      CA=T**3/(12.*(1.-XU**2))
      KUP=0
      ZAT=6./T
      DO31I=1,KU
      DO3J=1,7
      QA(I,J)=0.
    3 Q(I,J)=0.
      DO11I=1,NY
      CH(I)=COSF(V(I)/R)
    1 SH(I)=SINF(V(I)/R)
   16 READ104,N
  104 FORMAT(I3)
      XN=2*N-1
      AN=XN*PI/XL
      DO21I=1,ND
      C(I)=COSF(AN*X(I))
    2 S(I)=SINF(AN*X(I))
      CAT=CA*AN**2*(1.-XU**2)
      CAS=CA*(1.-XU)*AN
      DO41I=1,NY
      READ100,EN,EU
      HC(2)=EN(2)
      HC(4)=EN(4)
      HC(7)=(EU(2)*SH(I)+EU(3)*CH(I))/E
      HC(1)=XU*HC(2)+AN*T*EU(1)
      HC(3)=XU*HC(4)+CAT*EU(3)
      HC(5)=EN(1)
      HC(6)=-CAS*EU(4)
      HD(1)=HC(1)+HC(3)*ZAT
      HD(2)=HC(1)-HC(3)*ZAT
      HD(3)=HC(2)+HC(4)*ZAT
      HD(4)=HC(2)-HC(4)*ZAT
      HD(5)=HC(5)+HC(6)*ZAT
      HD(6)=HC(5)-HC(6)*ZAT
      HD(7)=HC(7)
      DO4K=1,ND
      L=K*NY-I+1
      DO9J=1,4
      Q(L,J)=Q(L,J)+HC(J)*C(K)
    9 QA(L,J)=QA(L,J)+HD(J)*C(K)
      DO8J=5,6
      Q(L,J)=Q(L,J)+HC(J)*S(K)
    8 QA(L,J)=QA(L,J)+HD(J)*S(K)
      Q(L,7)=Q(L,7)+HC(7)*C(K)
    4 QA(L,7)=QA(L,7)+HD(7)*C(K)
      IF(NN-N)15,15,16
   15 PUNCH100,R,XL,T,PHIK,E,XU
      PUNCH100,P,FA,FB,FR
      PUNCH101,NN,NB,NS,NC,IDENT,NY,ND,NDO
      PUNCH100,(X(I),I=1,ND)
      GO TO (20,21,20),NDO
   20 IF(KUP)22,22,21
   22 KUP=1
      PUNCH110
  110 FORMAT(//)
      PUNCH111
  111 FORMAT(5HGAUGE,8X,2HN1,8X,2HN2,8X,2HM1,8X,2HM2,7X,3HN12,8X,3HM12,5
     1X,5HDEFLN/11X,5HLB/IN,5X,5HLB/IN,7X,2HLB,8X,2HLB,6X,5HLB/IN,7X,2HL
     2B,7X,2HIN/)
      DO23I=1,KU
      PUNCH112,I,(Q(I,J),J=1,7)
  112 FORMAT(13,3X,2F10.1,2F10.3,F10.1,F10.3,F10.4)
      IF(I/NY*NY-I)23,24,24
   24 PUNCH113
  113 FORMAT(/)
   23 CONTINUE
      GO TO (27,21,15),NDO
   21 PUNCH213
  213 FORMAT(/17HSTRESSES IN LB/IN)
      PUNCH114
  114 FORMAT(5HGAUGE,9X,11HLONG STRESS,8X,12HTRANS STRESS,8X,12HSHEAR ST
     1RESS,7X,5HDEFLN/13X,3(3HINT,7X,3HEXT,7X),2HIN/)
      DO25I=1,KU
      PUNCH115,I,(QA(I,J),J=1,7)
  115 FORMAT(13,3X,6F10.1,F10.4)
      IF(I/NY*NY-I)25,26,25
   26 PUNCH113
   25 CONTINUE
      GO TO 27
      END
```

```
C     P.C.S. GEN. LINE-LOAD. CHAPTER 5
C
C
      DIMENSION A(40,10),B(40,10),W(5),IDENT(5),X(7)
      READ101,II,M,IDE
   17 DO21I=1,40
      DO21J=1,10
   21 B(I,J)=0.
  100 FORMAT(4E14.8)
  101 FORMAT(1015)
      READ100,(W(I),I=1,II)
      I=1
   11 READ100,R,XL,T,PHIK,E,XU
      READ100,P,FA,FB,FR
      READ101,NN,NB,NS,NC,IDENT(I),NY,ND,NDO
      READ100,(X(L),L=1,ND)
      READ107
  107 FORMAT(/23H12345678901234567890123/)
      READ108
  108 FORMAT(79H
     1
     2/79H
     3
     4/)
      NDE=NY*ND
    7 GO TO (1,2),M
    1 READ105,K,(A(K,J),J=1,7)
  105 FORMAT(I3,3X,2F10.1,2F10.3,F10.1,F10.3,F10.4)
      GO TO 3
    2 READ104,K,(A(K,J),J=1,7)
  104 FORMAT(I3,3X,6F10.1,F10.4)
    3 DO4J=1,7
    4 B(K,J)=B(K,J)+A(K,J)*W(I)
      IF(K/NY*NY-K)5,6,5
    6 READ106
  106 FORMAT(/)
    5 IF(NDE-K)8,8,7
    8 IF(II-I)9,9,10
   10 I=I+1
      GO TO 11
  117 FORMAT(19HTHEORETICAL RESULTS,I5//)
    9 PUNCH117,IDE
      PUNCH109,(IDENT(I),W(I),I=1,II)
  109 FORMAT(6HSUM OF/(12X,I5,2H *,F10.4)//)
      PUNCH100,R,XL,T,PHIK,E,XU
      PUNCH100,P,FA,FB,FR
      PUNCH101,NN,NB,NS,NC,NY,ND,NDO
      PUNCH100,(X(I),I=1,ND)
      PUNCH 107
      PUNCH 108
      DO12K=1,NDE
      GO TO (13,14),M
   13 PUNCH105,K,(B(K,J),J=1,7)
      GO TO 15
   14 PUNCH104,K,(B(K,J),J=1,7)
   15 IF(K/NY*NY-K)12,16,12
   16 PUNCH106
   12 CONTINUE
      GO TO 17
      END
```

A P P E N D I X V

LISTING OF MODEL SHELL RESULTS

The results in this appendix are given in three sections:

(a) Average reduced strains and deflections are given in pages 184 - 187. The numbers in the first column of the listings refer to the location of the strain gauge rosettes as given in figure 7.1.

(b) On pages 188 - 195 listings of experimental and theoretical actions and deflections for each of the 8 model tests are given.

(c) In table V.2 figures are given for the equilibrium between internal actions and applied external prestressing loads for all the model tests.

Symbol	Meaning
M1	m_1
M2	m_2
M12	m_{12}
N1	n_1
N2	n_2
N12	n_{12}
DEFLN	vertical deflection
GAUGE	location of strain gauge rosettes as given in figure 7.1.

Table V.1 Meaning of symbols in listings of actions and displacements

EXPERIMENTAL STRAINS AND DEFLECTIONS

MODEL TEST 1
P=1200 LB FR=00 LB
D=0.048 YM F=0.000 YM

STRAIN IN MICROSTRAIN DEFLECTION IN INCHES

	INTRADOS STRAIN			EXTRADOS STRAIN			
POINT	GAUGE 1	GAUGE 2	GAUGE 3	GAUGE 1	GAUGE 2	GAUGE 3	VERT DEFLN
1	137	-42		110	-35		-.0025
2	41	-3	-5	15	-3	4	.0040
3	-40	10		-64	17		.0090
4	-108	7	10	-122	-17	-16	.0100
5	-153	84		-163	10		.0215
6	-176	117		-192	-6		.0250
7	-186	52	42	-197	-54	-50	.0270
8	103	-32		97	-33		-.0050
9	36	-19		35	-5		
10	-33	6		-44	17		
11	-98	43		-111	19		
12	-145	91		-163	9		
13	-176	120		-194	-3		
14	-187	49	64	-210	-51	-60	.0255
15	28	-14		69	-25		-.0082
16	15	-18		52	-8		
17	-24	-17		-2	17		
18	-76	4		-76	31		
19	-136	66		-156	23		
20	-197	143		-223	-3		
21	-227	73	73	-250	-60	-72	.0210
22	14	-5		28	-10		-.0050
23	6	34	-37	29	-8	15	
24	-12	35	-57	21	7	19	
25	-42	11	-68	-11	-8	50	
26	-97	-29	-20	-94	-56	80	
27	-208	-17	98	-270	-118	32	
28	-292	95	128	-399	-84	-104	.0125
29	35	-11		-8	-4		
30	16	29	-31	-11	-13	-3	
31	-1	37	-45	-1	3	1	
32	-25	34	-51	5	-1	25	
33	-74	-3	-44	5	-53	94	
34	-254	-107	96	-151	-187	198	
35	-621	65	109	-539	-12	-28	

EXPERIMENTAL STRAINS AND DEFLECTIONS

MODEL TEST 4
P=1200 LB FR=00 LB
D=0.333 YM F=0.000 YM

STRAIN IN MICROSTRAIN DEFLECTION IN INCHES

	INTRADOS STRAIN			EXTRADOS STRAIN			
POINT	GAUGE 1	GAUGE 2	GAUGE 3	GAUGE 1	GAUGE 2	GAUGE 3	VERT DEFLN
1	58	-17		43	-12		.0160
2	-2	1	0	-15	-2	2	.0160
3	-54	19		-65	21		.0150
4	-98	-2	-2	-105	-3	1	.0145
5	-131	35		-132	46		.0140
6	-144	45		-155	49		.0135
7	-153	-2	-2	-160	-2	-1	.0140
8	54	-17		38	-13		.0142
9	0	3		-14	2		
10	-55	19		-65	18		
11	-100	37		-103	32		
12	-125	39		-134	43		
13	-142	41		-153	51		
14	-147	-9	-1	-164	0	-3	.0125
15	49	-16		45	-13		.0085
16	-1	0		-10	4		
17	-54	23		-67	15		
18	-100	49		-112	21		
19	-128	50		-139	35		
20	-143	38		-148	53		
21	-143	-17	-19	-151	16	7	.0080
22	23	-8		41	-12		.0035
23	-6	4	-17	12	5	4	
24	-43	-14	-1	-40	-11	15	
25	-113	-12	48	-129	-29	4	
26	-187	38	19	-187	2	-19	
27	-141	37	-51	-130	43	-29	
28	-105	-42	-42	-87	27	23	.0040
29	16	-6		17	-6		
30	2	14	-21	5	8	-8	
31	-20	-6	-22	2	-8	13	
32	-81	-78	44	-75	-76	63	
33	-321	38	54	-346	0	-46	
34	-88	53	-97	-80	99	-99	
35	-38	-34	-39	-8	13	14	

EXPERIMENTAL STRAINS AND DEFLECTIONS

MODEL TEST 3
P=1200 LB FR=00 LB
D=0.667 YM F=0.000 YM

STRAIN IN MICROSTRAIN DEFLECTION IN INCHES

	INTRADOS STRAIN			EXTRADOS STRAIN			
POINT	GAUGE 1	GAUGE 2	GAUGE 3	GAUGE 1	GAUGE 2	GAUGE 3	VERT DEFLN
1	-182	55		-151	47		.0185
2	-136	0	2	-112	3	-3	.0125
3	-101	37		-88	34		.0055
4	-77	-18	-2	-68	17	16	-.0015
5	-63	-18		-51	62		-.0085
6	-51	-46		-45	80		-.0125
7	-47	-55	-56	-41	56	57	-.0150
8	-144	45		-134	43		.0195
9	-127	43		-124	35		
10	-110	35		-104	33		
11	-84	11		-77	41		
12	-63	-20		-53	60		
13	-47	-59		-39	81		
14	-41	-61	-61	-33	55	58	-.0140
15	-58	22		-120	38		.0197
16	-107	47		-154	37		
17	-123	48		-146	40		
18	-99	21		-109	47		
19	-62	-20		-55	60		
20	-32	-52		-14	69		
21	-19	-53	-52	4	56	58	-.0120
22	10	3		-64	23		.0127
23	-101	-48	94	-170	-4	-29	
24	-166	-6	65	-218	18	-50	
25	-112	3	-13	-128	68	-59	
26	-51	-44	-27	-76	73	-24	
27	-23	-49	-25	17	54	11	
28	-14	-32	-34	28	32	32	-.0070
29	-37	10		50	-4		
30	-112	-95	91	-66	-24	38	
31	-327	5	86	-338	47	-73	
32	-77	8	-53	-83	123	-123	
33	6	-49	-6	-11	51	-46	
34	29	-35	-1	-13	13	-15	
35	36	-13	-17	-11	-3	-3	

EXPERIMENTAL STRAINS AND DEFLECTIONS

MODEL TEST 5
P=1200 LB FR=00 LB
D=0.833 YM F=0.000 YM

STRAIN IN MICROSTRAIN DEFLECTION IN INCHES

	INTRADOS STRAIN			EXTRADOS STRAIN			
POINT	GAUGE 1	GAUGE 2	GAUGE 3	GAUGE 1	GAUGE 2	GAUGE 3	VERT DEFLN
1	-337	101		-283	86		-.0210
2	-227	-15	13	-185	2	-10	-.0215
3	-135	46		-114	30		-.0225
4	-62	-2	1	-47	-1	3	-.0230
5	-21	0		-3	7		-.0245
6	10	-13		27	0		-.0240
7	23	-7	-7	40	10	9	-.0250
8	-306	94		-268	85		-.0182
9	-222	71		-200	60		
10	-135	39		-119	38		
11	-68	14		-51	22		
12	-20	-4		-3	10		
13	12	-15		29	2		
14	23	-7	-7	42	10	7	-.0225
15	-287	90		-283	85		-.0090
16	-219	66		-210	71		
17	-141	36		-127	51		
18	-66	-4		-52	39		
19	-15	-18		1	19		
20	13	-13		32	2		
21	24	1	3	43	1	6	-.0160
22	-188	66		-301	88		-.0012
23	-205	1	29	-278	-9	-31	
24	-122	-6	-38	-142	31	-15	
25	-48	-45	-32	-23	37	16	
26	-10	-35	-4	23	10	25	
27	8	-9	10	31	-5	14	
28	12	9	8	29	-4	0	-.0090
29	-156	56		-177	61		
30	-357	12	73	-364	38	-41	
31	-100	-10	-40	-82	98	-79	
32	-14	-54	0	0	19	7	
33	7	-31	10	7	-18	25	
34	11	-9	6	7	-21	13	
35	13	3	-1	11	-6	-3	

EXPERIMENTAL STRAINS AND DEFLECTIONS

MODEL TEST 2
P=1200 LB FR=00 LB
D=0.972 YM F=0.000 YM

STRAIN IN MICROSTRAIN DEFLECTION IN INCHES

	INTRADOS STRAIN			EXTRADOS STRAIN			
POINT	GAUGE 1	GAUGE 2	GAUGE 3	GAUGE 1	GAUGE 2	GAUGE 3	VERT DEFLN
1	-449	131		-416	126		-.0810
2	-305	-16	-15	-282	-10	18	-.0715
3	-170	39		-149	51		-.0615
4	-50	8	7	-29	-13	-12	-.0500
5	30	44		53	-72		-.0405
6	77	69		105	-121		-.0335
7	99	80	82	121	-72	-72	-.0310
8	-481	141		-403	130		-.0782
9	-318	74		-281	99		
10	-164	31		-134	48		
11	-50	24		-20	-11		
12	27	48		53	-73		
13	68	76		93	-123		
14	85	86	82	108	-77	-72	-.0275
15	-619	174		-469	143		-.0647
16	-341	67		-241	100		
17	-140	13		-66	41		
18	-26	22		20	-23		
19	30	55		55	-77		
20	52	81		58	-109		
21	57	77	77	58	-74	-72	-.0175
22	-723	201		-535	166		-.0417
23	-343	17	-145	-180	23	51	
24	-101	-18	-76	29	-22	83	
25	-6	20	0	53	-84	76	
26	30	56	34	32	-101	38	
27	38	61	47	12	-79	-7	
28	36	55	55	8	-45	-45	-.0085
29	-821	228		-770	212		
30	-192	-2	-180	-100	6	-10	
31	-35	-27	-45	48	-117	140	
32	-23	26	1	54	-129	137	
33	-42	45	14	54	-82	100	
34	-54	43	21	59	-29	57	
35	-62	30	35	56	15	14	

EXPERIMENTAL STRAINS AND DEFLECTIONS

MODEL TEST 6
P=1200 LB FR=31 LB
D=0.833 YM F=0.138 YM

STRAIN IN MICROSTRAIN DEFLECTION IN INCHES

	INTRADOS STRAIN			EXTRADOS STRAIN			
POINT	GAUGE 1	GAUGE 2	GAUGE 3	GAUGE 1	GAUGE 2	GAUGE 3	VERT DEFLN
1	-516	145		-447	140		-.0885
2	-311	-18	-25	-248	-12	22	-.0765
3	-153	39		-103	28		-.0620
4	-36	24	25	-2	-26	-28	-.0490
5	28	71		49	-94		-.0365
6	65	91		78	-130		-.0290
7	77	94	97	86	-87	-87	-.0260
8	-498	144		-399	131		-.0797
9	-311	65		-245	92		
10	-151	39		-104	32		
11	-44	43		-13	-27		
12	22	62		43	-79		
13	58	81		74	-115		
14	69	85	83	89	-75	-73	-.0250
15	-423	122		-378	110		-.0492
16	-276	64		-240	75		
17	-152	25		-113	46		
18	-51	12		-26	8		
19	11	24		34	-40		
20	47	47		63	-77		
21	56	60	59	73	-55	-52	-.0175
22	-234	79		-330	97		-.0207
23	-245	4	20	-291	-77	35	
24	-131	7	-55	-144	-42	54	
25	-39	-30	-41	-11	-30	72	
26	5	-8	2	37	-50	53	
27	26	24	31	43	-53	12	
28	32	40	40	42	-30	-28	-.0100
29	-68	34		-238	74		
30	-328	32	72	-443	-54	-13	
31	-81	-19	-47	-103	30	-21	
32	-10	-56	0	6	-50	70	
33	-3	-22	12	27	-69	76	
34	-9	5	13	39	-45	42	
35	-12	13	13	41	-5	-4	

EXPERIMENTAL STRAINS AND DEFLECTIONS

MODEL TEST 7
P=1200 LB FR=60 LB
D=0.667 YM F=0.305 YM

STRAIN IN MICROSTRAIN DEFLECTION IN INCHES

POINT	INTRADOS STRAIN GAUGE 1	GAUGE 2	GAUGE 3	EXTRADOS STRAIN GAUGE 1	GAUGE 2	GAUGE 3	VERT DEFLN
1	-627	171		-416	142		-.0895
2	-327	-43	-22	-191	15	17	-.0770
3	-136	38		-53	16		-.0625
4	-23	35	40	20	-27	-34	-.0475
5	28	84		45	-100		-.0350
6	52	102		53	-124		-.0275
7	59	95	98	57	-88	-86	-.0240
8	-506	145		-361	116		-.0742
9	-301	55		-206	89		
10	-143	37		-82	30		
11	-44	45		-10	-27		
12	17	62		34	-71		
13	49	74		61	-97		
14	57	74	74	70	-64	-63	-.0240
15	-178	61		-285	82		-.0315
16	-197	68		-260	52		
17	-156	18		-164	62		
18	-80	0		-67	38		
19	-10	-1		15	-2		
20	38	14		67	-43		
21	55	30	32	88	-25	-22	-.0195
22	15	5		-124	38		-.0087
23	-115	-78	122	-249	-62	15	
24	-165	-16	68	-259	-99	22	
25	-94	-41	-27	-117	-15	48	
26	-18	-55	-18	17	-4	55	
27	17	-19	13	65	-17	30	
28	29	16	16	74	-5	-5	-.0120
29	5	-3		11	5		
30	-100	-90	96	-128	-86	62	
31	-298	-29	129	-377	-65	-16	
32	-65	-66	-15	-71	46	-23	
33	5	-79	18	18	-28	47	
34	14	-34	16	33	-39	35	
35	16	-1	-1	36	-7	-9	

EXPERIMENTAL STRAINS AND DEFLECTIONS

MODEL TEST 8
P=1200 LB FR=87 LB
D=0.500 YM F=0.472 YM

STRAIN IN MICROSTRAIN DEFLECTION IN INCHES

POINT	INTRADOS STRAIN GAUGE 1	GAUGE 2	GAUGE 3	EXTRADOS STRAIN GAUGE 1	GAUGE 2	GAUGE 3	VERT DEFLN
1	-611	173		-481	141		-.0870
2	-316	-55	-47	-171	11	32	-.0745
3	-121	26		-15	8		-.0595
4	-17	40	42	37	-31	-37	-.0450
5	24	89		40	-102		-.0325
6	39	100		34	-114		-.0255
7	44	87	90	33	-84	-80	-.0230
8	-474	130		-329	112		-.0622
9	-282	44		-202	83		
10	-133	16		-73	40		
11	-47	32		-10	-8		
12	8	47		29	-51		
13	39	63		49	-81		
14	45	68	67	54	-58	-56	-.0230
15	-12	14		-185	52		-.0150
16	-126	58		-249	34		
17	-148	25		-203	43		
18	-102	-17		-102	57		
19	-33	-25		-6	27		
20	21	-16		60	-9		
21	45	3	5	86	-1	4	-.0215
22	72	-19		-19	11		-.0022
23	-49	-54	68	-148	-46	5	
24	-135	-69	176	-198	-152	-10	
25	-154	-105	82	-194	-59	42	
26	-70	-74	-12	-50	3	51	
27	-2	-53	-18	66	17	41	
28	18	-21	-23	100	23	25	-.0145
29	-18	-1		38	-10		
30	-54	-37	21	-5	-11	24	
31	-89	-147	152	-107	-136	72	
32	-264	-119	157	-336	-81	9	
33	-33	-90	-6	-49	30	-26	
34	27	-81	7	28	-17	15	
35	38	-22	-25	36	-7	-7	

EXPERIMENTAL STRESSES AND DEFLECTIONS

MODEL TEST 1
P=1200 LB FR=00 LB
D=0.048 YM F=0.000 YM

GAUGE	N1 LB/IN	N2 LB/IN	M1 LB	M2 LB	N12 LB/IN	M12 LB	DEFLN IN
1	165.0	-.9	.400	.009			-.0025
2	36.4	-4.5	.352	-.105	2.9	-.113	.0040
3	-70.6	-3.8	.358	.010			.0090
4	-155.2	-3.3	.358	.519	2.3	.025	.0100
5	-212.1	-1.6	.522	1.238			.0215
6	-246.5	-1.6	.856	2.051			.0250
7	-255.7	2.5	.820	2.115	-3.5	-.176	.0270
8	132.9	-2.1	.098	.044			-.0050
9	46.4	-1.6	-.051	-.214			
10	-51.8	-.6	.135	-.114			
11	-139.9	-1.2	.323	.454			
12	-205.1	3.8	.690	1.418			
13	-247.1	2.8	.908	2.081			
14	-263.1	8.7	1.080	2.404	3.5	.327	.0255
15	62.8	-6.5	-.605	-.029			-.0082
16	43.8	-3.7	-.643	-.339			
17	-18.9	-5.8	-.508	-.638			
18	-104.3	-8.2	-.134	-.438			
19	-195.2	-.4	.540	.790			
20	-278.5	8.4	1.144	2.480			
21	-314.0	16.1	1.260	2.992	-7.0	.151	.0210
22	27.3	-1.5	-.195	.010			-.0050
23	23.8	1.7	-.360	-.105	-28.7	-1.222	
24	6.5	1.7	-.627	-.511	-46.9	-1.335	
25	-37.8	-6.2	-.777	-1.046	-12.3	-1.751	
26	-131.0	-8.9	-.280	-.775	85.7	-1.637	
27	-318.2	6.8	1.455	1.768	156.7	-.466	
28	-453.2	30.5	2.911	4.373	7.6	.692	.0125
29	17.0	-4.6	.655	.101			
30	.7	-8.4	.429	.146	-29.9	-.894	
31	-1.9	-1.9	-.038	-.125	-50.5	-1.033	
32	-11.9	4.3	-.559	-.428	-35.2	-1.436	
33	-46.3	-1.6	-1.434	-.911	63.4	-2.419	
34	-268.7	7.8	-1.569	-.186	347.6	-2.343	
35	-749.1	88.6	-.481	2.333	17.0	.768	

THEORETICAL STRESSES AND DEFLECTIONS

MODEL TEST 1
D=0.048 YM F=0.000 YM
P=1200 LB FR=00 LB

GAUGE	N1 LB/IN	N2 LB/IN	M1 LB	M2 LB	N12 LB/IN	M12 LB	DEFLN IN
1	167.0	0.0	.199	0.000	0.0	0.000	-.0072
2	38.6	-1.2	.235	-.013	0.0	0.000	0.0000
3	-66.8	-2.2	.333	.204	0.0	0.000	.0074
4	-149.8	-1.3	.521	.803	0.0	0.000	.0149
5	-208.7	.7	.755	1.651	0.0	0.000	.0217
6	-243.5	2.7	.950	2.398	0.0	0.000	.0265
7	-255.0	3.6	1.026	2.695	0.0	0.000	.0282
8	139.9	0.0	-.094	0.000	0.0	-.153	-.0088
9	41.5	-1.3	-.014	-.127	-6.0	-.164	-.0020
10	-54.4	-2.8	.138	-.013	-.7	-.120	.0051
11	-141.0	-2.0	.410	.573	6.1	-.030	.0125
12	-209.1	.7	.748	1.560	9.0	.052	.0195
13	-251.6	3.8	1.030	2.514	6.2	.063	.0246
14	-265.4	5.0	1.137	2.910	0.0	0.000	.0265
15	63.6	0.0	-.605	0.000	0.0	-.526	-.0094
16	43.4	-.5	-.533	-.251	-13.3	-.556	-.0046
17	-16.0	-3.6	-.428	-.511	-6.9	-.575	.0004
18	-102.4	-6.7	-.109	-.361	10.8	-.457	.0062
19	-200.7	-3.4	.528	.757	26.7	-.162	.0126
20	-284.0	6.5	1.235	2.586	24.3	.066	.0181
21	-320.8	13.4	1.552	3.567	0.0	0.000	.0203
22	14.5	0.0	-.424	0.000	0.0	-.674	-.0056
23	27.9	1.7	-.439	-.072	-14.0	-.666	-.0033
24	7.5	.3	-.578	-.367	-18.9	-.744	-.0010
25	-41.9	-8.7	-.749	-.818	-3.2	-.883	.0017
26	-136.7	-19.8	-.427	-.599	40.6	-.874	.0053
27	-314.3	-1.1	.927	1.580	90.1	-.435	.0096
28	-501.3	56.1	2.077	3.891	0.0	0.000	.0119
29	3.4	0.0	-.185	0.000	0.0	-.679	-.0025
30	12.8	1.3	-.202	-.006	-12.0	-.638	-.0015
31	6.2	1.4	-.324	-.141	-23.1	-.647	-.0006
32	-13.4	-4.7	-.588	-.464	-17.9	-.807	.0004
33	-60.6	-20.3	-.721	-.631	23.9	-1.106	.0019
34	-207.4	-25.4	.011	.438	145.5	-1.084	.0041
35	-518.7	51.0	1.149	2.371	0.0	0.000	.0054

EXPERIMENTAL STRESSES AND DEFLECTIONS

MODEL TEST 4
P=1200 LB FR=00 LB
D=0.333 YM F=0.000 YM

GAUGE	N1 LB/IN	N2 LB/IN	M1 LB	M2 LB	N12 LB/IN	M12 LB	DEFLN IN
1	67.9	1.6	.226	-.001			.0160
2	-11.0	.8	.186	.005	1.7	-.062	.0160
3	-79.3	2.0	.162	.021			.0150
4	-135.9	1.0	.092	-.023	2.3	-.050	.0145
5	-176.5	0.0	-.042	-.183			.0140
6	-199.7	2.1	.153	-.009			.0135
7	-208.5	2.6	.095	-.013	.5	-.012	.0140
8	61.1	-1.0	.247	.019			.0142
9	-9.1	.5	.224	.083			
10	-80.7	-.3	.161	.063			
11	-134.0	5.1	.075	.108			
12	-172.7	1.8	.132	-.030			
13	-197.4	.8	.119	-.119			
14	-208.1	-.3	.217	-.080	2.9	.138	.0125
15	63.6	.3	.048	-.027			.0085
16	-7.1	.4	.121	-.019			
17	-81.2	.1	.242	.187			
18	-140.3	3.8	.327	.512			
19	-177.8	2.2	.264	.308			
20	-194.7	1.0	.001	-.226			
21	-196.9	-.6	-.077	-.622	-6.4	.088	.0080
22	42.9	0.0	-.278	-.028			.0035
23	3.3	-2.0	-.325	-.223	-12.9	-.251	
24	-56.3	-3.7	-.103	-.198	22.9	-.163	
25	-158.9	10.5	.425	.644	55.1	.352	
26	-241.5	27.3	.241	.787	-24.0	.012	
27	-179.9	4.7	-.248	-.299	-94.5	-.214	
28	-132.2	-12.9	-.713	-1.440	-2.3	.050	.0040
29	21.4	-1.3	-.015	-.004			
30	3.5	-3.5	-.064	-.072	-29.9	-.239	
31	-15.3	-10.9	-.417	-.337	2.9	-.466	
32	-110.6	-20.4	-.169	-.228	155.0	-.226	
33	-435.6	35.9	.821	1.469	-18.2	.793	
34	-118.7	-18.7	-.258	-.469	-206.1	.617	
35	-37.8	-21.5	-.773	-1.078	-2.3	-.075	

THEORETICAL STRESSES AND DEFLECTIONS

MODEL TEST 4
P=1200 LB FR=00 LB
D=0.333 YM F=0.000 YM

GAUGE	N1 LB/IN	N2 LB/IN	M1 LB	M2 LB	N12 LB/IN	M12 LB	DEFLN IN
1	77.0	0.0	.212	0.000	0.0	0.000	.0163
2	-12.2	0.0	.197	.030	0.0	0.000	.0156
3	-83.1	0.0	.180	.043	0.0	0.000	.0150
4	-137.6	0.0	.167	.038	0.0	0.000	.0144
5	-177.1	0.0	.163	.023	0.0	0.000	.0140
6	-201.3	0.0	.167	.010	0.0	0.000	.0138
7	-209.5	0.0	.169	.005	0.0	0.000	.0137
8	78.4	0.0	.245	0.000	0.0	.069	.0143
9	-12.7	0.0	.227	.051	.1	.069	.0138
10	-83.6	.1	.207	.109	0.0	.057	.0134
11	-137.4	.2	.186	.132	-.2	.020	.0131
12	-176.1	0.0	.169	.079	-.1	-.022	.0127
13	-201.3	-.1	.163	-.017	0.0	-.031	.0123
14	-210.0	-.3	.163	-.067	0.0	0.000	.0122
15	73.4	0.0	.053	0.000	0.0	.076	.0080
16	-9.0	-1.1	.114	-.046	-.5	.076	.0083
17	-82.4	-.5	.237	.155	3.5	.131	.0088
18	-142.9	2.7	.341	.562	2.7	.114	.0091
19	-184.7	4.0	.294	.550	-4.2	-.059	.0088
20	-198.2	-1.9	.117	-.160	-7.2	-.159	.0080
21	-201.3	-5.6	.018	-.631	0.0	0.000	.0075
22	41.7	0.0	-.361	0.000	0.0	-.099	.0030
23	3.1	-2.4	-.329	-.205	-7.3	-.132	.0033
24	-55.9	-8.0	-.190	-.257	7.7	-.134	.0039
25	-151.6	-.7	.345	.523	32.9	.017	.0047
26	-276.0	35.7	.728	1.425	-12.6	.051	.0049
27	-177.6	-8.3	-.170	-.375	-50.3	0.000	.0036
28	-133.4	-22.4	-.773	-1.462	0.0	0.000	.0027
29	17.5	0.0	-.269	0.000	0.0	-.164	.0011
30	4.3	-1.3	-.297	-.123	-13.1	-.157	.0013
31	-23.8	-8.7	-.348	-.268	-1.5	-.246	.0015
32	-94.6	-14.2	-.058	.095	53.8	-.265	.0020
33	-315.7	45.4	.488	1.105	-15.6	.165	.0022
34	-103.8	-18.4	-.426	-.390	-79.5	.432	.0013
35	-57.6	-21.0	-.890	-1.028	0.0	0.000	.0008

EXPERIMENTAL STRESSES AND DEFLECTIONS

MODEL TEST 3
P=1200 LB FR=00 LB
D=0.667 YM F=0.000 YM

GAUGE	N1 LB/IN	N2 LB/IN	M1 LB	M2 LB	N12 LB/IN	M12 LB	DEFLN IN
1	-222.7	.3	-.447	-.023			.0185
2	-164.3	5.8	-.332	.030	-2.3	.100	.0125
3	-123.5	9.0	-.189	-.015			.0055
4	-94.2	9.1	-.312	-.552	8.8	.214	-.0015
5	-74.8	6.1	-.582	-1.342			-.0085
6	-63.2	3.0	-.734	-2.070			-.0125
7	-57.6	2.6	-.819	-2.390	0.0	-.025	-.0150
8	-185.7	2.5	-.147	-.016			.0195
9	-168.4	.5	-.003	.126			
10	-142.4	1.2	-.084	.002			
11	-107.1	2.1	-.258	-.519			
12	-77.1	2.7	-.551	-1.332			
13	-58.5	-3.4	-.833	-2.299			
14	-50.0	-2.9	-.883	-2.505	1.7	-.037	-.0140
15	-117.7	4.1	.920	.041			.0197
16	-173.7	2.8	.804	.403			
17	-178.6	4.0	.419	.256			
18	-137.8	3.3	.026	-.374			
19	-77.9	2.5	-.504	-1.318			
20	-30.5	1.8	-.898	-2.049			
21	-8.5	4.6	-1.043	-2.331	1.7	-.012	-.0120
22	-33.6	6.8	1.094	.052			.0127
23	-177.8	11.6	1.264	.820	69.8	2.154	
24	-250.8	20.6	1.048	.954	1.7	1.776	
25	-159.7	3.6	.161	-.216	-84.5	1.436	
26	-54.5	-8.7	-.763	-1.280	-47.5	1.474	
27	-5.9	-4.2	-1.033	-1.463	-11.1	.869	
28	9.5	-1.2	-1.039	-1.388	-1.1	-.025	-.0070
29	10.8	7.2	-1.327	-.208			
30	-116.4	8.3	-.722	-.169	146.8	1.587	
31	-431.4	45.2	.556	1.254	-23.4	2.595	
32	-113.6	-19.3	-.063	-.485	-182.0	2.393	
33	-10.9	-24.8	.043	-.647	-32.2	1.801	
34	5.3	-19.4	.494	-.385	4.1	.793	
35	11.7	-18.1	.601	-.271	-2.3	-.050	

THEORETICAL STRESSES AND DEFLECTIONS

MODEL TEST 3
P=1200 LB FR=00 LB
D=0.667 YM F=0.000 YM

GAUGE	N1 LB/IN	N2 LB/IN	M1 LB	M2 LB	N12 LB/IN	M12 LB	DEFLN IN
1	-211.3	0.0	-.119	0.000	0.0	0.000	.0262
2	-164.8	1.2	-.132	-.035	0.0	0.000	.0173
3	-130.0	2.3	-.208	-.290	0.0	0.000	.0083
4	-102.9	1.5	-.386	-.917	0.0	0.000	-.0005
5	-83.1	-.6	-.629	-1.792	0.0	0.000	-.0083
6	-70.8	-2.9	-.842	-2.564	0.0	0.000	-.0138
7	-66.6	-3.8	-.927	-2.872	0.0	0.000	-.0157
8	-184.8	0.0	.142	0.000	0.0	.051	.0270
9	-167.1	1.5	.086	.054	6.0	.060	.0182
10	-141.8	2.7	-.046	-.165	.9	.031	.0092
11	-112.6	1.8	-.298	-.831	-6.0	-.002	.0002
12	-83.6	-.8	-.629	-1.791	-9.3	-.017	-.0076
13	-62.0	-3.5	-.917	-2.638	-6.7	-.013	-.0132
14	-54.0	-4.7	-1.032	-2.973	0.0	0.000	-.0152
15	-94.1	0.0	1.078	0.000	0.0	.488	.0249
16	-175.9	2.3	.866	.414	15.1	.507	.0175
17	-187.9	5.0	.526	.348	1.0	.393	.0098
18	-143.8	1.1	-.005	-.572	-16.3	.285	.0017
19	-82.9	-3.2	-.602	-1.741	-20.9	.274	-.0055
20	-33.3	-4.8	-1.052	-2.476	-13.2	.202	-.0106
21	-14.7	-4.8	-1.213	-2.692	0.0	0.000	-.0124
22	12.7	0.0	1.321	0.000	0.0	1.024	.0153
23	-175.0	1.1	1.331	.557	37.4	1.038	.0113
24	-297.5	32.4	1.237	1.190	-3.4	1.016	.0068
25	-161.2	-6.8	.114	-.487	-47.8	.944	.0014
26	-56.8	-11.9	-.753	-1.559	-22.3	.840	-.0034
27	-5.9	-3.3	-.949	-1.573	-5.3	.476	-.0063
28	8.7	.6	-.934	-1.451	0.0	0.000	-.0072
29	34.3	0.0	.544	0.000	0.0	1.121	.0070
30	-106.3	-10.7	.588	.188	46.2	1.054	.0052
31	-329.3	42.9	.820	.967	-7.8	1.343	.0033
32	-100.1	-18.2	-.170	-.435	-67.5	1.473	.0005
33	-24.4	-10.9	-.613	-.895	-9.6	1.016	-.0016
34	.5	-1.3	-.545	-.726	3.6	.464	-.0029
35	6.8	1.8	-.468	-.605	0.0	0.000	-.0033

EXPERIMENTAL STRESSES AND DEFLECTIONS

MODEL TEST 5
P=1200 LB FR=00 LB
D=0.833 YM F=0.000 YM

GAUGE	N1 LB/IN	N2 LB/IN	M1 LB	M2 LB	N12 LB/IN	M12 LB	DEFLN IN
1	-416.2	-2.7	-.805	-.034			-.0210
2	-274.8	3.1	-.588	.080	9.3	.503	-.0215
3	-166.7	-.2	-.262	.160			-.0225
4	-72.3	2.6	-.235	-.024	4.1	-.012	-.0230
5	-15.9	-.2	-.315	-.196			-.0245
6	24.1	-1.1	-.328	-.285			-.0240
7	42.2	1.2	-.346	-.339	-.5	.012	-.0250
8	-383.6	1.9	-.567	-.046			-.0182
9	-281.9	1.3	-.307	.061			
10	-170.1	-.6	-.256	-.050			
11	-79.5	-.6	-.320	-.211			
12	-15.4	-.7	-.333	-.301			
13	27.7	0.0	-.363	-.352			
14	43.2	.2	-.368	-.317	-1.7	.037	-.0225
15	-381.6	-.1	-.054	.054			-.0090
16	-285.7	4.2	-.180	-.126			
17	-178.1	3.5	-.311	-.322			
18	-79.5	-.6	-.430	-.756			
19	-9.9	-2.4	-.438	-.688			
20	31.1	2.2	-.385	-.331			
21	45.7	4.0	-.278	-.023	4.1	-.037	-.0160
22	-326.4	2.9	1.727	.218			-.0012
23	-322.3	4.5	1.292	.724	3.5	.655	
24	-179.2	-8.0	.086	-.648	-46.3	.188	
25	-51.0	-10.3	-.799	-1.395	-4.6	.428	
26	7.8	-2.6	-.708	-.773	27.5	.214	
27	27.1	4.1	-.350	-.074	22.3	0.000	
28	28.9	5.5	-.172	.227	1.7	-.052	-.0090
29	-219.4	11.3	.304	.022			
30	-466.4	54.6	.385	.931	-11.1	1.801	
31	-125.2	-11.6	-.497	-.737	-122.7	1.902	
32	-13.4	-13.4	-.462	-.854	24.6	.856	
33	7.1	-7.1	-.090	-.293	49.3	-.025	
34	10.2	-5.7	.072	.050	28.7	-.239	
35	14.7	-3.8	.063	.114	-.5	-.088	

THEORETICAL STRESSES AND DEFLECTIONS

MODEL TEST 5
P=1200 LB FR=00 LB
D=0.833 YM F=0.000 YM

GAUGE	N1 LB/IN	N2 LB/IN	M1 LB	M2 LB	N12 LB/IN	M12 LB	DEFLN IN
1	-427.3	0.0	-.344	0.000	0.0	0.000	-.0204
2	-281.0	.2	-.325	-.047	0.0	0.000	-.0212
3	-164.8	.4	-.320	-.121	0.0	0.000	-.0222
4	-75.8	.4	-.340	-.247	0.0	0.000	-.0233
5	-11.8	0.0	-.385	-.414	0.0	0.000	-.0244
6	27.2	-.5	-.431	-.560	0.0	0.000	-.0252
7	40.3	-.8	-.451	-.619	0.0	0.000	-.0254
8	-423.7	0.0	-.349	0.000	0.0	-.092	-.0172
9	-280.2	.2	-.325	-.073	1.1	-.087	-.0183
10	-167.0	.5	-.317	-.184	.3	-.067	-.0197
11	-78.1	.2	-.342	-.336	-1.0	-.025	-.0210
12	-12.3	-.1	-.393	-.472	-1.8	.015	-.0221
13	29.0	-.5	-.444	-.551	-1.3	.024	-.0229
14	43.3	-.6	-.465	-.575	0.0	0.000	-.0231
15	-402.2	0.0	-.079	0.000	0.0	-.161	-.0078
16	-287.9	1.6	-.154	-.042	2.7	-.159	-.0101
17	-175.8	-.5	-.305	-.455	-3.0	-.139	-.0125
18	-79.8	-2.8	-.454	-.834	-3.6	.005	-.0145
19	-8.8	-2.0	-.495	-.739	-.1	.131	-.0155
20	32.1	.8	-.428	-.365	1.6	.117	-.0158
21	45.2	2.3	-.380	-.170	0.0	0.000	-.0158
22	-312.0	0.0	1.298	0.000	0.0	.334	-.0006
23	-356.8	26.9	.892	.620	4.0	.288	-.0031
24	-177.2	-10.5	-.201	-.754	-28.5	.244	-.0060
25	-53.9	-13.3	-.814	-1.300	-.8	.263	-.0079
26	3.1	-3.3	-.558	-.737	13.2	.139	-.0085
27	24.3	3.4	-.291	-.055	10.6	.033	-.0082
28	29.1	5.4	-.127	.215	0.0	0.000	-.0080
29	-140.8	0.0	1.178	0.000	0.0	.815	.0004
30	-359.8	43.5	.938	.703	-5.9	.866	-.0009
31	-108.5	-20.8	-.272	-.629	-46.8	.830	-.0026
32	-22.8	-12.4	-.669	-.837	13.6	.366	-.0037
33	4.3	-1.8	-.432	-.386	23.5	0.000	-.0038
34	12.0	2.5	-.143	.016	14.5	-.089	-.0036
35	13.4	3.4	-.031	.161	0.0	0.000	-.0035

EXPERIMENTAL STRESSES AND DEFLECTIONS

MODEL TEST 2
P=1200 LB FR=00 LB
D=0.972 YM F=0.000 YM

GAUGE	N1 LB/IN	N2 LB/IN	M1 LB	M2 LB	N12 LB/IN	M12 LB	DEFLN IN
1	-581.3	-6.5	-.503	-.069			-.0810
2	-392.7	.1	-.450	-.399	17.0	-.340	-.0715
3	-215.4	-5.9	-.391	-.304			-.0615
4	-54.2	-3.3	-.182	.428	0.0	-.025	-.0500
5	55.0	-1.6	.201	1.764			-.0405
6	123.2	2.7	.483	2.915			-.0335
7	148.9	4.5	.700	3.305	1.1	.025	-.0310
8	-592.1	-.5	-1.211	-.201			-.0782
9	-403.2	-8.0	-.715	-.574			
10	-201.8	-9.0	-.572	-.431			
11	-48.7	-5.6	-.312	.414			
12	53.5	0.0	.178	1.828			
13	108.4	2.2	.594	3.091			
14	130.6	5.5	.708	3.421	.5	-.113	-.0275
15	-732.2	-13.1	-2.274	-.244			-.0647
16	-392.2	-8.6	-1.772	-1.012			
17	-139.5	-6.4	-1.330	-.819			
18	-4.6	-2.0	-.525	.505			
19	57.8	3.2	.246	2.005			
20	75.5	4.6	.848	3.042			
21	76.9	1.6	.978	3.233	1.1	-.025	-.0175
22	-846.9	-13.9	-2.866	-.369			-.0417
23	-355.4	-16.7	-3.027	-2.103	-79.2	-2.456	
24	-53.0	-14.7	-2.392	-1.613	27.5	-2.104	
25	32.7	4.9	-.771	.319	82.2	-2.318	
26	44.8	12.0	.477	1.648	68.7	-2.078	
27	36.2	9.7	1.011	2.088	34.0	-1.108	
28	31.9	8.9	1.053	2.129	0.0	0.000	-.0085
29	-1076.6	-36.2	-.748	.011			
30	-221.9	-86.2	-1.915	-1.871	-115.0	-2.091	
31	1.2	-24.2	-1.513	-.982	141.5	-3.565	
32	25.6	16.5	-1.055	.232	142.6	-3.741	
33	19.3	36.9	-1.249	.481	89.2	-2.746	
34	17.2	45.4	-1.506	.436	38.1	-1.398	
35	10.1	46.1	-1.580	.427	2.3	.075	

THEORETICAL STRESSES AND DEFLECTIONS

MODEL TEST 2
P=1200 LB FR=00 LB
D=0.972 YM F=0.000 YM

GAUGE	N1 LB/IN	N2 LB/IN	M1 LB	M2 LB	N12 LB/IN	M12 LB	DEFLN IN
1	-633.2	0.0	-.326	0.000	0.0	0.000	-.1074
2	-400.9	-2.0	-.322	.091	0.0	0.000	-.0895
3	-203.2	-3.8	-.214	.530	0.0	0.000	-.0716
4	-48.1	-2.6	-.065	1.562	0.0	0.000	-.0546
5	61.6	.9	.461	2.993	0.0	0.000	-.0400
6	126.6	4.8	.813	4.255	0.0	0.000	-.0300
7	148.0	6.4	.954	4.758	0.0	0.000	-.0264
8	-674.1	0.0	-.697	0.000	0.0	.007	-.1035
9	-397.6	-2.2	-.640	-.009	-9.9	-.012	-.0856
10	-182.9	-4.4	-.455	.401	-1.6	.005	-.0678
11	-31.8	-2.9	-.061	1.501	10.0	.021	-.0507
12	62.6	1.3	.470	3.032	15.3	.017	-.0360
13	112.1	5.7	.936	4.362	11.0	.005	-.0258
14	127.1	7.5	1.121	4.886	0.0	0.000	-.0222
15	-830.8	0.0	-2.215	0.000	0.0	-.478	-.0856
16	-381.6	-5.1	-1.868	-.437	-24.1	-.522	-.0694
17	-113.1	-5.7	-1.269	.058	0.0	-.462	-.0531
18	16.8	-.6	-.408	1.482	25.3	-.481	-.0373
19	60.7	4.5	.489	3.006	31.9	-.495	-.0240
20	66.5	6.7	1.130	4.000	20.6	-.333	-.0150
21	65.1	7.0	1.355	4.324	0.0	0.000	-.0119
22	-1095.7	0.0	-5.241	0.000	0.0	-1.880	-.0541
23	-326.3	-32.0	-4.384	-1.561	-38.5	-1.857	-.0431
24	-25.3	-8.6	-2.631	-.421	24.3	-1.753	-.0317
25	43.8	10.0	-.705	1.413	42.2	-1.689	-.0207
26	39.9	10.7	.478	2.348	31.9	-1.349	-.0120
27	25.4	5.0	.932	2.523	15.5	-.738	-.0066
28	19.5	2.2	1.024	2.500	0.0	0.000	-.0048
29	-1001.0	0.0	-4.609	0.000	0.0	-3.154	-.0262
30	-185.4	-59.5	-3.964	-1.512	-9.0	-2.965	-.0207
31	5.4	-10.8	-2.163	-.381	66.7	-3.067	-.0149
32	28.1	8.6	-.525	.814	50.6	-2.621	-.0094
33	18.6	7.6	.265	1.217	25.8	-1.781	-.0052
34	9.4	2.6	.485	1.186	9.6	-.868	-.0027
35	6.2	.5	.510	1.127	0.0	0.000	-.0019

EXPERIMENTAL STRESSES AND DEFLECTIONS

MODEL TEST 6
P=1200 LB FR=31 LB
D=0.833 YM F=0.138 YM

GAUGE	N1 LB/IN	N2 LB/IN	M1 LB	M2 LB	N12 LB/IN	M12 LB	DEFLN IN
1	-647.1	-7.5	-1.088	-.263			-.0885
2	-375.8	-5.2	-1.095	-.550	15.8	-.541	-.0765
3	-173.8	-8.4	-.741	-.057			-.0620
4	-26.4	-1.6	-.149	1.137	-.5	.037	-.0490
5	51.5	0.0	.473	2.557			-.0365
6	97.1	4.0	.888	3.494			-.0290
7	110.5	5.1	1.060	3.919	1.7	.037	-.0260
8	-600.7	-.5	-1.530	-.271			-.0797
9	-374.7	-9.8	-1.195	-.750			
10	-172.2	-5.2	-.713	-.105			
11	-38.7	-1.3	-.155	.974			
12	44.3	2.3	.352	2.166			
13	90.2	5.2	.720	3.087			
14	107.7	6.7	.747	3.409	0.0	-.050	-.0250
15	-539.5	-10.2	-.673	-.022			-.0492
16	-350.2	-14.2	-.632	-.350			
17	-179.5	-7.5	-.732	-.537			
18	-52.4	-2.8	-.388	-.062			
19	30.0	-1.3	-.058	.918			
20	74.3	2.9	.349	1.923			
21	87.4	3.3	.486	2.421	1.1	-.050	-.0175
22	-377.0	1.9	1.464	.194			-.0207
23	-358.4	1.6	.897	.693	75.1	-1.234	
24	-188.0	-12.7	-.012	-.645	20.5	-2.028	
25	-37.9	-13.2	-.780	-1.195	53.4	-1.448	
26	27.8	-2.2	-.495	-.080	67.5	-1.196	
27	47.5	5.5	.075	1.035	42.2	-.755	
28	52.0	9.3	.316	1.494	1.1	-.025	-.0100
29	-201.2	10.3	2.544	.199			
30	-505.6	33.0	2.231	1.787	47.5	-.012	
31	-130.5	-24.7	.073	-.828	-46.9	.302	
32	-8.0	-17.5	-.477	-.812	103.3	-.831	
33	15.3	-1.9	-.478	-.166	106.2	-1.423	
34	22.6	6.7	-.624	.240	56.9	-1.020	
35	21.6	7.7	-.664	.390	.5	-.012	

THEORETICAL STRESSES AND DEFLECTIONS

MODEL TEST 6
D=0.833 YM F=0.138 YM
P=1200 LB FR=31 LB

GAUGE	N1 LB/IN	N2 LB/IN	M1 LB	M2 LB	N12 LB/IN	M12 LB	DEFLN IN
1	-725.7	0.0	-1.691	0.000	0.0	0.000	-.1037
2	-376.7	-5.8	-1.339	-.141	0.0	0.000	-.0854
3	-153.2	-1.9	-.704	.714	0.0	0.000	-.0673
4	-18.5	1.3	-.019	1.966	0.0	0.000	-.0504
5	57.6	3.5	.558	3.146	0.0	0.000	-.0367
6	95.8	4.5	.932	3.951	0.0	0.000	-.0276
7	107.2	4.6	1.059	4.232	0.0	0.000	-.0245
8	-691.2	0.0	-1.485	0.000	0.0	-.912	-.0897
9	-368.2	-6.3	-1.235	-.267	13.8	-.877	-.0745
10	-158.5	-2.4	-.711	.371	14.0	-.775	-.0594
11	-27.3	.6	-.112	1.469	9.8	-.594	-.0451
12	50.5	3.0	.411	2.610	5.1	-.378	-.0331
13	91.6	4.2	.756	3.453	2.0	-.175	-.0251
14	104.6	4.6	.877	3.763	0.0	0.000	-.0223
15	-567.8	0.0	-.521	0.000	0.0	-1.390	-.0519
16	-350.3	-5.6	-.636	-.287	25.9	-1.365	-.0448
17	-174.2	-4.9	-.644	-.491	23.5	-1.274	-.0377
18	-46.4	-3.8	-.435	-.023	18.4	-.954	-.0302
19	34.8	-.1	-.055	1.094	15.1	-.564	-.0228
20	75.9	4.6	.338	2.250	9.2	-.250	-.0173
21	88.0	6.8	.508	2.733	0.0	0.000	-.0154
22	-384.8	0.0	1.493	0.000	0.0	-.765	-.0208
23	-391.4	16.4	.945	.693	31.2	-.824	-.0194
24	-177.4	-17.1	-.415	-1.034	6.2	-.892	-.0182
25	-35.7	-15.4	-.913	-1.108	29.7	-.799	-.0157
26	26.7	-2.3	-.499	.098	34.2	-.701	-.0122
27	47.1	5.8	.087	1.260	20.9	-.433	-.0090
28	50.9	8.3	.332	1.701	0.0	0.000	-.0078
29	-170.7	0.0	1.394	0.000	0.0	-.151	-.0082
30	-374.3	35.8	1.079	.839	23.3	-.104	-.0078
31	-108.4	-25.1	-.371	-.808	-7.0	-.216	-.0078
32	-14.3	-13.7	-.737	-.793	48.0	-.710	-.0070
33	14.9	-1.3	-.375	-.032	46.6	-.890	-.0053
34	22.0	3.6	.021	.592	25.7	-.590	-.0039
35	22.9	4.7	.173	.816	0.0	0.000	-.0034

EXPERIMENTAL STRESSES AND DEFLECTIONS

MODEL TEST 7
P=1200 LB FR=60 LB
D=0.667 YM F=0.305 YM

GAUGE	N1 LB/IN	N2 LB/IN	M1 LB	M2 LB	N12 LB/IN	M12 LB	DEFLN IN
1	-700.2	-5.9	-3.271	-.578			-.0895
2	-348.8	-6.0	-2.297	-.981	13.5	.264	-.0770
3	-127.1	-2.6	-1.221	-.048			-.0625
4	.1	6.9	-.184	1.488	-1.1	.151	-.0475
5	50.4	4.9	.631	2.890			-.0350
6	73.2	7.9	1.100	3.630			-.0275
7	79.2	7.0	1.236	3.935	2.9	.012	-.0240
8	-581.2	-3.8	-2.190	-.246			-.0742
9	-342.8	-9.3	-1.703	-1.019			
10	-150.5	-1.2	-.948	-.177			
11	-36.1	.8	-.192	.991			
12	35.9	5.0	.376	2.059			
13	75.6	7.3	.642	2.694			
14	87.4	7.8	.714	2.976	.5	-.012	-.0240
15	-309.2	.9	1.622	.200			-.0315
16	-310.9	-15.4	1.100	.579			
17	-218.4	-13.4	-.091	-.666			
18	-100.0	-4.9	-.391	-.673			
19	2.9	-1.0	-.386	-.104			
20	70.9	2.5	-.186	.780			
21	97.1	4.5	-.116	1.200	-2.9	-.012	-.0195
22	-71.1	7.2	2.075	.155			-.0087
23	-242.2	5.6	2.236	.919	163.8	1.600	
24	-284.8	-3.4	1.796	1.345	120.9	-.478	
25	-145.0	-13.5	.004	-1.101	45.8	-.629	
26	-4.1	-11.2	-.903	-1.318	56.9	-.289	
27	55.7	1.8	-.753	-.179	46.3	-.188	
28	71.8	8.7	-.514	.459	0.0	0.000	-.0120
29	12.1	5.0	-.132	-.154			
30	-153.7	-4.8	.509	.313	197.8	.491	
31	-445.0	22.4	1.726	1.908	122.7	1.398	
32	-98.9	-25.7	-.242	-1.115	-10.5	1.537	
33	8.8	-20.9	-.447	-.855	102.1	.277	
34	27.6	-11.6	-.313	-.139	72.8	-.302	
35	31.5	-9.8	-.237	.155	-1.1	.025	

THEORETICAL STRESSES AND DEFLECTIONS

MODEL TEST 7
P=1200 LB FR=60 LB
D=0.667 YM F=0.305 YM

GAUGE	N1 LB/IN	N2 LB/IN	M1 LB	M2 LB	N12 LB/IN	M12 LB	DEFLN IN
1	-837.3	0.0	-3.266	0.000	0.0	0.000	-.1052
2	-358.7	-10.9	-2.480	-.451	0.0	0.000	-.0859
3	-106.4	1.0	-1.325	.689	0.0	0.000	-.0667
4	10.4	6.2	-.103	2.366	0.0	0.000	-.0489
5	57.5	6.4	.708	3.460	0.0	0.000	-.0349
6	73.1	4.5	1.125	3.973	0.0	0.000	-.0260
7	76.5	3.5	1.247	4.107	0.0	0.000	-.0229
8	-696.1	0.0	-1.775	0.000	0.0	-1.835	-.0803
9	-348.9	-9.2	-1.582	-.541	40.2	-1.740	-.0675
10	-140.2	-2.4	-1.069	-.060	30.9	-1.542	-.0546
11	-21.7	2.9	-.260	1.254	11.2	-1.160	-.0423
12	44.1	4.3	.340	2.311	-1.9	-.728	-.0318
13	77.6	4.0	.676	2.954	-4.4	-.335	-.0249
14	87.9	3.7	.780	3.163	0.0	0.000	-.0225
15	-310.1	0.0	1.857	0.000	0.0	-1.172	-.0291
16	-311.6	-2.2	1.211	.696	65.5	-1.219	-.0279
17	-225.3	-10.6	-.018	-.787	54.7	-1.403	-.0269
18	-100.9	-7.3	-.426	-.858	26.6	-1.208	-.0251
19	8.1	-2.9	-.441	-.173	7.8	-.755	-.0223
20	79.3	2.6	-.289	.849	1.2	-.311	-.0196
21	103.4	5.4	-.200	1.337	0.0	0.000	-.0185
22	-26.3	0.0	2.764	0.000	0.0	.187	-.0061
23	-251.5	-6.3	2.689	1.520	79.8	.246	-.0072
24	-332.8	0.0	1.788	1.273	62.3	.060	-.0092
25	-142.7	-25.9	-.297	-1.506	20.9	-.233	-.0115
26	-4.1	-16.1	-1.008	-1.380	31.1	-.213	-.0121
27	59.8	2.0	-.723	-.018	23.3	-.157	-.0112
28	76.9	9.1	-.480	.657	0.0	0.000	-.0106
29	30.1	0.0	1.395	0.000	0.0	.537	-.0016
30	-141.0	-16.5	1.454	.716	78.8	.465	-.0022
31	-341.1	18.1	1.485	1.493	63.7	.836	-.0032
32	-91.3	-31.5	-.345	-1.053	18.3	.656	-.0050
33	.2	-14.1	-.797	-.936	56.6	-.011	-.0054
34	30.7	1.3	-.480	-.063	38.4	-.235	-.0051
35	37.8	6.3	-.279	.337	0.0	0.000	-.0048

EXPERIMENTAL STRESSES AND DEFLECTIONS

MODEL TEST 8
P=1200 LB FR=87 LB
D=0.500 YM F=0.472 YM

GAUGE	N1 LB/IN	N2 LB/IN	M1 LB	M2 LB	N12 LB/IN	M12 LB	DEFLN IN
1	-736.5	-16.4	-1.940	-.127			-.0870
2	-332.2	-19.3	-2.586	-1.502	17.0	-.163	-.0745
3	-92.4	-5.8	-1.621	-.242			-.0595
4	15.2	6.4	-.295	1.639	-2.3	.100	-.0450
5	44.5	5.0	.681	3.004			-.0325
6	50.8	6.3	1.152	3.475			-.0255
7	52.6	4.8	1.280	3.658	4.1	-.012	-.0230
8	-538.7	-3.3	-2.243	-.419			-.0622
9	-329.1	-16.3	-1.477	-1.021			
10	-139.1	-5.0	-1.091	-.689			
11	-36.7	5.2	-.398	.459			
12	26.8	5.5	.136	1.460			
13	60.9	6.8	.539	2.265			
14	68.6	9.3	.694	2.680	.5	-.037	-.0230
15	-131.0	4.0	2.601	.245			-.0150
16	-255.9	-17.0	2.110	1.002			
17	-243.7	-29.1	.801	-.023			
18	-141.4	-16.9	-.365	-1.190			
19	-28.7	-7.5	-.698	-.980			
20	54.2	.1	-.660	-.302			
21	88.6	2.8	-.577	.069	4.1	-.037	-.0215
22	37.6	6.2	1.328	-.017			-.0022
23	-135.1	-9.3	1.611	.555	101.5	.919	
24	-229.0	-20.9	1.808	2.870	229.0	1.335	
25	-237.2	-12.7	.560	-.079	170.2	1.108	
26	-84.5	-13.3	-.760	-1.502	64.5	.176	
27	40.2	-7.5	-1.417	-1.367	34.6	.138	
28	78.3	-.3	-1.496	-.972	0.0	-.050	-.0145
29	12.1	-3.5	-.865	-.137			
30	-39.9	-.3	-.800	-.283	54.6	.289	
31	-138.6	-25.0	.497	.737	300.0	1.171	
32	-402.9	-4.9	1.406	1.144	216.0	2.393	
33	-67.9	-43.9	-.105	-1.087	17.0	1.801	
34	24.6	-38.7	-.249	-.765	71.0	.718	
35	39.5	-31.2	-.078	-.347	-1.7	-.037	

THEORETICAL STRESSES AND DEFLECTIONS

MODEL TEST 8
P=1200 LB FR=87 LB
D=0.500 YM F=0.472 YM

GAUGE	N1 LB/IN	N2 LB/IN	M1 LB	M2 LB	N12 LB/IN	M12 LB	DEFLN IN
1	-966.4	0.0	-4.885	0.000	0.0	0.000	-.1114
2	-354.4	-17.0	-3.674	-.916	0.0	0.000	-.0905
3	-69.3	2.7	-1.837	.741	0.0	0.000	-.0696
4	38.8	11.5	-.341	2.452	0.0	0.000	-.0506
5	64.8	10.0	.841	3.862	0.0	0.000	-.0354
6	64.5	5.6	1.361	4.305	0.0	0.000	-.0260
7	62.2	3.4	1.493	4.382	0.0	0.000	-.0226
8	-701.4	0.0	-1.472	0.000	0.0	-2.566	-.0759
9	-346.8	-13.6	-1.659	-.790	66.1	-2.437	-.0651
10	-132.9	-6.8	-1.293	-.475	46.4	-2.236	-.0538
11	-11.4	3.2	-.661	.584	14.2	-1.654	-.0425
12	47.6	6.2	.204	2.100	-4.5	-.999	-.0325
13	74.0	5.6	.689	2.888	-7.2	-.458	-.0258
14	81.5	5.0	.838	3.132	0.0	0.000	-.0234
15	-122.7	0.0	3.445	0.000	0.0	-.602	-.0179
16	-283.5	-5.7	2.953	1.948	87.8	-.562	-.0189
17	-248.0	-24.4	.798	-.128	86.5	-.994	-.0208
18	-134.4	-13.0	-.621	-1.504	49.6	-1.319	-.0226
19	-12.1	-3.1	-.767	-.836	15.3	-1.015	-.0227
20	75.4	2.0	-.697	-.082	-.1	-.533	-.0219
21	107.3	3.6	-.661	.263	0.0	0.000	-.0215
22	91.7	0.0	1.937	0.000	0.0	.469	-.0020
23	-156.2	-21.9	2.009	.485	55.2	.506	-.0032
24	-248.8	-35.1	3.030	3.223	124.0	.774	-.0045
25	-277.9	-20.5	1.528	1.064	89.2	.288	-.0078
26	-76.2	-27.5	-.745	-1.718	29.0	-.081	-.0115
27	55.4	-10.2	-1.514	-1.429	19.1	-.004	-.0133
28	95.3	1.0	-1.565	-.884	0.0	0.000	-.0136
29	65.5	0.0	.593	0.000	0.0	.481	-.0004
30	-66.4	-17.8	.633	-.163	19.2	.298	-.0008
31	-142.5	-36.7	1.835	2.066	132.9	.568	-.0010
32	-307.1	0.0	1.603	1.692	109.7	1.217	-.0026
33	-58.2	-34.2	-.550	-1.202	42.2	.952	-.0050
34	31.0	-10.8	-1.103	-.971	45.8	.302	-.0062
35	52.0	.5	-1.059	-.548	0.0	0.000	-.0065

Model	Cross section	Longitudinal thrust			Longitudinal moment		
		Applied external lb.	Internal actions lb.	% diff.	Applied external lb./in.	Internal actions lb./in.	% diff.
1	A	1200	1234	2.9	1080	1113	3.0
	B		1158	3.5		1073	0.7
	C		1191	0.7		1055	2.4
	D		1044			887	
	E		434			570	
2	A	1200	1214	1.2	-1973	-1931	2.1
	B		1289	7.5		-1916	2.8
	C		1270	5.7		-2009	3.2
	D		1227			-1962	
	E		1107			-1916	
3	A	1200	1195	0.4	-368	-393	6.8
	B		1180	1.7		-391	6.3
	C		1201	0.1		-354	3.8
	D		1184			-335	
	E		934			-192	
4	A	1200	1173	2.3	722	719	0.2
	B		1159	3.3		703	2.5
	C		1181	1.6		723	0.1
	D		1086			685	
	E		309			-118	
5	A	1200	1200	0.0	-1175	-1157	1.4
	B		1198	0.2		-1153	1.8
	C		1206	0.5		-1165	0.8
	D		1153			-1190	
	E		1320			-1329	
6	A	1169	1172	0.3	-1920	-1925	0.3
	B	1177	1229	4.4	-1854	-1821	1.8
	C	1183	1221	3.2	-1632	-1651	1.2
	D	1186	1178		-1405	-1387	
	E	1187	1302		-1271	-1462	
7	A	1140	1119	1.8	-1873	-1868	0.3
	B	1152	1155	0.3	-1723	-1699	1.4
	C	1153	1175	1.9	-1247	-1233	1.0
	D	1148	1118		-793	-719	
	E	1144	846		-543	-355	
8	A	1122	1122	0.6	-1829	-1807	1.2
	B	1125	1131	0.6	-1594	-1581	0.8
	C	1112	1139	2.4	-891	-815	8.5
	D	1093	1086		-285	-293	
	E	1080	1804		-220	125	

Table V.2 Overall equilibrium of model results